12-2017

Process Intensification through Spherical Crystallization: Novel Experimental and Modeling Approaches

Ramon Peña
Purdue University

PROCESS INTENSIFICATION THROUGH SPHERICAL CRYSTALLIZATION: NOVEL EXPERIMENTAL AND MODELING APPROACHES

by

Ramon Peña

A Dissertation

Submitted to the Faculty of Purdue University

In Partial Fulfillment of the Requirements for the degree of

Doctor of Philosophy

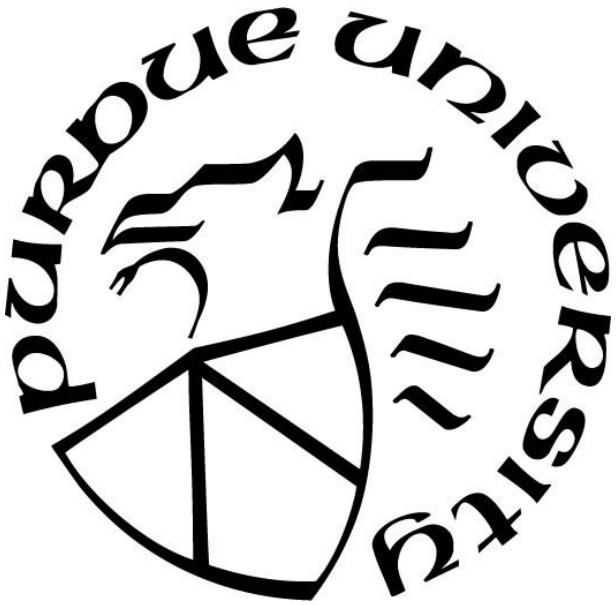

Davidson School of Chemical Engineering

West Lafayette, Indiana

December 2017

THE PURDUE UNIVERSITY GRADUATE SCHOOL
STATEMENT OF COMMITTEE APPROVAL

Dr. Zoltan K. Nagy, Chair
Davidson School of Chemical Engineering
Dr. James D. Litster
Davidson School of Chemical Engineering
Chemical and Biochemical Engineering, The University of Sheffield
Dr. Doraiswami Ramkrishna
Davidson School of Chemical Engineering
Dr. Michael T. Harris
Davidson School of Chemical Engineering

Approved by:
Dr. Sangtae Kim
Head of the Graduate Program

"There's a few things, about three things to my account, that I need each day. One of them is something to look up to, another is something to look forward to, and another is someone to chase. First off, I want to thank God because that's who I look up to. He has graced my life with opportunities that I know are not of my hand or any other human hand. He has shown me that it is a scientific fact that gratitude reciprocates. To my family, that's who and what I look forward to. To my father […] to you Dad, you taught what it means to be a man. To my mother […] who taught me and [my sisters] to respect ourselves and what we in turn learned was that we were better able to respect others. Thank you for that momma. To my [sisters Claritza, Ariana, and Ana along with Mom, Dad and Milan] the courage and significance you have given me [through this journey] is unparalleled you are the [six] people who I want to make most proud of me. Thank you. To my hero, that's who I chase. [My hero is me in ten years]. You see every day, every week, every month, and every year of my life, my hero is always ten years away. I'm never going to be my hero. I'm not going to attain that. I know I'm not. And that's just fine with me because that keeps me with someone to keep on chasing."

Rephrased Matthew McConaughey speech - Best Actor for Dallas Buyers Club

ACKNOWLEDGMENTS

I want to thank my advisor Professor Zoltan K. Nagy for giving the opportunity to pursue my Ph.D. under his guidance. I can truly say that my experience throughout these years would have paled in comparison had I joined any other research group. I want to thank him for allowing me to be creative and independent in my research and having trust in my decisions. Whether I wanted to go on internships or go to conferences, he was always supportive of professional endeavors as well. I'll always remember my first group meeting presentation; he was running late. When he finally got in and sat down, I said "Boss, are we ready to rock and roll?" His response was "Yeah, let's see how these spheres roll." And that was the start to my spherical crystallization dissertation and Ph.D. experience.

I would like to thank the good friends from my cohort that started their graduate school journey with me, specifically Omar, Jonatan, and Mariana. Had we not stuck together in our first year, the story would have ended differently. I would like to also thank the entire Nagy research group. As the middle child of the group, I had the opportunity to collaborate and share good times with older members who graduated before me including Elena, Andy, Elcin, Yang, David, and Jennifer, and new members who will guide the group after me including Claire, Pal, Joe and Jaron. You were all great colleagues and very helpful to me, thank you for the countless discussions. To my friends within and outside the engineering realm including Lizbeth, Oscar, David, Vu, Sherryl, Andres, and others, you all made the PhD experience much more enjoyable.

Special thanks go to EOF and the OSD office at the Rutgers University School of Engineering. They set me on the path I am on today. Special thanks go to Dean Candiece White. I would also like to thank the McNair program at Rutgers, without them I would not have considered graduate school. Special thanks to James Whitney and Crystal Bedley.

Last, but not least, I would like to thank my family. Mom and Dad, you are who I do this for. Thank you for always supporting me in everything I do. Claritza, Ariana, and Ana, thank you for holding down the fort, I look up to each one of you. To Milan, you give me motivation and energy. I cannot wait to watch you grow into the beautiful and special person you are. To all my friends at home, especially Mark, Kareem, Giancarlos, Cody, Dairon, Gage, Jeff, Saury, Sally, my church, le Frat and Clutch, this marks the homecoming!

TABLE OF CONTENTS

LIST OF TABLES

LIST OF FIGURES

LIST OF ABBREVIATIONS

API	Active pharmaceutical ingredient
ASD	Agglomerate size distribution
BA	Benzoic acid
BASR	Bridging liquid to anti-solvent ratio
BSC	Batch spherical crystallization
BSR	Bridging liquid to solute ratio
CBD	Conditioned bulk density
CFC	Continuous filtration carousel
CIP	Clean-in-place
CLD	Chord length distribution
COBC	Continuous oscillatory baffled crystallizer
CPS	Compression percentage
CPSR	Crystal to droplet size ratio
CSC	Continuous spherical crystallization
CSD	Crystal size distribution
CSO	Controlled state operation
ESD	Emulsion solvent diffusion
FBRM	Fourier beam reflectance measurement
FRI	Flow rate index
MOM	Method of moments
MSMPR	Mixed Suspension mixed product removal
ODE	Ordinary differential equation
OFBC	Oscillatory flow baffled crystallizer
PAT	Process analytical technology
PBE	Population balance equation
PBM	Population balance model
PCA	Principal component analysis
PCM	Paracetamol
PD	Product difference

PFC	Plug flow crystallizer
PI	Process intensification
PVM	Particle vision microscopy
PSD	Particle size distribution
QESD	Quasi-emulsion solvent diffusion
QMOM	Quadrature method of moments
SA	Spherical agglomeration
SASR	Solution to anti-solvent ration
SC	Spherical crystallization
SEM	Scanning electron microscopy
SI	Stability Index
SWMCL	Square weighted mean chord length
UPLC	Ultra-performance liquid chromatography
UV	Ultra violet

ABSTRACT

Author: Peña, Ramon. PhD
Institution: Purdue University
Degree Received: December 2017
Title: Process Intensification through Spherical Crystallization: Novel Experimental and Modeling Approaches
Major Professor: Zoltan K. Nagy

Process intensification is defined as the use of innovative techniques and technologies to create sustainable solutions to industrial production difficulties. Continuous spherical crystallization is a process intensification technique that could resolve production issues for pharmaceutical and solids processing industries, consequently, allowing for the integration of upstream and downstream manufacturing units. Spherical crystallization is carried out through emulsion based crystallization and/or agglomeration in suspension of fine crystals to produce aggregates of improved bulk and micromeritic properties. The advantages of spherical crystallization include: (i) replacing downstream particle correction units (i.e., milling, granulation), (ii) providing control of crystalline properties by decoupling crystallization and agglomeration mechanisms, and (iii) reducing plant foot print and allowing for reconfigurable units. The overall aim of the thesis is to further develop the scientific understanding of spherical crystallization mechanisms and introduce a systematic approach for implementing continuous spherical crystallization as a smart manufacturing platform enabled by a quality-by-design framework.

Experimentally, the thesis achieves: (i) better mechanistic understanding of spherical crystallization in semi-batch systems using process analytical technologies (PAT); and (ii) the assessment of the feasibility of continuous spherical crystallization in mixed suspension mixed product removal (MSMPR) and oscillatory flow baffled crystallizer (OFBC) systems. Computationally, a coupled population balance model is developed that leads to an optimization framework for bioavailability and manufacturability through spherical crystallization. Together the experimental and modeling approaches deliver a model-based framework for process intensification that can lead to adaptive manufacturing systems for high value-added particulate products.

1. INTRODUCTION

1.1 Motivation

Crystallization, originally conceived as a purification and separation process, has become a predominant technique in particle design technology. Crystallization is a unit operation in process systems in a broad range of industries including pharmaceuticals, bulk and fine chemicals, food, and electronics. Crystallization is the characteristic-and property-determining step in most solid processes. Given that it is also one of the initial steps, it has a major impact on downstream processes (e.g., filtering, drying, milling, handling, and storage).[1] The pharmaceutical industry, with an estimated worth of USD $300 billion/year[2], is a major dependent of crystallization as 90% of its active pharmaceutical ingredients (API) are derived from a crystallization step.[3]

Due its industrial importance and economic significance, crystallization has been studied extensively within academia and industry research. Advancements have been made in the area of crystal size[4,5] and shape[1,6,7] distribution design, in-situ measurement/online monitoring[8-11], modeling[12-15], optimization[7,8,14,16] and control.[16-19] The introduction of process analytical technology (PAT) allowed for major advancement in the monitoring of both batch and continuous processes. The pharmaceutical industry, through initiatives supported by the U.S. Food and Drug Administration (FDA), has been one of the main beneficiaries of the technology avoiding major product loss from its traditional recipe-based batch operation approach.[20] Application of predictive models in combination with real-time in-situ sensors has allowed the ability to not only monitor and control but also optimize the crystal product properties.[17,21] The ability to monitor processes online along with continued advances in computation speed can lead to the development of improved models and improved real-time control, which in turn will improve crystal product quality.

Crystal properties are directly related to the efficiency of downstream processes that are used to achieve the final dosage form. For example, fine crystals are preferred for pharmaceutical application due their bioavailability properties, but their subpar flow properties make them undesirable for processing.[22] There are many techniques available (e.g., wet/dry granulation, roller compaction, milling) to help improve crystal properties to

improve manufacturability; however, these processes often require extra unit operations which comes with more capital, labor, and operational costs. Moreover, given the historically batch nature of pharmaceutical processes, increasing the number of unit operations can cause increases in variability at each stage of production.

To achieve consistent product quality, the pharmaceutical industry has begun to investigate innovative continuous manufacturing platforms. With the goal for the industry being continuous end to end manufacturing, from drug substance to final drug product. The motivation for the aim is not only product quality, but due to expiring patents and the fluctuating cost of energy, the economic burden of inefficient manufacturing can no longer be ignored.[23] Thus the need to reduce operating costs, limit energy consumption and improve process efficiency has also become very significant. The adoption of continuous manufacturing technologies can be a key stride in achieving their objective.

It is estimated that the shift from batch to continuous manufacturing will have significant impact on high value-added solids manufacturing, through improved flexibility, agility, and sustainability in the process design (see Figure 1.1). This can result in plant footprint reduction (40-90% space, 25-60% reduced capital expenditure), lower operating costs (25-60%), and reduced energy requirements (40-70%).[25] Crystallization becomes a key focus in efforts to go continuous given it is one of the first steps in drug substance separations, accounts for 90% of API purification processes[3] and more than 70% of all pharmaceutical formulations are in the solid dosage form.[26] However, little implementation of continuous crystallization or other process alterations/intensifications has occurred. Intensifying the processes involved in pharmaceutical formulations within a continuous system can greatly improve efficiency, integrate processes for drug substance with drug product, decrease development time, and afford line-of-sight from the laboratory to full commercial scale operations. When applied to pharmaceutical manufacturing, process intensification (PI) techniques present integrative and adaptive attributes that make them the key framework for smart manufacturing techniques.

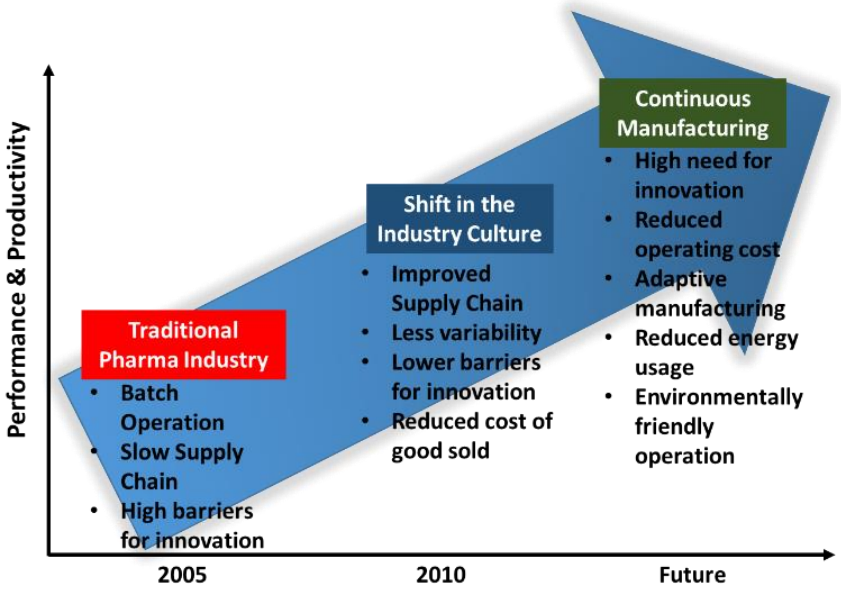

Figure 1.1 Schematic of increase process performance due to innovation and shift in focus from batch to continuous. Adapted from [24].

Spherical crystallization is a PI technique that produces large (micron to millimeter) particles of spherical shape with improved micromeritic properties using a minimum number of unit operations. Spherical crystallization is the agglomeration of fine crystals during the crystallization process. This eliminates the need for further unit operations (e.g., milling or granulation) to overcome negative physical properties typical to micronized drug substance or poor powder flow common to most APIs. Spherical crystallization produces ready to formulate material with specific dissolution properties, improved drug homogeneity, and decreased energy usage[27-30]; incorporating both the beneficial biopharmaceutical and manufacturability properties of the fine crystals and agglomerates, respectively. Spherical crystallization via spherical agglomeration (SA) is a technique that was first introduced in the 1960s. Sirianni et al.[31] (1969) described SA as a separation technique that allows particles to be removed from liquid suspension through selective wetting and agglomeration by the addition of an immiscible solvent, termed the bridging liquid.

Industrial processes that have benefited from spherical crystallization (SC) technique include coking of coals, pelletization of fine crystals, and beneficiation of ores. Current API manufacturing processes are poised to also benefit from SC. The most significant

challenges in manufacturing APIs is their common needle or plate-like morphologies that are difficult to isolate and process. Micronization is also often required for increased surface area to tailor bioavailability, which hinders downstream manufacturing. Properly understood and designed SC processes may provide a manufacturing platform that can solve many of the current processing and handling issues related to API size and morphology. Moreover, successfully designed continuous spherical crystallization (CSC) processes can provide the medium by which to integrate drug substance and drug product; allowing for end to end production that pharmaceutical industry desperately seeks.

1.2 Research Aims

The overall aim of this thesis is to investigate the viability of SC as a PI technique as well as assess continuous crystallization technologies to perform CSC. The aims are examined through a combined experimental and computational analysis.

The aims of this thesis work can be summarized as follows:

- To recognize the advancements in SC, gain a broad understanding of its potential impact on pharmaceutical processes, and identify areas of research interest within the field via a thorough review of the literature.
- To develop of deeper scientific understanding of the mechanisms that govern the agglomeration of fine crystals during SC using PAT tools with a detailed investigation of the effects of process parameters on particle properties and process efficiency.
- To develop a first principles modeling framework that describes the primary particle formation (via crystallization) and agglomerate formation (via SA) using a coupled population balance.
- Use the coupled population balance model (PBM) to develop a multi-objective optimization framework to design and achieve processes of both desired bioavailability (primary crystal size) and improved manufacturability (agglomerate size).
- Investigate, validate and assess the use of different continuous crystallization technologies for the purposes of the CSC with decoupled crystallization and agglomeration mechanisms.

- To develop a set of dimensionless quantities that describe the critical process parameters of SC to allow regime map development and dimensional analysis that will enable rapid design of SC processes.
- Consolidate the literature data of compound and solvent system combinations used for different SC processes and use principal component analysis for bridging liquid selection.
- Evaluate the coupling of continuous downstream unit operations with continuous crystallization to assess the feasibility of PI via multiple unit operations.

1.3 Research Contributions

The main contributions of this thesis can be summarized as follows:

- Identification of key agglomeration mechanisms during SC processes using modern PAT providing greater insight for the design of such processes. Agglomerates produced via different mechanisms were characterized for different flow and bulk properties, and the mechanism leading to favorable downstream process performance was identified.
- A coupled PBM was developed to simulate the evolution of crystals and agglomerates in a SC. The model allowed for decoupled kinetic parameters as the populations are tracked independently as opposed to traditional lumped kinetic parameters. The model provides first principles based process properties; for example, agglomeration efficiency and porosity.
- Implementation of a multi-objective framework for targeted bioavailability and manufacturability. The framework identifies different phases of a semi-batch SC process required to achieve different biopharmaceutical and manufacturing targets.
- The design of CSC in a mixed suspension mixed product removal (MSMPR) crystallizer with decoupled nucleation/growth and agglomeration mechanisms. Validating the concept of PI through CSC.
- The design of CSC in an oscillatory flow baffled crystallizer (OFBC) with spatially distributed solvent injection along the length of the crystallizer. The optimal

operating parameters for achieving efficient agglomeration and difference between an oscillatory flow system and traditional crystallizers were identified.

- A continuous filtration carousel (CFC) coupling with a mixed suspension mixed product removal crystallizer was evaluated for performance and validation of PI via coupled unit operations.
- Enabling the rapid design of SC process via mechanistic and process regime maps, and the selection of an appropriate bridging liquid via principal component analysis.

1.4 Thesis Structure

Chapter 2 is a literature review of crystallization which includes the fundamentals of crystallization, various crystallization techniques and their mode of operation. The description of the various process analytical technologies and characterization tools used in the experimental work is also given. An overview of modeling of crystallization via population balance equations (PBEs) using method of moments and quadrature method of moments (QMOM) is provided. The basics of using principal component analysis for multivariate data analysis is also discussed. The definition PI and its role in pharmaceutical manufacturing is presented. Lastly, most of the literature review focuses on critically reviewing all the relevant SC literature to provide the proper context for assessing the contributions of this thesis work.

Chapter 3 is a literature review specific to SC which includes an understanding of the parameters affecting SC and the fundamental mechanisms of the process. The review also details the work accomplished in the modeling and simulation of SC processes. The chapter also briefly discusses some CSC applications.

Chapter 4 describes the use of process analytical technologies to identify the agglomeration mechanism for various bridging liquid addition methods for a semi-batch process. For bridging liquid additions methods that are decoupled from solution addition, i.e., post crystallization, the effect of primary particle size on the final agglomerate size is evaluated. A critical bridging liquid to primary particle size ratio is established as the inflection point where the agglomeration mechanism changes from immersion to distributed. For successful bridging liquid addition methods, i.e., methods that create agglomerates, bulk and flow properties for the different methods are compared. The

combination of results lead to the development of guidelines for designing processes based on mechanism and flow properties.

Chapter 5 describes the development of the coupled PBM, the efficient solution method employed, and the implementation of a multi-objective optimization framework. The chapter describes how using the mass balance equations it is assured that mass is conserved and that the set of PBEs are coupled. It also describes the transformation of the PBEs using a QMOM approach that allows for efficient solution of the model while still handling otherwise difficult integral terms. Lastly, the targeted primary particle size and agglomeration size multi-objective framework is demonstrated for various scenarios.

Chapter 6 initiates the use of CSC as a PI technique. In this chapter, a two-stage MSMPR crystallizer is employed. The first stage serves as a nucleation and growth stage controlled by solution and anti-solvent addition. The second stage serves as the agglomeration stage controlled by bridging liquid addition and increased agitation rate. The chapter experimentally demonstrates that decoupling of nucleation/growth from agglomeration allows for tailored product design.

Chapter 7 extends the work of Chapter 6 to flow based system. In this chapter, an OFBC is employed. The OFBC is divided into different zones: nucleation, growth, and agglomeration. While the oscillatory flow baffled crystallizer superimposes an oscillatory motion on the net flow causing significant back-mixing, the zones are dominant by the specific crystallization mechanisms. The chapter presents the optimal conditions for design a CSC process in an OFBC and how the product quality and process efficiency are affected by changes in operating parameters.

Chapter 8 extends the PI concept to the coupling of two continuous unit operations: MSMPR crystallizer and CFC. The CFC is evaluated for its use in combination with a cooling and anti-solvent crystallization in a mixed suspension mixed product removal system. The process was evaluated in regards to its ability to reach a controlled state of operation (CSO) and for final moisture content of crystals.

Chapter 9 summarizes the finding of the thesis into main conclusions and future work. It provides suggestions on which areas of research should be expanded upon and what new directions can be explored. The emphasis of this chapter is to provide suggestions for achieving end to end integration of drug substance and drug product.

2. LITERATURE REVIEW

Crystallization is the leading solid-liquid separation technique in industrial processes. During crystallization, randomly organized molecules in solution undergo a phase change, coming together to create crystalline structures (solids) with three dimensional arrangements of periodic repeating patterns.[32] The conditions (i.e., supersaturation) under which the crystalline structures are created determines morphology and properties. Proper design of the crystallization process by controlling the conditions of the solution environment is required to achieve the desired level of yield, purity, micromeritic properties.

2.1 Solubility and Phase Equilibrium

Crystallization is a rate driven, kinetic process, with supersaturation as the driving force. Most practical crystallization processes use some type of solution crystallization technique. A solution is a homogeneous, single phase, mixture of two or more components. In crystallization, a solution is usually composed of a solvent (liquid phase) and a solute (solid phase).[32,33] Dissolving the solute in the solvent at a given temperature forms a homogeneous solution. At a specific temperature, there is a maximum amount of solute that can dissolve in a specific amount of solvent. This is known as solubility of the solute in the solvent.

Solubility depends on temperature and composition of the system. At solubility, the solution is said to be saturated. A saturated solution is in equilibrium with the dissolved solute. An undersaturated solution represents a solute concentration that is below the equilibrium concentration and the solute present will readily dissolve. Undersaturated solutions lie below the solubility curve. A supersaturated solution represents a solute concentration that exceeds the equilibrium concentration and lies above the solubility curve.[32,34] Due to the excess amount of solute in supersaturated solutions, the solute molecules crystallize to reach the equilibrium concentration in solution. The solubility curve describes the change in solute solubility with respect to temperature and concentration. A phase diagram can be used to understand the solubility of a compound

and identify its phase equilibrium point (Figure 2.1). Solubility and phase diagrams can be altered by using solvent mixtures instead of pure solvent solutions. Solvent mixtures are important when temperature changes do not significantly affect solubility and phase changes.[32]

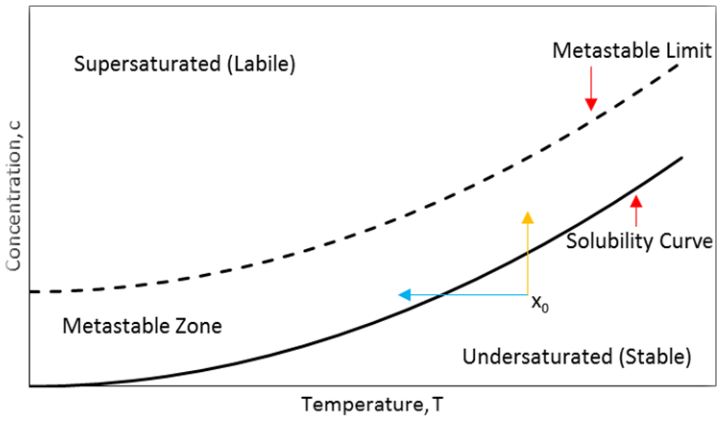

Figure 2.1 Phase diagram.

The most common way of expressing supersaturation (S) is shown in equation 2.1 as the difference in concentration. This expression is formulated under the assumption of ideal solution. The assumption of ideal solution allows for simpler, kinetic based, expressions of supersaturation. Otherwise the expression would depend on values of the activity coefficient and other thermodynamic parameters.[32]

$$S = \Delta c = c - c^* \qquad 2.2$$

In equation 2.1, c^* represents the solubility point or saturation concentration and c is the concentration in solution. Equation 2.3 shows the supersaturation expressed as a ratio where σ represents the relative supersaturation; as opposed to S the absolute supersaturation.

$$\sigma + 1 = \frac{c}{c^*} \qquad 2.4$$

Supersaturation, although the driving force in crystallization, does not guarantee crystallization. Supersaturated solutions exhibit a metastable zone. The metastable zone is a region between the solubility curve (saturation level) and supersaturation region where crystallization is not spontaneous (Figure 2.1). The width of this region depends on the

process conditions and the metastable zone limit which indicates the supersaturation level at which crystallization is spontaneous due to instability. In the metastable region, crystallization is governed by nucleation and growth mechanisms. Nucleation refers to the birth of new crystals. However, there is a free energy barrier that needs to be overcome for nuclei to be created. The energy barrier is overcome when nuclei reach a critical size. A size above which growth is favored over dissolving back into solution. As the supersaturation increases the energy barrier and cluster critical size decrease.[32] For this reason, supersaturation does not guarantee spontaneous crystallization, unless the supersaturation level is near the metastable zone limit. Near the metastable limit small crystals will begin to nucleate because of the reduced free energy barrier. In practice, however, the metastable limit is never closely approached as process conditions dictate the width of the metastable zone, and operating within the metastable zone (away from the metastable limit) makes it is easier to control crystalline properties.

2.2 Kinetic Process in Crystallization

Solution crystallization occurs in a two-step process that includes the initial phase separation, termed nucleation, and the growth of these nuclei, termed crystal growth. For either of these processes to occur the solution must be supersaturated. Once crystallization begins, both nucleation and crystal growth will commence, reducing supersaturation with the more significant of the two-determining size and shape characteristics.[32] In the metastable zone, the supersaturated solution can exist as a complete solution or as a crystal-liquid mixture (slurry). In this region, nucleation will not occur spontaneously; it must be induced by agitation or some other mechanical force.[33] At the metastable limit (i.e., very high supersaturation) nucleation will occur spontaneously. The region between the solubility curve and the metastable limit (metastable zone width) is governed by both nucleation and growth.[32] The metastable zone width becomes an important parameter and measurement in the design of particles of a desired shape and size.

2.2.1 Nucleation

Nucleation is often the more dominant of the rate process during crystallization. Nucleation may or may not be a spontaneous process. Because of the ambiguity of a nucleation event, nucleation has been studied in two separate mechanisms: primary and secondary nucleation (Table 2.1). Primary nucleation is categorized as either homogeneous or heterogeneous, and refers to nucleation in the absence of another crystalline surface. Secondary nucleation refers to nucleation induced by the presence of an already existing crystal.[32,33]

Table 2.1 Nucleation mechanisms

Primary Nucleation	***Secondary Nucleation***
Homogeneous – spontaneous	Induced by crystals
Heterogeneous – induced by foreign entity	

Homogeneous nucleation, although unpractical in industrial and research settings, has been the basis for many nucleation theories. One of these theories is classical nucleation theory (CNT). Classical nucleation assumes that the formation of a nucleus occurs by the molecular additions of two molecules until a critical cluster size is reached. Equation 2.5 depicts the addition of molecules (A) onto each other until the critical cluster size is reach (A_n). Following this theory, nucleation rates that consider a viscous energy term have been developed.[35]

$$A + A = A_2$$
$$A_2 + A = A_3$$
$$\ldots$$
$$A_{n-1} + A = A_n \ (critical\ cluster\ size) \qquad 2.6$$

Once this critical cluster size is reached, the addition of more molecules would cause phase separation, nucleation and later growth. This can be explained thermodynamically in terms of Gibbs free energy. Assuming the critical cluster is a sphere of radius r, the total change in free energy is equal to the sum of the change in free energy from the formation a nucleus (surface free energy) plus the change in free energy from the phase separation and transformation (volume free energy).

$$\Delta G = \Delta G_S + \Delta G_V = 4\pi r^2\gamma - \frac{4}{3}\pi r^3 \Delta G_v \qquad 2.7$$

In the above equation, γ is surface tension at the interface between the surface of the nucleus and the supersaturated solution and ΔG_v is the phase transformation change in free energy on a per unit volume basis.[32,33] The surface free energy term is positive due the increase in surface tension as the nucleus grows larger. The phase transformation term is negative because transformation decreases as the nucleus grows larger. Due to this relationship between surface and volume free energy, and the fact that the phase transformation term has a higher dependence on r, the total change in free energy has a maximum value. This maximum value corresponds to the critical cluster size (r_c) which is calculated by maximizing equation 2.5.

$$\frac{\mathrm{d}\Delta G}{dr} = 8\pi r\gamma - 4\pi r^2 \Delta G_v = 0 \qquad 2.8$$

$$\Delta G_{crit} = \frac{16\pi\gamma^3}{2(\Delta G_v)^2} = \frac{4\pi\gamma r_c^2}{3} \qquad 2.9$$

The rate of nucleation (B_{nuc}) derived from classical nucleation theory can now be describe by an Arrhenius equation of the form:

$$B_{nuc} = Aexp(-\frac{\Delta G_{crit}}{kT}) \qquad 2.10$$

where k is the Boltzmann constant and A is a pre-exponential factor. Using the Gibbs-Thompson equation describing growth of clusters, B_{nuc} can be expressed in terms of temperature, T; supersaturation, S; and surface tensions, γ.[32,33]

$$\ln\left(\frac{c}{c^*}\right) = \ln(S) = \frac{2\gamma v}{kTr} \qquad 2.11$$

$$G_{crit} = \frac{16\pi\gamma^3 v^2}{3\left(kTln(S)\right)^2} \qquad 2.12$$

$$B_{nuc} = Aexp\left(-\frac{16\pi\gamma^3 v^2}{3k^3T^3(\ln(S))^2}\right) \qquad 2.13$$

This nucleation rate developed by CNT increases indefinitely with increasing supersaturation. This is not observed in practice, and because of the difficulty to observe this in practice the equations derived from CNT will never completely describe real systems. Heterogeneous nucleation is more widely accepted as the principal form of primary nucleation. During crystallization, there almost always exist some form of impurity, foreign substance or surface where heterogeneous nucleation can take place.

Impurities lower the free energy barrier and allow nucleation to take place at lower supersaturation levels. Hence, why the metastable limit is rarely ever reached in practice.[32,33] One way of deriving nucleation rates experimentally is through induction time experiments. Induction time is defined as the time elapsed between the onset of supersaturation and the creation of an observable new phase.[32] Nucleation rate is proportional to the inverse of induction time.[34]

It is common practice in pharmaceutical crystallization to use secondary nucleation whenever possible. Secondary nucleation is nucleation caused by the presence of crystal surfaces in solution. When crystals are already present solution, whether by previous nucleation or crystal seeding, it lowers the supersaturation level while also lowering the free energy barrier for nucleation. In turn, nucleation occurs at a much lower supersaturation level than for homogeneous nucleation. Initial breeding or seeding is a commonly used technique because it allows for growth dominant crystallization processes.

Contact nucleation theory (Table 2.2) is believed to be the most common form of secondary nucleation in a crystallizer because of the various contact surfaces available in a crystallizer. Some forms of contact include: crystal-wall, crystal-stirrer, and crystal-crystal.[32,33] Supersaturation levels have the most significant impact on secondary nucleation as supersaturation allows nuclei to form around a parent crystal or another secondary nucleation mechanism. Secondary nucleation is also influenced by process conditions such as cooling rate, agitation rate, and impurities. Even factors such as crystal hardness and impeller material have an impact on secondary nucleation as they present different surface contacts that induce or reduce secondary nucleation.[32]

Table 2.2 Secondary nucleation theories

Originates from Parent Crystal	***Originates from Solute in Liquid Phase***
Initial (dust) breeding	Impurity concentration gradient
Needle/polycrystalline breeding	Fluid shear
Collision breeding	Local supersaturation
Contact nucleation	

Due to the lack of practicality from nucleation rates developed from CNT, and the fact that secondary nucleation is also influenced by hydrodynamic properties within the crystallizer and solution, more empirical nucleation rates were developed.

$$B_{nuc} = k_N \Delta C^n \quad (2.14)$$

$$B_{nuc} = k'_N W^i M_T^j \Delta C^n \quad (2.15)$$

Equations 2.11 and 2.12 are nucleation rates derived from the general power law function where k_N is the rate constant and ΔC the absolute supersaturation. Equation 2.12 includes the agitation rate (W) and suspension density (M_T) in take into account the hydrodynamics in the solution.[32,34] Both the constants and the exponents are determined by fitting the equations to experimental data. Experimental methods for determining these values include metastable zone width measurement, induction time experiments, and measuring the counts of nuclei.

2.2.2 Growth

When nuclei have surpassed the critical cluster size the growth process begins. Crystal growth is as important as nucleation rate in determining final product properties. Crystal growth rates can describe different phenomena; crystal face or characteristic length growth. A growth rate could be referring to a crystal face, which most likely has a different growth rate than other crystal faces. In general, of the growth of a crystal face can be explained by three processes: diffusion of solute molecules from the bulk solution to the crystal face, bulk transportation; solute molecules desolvate allowing other solute molecules to incorporate themselves at kink sites, surface integration; and latent heat of crystallization is exchanged in the system, heat transport. A kink site is a position on the crystal surface where solute molecules can easily detach and incorporate themselves onto the crystal lattice.[1] A growth rate could also describe the growth of a characteristic length of the crystal; e.g., a diameter for spherical crystals. Growth rates describing a crystal face are more appropriate for fundamental understanding as the processes describing crystal face growth have led to the development of many crystal growth theories. While growth rates describing a characteristic length and overall growth have more industrial relevance and practical application.[32] There have been numerous growth models developed to describe the crystal growth process (Table 2.3).

Table 2.3 Crystal growth theories

Surface energy theories	Shape of crystal is that of minimum free surface energy
Adsorption layer theories	2-D nucleus on crystal surface promotes growth layer by layer
Kinematic theories	Generation of growth steps and their movement across a crystal face in the presence of other growth steps
Diffusion reaction theories	Disposition of solute molecules on the surface of a crystal face governed by diffusion and the concentration gradient between the solid surface and bulk solution

The Burton-Cabrera-Frank (BCF) model is a combination of adsorption layer theories and kinematic theories. It has received attention due to its ability to better explain the relation between crystal growth and supersaturation. The idea behind the BCF model is that dislocations in the crystal structure could provide a step (a kink site) where growth could occur continuously. The BCF model was specifically based on screw dislocations that promote spiral growth (Figure 2.2). At these screw dislocations, the internal crystal structure is exposed to supersaturated solution. This exposure will promote the incorporation of solute molecules along the length of that step. The incorporation of solute molecules then causes the step to move in the direction of its outward normal. This process repeats itself forming a spiral. The spiral will continue to grow so long the solution remains supersaturated or the crystal meets a boundary.[1]

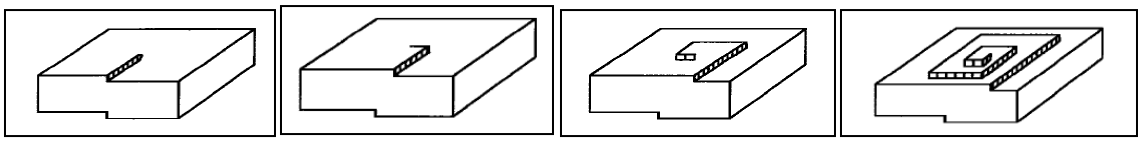

Figure 2.2 Spiral growth schematic. Adapted with permission from [1]. Copyright 2008 American Chemical Society.

The BCF model describes the dependence of crystal growth on supersaturation to be parabolic at low levels of supersaturation and linear as supersaturation increases. This relationship is observed experimentally. However, the limitation of the BCF model is that it was developed for crystal growth from evaporation where diffusion onto the crystal surface is dominant. While in crystal growth from solution, diffusion from bulk solution to the crystal surface-solution interface is believed to be more dominant. These diffusion

differences along with the differences in transport phenomena within a vapor and solution make the application of the BCF model for solution crystallization questionable.[32,33]

A second model derived from the BCF model, called the bulk diffusion model, attempts make up for the difference in diffusion between the vapor and solution crystallization. This model considers the boundary layer between solute molecules in solution and the crystal surface. Accounting for this boundary layer brings the model closer to actual practice where the boundary layer thickness can be affected by process conditions such as temperature and agitation rates. This boundary layer concept led to a more applicable model called the diffusion layer model.[32] The diffusion layer model considers the diffusion of solute molecules from the bulk solution, where the concentration of solute molecules is high; through crystal-solution interface, where the concentration of solute molecules is depleted due to crystal growth; and onto the crystal surface, where solute molecules are incorporated into the crystal structure.[32] The concentration gradient at the limit between the bulk solution and crystal-solution interface will always be present under supersaturation; providing a constant boundary layer. The rate of change of crystal mass can be expressed by a diffusion rate across the boundary layer:

$$\frac{dm_c}{dt} = k_d A(C_\infty - C_i) \tag{2.16}$$

$$k_d = D/\delta \tag{2.17}$$

In Equations 2.13 and 2.14, C_∞ is the bulk concentration, C_i is the concentration at the interface, A is the surface area of the crystal, D is the diffusion coefficient, and δ is the boundary layer thickness. The rate of solute integration into the crystal surface can then be expressed by:

$$\frac{dm_c}{dt} = k_i A(C_i - C)^i \tag{2.18}$$

Equations 2.13 and 2.15 are combined and expressed as:

$$\frac{dm_c}{dt} = K_G A \Delta C^g \tag{2.19}$$

$$\frac{1}{K_G} = \frac{1}{k_d} + \frac{1}{k_i} \tag{2.20}$$

The combination of equations 2.13 and 2.15 eliminates the concentration at the interface from the growth rate expression. Equation 2.16 is the most commonly used growth rate expressions in industrial practice. K_G is the overall mass transfer coefficient and ΔC is the supersaturation. The growth order g is usually between 1 and 2 and is determined from experimental data.[32]

Overall, crystal growth is a complex phenomenon and each of the above theories has limitations. Surface energy theories, although logical thermodynamically, fail to account for the effects supersaturation.[33] Adsorption layer theories fail at low levels of supersaturation due inaccurate surface energy relationships.[32] The one-dimensional growth rate expression, derived from the diffusion layer model, most commonly used is:

$$G = k_g \Delta C^g \qquad 2.21$$

Here k_g is temperature dependent and can be expressed as an Arrhenius equation. Many experimental methods exist to obtain data that can be fitted to the above equations. Some experiments include single crystal experiments grown at a constant supersaturation, fluidized bed and agitated vessel experiments where a known mass of crystal seeds is added to the solution, rotating disc method where boundary layer dynamics can be analyzed more closely, etc.[33]

2.2.3 Agglomeration and breakage

Nucleation and growth have a significant effect on crystal size and shape; however, in industrial crystallization, other mechanisms are also taking place. Agglomeration and breakage are two mechanisms that also greatly affect final product properties. Sometimes these additional mechanisms are beneficial while other times they ought to be avoided. Agglomeration can also occur at any point in the process (e.g., crystallization, drying, storage).[36]

Agglomeration occurs when two (or more) particles collide to form an aggregate. Interparticle growth and attractive forces between the particles then determine whether the aggregate disintegrates or agglomerates. Aggregates are loosely bonded particles resulting from the initial particle collision. While agglomerates refer to the more tightly packed particles that result from solid bridges or agglomerative bonds; agglomerates are not easily disintegrated.[36,37] Agglomeration mechanisms depend on process conditions, mainly

supersaturation and agitation rate, but also on the size of the particles in suspension. Smaller particles necessitate lesser forces to become agglomerates while larger particles require phenomena such as solid or liquid bridges to become agglomerates.[36] During the formation of an aggregate there is solution between the crystals that have collided, this is often referred to as a liquid bridge. The strength of the liquid bridge determines whether the crystals will adhere long enough for an agglomerative bond to form through intergrowth and cementation.[37]

Breakage can occur from continued collisions between particles. At high agitation rates, it becomes more difficult to form aggregates as the initial forces holding the particles together may not be able to withstand the shear forces in the fluid. Breakage is mainly influenced by agitation but can depend on suspension density as well. As the concentration of crystals in a suspension increases the aggregation process is more greatly influenced by breakage rather than agglomeration. For that reason, higher suspension concentrations and higher mixing intensities, tend to produce smaller particle sizes and less agglomeration.[36] At high suspension concentrations are particles usually smaller, aggregation forces are weaker, and supersaturation levels are lower. These factors all inhibit agglomeration especially under agitation. Agglomeration is predominant at high levels of supersaturation because colliding particles can bind more firmly as intergrowth and cementation are faster and stronger.[36,37]

Rates for agglomeration have been derived empirically throughout the literature. These empirical rate expressions encompass the both physical (e.g., particle size) and environmental (e.g., supersaturation and agitation rate) conditions affecting agglomeration and breakage. Initial aggregation and breakage rates where simply size dependent expressions that were proportional to the volume of particle:

$$K_{agr} = \beta_{agr}[L_i + L_j]^3 \qquad 2.22$$

$$K_{bre} = \beta_{bre}[L_i + L_j]^3 \qquad 2.23$$

In equations 2.19 and 2.20, K_{agr} and K_{bre} represent aggregation and breakage kernels. This kernels are used in population balance equations (PBEs) that describe various crystallization processes. β_{agr} and β_{bre} represent the aggregation and breakage rates, respectively. L_i and L_j are the sizes of the particles aggregating or breaking.[37] The breakage

term is also a function of the crystallizer conditions such as supersaturation and agitation. It can be expressed as:

$$K_{bre} = \beta_{bre}\epsilon^{r}S^{s}f(L_i, L_j) \quad 2.24$$

In this equation, S represents the supersaturation and ϵ is the energy dissipation in the tank which is indicative of the shear field produced from agitation. Considering the aggregation and breakage rates there will be a net agglomeration rate that can be expressed as:

$$K_{agg} = \beta_{agg}\epsilon^{p}S^{q}f(L_i, L_j) \quad 2.25$$

Equation 2.22 considers the effects of supersaturation and energy dissipation. In the equation, β_{agg} accounts for both aggregation and breakage. The powers in equations 2.21 and 2.22 (r, s, p, and q) can be fitted to experimental data.[37] The section refers to agglomeration and breakage on from a broadly scope. Agglomeration as it pertains to SC will be discussed in proceeding chapters.

2.2.4 Crystal morphology and polymorphism

The morphology, or shape, of a crystal is an important property of a crystal structure. It affects flow properties, filtration, bulk density, and other rheological properties.[32] The morphology of a crystal is a function of both internal structure (e.g., the internal symmetry of the crystal) and external conditions (e.g., growth rates, choice of solvent, impurities).[34] Shape factors for both volume and area are a mathematical way of describing the shape of crystal as a function of its characteristic length.[32]

Polymorphism is a molecule's ability to exhibit more than one crystal structure. Each polymorph has different physical properties; which could include different morphologies. The crystallization conditions will affect which polymorph(s) crystallize. Molecules that have different polymorphs present crystallization challenges. In many pharmaceutical crystallization cases, one polymorph is preferred over another. However, it can be difficult to control which polymorph crystallizes outs of solution or to identify which polymorph is present because one polymorph can also transform to another.[32] Transformation of one polymorph to another usually occurs at a specific transition temperature and can be characterized by changes in thermodynamic properties.[34] Control and understanding of

nucleation and growth mechanisms help produce the desired polymorph and subsequent morphology.

2.3 Crystallization techniques

Supersaturation is the key parameter in crystallization. For this reason, generation and control of supersaturation is the focus of most crystallization techniques. There are many different methods to generate and maintain supersaturation, but they all rely on the two properties that most significantly influence the level of supersaturation; concentration and temperature.

Cooling crystallization is a very common type of crystallization technique. For most compounds, solubility decreases with decreasing temperature. If solubility changes significantly with temperature, and the temperature range required to create a significant change is attainable, then cooling crystallization is a viable option. In such cases, cooling crystallization results in high product yield.[32,34] Cooling crystallization is carried out by preparing a saturated solution at given temperature and then cooling the solution until the system becomes supersaturated. Supersaturation then results in nucleation and growth of crystals. Controlling the cooling rate will control the rate at which supersaturation is generated. Cooling rate, or the rate of supersaturation generation, will also have a significant influence on the nucleation and growth processes.

Anti-solvent crystallization, also referred to as drowning-out, is a viable crystallization option when the solubility changes are negligible with significant changes in temperature, or when the necessary operating temperature range is unachievable. The anti-solvent method changes the saturation level of solution by adding a solvent mixture to the system. The solvent mixture should be miscible and significantly decrease the solubility of the solute in the system.[32] The solvent used for the mixture is often referred to as the anti-solvent or poor solvent. Controlling the rate of anti-solvent addition will control the rate at which supersaturation is generated. Anti-solvent addition rate will be the main parameter governing the nucleation and growth processes for this technique. Reverse anti-solvent crystallization also works by introducing a solvent mixture the system, but instead the solution is added to the anti-solvent. The reverse addition technique causes the system to

approach the metastable zone limit rapidly which in turn produces small crystals or amorphous solids.

Evaporation crystallization is also viable option when changes in solubility with respect to temperature are insignificant and/or a third miscible solvent is not available. This technique is especially useful for non-aqueous, high vapor pressure solvents. The saturation level increases by evaporating the solvent until the system finally becomes supersaturated. The process is typically run under vacuum and constant temperature to better control the evaporation rate.[32] The rate of evaporation will control the crystallization kinetics in this technique.

Crystallization can also be carried out through a chemical reaction. This is often referred to as reaction precipitation. In reaction precipitation, two soluble compounds are mixed in solution and react with each other. The resulting product from the reaction then has low solubility in the solution causing the solution to become supersaturated and crystallize or precipitate.[32] The key parameter controlling supersaturation in this case is the reaction rate. Reaction crystallization can be more difficult to control when compared to key parameters of other techniques because the reaction rate itself depends on many other parameters and reaction conditions.

In all crystallization techniques, the key is to maintain uniform supersaturation levels. This is done by ensuring proper mixing throughout the system. Local supersaturation can cause many problems including fines and wide particle size distributions (PSDs).

2.4 Operating modes

A crystallization process can be operated in either batch or continuous mode. Batch crystallization is a versatile, recipe based, mode of operation that can be adapted for specific product properties and can be used for different products. Batch crystallizers are also relatively inexpensive when compared to other methods of operation and are simple to use. Continuous operation allows for lower overall capital investment, more efficient production, easier scalability, and better waste or off-specification product management. Batch operation is difficult to scale up because the inherent science is unknown and operation occurs dynamically (unsteady state). Continuous operation, although easier to scale, makes the process design more difficult because of all the interplaying parameters.

However, continuous operation is primarily viable when production rates are very large (> 50 tons/day).[32]

2.4.1 Batch

Batch crystallization can be carried using out any of the techniques described previously or in combination with one or more techniques. Cooling crystallization carried out in batch is most common because of the ease with which the temperature of the crystallizer can be controlled. Anti-solvent crystallization in batch can be carried out alone or combined with cooling crystallization to create supersaturation and/or change the solubility of the solute. One downside to this method is the potential for local high supersaturation at the addition point of the anti-solvent. This can cause spontaneous nucleation which can have a major effect on the final CSD.[36] One common technique used in batch crystallization is seeded crystallization. Here crystal seeds are used to initiate the crystallization process. The seeds are usually crystalline material of the solute and help reduce spontaneous nucleation and control polymorphism and CSD.[36]

2.4.2 Continuous

For continuous crystallization, the two most common operation configurations are mixed suspension mixed product removal (MSMPR) crystallizer and plug flow crystallizer (PFC). The MSMPR is like the ideal continuous stirred tank reactor in that it assumes perfect mixing without spatial variations. Figure 2.3 shows the two-stage MSMPR used in this thesis work. The system employs a vacuum and nitrogen based transfer line to remove slurry from one vessel to the another. By using nitrogen, an inert gas, impurities are kept away from the slurry so to not affect the crystallization process. A control box is used to set the cycle time, vacuum buildup time, sampling time, pressure buildup time and purging times that control the rate of removal from each stage. The MSMPR system is versatile in that it can be constructed from vessels used in previous batch systems and employs the same mixing mechanism as a batch system. Several literature examples exists displaying the design and evaluation of the MSMPR for crystallization processes.[18,19,38-40]

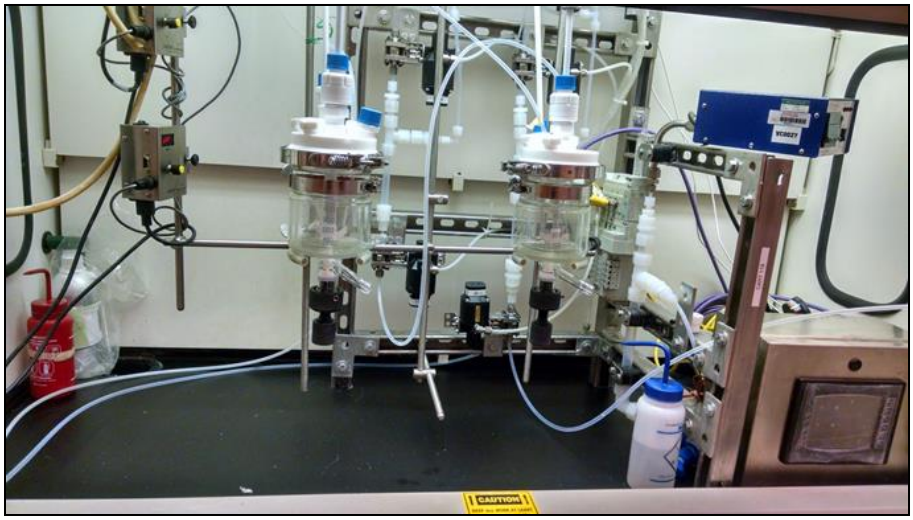

Figure 2.3 Two-stage mixed suspension mixed product removal (MSMPR).

The PFC is assumed to have plug flow behavior meaning that it has complete radial mixing and negligible axial mixing.[41] However, it is difficult to attained sufficient mixing to model a system as plug flow because that usually requires very high flow rates or very long reactors. Both of which are not common in industrial crystallization. Because of this, crystallizers have been design to induce this mixing through turbulent flows generated by process enhancements. One such crystallizer is the continuous oscillatory baffled crystallizer (COBC). The COBC has periodically spaced baffles along the length of the reactor and superimposed oscillatory motion on the fluid, at a set frequency and amplitude, which promotes the necessary radial and axial mixing for plug flow behavior to be achieved.[42,43]

2.5 Process analytical technologies (PAT)

Prior to 2004, process analytical technologies were not common in pharmaceutical development and manufacturing processes. The industry had become accustomed to predominantly batch processes and end-point laboratory testing to assess product quality. Given their familiarity with regulatory standards and fearing an increase in regulatory hurdles, the industry was hesitant to introduce any innovation into their development and manufacturing systems.[44] This widespread sentiment prompted the U.S. Food and Drug Administration (FDA) to issue its "Guidance for Industry: PAT – A Framework for

Innovative Pharmaceutical Development, Manufacturing, and Quality Assurance." The goal of the guidance was to encourage innovation and process understanding that would lead to more accurate and efficient processes with improved product quality by taking advantage of the significant advances in PAT tools. The guidance defined PAT as "a system for designing, analyzing, and controlling manufacturing through timely measurements (i.e., during processing) of critical quality and performance attributes of raw and in-process materials and processes, with the goal of ensuring final product quality." The tools can be categorized as: multivariate tools for design, data acquisition and analysis; process analyzers; process control tools; and continuous improvement and knowledge management tools.[20] Process analyzers have quickly become of interest in the pharmaceutical industry, especially for crystallization processes, due to the various measurement types and large volume of process information and insight produced by these tools.

Process analyzers are typically senor-based and can be categorized to have at-, on-, or in-line measurement. A measurement is considered: at-line when produced from a sample that is removed and isolated from the process, and analyzed in close proximity to the process stream; on-line when produced from a sample that is diverted from, and possibly returned to, the process stream; and in-line when produced from a sample that is not removed from the process stream through either invasive or noninvasive means.[20] By providing various measurement types, process analyzers allow for flexible implementation. The most insightful type of measurement is often a real-time in-line measurement because it requires no sample preparation and provides in process attributes. These features provide a method by which processes can be understood mechanistically and frequently assessed for rapid troubleshooting. Crystallization processes are a great beneficiary of real-time in-line process analyzers because its process parameters ultimately determine purity, morphology, polymorphic form, crystallinity, crystal size and size distribution, dissolution, bioavailability, and pharmacokinetics/pharmacodynamics (PK/PD).[0,46]

Examples of PAT implementation in crystallization processes are abundant throughout the literature.[17,21,47-49] However, there is a general lack of use of PAT tools in SC systems. Some of the most common PAT tools are used in this thesis and include the focused beam reflectance measurement (FBRM), particles vision microscopy (PVM), and attenuated

total reflectance (ATR)-UV/Vis. Other common tools include the ATR-FTIR, Raman spectroscopy, and NIR. These tools are used to monitor solute concentration. The proceeding sections will a detailed explanation of the PAT tools used in this thesis and their implementation.

2.5.1 Focused beam reflectance measurement (FBRM)

Particle size, morphology, and size distribution information are critical quality attributes of a crystallization process that effect other downstream processes and final product application. The ability to characterize these properties, particularly *in-situ*, can significantly aid in the design and optimization of a pharmaceutical manufacturing line. The FBRM is an *in-situ* laser reflectance technique that can be used in many crystallization applications including: solubility and metastable zone width determination[50], evaluation of seed effectiveness[51], identification of polymorphic transformations[52], effects of different impurity profiles[53], estimation of nucleation kinetics[54], particle size optimization[55], and process control.[56-58] The FBRM uses a solid state laser light source to produce a continuous beam of light that is highly focused on a spot near the surface of the probe's window. An electric motor then rotates the optics, allowing the focused beam of laser light to continuously scan over particles passing through the probe window. As the rotating laser crosses the path of a particle, light is backscattered to the probe where the reflectance is detected.[58] Given the known rotation speed of the optics (2 m/s), the duration of the reflectance determines the distance the beam has scanned on the particle's surface. This measured distance is known as the chord length and the resulting measurement of the system is a chord length distribution (CLD). An assumption in this measurement is the particle velocity is much smaller than the rotating laser velocity, relative to the probe window.[58,59] Figure 2.4 depicts the how the ParticleTrack with FBRM technology by Mettler Toledo works.

Many attempts and methods have been proposed to determine the CSD from the CLD.[61-65] Ultimately, the CLD is correlated but not the same as the CSD because the random motion and orientation of the particles in suspension does not guarantee measurement of the true characteristic length of a particle (e.g., diameter). However, the CLD is a function of particle concentration, size and shape and is highly sensitive to

changes in these properties. This sensitivity allows the FBRM to be used as a process analyzer that can provide a process signature[20] of the system dynamics for design and optimization. An advantage of the FBRM, over traditional offline laser diffraction techniques, is the measurement principle does not require assumptions regarding particle shape and the FBRM has much higher statistical robustness. A typical FBRM probe can also be exposed to a wide range of operating temperatures and pressures.[58] An important consideration when using the FBRM is the optical property of the material of interest as the measurement technique requires light backscattering.[66] Other considerations when using an FBRM include understanding the effects of stirring conditions, particle properties, particle concentration, laser beam spreading, and particle weighting.[58,59,67]

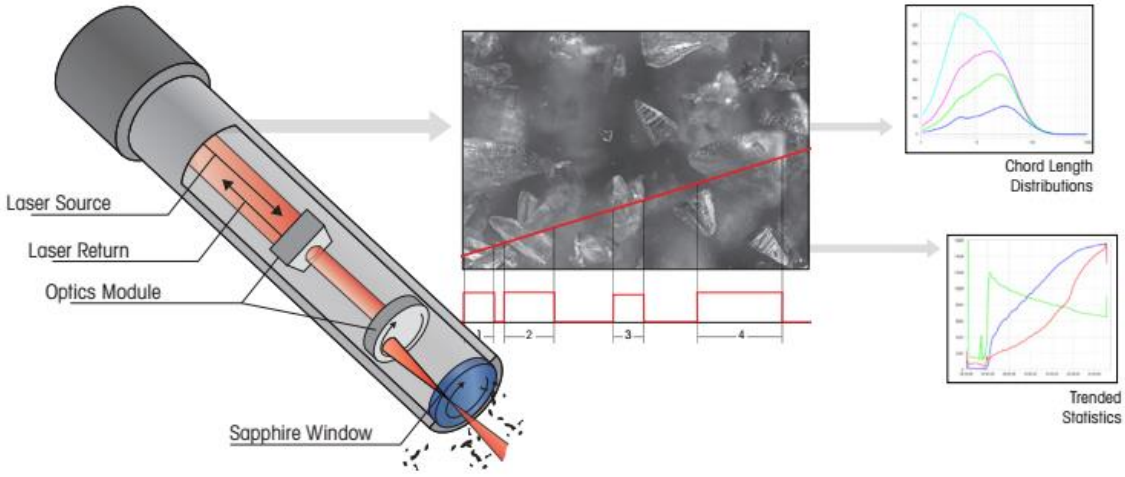

Figure 2.4 Schematic representation of the ParticleTrack (FBRM) by Mettler Toledo. Reprinted with permission from [60] Mettler Toledo.

2.5.2 Particle vision measurement (PVM)

Due to the relative data produced by the FBRM, i.e., chord length distribution as opposed to size distribution, it is often used in tandem with *in-situ* microscopy techniques. These techniques capture images of a process which aid in interpreting data from other process analyzers like the FBRM. *In-situ* microscopy has origins in the early 1990s where it was commonly used to observe bioprocess (e.g., yeast cells in brewery tanks).[68] These techniques can be characterized into two categories: incident light microscopes and transmitted light microscopes.[69] Today there are numerous examples in the literature of

crystallization monitoring via *in-situ* microscopy techniques, in particular the use of PVM in combination with FBRM.[17,21,44,46,50,52,54] Applications include process understanding, polymorph transformation, agglomeration, and breakage.[70,71] The PVM is a probe-based instrument that produces high resolution images of particles and their interactions in suspension, in real-time. Allowing the in the visualization of process mechanisms without process sampling. The latest version Mettler Toledo's ParticleView V19, which is used in this thesis consists of four front lasers and four back lasers. The lasers serve as light sources with the front lasers focused on the field of view to provide backscatter from particles and the back lasers are focused beyond the field of view to provide trans-illumination lighting. The high resolution (>2 µm) images produced by the PVM provide size and shape characteristics of the particles (or droplets[72]) in suspension. Like the FBRM, the PVM can operate under a board range of operating temperatures and pressures. The high frequency of high quality images the PVM can capture also provides the statistical robustness necessary for image analysis techniques.[21] Figure 2.5 depicts the how the ParticleView with PVM by Mettler Toledo works.

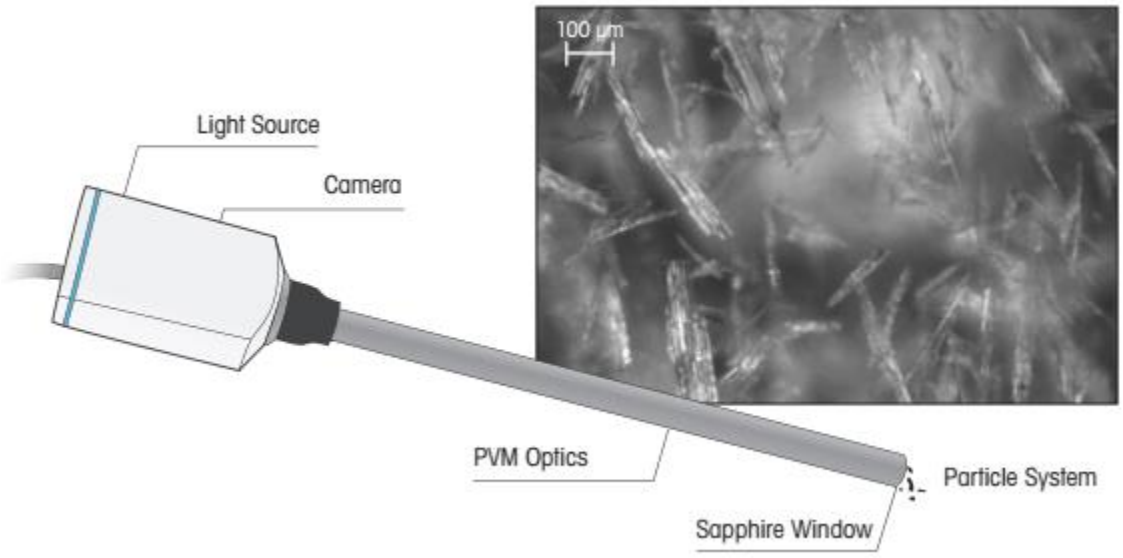

Figure 2.5 Schematic of the ParticleView (PVM) by Mettler Toledo. Reprinted with permission from [73] Mettler Toledo.

2.5.3 UV-Vis Spectroscopy

UV-Vis spectroscopy is a simple, versatile, quick and accurate technique that measures photon absorption in the ultra-violet (UV) (200-400 nm) and visible (Vis) (400-800 nm) ranges of the electromagnetic spectrum. The instrument measures the discrete transition from one electronic state to another upon light radiation. The measurement (absorbance) is correlated with the molecular structure and geometry of a compound.[74] Hence, the technique is often utilized to measure solute concentration in solution. The absorbance is related to solute concentration in solution via Bouguer-Lambert-Beer law:

$$A = \varepsilon C l \qquad 2.26$$

where ε is the molar absorption (extinction) coefficient, C is the concentration of the absorbing species, and l is the length of the radiation path through the sample.[75]

Given its versatility, *in-situ* UV-Vis spectroscopy has been widely employed to monitor solution concentration and implement control schemes for crystallization processes.[9,76-78] However, for optimal use of such spectroscopy the solvent of choice, material properties (e.g., refractive index), and process conditions (e.g., solids concentration) must be considered. Some solvents can have different wavelength cutoffs than necessary for a specific compound while other solvents can cause band broadening making identification and monitoring more difficult and less sensitive.[75] In cases where compounds have overlapping bands (peaks) or weak resolution, the derivative of the absorbance can be used for more precise identification of the solute molecule of interest.[74]

2.6 Principal component analysis (PCA)

Per the definition of PAT, designing, analyzing and/or controlling a process are key applications for PAT tools. Some of the common process analyzers aid in gaining process understanding via real-time, *in-situ* process measurements. Modeling via PBEs can allow for better experimental design, process understanding and reduced experiments. Combining PBMs with an optimization framework can provide optimal process conditions to achieve desired final product properties. However, none of these techniques provide a method by which process data can be easily analyzed and interpreted. In fact, in the case of process analyzers, many times the process data can become even more complex and

multivariate with less conclusive trends to help identify key process signatures. Principal component analysis (PCA) forms the basis for multivariate data analysis, and approximates a data set via a reduction in the data matrix. PCA has many different applications from data simplification and reduction to variable selection, classification and outlier detection to modeling and predicting.[79] Examples of PCA applications in crystallization include simplification and calibration of spectroscopy data (e.g., UV/Vis, FTIR, Raman), image analysis, solvent selection, process monitoring, prediction, and control.[10,17,74,80-82]

A data matrix X is composed of N rows representing objects and K columns representing variables. By selecting the appropriate objects and variables, the data matrix X of K-dimensional space can be well modeled or explained by a submatrix on an A-dimensional subspace. The reduction into a lower-dimensional subspace is done by projecting the X into vectors t and p' which compose the columns of matrix T and the rows of matrix P', respectively.[79] The number of rows of P' and columns of T correspond to the number of principal components used to reduce X. The PCA model for X then becomes:

$$X = 1\bar{x} + TP' + E \qquad 2.27$$

E represents the matrix of deviations or residuals between the projections (TP') and the original data X. The residuals contain the unexplained variance within the data set. $\bar{x}$ is the mean vector and is used to mean center and scale the original data to ensure that all variables are weighted equally by the statistical model; avoiding any bias due to differences in magnitude. Other matrix transformations can be applied to smooth or centralize the data. Vectors are t_i known as score vectors and explain the correlation or dominant patterns between objects while the vectors p_i are known as loadings and contain the dominant variable patterns of the data set. Score plots, i.e., plots of score vectors against each other (e.g., t_1 vs t_2), can help identify clusters or classes between the objects.[79] Score plots can be superimposed with loading plots to provide information about the relationship with classes of objects and classes of variables. Scores and loadings correspond to the eigenvalues containing the most information. The larger the eigenvalue of a principal component the more information the component contains about the original data set. The rule of thumb is principal components with eigenvalues larger than one have significant

capability in describing the original data set. Principal components with eigenvalues less than one are mainly comprised of the noise in the data. The evaluation of eigenvalues is a mathematical technique, where the eigenvectors of large eigenvalues represent the directions of maximum variance and hence the most amount of information. If the data exhibits high levels of similarity, a fewer number of principal components is required to approximate the data set.[79]

2.7 Crystallization modeling

Polymorphism, crystal morphology, and CSD are crystal product properties that are a direct result of the crystallization process and its operating conditions. The CSD inside a crystallizer affects the consumption of supersaturation, which in turn influences nucleation and growth rates, morphology, operation stability, and many other product and process properties.[34] Prediction, monitoring and control of the CSD is essential in understanding the crystallization process and producing particles of high quality. The most widely applied method of understanding and modeling the interactions between CSD and process and product properties is the use of PBEs first introduce by Randolph & Larson (1988).[83]

The population balance essentially requires a number balance be satisfied in the crystallization process. The equations for the population balance are therefore expressed in terms of number distributions. The population balance can then be expressed in a similar manner as the energy and mass balances:

$$Accumulation = Input - Output + Net\ Generation \qquad 2.28$$

If the $Net\ Generation$ of particles is taken to be $(B - D)dL$, where B and D are the birth and death functions, respectively, and the region of interest is said to move convectively with the particles so that there is no $Input$ or $Output$. The total population can be described as:

$$\frac{d}{dt}\int n\ dL = \int (B - D)\ dL \qquad 2.29$$

Using various mathematical techniques, the above can simplified and written as:

$$\frac{\partial n}{\partial t} + \nabla * (\boldsymbol{v}n) - B + D = 0 \qquad 2.30$$

Here $\boldsymbol{v}$ refers to the rate of change of the set of external and internal coordinates.[34,83] The internal coordinate can be taken to be crystal size (L) or any other internal property of interest, and the external coordinate can be taken to be the crystallizer length (x). Considering a steady state case with negligible birth and death, equation 2.25 can be rewritten as:

$$\frac{\partial}{\partial x}(v_x n) = -\frac{\partial}{\partial L}\left(\frac{\partial L}{\partial t} n\right) = -\frac{\partial}{\partial L}(Gn) \qquad 2.31$$

where G is the linear growth rate equal to $\partial L/\partial t$. Equation 2.27 describes the PSD along both the spatial and size coordinates. In practice, the spatial distribution is insignificant as most applications are implemented under ideal conditions. Therefore, equation 2.26 and 2.27 are usually averaged over the external coordinate so to describe a more specific region of the system.[83] This concept is applied to both batch and continuous MSMPR crystallizers. For a batch case that assumes perfect mixing, negligible agglomeration/breakage, and size independent growth, the PBE can be expressed as:

$$\frac{\partial n}{\partial t} + G\frac{\partial n}{\partial L} = 0 \qquad 2.32$$

For a continuous MSMPR with the same assumptions and if there are no crystals in the inlet stream, the population equation balance can be expressed as:

$$\frac{\partial n}{\partial t} + G\frac{\partial n}{\partial L} + \frac{n}{\tau} = 0 \qquad 2.33$$

where $\tau = V/Q$, V is the operating volume of crystallizer and Q is the inlet and outlet flow rate. The residence time (τ) becomes an important parameter controlling or affecting the final crystal properties. For a continuous MSMPR operating under steady state conditions equation 2.29 simplifies to:

$$G\frac{\partial n}{\partial L} + \frac{n}{\tau} = 0 \qquad 2.34$$

This equation can be integrated to solve for the CSD with the appropriate boundary conditions.[34,41,83]

$$Initial\ Condition: n(0, L) = n(L) = n_0 \qquad 2.35$$

$$Boundary\ Condition: n(t, 0) = B_{nuc} \qquad 2.36$$

The given equations that represent batch and continuous MSMPR crystallization can now be coupled with various definitions for nucleation and growth rates, as well as with the respective mass balances. Numerous solution methods exist to solve the PBM for a crystallization system. Two of the most common and efficient solution methods are the method of moments (MOM) and the QMOM. The two methods will be discussed in the proceeding sections with QMOM used as the method of choice throughout thesis work.

2.7.1 Method of moments (MOM)

Solving the various forms of equation 2.25 permits the calculation of the CSD and other crystal properties. The PBE also serve as a tool for modeling and understanding the different mechanisms occurring during crystallization. Because a crystallization does not produce monodispersed crystals, information about the crystal size distribution is usually expressed as an average. The most common method of solving PBEs is by using a moment transformation. The moment of a distribution is expressed as:

$$\mu_k = \int_0^\infty L^k n \, dL \qquad 2.37$$

The different moments of the distribution are representative of different physical properties. The zeroth moment represents the number of crystals; the first represents the sum of the characteristic lengths of the all crystals in the distribution; the ratio of the first and zeroth moment represents the mean size of the crystals; the third moment multiplied by crystal density represents the total concentration of crystals in the slurry.[83] Substituting equation 2.33 into equation 2.28 yields:

$$\frac{d\mu_k}{dt} + kG\mu_{k-1} = 0 \qquad 2.38$$

Equation 2.34 is consistent since $k = 0$ represents the zeroth moment, or total particles, and would not be affected by growth.

Moment transformation of the PBE converts the system of equations into a set of ordinary differential equations (ODEs) that describe the evolution of the moments of a distribution and can be relatively simple to solve; often having analytical solutions. As opposed to the original partial differential equation (PDE), which is computationally cumbersome to solve. However, it requires the set of ODEs to be in the closed form; meaning the moments are to be described only as a function of themselves. The closure

condition becomes very restricted and limits the types of growth functions and agglomeration kernels implemented.[84,85] For example, the necessary and sufficient condition for closure of a growth-only crystallization process is:

$$G(L) = a + bL \qquad 2.39$$

where a and b are independent of the crystal size, L. The case of $b = 0$, is the well-studied size independent growth scenario (equation 2.28).[34,83] Fortunately, in practice this growth rate condition is relevant, given that crystallization properties are usually examined as an average of the distribution and not on an individual basis.

2.7.2 Quadrature method of moments (QMOM)

The QMOM technique is much like MOM, except QMOM can handle a much broader range of growth functions and agglomeration kernels. QMOM replaces the closure requirement that restricts MOM by approximating the closure condition. The technique uses the summation of abscissas (L_i) and weights (w_i) to approximate and completely specify the low-order moments of the unknown distribution, $n(L)$. The MOM technique is not able to accurately specify the low-order moments unless the equations meet the closure condition or some other type of simplification is made.[85] Moreover, the QMOM approximation becomes completely independent of the growth function and agglomeration kernel.[84]

$$\mu_k = \int L^k n(L) dL = \sum_{i=1}^{N} L_i^k w_i \qquad k = 0, \dots, 2N-1 \qquad 2.40$$

Equation 2.36 is the quadrature approximation of the moments for N quadrature points. Substituting equation 2.36 into equation 2.28 yields:

$$\frac{d\mu_k}{dt} + kG \sum_{i=1}^{N} L_i^{k-1} w_i = 0 \qquad k = 0, \dots, 2N-1 \qquad 2.41$$

The number of quadrature points used determines the number of nodes used to approximate the integral, i.e., the distribution. N also determines the moments whose evolutions are being tracked and used to solve the weights and abscissas, i.e., the first $2N$ moments determine the first N weights and abscissas.

The most efficient and commonly used technique to solve for the weight and abscissas is the Product Difference (PD) algorithm.[86] The PD algorithm minimizes the error committed by replacing terms in the PBM with their quadrature approximation. The

algorithm works by using the moment sequence (N moments) to construct a tridiagonal Jacobian matrix (of rank $N/2$) whose eigenvalues and eigenvectors correspond to ($N/2$) weights and abscissas.[84,85] Although the QMOM procedure does not directly provide the CSD, the abscissas are related to the particle class sizes and the weights are related to the volume fraction in the respective class size. In general, increasing the number of quadrature points (or nodes) decreases the error of the approximation. However, $N = 3$, has been found to be the best tradeoff between accuracy and the size of the problem.[84,85,87,88] A more complex and detailed example of the use of the QMOM technique will be discussed in the proceeding sections.

2.8 Optimization

Optimization of a process can be examined from both a physical sense, i.e., running experiments and adjusting process parameters to achieve improved results, and a mathematical sense, i.e., developing a model that accurately predicts the process and then optimizing the input variables so to achieve desired final properties. In the mathematical sense, optimization of a crystallization process requires the kinetic information discussed in Section 2.2, a PBM that considers the relevant process mechanisms and an efficient solution method to accurately predict the process as discussed in Section 2.6. The PAT tools discussed in Section 2.4 can also provide insight that can be used to improve models and ultimately lead to better optimization results. Optimization of crystallization properties like shape, size, yield, and purity via optimal heating/cooling profiles, anti-solvent addition profiles, and addition location(s) has been well studied in the literature.[7,14,15,18,51] Although well studied, optimization of a crystallization system can be a very complex problem depending on the mechanisms incorporated in the PBM and the solution method chosen. Even when expressed in terms of moments, the optimization problem would represent the minimization of a nonlinear system. Nonlinear systems can have several local minima and finding the global minima is not easily achievable. Several approaches exist to handle these cases.[89]

A typical optimization problem for crystallization is the maximization of the mean crystal size. The manipulative variable is either the temperature or anti-solvent addition profile for a cooling process or anti-solvent process, respectively. For batch process, the

batch time can either be fixed or a manipulative variable as well; the equivalent for continuous processes would be the residence time. Fixing the batch or residence time significantly reduces the computationally burden of the optimization problem and is common practice. The optimization formulation for the maximization of mean crystal size via temperature profile of a batch process can be expressed as:

$$\min_{x(k)}(-\mathcal{L}_{10,end}) \tag{2.42}$$

subject to:

$$T_{min} \leq T(t) \leq T_{max} \tag{2.43}$$

$$r_{min} \leq \frac{dT}{dt} \leq r_{max} \tag{2.44}$$

$$C(t_{end}) \leq C_{max}(t_{end}) \tag{2.45}$$

x represents the vector of the variable to be optimized. It contains k elements which is the number of discretization of the variable representing the number of stages the variable is divided into to describe the process.[90] Each optimization problem has its own optimal level of discretization for the manipulative variables. Significantly below this optimal *k* value the optimal solution may be inaccurate and significantly above this optimal *k* can make convergence infeasible. The objective function is $-\mathcal{L}_{10,end}$ and represents the moment based final number mean diameter.[91] It is expressed as the ratio of the first and zero moment:

$$-\mathcal{L}_{10,end} = \frac{\mu_{1,end}}{\mu_{0,end}} \tag{2.46}$$

Optimization problems are subject to constraints the allow the optimal variable to be achievable in a practical application. Otherwise the unconstraint optimal solution is likely either infeasible or unrealistic in application. In this example case, there are three constraints on temperature, heating/cooling rate, and yield. T_{min}, T_{max} represent the lower and upper bounds for the temperature. r_{min}, r_{max} represent the lower and upper bounds for heating/cooling rates. $C(t_{end})$ represents the concentration in solution at the end of the batch process and $C_{max}(t_{end})$ represent the maximum allowable concentration at the end of the batch experiment.

2.8.1 Multi-objective optimization (MOO) framework

A multi-objective optimization (MOO) framework arises from the desire to achieve multiple, many times conflicting, objectives. A typical conflict of interest is to increase the crystal mean size ($\mathcal{L}_{10,end}$) while decreases the aspect ratio (AR) of crystals. Larger crystals with smaller aspect ratios have improved processing properties. It has been shown that an MOO framework for increasing the mean size while simultaneously decreasing the aspect ratio can be implement for a batch cooling crystallization.[7] Another practical example is to minimize the coefficient of variation of the distribution, minimize the nucleation and maximize growth. Broad distributions are lead to downstream processing difficulties, specifically they prevent uniform dosing of pharmaceuticals. A MOO framework has proven to be more effective than a single objective in reducing fines leading to increased growth and a narrower distribution.[92] An example of a multi-objective optimization (MOO) framework for the case of maximizing crystal mean size while decreasing aspect ratio is formulated as follows:

$$\min_{x(k)}(-\mathcal{L}_{10,end} \mid AR) \tag{2.47}$$

subject to equations 2.39, 2.40, and 2.41. Equation 2.43 can be rewritten as:

$$\min_{x(k)}(-w_1\mathcal{L}_{10,end} + w_2\, AR) \tag{2.48}$$

where w_1 and w_2 represent the weighting of each objective. By varying the weightings, a set of solutions can be obtained, depicting the tradeoff between the objectives. This is known as the Pareto optimality and plotting set of optimal solutions is known as the Pareto optimality. Along the Pareto frontier, a move from a single point along the curve results in a favorable reduction in one objective and an undesirable increase in the other objective.[93]

Numerous optimization algorithms exist to implement desired optimization schemes. There are ideal algorithms for linear, quadratic and nonlinear problems. However, discussions of these algorithms are outside the scope of this thesis work. For details of various optimization algorithms, the readers are referred to *Numerical Optimization* by Nocedal & Wright (2006).[94] The interior point algorithm is employed in the proceeding sections and is described by Nocedal & Wright (2006) and Byrd et al. (1999). [94,95]

2.9 Process intensification (PI)

PI is the combination of innovative processing techniques and technologies to improve overall process efficiency, increase yield of desire final product, and produce final product of desired properties. While there exist many definitions for PI, generally it includes: increasing productivity and selectivity through multi-scale designs and intelligent intensification of unit operations, designing novel equipment based on scientific process knowledge (e.g., multi-functional reactors, microtechnology), and the development and implementation of multi-scale modeling frameworks to appropriately predict, design and control processes. The aim of PI is to advantageously increase or decrease process complexity allowing for the elimination of large, cumbersome, costly, and energy-intensive processes; replacing them with smaller, less-expensive, and more efficient ones. The smaller operation decreases the operational footprint resulting in greener, safer processes (due waste and exposure minimization), and improved control and automation.[96,97] PI via hybridization of unit operations (or multi-functional equipment) reduces the overall number of unit operations; leading to reduced capital and energy costs. By increasing overall yield, the consumption and waste of raw materials is also reduced, further adding to savings in operational costs. In the pharmaceutical indsutry, the increased savings can be used to further drug discovery, research and development. Microscale technology offers improved mixing dynamics resulting in reduced maldistribution or local hotspots in a process, increase heat transfer, and an improved the design space (offers operating conditions unattainable in convential equipment).[96,97] In crystallization, improved mixing leads to improve yield and improved uniformity throughout the product properties.

To date, PI has been mostly exploited in reaction chemistry. Examples include: the heat exchanger (HEX) reactor shown to decrease process time and byproduct formation, the in-line monolithic reactor shown to decrease equipment size by two orders of magnitude, spinning disk reactor shown to 90%+ reduction in process time, inventory and impurity levels, and the reactive distillation which uses the heat of reaction to vaporize reaction products resulting in the distillation of the products (separation).[98-101] Figure 2.6 shows a methyl acetate process that was reduced from 28 unit operations to 3, a prime example of PI.

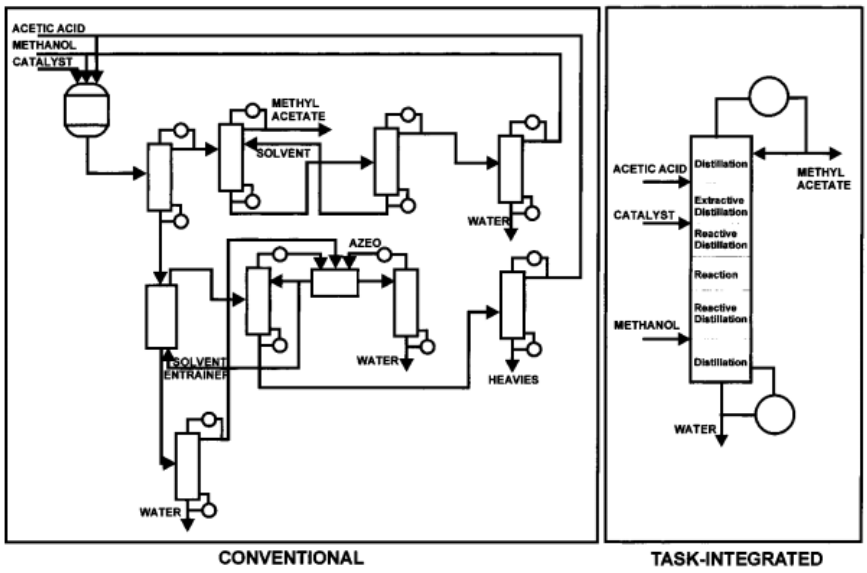

Figure 2.6 PI of Eastman Chemical methyl acetate plant: (left) conventional process, (right) intensified process. Reprinted with permission from [96]. Copyright 2002 American Chemical Society.

Early adoption of PI was not widespread because of a number of barriers, particularly in the pharmaceutical industry. Barriers to PI included: industrial growth strategies that focus on mergers and acquisitions rather than innovation, an R&D focus on new products as opposed to new manufacturing methods, fear of being first and waiting for innovation to pass regulation before attempting implementation, lack of familiarity and exposure to such techniques, lack of standardized lab-scale PI equipment, lack of modeling capability and concerns over scale-up.[96] However, in the last five years, examples of end-to-end integrated continuous manufacturing of pharmaceuticals have been presented with integration of drug synthesis, purification (e.g., crystallization, extraction), filtration, formulation, automation and control.[102-105]

Many of the PI techniques implemented in pharmaceutical processes have been driven by innovation in the technology (i.e., in equipment), specifically the emergence of microtechnology for use in reaction applications. Very few PI techniques in the pharmaceutical industry have revolved around innovation in the processing technique. Moreover, there is a need to address the integration of upstream and downstream processes. Spherical crystallization has a long history as a size enlargement technique for particulate processes, and has the potential to be the key processing technique to integrate and intensify

drug substance and drug product. The remaining chapters of this thesis will focus on SC and its application as a PI technique.

2.10 Conclusions of the literature review

The discussion presented in this chapter covered crystallization fundamentals, techniques, modes of operation, as well as PAT and modeling to provide the sufficient background necessary to comprehend the proceeding chapters. Various modes of operation for SC processes are implemented in the following chapters to assess their PI capabilities. Each mode of operation incorporates PAT tools for process monitoring and understanding. A PBM designed to track both constituent and agglomerate properties for superior process development will also be presented. The coupling of downstream continuous unit operations with a continuous crystallization process is also discussed to complete the overall PI theme.

3. A REVIEW OF SPHERICAL CRYSTALLIZATION

3.1 Introduction

Spherical crystallization originates from SA techniques used in the 1960's to preferentially agglomerate and recover common commodity materials. Early examples include the agglomeration of barium sulfate[106], calcium carbonate[107], graphite[107,108], coal[31] and sand.[109] In these early applications, the process was an agglomeration in suspension technique. The key was to identify suitable agglomeration agents, called the bridging liquid or binder, to agglomerate suspended particles. In the early 1980's, SA expanded into pharmaceutical applications where simultaneous precipitation (via crystallization) and agglomeration became of interest, and the term SC was adopted.[22,30] Spherical crystallization is a particle size enlargement technique designed to improve processing properties (flowability, compressibility) while maintaining or improving micromeritic properties (size, size distribution, dissolution rate).[110] The technique is of interest in the pharmaceutical industry because of the frequently undesired functional properties of APIs. Moreover, in conventional pharmaceutical operations, designing particles of enhanced micromeritic and functional properties would require multiple unit operations (e.g., milling, granulation). However, with SC those additional downstream unit operations can be eliminated while other operations (i.e., filtration, washing, drying) become more efficient.[111,112]

Spherically crystallized particles of salicylic acid were first studied by Kawashima et al.[22,113] and reported improved properties including particle size, angle of repose, compressibility, and tablet hardness. Since then many other compounds have exhibited improved physio-mechanical properties from SC over conventional crystallization including the following APIs: tolbutamide[114], bucillamine[115], aceclofenac[116], cefotaxime sodium[117], carbamazepine[118], and ibuprofen.[119] The improvement in the compression properties is believed to come from the higher tensile strength of compressed agglomerated crystals. Agglomerates are composed of numerous small crystals of very high surface area to volume ratios. This internal structure, along with their sphericity, increases the number of contact points of spherical agglomerates and enhances inter-particle bonding upon compression; leading to increased strength.[119,120] Due to the nature of their internal

structure, spherical agglomerates can also have desirable biopharmaceutical characteristics. Spherical agglomerates of fine crystals have exhibited significantly improve dissolution rates for some APIs.[116,121,122] Bioavailability and dissolution are properties largely dependent on particle size. The size of the agglomerated crystals and the porosity of the agglomerates can allow for improved dissolution rates.

3.2 Spherical crystallization methods

Spherical crystallization can be achieved in five different ways: spherical agglomeration (SA), quasi-emulsion solvent diffusion (QESD), ammonia diffusion (AD), crystallo-co-agglomeration (CCA), and neutralization technique (NT).[23,123] SA depends on the miscibility of the solvents in the system and solubility of the solute. This technique typically employs three solvents: a (good) solvent to dissolve the solute; an anti-solvent, miscible with the solvent, to precipitate the solute; and a bridging liquid, of high affinity for the solute and immiscible with anti-solvent (and solvent system), to preferentially wet the solute crystals.[23,123] There are instances in which the solvent itself promotes agglomeration and behaves as the bridging liquid, in which only two solvents are necessary.[119,123] QESD requires two solvents. The solute is dissolved in the solvent and added to the anti-solvent. Emulsion droplets then form if the affinity between the solute and solvent is much greater than the affinity between the solvent and anti-solvent. The emulsion formation is followed by counter-diffusion where concentration gradients cause the solvent diffuses out of the droplets into the anti-solvent and vice versa. Counter-diffusion reduces the solubility of the solute in the droplet inducing supersaturation and crystallization. Residual solvent within the droplet serves as the bridging liquid, promoting agglomeration and maintaining sphericity.[125,126] AD uses a system of three partially immiscible with ammonia-water as the solvent and bridging liquid, an organic solvent as the anti-solvent, and a hydrocarbon to promote immiscibility and agglomeration. The immiscibility of the solvents creates emulsions which then follow a process like QESD and two-solvent SA. This technique is typically used with amphoteric drugs.[23,123,127] CCA is the crystallization and agglomeration of a solute (drug) with another solute (drug or excipient) using a bridging liquid. The second solute may remain in solution, particularly in the case of excipients. The technique is very useful for poorly compressible materials as

the inclusion of excipients can improve compressibility. However, given that the physio-chemical properties of drugs and excipients differ drastically, and the selection of an appropriate solvent system is often very challenging.[23,128] For simplicity, the CCA method maybe be referred to as co-agglomeration. Lastly, with NT, crystal formation is induced neutralization of a basic solution containing dissolved acid and subsequent agglomeration is caused by the addition of a bridging liquid.[23,123,129] QESD and SA are the most common applications of SC and their mechanisms are illustrated in Figure 3.1.

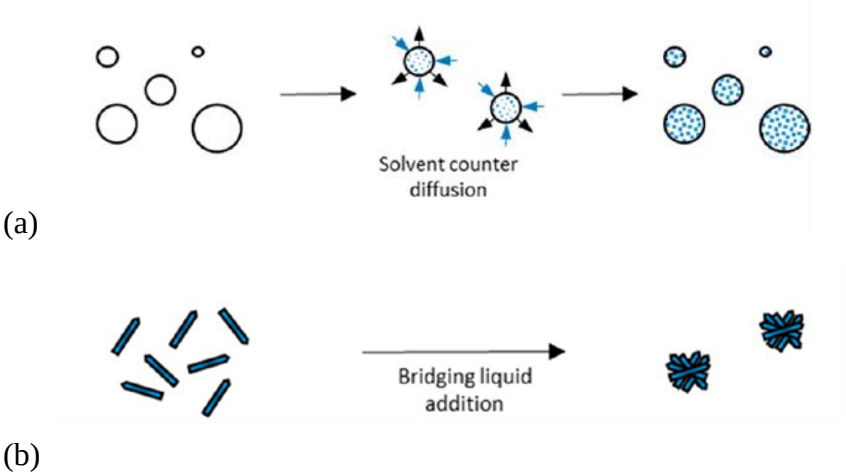

Figure 3.1 Schematic diagrams showing: (a) QESD and (b) SA. Adapted with permission from [130] Copy Right 2015 American Chemical Society.

While SC offers many benefits from product quality to PI, it also increases process complexity which may be disadvantageous or too difficult to design due to lack of fundamental understanding. One of the most common challenges in designing a SC process is the selection of the appropriate solvent system for both crystallization and agglomeration, particularly finding a suitable bridging liquid.[131] APIs with polymorphs pose an even bigger challenge to selectively precipitate and agglomerate the desired form without transformation.[131,133] Moreover, SC is only attainable under a certain range of operating conditions which can require an extensive amount of experiments to identify.[23] The proceeding sections will explore SA, discussing the process parameters which influence final product properties, agglomeration mechanisms, differences in operating modes and modeling of the process.

3.3 Spherical crystallization via SA

SA can consist of simultaneous crystallization and agglomeration or the agglomeration in suspension of fine crystals to produce spherical agglomerates. For SA applications, crystallization is usually carried out through an anti-solvent method, sometimes referred to as “drowning-out”, “salting-out” or “solvent change.” Anti-solvent crystallization methods involve the addition of a miscible anti-solvent to a solution (solute dissolved in solvent) which reduces the solubility of the solute and induces crystallization. When fine crystals are desired or a very low solution to anti-solvent ratios (SASR), a reverse addition technique is used where the solution is added to the anti-solvent which causes “crashing-out” or “oiling out” to produce fine crystals. Reverse addition is commonly used for SA processes, since agglomerates of fine crystals possess advantageous functional and biopharmaceutical properties. However, the high degree of supersaturation generated by this approach can also form emulsions and cause some agglomeration. In such cases, the agglomeration caused by crystallization often goes unnoticed because of the agglomeration caused by the bridging liquid.

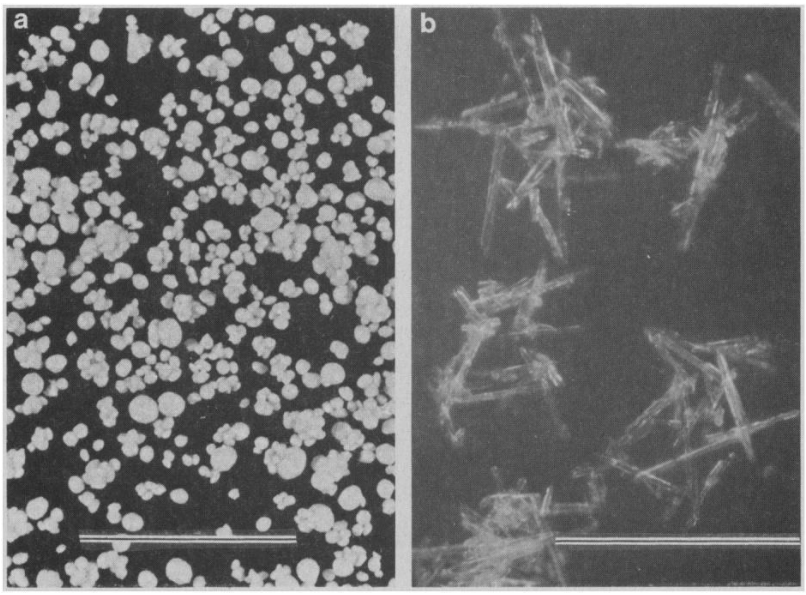

Figure 3.2 Salicylic acid particles (left) spherically agglomerated (scale bar = 10mm), (right) crystals via conventional crystallization (scale bar = 200μm). Reprinted with permission from [22]. Copyright 1982 The American Association of the Advancement of Science.

In cases with simultaneous crystallization and agglomeration, the bridging liquid is present at the onset in either the solution or anti-solvent, typically in the solution. Due to the immiscibility of the bridging liquid in the solvent system, bridging liquid droplets or emulsions are created that contain solution. The emulsions make the process resemble QESD.[28] However, further agglomeration of the emulsions takes place. In agglomeration in suspension cases, the bridging liquid is added after the crystallization process. Addition of bridging liquid post crystallization, allows for various crystallization techniques to be employed for the formation of the crystals.[134] Figure 3.2 shows images of crystals of salicylic acid (right) which have been spherically agglomerated in a water-ethanol solvent system using chloroform as the bridging liquid (left). The following section will review operating parameters affecting SA.

3.4 Parameters affecting spherical agglomeration

Many operational parameters have significant impact on a SA process and the quality of its final product. One of the key considerations in developing a SA process is the choice of bridging liquid. The main characteristic is its ability to wet the crystals of interest, in suspension. Chow & Leung (1996) proposed some general rules for solvent and bridging liquid selection which explicitly detailed the dependency on the miscibility of the solvent, anti-solvent and bridging liquid, and mentioned the use of the contact angle between the bridging liquid and crystals as a measurement to assess compatibility of a bridging liquid.[135] In addition to the solvent-bridging liquid system, other operational parameters that must be considered include: the solvent addition method and rate; bridging liquid addition method, rate, and amount; agitation rate, temperature and residence time.[30] These operational parameters not only the affect the precipitation process but also the agglomeration rate and resultant particle properties.

3.4.1 Effect of solvent system

As discussed previously, the miscibility of the solvent system is of critical importance in establishing a functional SA process. Moreover, there critical concentrations of each solvent that dictate the feasibility. As an evaluation tool, ternary phase diagrams of the solvent, anti-solvent, and bridging liquid have been developed and various points along the

phase diagram have been explored to assess the feasible regions for the compositions for each solvent. From the first reported SA study to more recently, ternary phase diagrams have been consistent in their ability to identify the compositions at which miscibility is optimal and within that the compositions at which SA is achieved. Examples of ternary phase diagrams are available for the following compounds: salicylic acid[22], tolbutamide[131], acebutolol hydrochloride[123], fenbufen[136], cefotaxmine[103], benzoic acid[137], simvastation[122], and etodolac.[138] Figure 3.3 shows the ternary phase diagram for benzoic acid SA in a water-ethanol-toluene solvent system. The region of SA feasibility is only a small portion of the ternary phase diagram. The lines depict the region of optimal miscibility while the points represent feasible operating compositions for agglomeration. As evident from the ternary phase diagram, for benzoic acid the ideal miscibility and agglomeration feasibility regions consist of a large anti-solvent composition (water), and small solvent (ethanol) and bridging liquid (toluene) compositions. This finding is observed generally for water insoluble compounds.

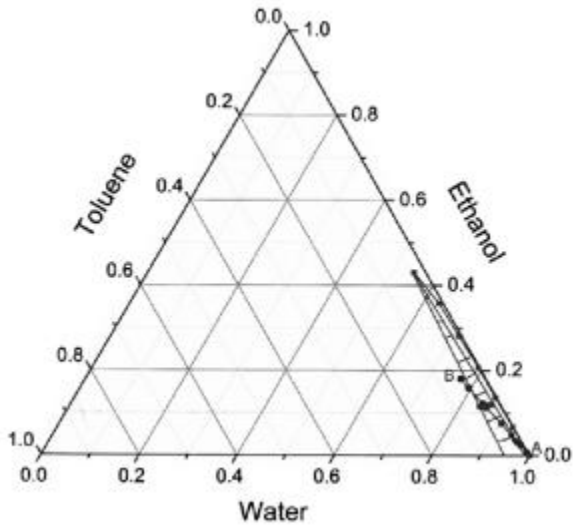

Figure 3.3 Solvent phase diagram for ethanol, water, toluene at $T = 20℃$. Reprinted with permission from [137] Copyright 2011 Elsevier.

While ternary phase diagrams aid in developing the SA experiments, selecting the appropriate bridging liquid takes precedence. Testing solvents for their wettability of the solute of interest is a good starting point. The Washburn's test, which measures the capillary rise of liquid in a column of packed power, is one method of evaluating wettability.

The test measures the contact angle of the liquid with the crystals interest, perfect wetting is equivalent to a contact angle of zero.[29] Amaro-González & Biscans (2002) investigated different solvents to serve as the bridging liquid for the SA of lobenzarit. They observed and experimentally validated that the most suitable wetting agent was that of the lowest contact angle produced by the Washburn's test. In their experiments, n-hexane had the lowest contact angle and produced larger, compact, and good sphericity agglomerates of narrow size distribution.[29] While n-hexane produced the best agglomerates, other bridging liquid test also produced agglomerates of lesser quality; proving that the Washburn's test can be a good tool for bridging liquid selection and optimization. Other studies in the literature have shown different bridging liquids to produce very different final product properties. Differences observed include yield, strength, size, size distribution and sphericity. Along with a low contact angle with the solid, other properties of a bridging liquid should be a low solubility in the anti-solvent, low solubility for the solid, and a high interfacial tension between the liquid and anti-solvent.[139]

3.4.2 Effects of solvent addition methods

The order in which the various solutions and solvents are mixed together can vary. Different addition methods examples include: (i) the addition of the anti-solvent to the solution to induce crystallization then bridging liquid addition to induce agglomeration[140], (ii) the addition of solution to an anti-solvent/bridging liquid mixture to induce simultaneous crystallization and agglomeration[140], and (iii) the addition of bridging liquid to the solution then the addition of the bridging liquid-solution mixture to the anti-solvent to induce simultaneous crystallization and agglomeration.[26,137] When comparing method 1 and method 2, method 2 produced more compact and spherical agglomerates with much less fines left in suspension.[26] Method 3 has not been explicitly compared to the other methods in the literature, however it is a commonly used method due to its ability to produce dense agglomerates of very fine crystals.[137,139] A recent study of the SA of atorvastin calcium showed that method 3 produced agglomerates of improved flowability and compressibility compared two method 1.[141] The solvent addition method also becomes important for polymorphic systems. Several studies have shown that the solvent

composition at the onset of nucleation determines the polymorph formed.[131,133,141] The addition method should be tailored to the produce the polymorph of interest.

Along with the addition method, the rate of addition also impacts the crystallization and agglomeration behavior, resulting in different final properties. The general observation is the decrease in agglomerate size with increasing feed rates.[30,137] The smaller size is attributed to the increased supersaturation achieved by the higher feed rate. The morphology of the crystals and shape of the agglomerates was observed to be unaffected by feed rate. Mechanical strength tests showed that the fracture force of agglomerates increased with increasing feed rates. This observation could be related to the internal structure of the agglomerate being composed of smaller crystals can create stronger bonds upon compression. In agglomeration-only studies, bridging liquid addition post crystallization (method 1), increasing the feed rate of the bridging liquid also produced smaller final agglomerates. The increased feed rate promotes dispersion of the bridging liquid into small droplets creating smaller agglomerates.[142] It is important to note that the effect of droplet size is also correlated to the agitation rate and the size of the primary crystals undergoing agglomeration.

3.4.3 Effect of bridging liquid content

After establishing the solvent system, operating region with in the phase diagram and addition method, the amount of bridging liquid added (within the region of feasibility) becomes of the most important process parameter in tuning the final product properties.[26,110,141-143] The bridging liquid content is usually quantified as the bridging liquid to solute ratio (BSR) on a volume basis. The BSR range is highly dependent on the system of study, and is found empirically. Each system has a critical BSR range that determines agglomeration feasibility and efficiency. Below this range, there is no significant agglomeration, and above this range a paste-like product is produced. The widely-observed trend for a wide range of compounds is increasing agglomerate size with increasing BSR within the critical range.[29,137,139,142-147] Increasing the BSR within the critical range increases the amount of bridging liquid available for agglomeration. Increased bridging liquid availability in turn increases the probability of cohesion and deformability. The increased cohesion and deformability allows for higher agglomeration

efficiency resulting larger, more spherical agglomerates.[137] The increased deformability also creates more compact agglomerates leading to increased agglomerate strength using increasing BSR. Lastly, the higher availability of bridging liquid with increasing BSR reduces, and ultimately eliminates, fine crystals in the system leading to a narrower size distribution.[142,146]

3.4.4 Effect of agitation rate and duration

The hydrodynamics of the SA system must be sufficient to allow for mixing and particle collisions to take place. Furthermore, an optimized solvent system with the appropriate BSR will not produce spheres without the adequate amount of mixing. Like the BSR, the agitation rate has a lower and upper bound. Operating below the lower bound leads to maldistribution of the bridging liquid often causing phase separation and flocculation. Operating above the upper bound can lead to the disruption of the agglomeration process causing breakage of agglomerates. The agitation rate bounds are much broader than those of the BSR, for this reason there have not been studies that specifically aim to identify those bounds. However, studies have shown that within the apparent optimal bounds increasing the agitation rate to a certain point leads to rapid agglomerate growth and increased agglomerate size, followed by a rapid decrease in agglomerate size due to compaction with further increase in the agitation rate.[22,26,116-118,143,148,149] The agitation rate can serve as the design variable that leads to the desired agglomerate size.

Studies have shown the agitation rate plays an important role in the dispersion of the bridging liquid droplets and the suspension of the agglomerates. An increase in agitation rate leads to smaller droplet sizes.[142] Collisions between crystals, bridging liquid droplets and wet crystals are higher with increasing agitation rates, increasing the probability of agglomeration.[29] Final product properties influenced are also influenced by the agitation rate. Properties affected include the agglomerate size distribution, porosity and compressive strength. The increased shear forces at higher agitation rates leads greater compaction and consolidation, producing denser agglomerates of reduced porosity, improved flowability and sphericity, and increased compressive strength.[116-118,143] Compaction and consolidation also contribute to the observed decrease in agglomerate size with increases in agitation rate. While most studies report a decrease in the mean size with

increasing agitation rates, there are cases that report a broadening of the overall size distribution with increasing agitation.[117] A recent study by Wu et al. (2015), observed a decrease in the critical BSR with increasing agitation speed.[141] This finding suggests that due to the more uniform distribution of bridging liquid at higher agitation rates, particle wetting and agglomeration become more efficient therefore requiring less bridging to obtain agglomerates. Consolidation of agglomerates at higher agitation rates can also lead to less entrapment of bridging liquid within the agglomerate pores making it available for further agglomeration with other particles. In addition to agglomeration, the agitation rate can also affect crystallization, influencing the nucleation and growth mechanisms of the primary crystals; higher agitation rates can cause higher nucleation or secondary nucleation and lead to formation of smaller primary crystals.[34]

A disadvantages of high agitation rates is the short contact times between colliding particles. Reduced contact times can inhibit agglomeration leading to smaller agglomerates and changes in the size distribution.[117] Very high agitation rates can reduce the efficiency of the agglomeration process due to disruptive forces overcoming the adhesive forces during a particle-particle collision. In extreme cases, even already adhered particles can be broken have excessive agitation. However, studies in this regard are limited because the focus of the literature has been to optimize the process and extreme cases have rarely been explored. Generally, the SA processes are operated in a regime where disruptive forces can be ignored.

The duration under agitation, or residence time, is another important parameter effecting SA product properties. In a couple studies, a modest increase in the agglomerate size has been observed with an increase in residence time.[150,150] Longer durations under agitation can also lead to consolidation which in some instances can liberate entrapped bridging liquid promoting continued coalescence. Eventually, an equilibrium size is reached once the particles are sufficiently dense and can no longer consolidate, or there is no more bridging liquid available for continued coalescence. As with increased agitation rate, increased residence time can also impact properties like porosity and compressive strength. Studies of salicylic and benzoic acid SA have shown decreases in porosity and increases in sphericity and compressive strength with longer residence times.[111,139] With longer residences times, once the bridging liquid is consumed, collisions between

agglomerate particles with each other, impeller, and vessel wall cause deformation that leads to compaction followed by densification of the agglomerates.[150] The results suggest that a minimum batch time for agglomeration exists for each system. However, above the minimum, for sufficiently long residence times an equilibrium size is reached after which further increasing the residence time will have minimal effects.

3.4.5 Effect of temperature

Cooling crystallization has long been one of the predominant techniques for creating supersaturation and inducing nucleation and growth in crystallizing systems. Temperature changes can significantly change the solubility and dictate the supersaturation of a crystallization process; directly impacting crystal properties.[34] More importantly for SA processes, temperature also affects the relative solubility of the solvent mixture. Resulting in changes in the ternary phase diagram which can alter miscibility and availability of bridging liquid in the system. Therefore, temperature changes can influence the agglomeration process.

Interpreting the effects of temperature on SA processes can be complicated because of competing mechanisms. For example, Kawashima et al. (1984) studied the effect of temperature on the SA of salicylic acid in an ethanol-water-chloroform solvent system. With an initial increase in temperature, there was a decrease in agglomerate size; potentially due to the dissolution from the surface of the agglomerates. However, with further increases in temperature, the size of the agglomerates increased and the size distribution broadened.[113] The results identified that changes in temperature affect the solubility of both the solid and the bridging liquid in the system. As the temperature increased, the solubility of chloroform decreased slightly while the solubility of the solid increased significantly; reducing the amount of solid crystallized. Thus, the amount of bridging liquid available for agglomeration increased relative to the amount of solid leading to larger agglomerates at higher temperature. The constituent particles within the agglomerates were also observed to increase with increasing temperature. Larger primary particles are related to the growth driven tendency of crystallization processes at higher temperatures. At lower temperatures, the crystallization process has a nucleation driven tendency resulting in smaller particles and the immiscibility of the bridging liquid is

increased. The combination of smaller particles and increased bridging liquid availability results increase agglomerate size due to continued coalescence. This effects have also been observed for carbamazepine agglomerates.[118] Both studies also noted a decrease in agglomerate bulk density and sphericity with an increase in temperature.

Contrarian results exist that report decreases in agglomerate size with increasing temperature for benzoic acid and cefotaxime.[110,139] Yield has also been reported to decrease with increasing temperature which is usually the case for crystallization processes. Changes in the constituent particles with temperature were consistent through the studies depending on whether the process driven by growth (higher temperature, larger particles) or nucleation (lower temperature, smaller particles).

3.4.6 Effect of primary crystal properties

For agglomeration in suspension process (post crystallization) the properties of particles can also affect the final process outcome. The properties of interest being morphology and particle size and their impact on agglomerate properties. Studies of salicylic acid have been conducted comparing the SA of smaller crystals with equant morphology with larger crystals of acicular morphology.[142] The results showed larger crystals, due to their morphology, agglomerated less efficiently with reduce sphericity than the smaller isotropic crystals. Suggesting that the compaction process, which usually improves sphericity and helps eliminate fines, was not effective for the larger acicular particles. Moreover, multiple studies found a higher initial particle size results in a lower surface area reducing deformability and coalescence efficiency.[142,144] Smaller particles have also been shown to require less bridging liquid for efficient agglomeration.[109] The adhesive forces between smaller particles are much stronger than for larger particles; making disruptive forces less effective, and agglomeration more efficient. The finding is somewhat counterintuitive and may be system not be generalized. Given the higher surface area of smaller particles, a SA process should more bridging liquid to achieve the appropriate amount of wetting.

One process parameter related to the initial particles is slurry density or solids concentration prior to agglomeration. Blandin et al. (2003) observed, below a certain solids concentration (C_s), increasing C_s led to a faster agglomeration process with larger final agglomerates of salicylic acid. For further increases in C_s, above the limiting C_s, no change

in the final agglomerate size was observed. However, the porosity of the final agglomerates did decrease with increasing C_s within the range studied.[143] The porosity results suggest that, at higher solids concentrations, more contact points are available for collisions contributing to the compaction process, and thereby, decreasing porosity.

3.4.7 Effect of combined process parameters

To achieve the desired final properties, a combination of process parameters can be adjusted. Blandin et al. (2003) established some empirical equations (3.1, 3.2) relating solids concentration (C_s), BSR (BSR), and agitation rate (N) to the final agglomerate size (L_{nb}) and the coefficient of variation (CV_{nb}) for size distribution. When fit to experimental data, the equations found the BSR to be the most significant parameter, followed by the agitation rate.[143] Empirical equations of this type can potentially be used to design and predict the final properties for any system as parameters α and β are material specific. It is also important to note that process parameters can be combined to intensify their effects on the process and final product properties. For example, increasing addition rates of solution or bridging liquid decreases the agglomerate size. This effect can be combined with an increase in agitation rate, which has also shown to decrease agglomerate size, to further decrease the attainable agglomerate size.

$$L_{nb} = \alpha C_s^{0.3} N^{-0.6} BSR^{2.1} \quad 3.1$$

$$CV_{nb} = \beta C_s^{0.4} N^{0.4} BSR^{-0.6} \quad 3.2$$

3.5 Mechanisms in spherical agglomeration

Many studies in the literature have thoroughly developed an understanding of how process parameters affect a SA process and its final agglomerate properties. Effects on properties like agglomerate size, size distribution, sphericity, porosity, compressibility and flowability are well understood from an operational perspective. However, most of the studies have been empirical with less emphasis on the understanding the complex mechanisms occurring during SA. To better design, model and control SA systems mechanistic understanding is imperative.

Kawashima & Capes (1974) took a quantitative approach to understanding the kinetics of the SA of sand.[152] Although many assumptions and experimental pitfalls limited their results, the study found the agglomeration kinetics in their system to be well described by a first-order rate process. Other early studies also concluded agglomerate growth as a first-order process. The studies described agglomerate growth as growth via layering mechanism and correlated the rate constant to process parameters like agitation rate, primary particle size and concentration of bridging liquid.[109,113,146,153] Bemer (1979) took a mechanistic approach to understanding SA process by analyzing the agglomeration in suspension of powdered glass in a carbon tetrachloride-water-glycerol solvent system. Measuring the agglomerate size at different times in a batch process, Bemer (1979) was able to suggest four main size enlargement regimes which occur during an agglomeration process: flocculation, zero growth, fast growth and the equilibrium regime.[154] The flocculation regime refers to the formation of loose flocs of particles initially created by the addition of bridging liquid. During the zero-growth regime, immediately following the flocculation regime, the particle mean size remains unchanged largely due the reduced availability of bridging liquid following flocculation. The zero-growth regime can vary depending on the agglomeration system (compound, solvents) and the operating conditions. The zero-growth regime is followed by a fast growth regime, where loose flocs are transformed into closely packed pellets by consolidation and further agglomeration occurs via coalescence due to bridging liquid moving to the surface of the flocs. Finally, an equilibrium is reached in which the mean size remains unchanged or reduces slightly due to further consolidation.[154] Later, Kawashima et al. (1981) developed another quantitative relationship between the final agglomerate size and the contact angle and interfacial tension of the bridging liquid with the particles, the size of the primary particles and their bridging liquid saturation (related to porosity).[144] These studies formed the basis of the mechanistic understanding literature.

The initial flocculation regime, also known as the wetting phase, describes the initial interaction between particles and bridging liquid droplets. It has been proposed the particles and droplets interact via two mechanisms, depending on the relative size of one another: (i) a distribution mechanism occurs when droplets are smaller than the crystals, and (ii) an immersion mechanism occurs when the liquid droplets are larger than the particles.[29,155]

The distributive mechanism describes the distribution of the bridging liquid droplet on the surface particles; coating the particles and forming agglomerates upon collision with other particles. The immersive mechanism describes the immersion of the particles into the bridging liquid droplet; as more particles become immersed by a droplet, they agglomerate and consolidate within the droplet until the droplet is fully saturated with particles. Similar mechanisms have been proposed for the 'nucleation' phase during granulation.[156,157] In granulation, the immersive mechanism is known to produce granules of higher sphericity, more density, and narrower size distributions when compared to the distributive mechanism. Other studies compare growth mechanisms in SA to granulation as well.[113,139,142] However, care must be taken when directly relating granulation and SA mechanisms as the continuous phases are different; a solid particle bed in granulation, a liquid suspension in SA.

In a more focused study, Subero-Couroyer et al. (2006) used a visualization flow cell under an optical microscope to investigate the wetting phase more thoroughly.[142] The experimental setup allowed a closer observation of the interactions between bridging liquid droplets and particles. However, the study was limited to only immersive cases as the droplets were considerably larger than the particles. In the study, particles of salicylic acid were observed to enter chloroform droplets due to the high affinity of chloroform for the particles.[29,142] The results suggest that the immersive mechanism is determined by the droplet size and the affinity between the droplets and particles. When attempting to scale the experiments from a flow cell to a stirred vessel, using an imaging probe for visualization, distinguishing between droplets and particles proved to be difficult. However, flocculation was clearly evidenced at the onset, further validating flocculation as the initial agglomerate growth regime.[142] The presence of flocculation made the it difficult to assess whether the mechanisms occurring were distributive or immersive; although, it is likely a combination of both mechanisms. At high agitation rates, the droplet sizes were observed to be smaller and better dispersed through the system. At well-dispersed conditions, the agglomeration rate was observed to be faster, provide much smaller agglomerates. Again, no conclusive interpretations could be made as smaller droplets could lead to a change in mechanism from immersive to distributive. Some studies in the literature have explored the use of a micro force balance to investigate the forces, geometry and interactions between bridging

liquid and particles.[158,159] While promising, the studies were also isolated small scale investigations that likely will not transfer well in a stirred vessel.

Blandin et al. (2000, 2003) developed an *in-situ* visualization tool to monitor the SA process and studied all phases of agglomerate growth proposed by Bemer (1979).[143,154,160] After the flocculation and zero growth phases, the fast growth and equilibrium phases are dominated by coalescence and compaction. In their study of a reactive crystallization and SA, Blandin et al. (2003) observed a decrease in the mean agglomerate size immediately following the flocculation period.[143] This period of decreasing agglomerate size correlates well with the zero-growth regime outlined by Bemer (1979) and is attributed to the compaction of flocs due to the hydrodynamics in the system. After a minimum size is reached due to compaction, rapid growth of the agglomerates is observed due to coalescence. This observation, again, agrees with those of Bemer (1979) and is attributed to bridging liquid being squeezed to the surface of agglomerates during compaction.[137] The increased availability of bridging liquid promotes the rapid-growth regime via coalescence. A more recent study has also confirmed this finding for a benzoic acid in ethanol-water-toluene system.[137] As the bridging liquid is consumed, the size distribution narrows. Once the bridging liquid is completely consumed, the agglomerate size plateaus.[143] Moreover, all fine particles were eliminated by the end of the process. Agreeing with other studies that suggest smaller particles, due to their higher surface area, are more susceptible to wetting and agglomeration.[142] This also suggest that the agglomeration kinetics for fine particles is much higher than that for large particles. It has been observed that fine crystals form flocs or nuclei at a higher rate during the flocculation phase as well.[150] The study by Blandin et al. (2003) served as the first example of the use of in-line PAT tools to gain process insight.

Post processing scanning electron microscopy (SEM) images of agglomerates from Blandin et al. (2003), showed possible “compaction and rearrangement” and “adhesion” coalescence mechanisms taking place during fast growth and equilibrium growth regimes. When coalescence was driven by compaction and rearrangement, primary particles were arranged in a compact manner, giving very spherical and dense agglomerates. When coalescence was driven by adhesion, the previously mentioned growth via layering mechanism takes place.[137,146,153] Layers of particles become apparent in the structure of

agglomerates, delimited by porous/breakable areas. Particles that underwent the adhesion mechanism also fractured easily due the voids in their structure. At-line and post processing agglomerate strength studies showed significantly higher compressive strength for dried agglomerates compared to agglomerates from the liquid suspension.[143] This is a common observation due to the volatility of bridging liquid and the slight solubility of the compound in the bridging liquid. The bridging liquid bonds that bind the wet agglomerates in suspension are replaced by solid crystalline bridges during the drying process due to evaporation of the bridging liquid.[112] The differences in agglomeration strength from in suspension to dried point out changes occurring in the internal structure of the agglomerate post processing. Suggesting that the use of in-line PAT tools should be even more prominent so that mechanisms are studied and interpreted correctly.

Due to the deformable nature of the agglomerates upon initial wetting, disruptive forces during coalescence due to shear are more likely than breakage of agglomerates.[111] However, there are conflicting views on whether a breakage mechanism exist for SA processes. At high agitation rates, breakage may be factor and can lead to fragmentation of particles and agglomerates.[137] Without conclusive evidence of occurrence during SA, a comprehensive mechanistic study of breakage in SA does not exist.

3.6 Modeling spherical agglomeration

The first few attempts to model SA resulted in first order approximations for agglomeration kinetics.[22,30,109,145-147,150,152] These approximations did not differ from other rates processes as agglomerate growth was estimated as a growth rate (length/time) as opposed to an agglomeration rate (based on an agglomeration kernel/rate). Growth rate approximations do not truly describe the agglomeration mechanisms since it does not account for coalescence. Since then, several modeling approaches have been developed for SA systems. Much of the modeling work has focused on agglomeration in suspension systems to reduce the complexity of the problem; focusing solely on developing more accurate and physically relevant agglomeration kernels. The literature is divided between studies of crystallization that exhibit agglomeration and studies of agglomeration suspension. The modeling studies discussed henceforth extend the initial modeling work and focus on the development of agglomeration kernels and PBMs that improve the predictability of SA process.

3.6.1 Modeling agglomeration in suspension processes

Bemer's (1979) study on the SA of powdered glass also included a modeling perspective. Based on the previously mentioned experimental observations, a PBM was developed to predict the changes in the agglomerate size distribution (ASD). In the study, it was observed that traditional granulation (agglomeration via coalescence/consolidation only) PBMs predicted continuous agglomerate growth; contradictory to experimental observations. To overcome the inaccuracies of coalescence only models, a model that included coalescence from collisions, growth mechanisms (e.g., layering) and breakage mechanisms (e.g., crushing) was developed. Referred to as the "coalescence-breakage" model, the coalescence term was redefined from a coalescence frequency and efficiency model; the model worked well at predicting steady-state ASDs.[154] However, as previously mentioned, the suggestion that there is a breakage mechanism during SA has yet to be validated experimentally and cannot be generalized to all systems.

Most of the common agglomeration kernel depend solely on the size of the interacting particles. Given the mechanisms occurring in SA, describing agglomeration solely on the size of the particles would depict experimental results. Madec et al. (2003) developed a multidimensional kernel that used a Monte Carlo solving approach.[161] The kernel, specific to agglomeration in suspension systems, incorporated the composition of bridging liquid, which made the model more representative of experimental agglomeration mechanisms discussed in Section 3.3 and 3.4. As mentioned in Section 3.4.3, there is an optimal range for the ratio of bridging liquid to solute volume (BSR); below or above this critically optimal range would produce loosely compacted agglomerates or paste-like amorphous agglomerates, respectively.[130,140,162] Equation 3.3 represents the agglomeration kernel used in the study.

$$\beta = \beta_0\left(L_i^3 + L_j^3\right)\left(\left(c_i + c_j\right)^{\alpha}\left(100 - \frac{c_i + c_j}{2}\right)^{\delta}\right)^{\alpha} \quad 3.3$$

$$c_i = \frac{\text{volume of liquid}}{\text{volume of the agglomerate}} * 100 \quad 3.4$$

$$\delta = \left(\frac{1 - c_{opt}}{c_{opt}}\right)\alpha \quad 3.5$$

Here, β is the agglomeration rate, β_0 is the agglomeration rate constant, L_i (L_j) is the size of the agglomerating particles, c_i (c_j) is the composition of bridging liquid in each particle, δ is the weight coefficient for the solid particles, α is the weight coefficient for the liquid droplets, and c_{opt} is the optimal bridging liquid composition. The composition function (last term in equation 3.3) is derived such that the collisions can only occur between particles with sufficient, not excess, bridging liquid composition, i.e., $c_i = 0$ and $c_i = 100$ will not yield a collision. The weighting coefficient for the solid particles is a function of the optimal bridging liquid composition and weighting coefficient of the droplets (equation 3.5) to assure that an agglomeration event cannot occur until wetting has occurred.[161] This unique incorporation of the bridging liquid composition served as the efficiency term by which the process would reach equilibrium. The multidimensional kernel (size, composition) resulted in simulations of the ASDs which could better predict the growth mechanisms explained in experimental literature.[154] The study was limited to agglomeration only systems (no nucleation, growth) and required some prior knowledge of the system composition. Moreover, the study did not consider the hydrodynamics of the system, the internal structure of the agglomerates, and did not track the population of bridging liquid droplets. To address some these issues, a coupled simulation approach using computational fluid dynamics (CFD) and Monte Carlo to track droplet and particle populations was suggested referring to a previous study by Madec et al. (2001).[163]

As outlined in Section 3.4, the key mechanisms of agglomeration in suspension are: 1) bridging liquid droplets capture solid particles and form agglomerate nuclei, 2) compaction of the agglomerate nuclei occurs due to collisions causing a rapid decrease in mean diameter, 3) growth via coalescence and consolidation then occurs due to the hydrodynamics and process conditions (i.e., agitation rate and BSR), and 4) the limit of compactibility determines when agglomeration ends.[111,143,154] Based on experimental observations, a "growth via coalescence only" model was developed by Blandin et al. (2005).[111]

$$\frac{\partial \Psi(L,t)}{\partial t} = R_A(L,t) \qquad 3.6$$

In equation 3.6, Ψ represents the number density function and R_A represents the agglomeration rate distribution. The agglomeration model considered the size (L) and

concentration of the agglomerating particles (N_i or N_j) . The agglomeration rate distribution can be broken down into its agglomeration rate (r_{agg}), a function of the meeting probability (f), the agglomeration efficiency (eff) and the concentration of particles (N_i or N_j) in the process (equations 3.7-3.10).

$$r_{agg}(l,t) = K(i,j,t)N_i(t)N_j(t) \quad 3.7$$

$$K(i,j,t) = f(i,j,t)\text{eff}(i,j,t) \quad 3.8$$

$$f(i,j,t) = C_{coll}\alpha(i,j,t)\left(\frac{\pi}{4}\right)\left(S_i + S_j\right)^2\left[\overline{u(S_i)^2} + \overline{u(S_j)^2}\right]^{1/2} \quad 3.9$$

$$\begin{cases} \text{eff}(i,j,t) = \frac{f_{adh}(i,j,t)}{f_{sep}(i,j,t)} - 1 & if\ f_{adh}(i,j,t) \geq f_{sep}(i,j,t) \\ \text{eff}(i,j,t) = 0 & otherwise \end{cases} \quad 3.10$$

$$F_{adh}(i,j,t) \propto \left[\frac{def^{max}(i,j,t)}{L_p/2}\right]^2 \left(1 - \mathcal{P}(t)\right)F_{bridge}\left(\frac{S_i^2 + S_j^2}{S_i^3 + S_j^3}\right) \quad 3.11$$

In equation 3.9, f, is described by a function of the target efficiency (α), characteristic size of size distribution class (S_i, S_j), and collision velocity (u).[164] The target efficiency is a function of the agglomerate and fluid densities as well as the fluid viscosity. The collision velocity is calculated from the particle-fluid relative velocity and is a function of energy dissipation. In equation 3.10, the agglomeration efficiency, eff, is defined as the ratio of adhesive to disruptive force. The disruptive force (f_{sep}) is a function the shear stress, dissipation energy, and the corresponding characteristic area. The adhesive force (f_{adh}) is a function of the deformation energy, which is calculated by the agglomerate strength (based on porosity, BSR) and the collision energy (based on primary particle size, interfacial energy, binding force). The adhesive force is then proportional to the deformation, porosity, binding force, and area to volume ratio (equation 3.11).[111] The simulations from the proposed model showed very good predicting ability, agreeing with experimental data when the necessary parameters were fit to the data. An additional benefit of the model is the incorporation of the system hydrodynamics and properties like porosity and deformability, predicting final properties another than size. One downside is the model development is very extensive and complex to understand. Additionally, the work did not provide values for all parameters making it difficult to assess its validity or extend it to other systems.

The key difference between the "coalescence-breakage" model and the "growth via coalescence only" model is the latter ignores breakage and fragmentation due to the experimental observations. Agglomerates created through an agglomeration in suspension process remain soft and do not fragment/break, but rather deform and compact upon collisions. Madec's et al. (2003) multidimensional agglomeration model directly addresses the agglomeration mechanism by incorporating the bridging liquid content in each agglomerate. If the agglomerate is saturated with bridging liquid an agglomeration event will not occur or if two particles do not contain bridging liquid, then an agglomeration will also not occur. Some limitations in their model include the negligence of hydrodynamics and the solving method as stochastic method can be computational heavy.

3.6.2 Modeling simultaneous crystallization and agglomeration

While a majority of the SA modeling work covers agglomeration in suspension, many of the experimental SA studies are combined crystallization and agglomeration studies.[137,139] There is an opportunity to further improve modeling in this area by using the experimental understanding of the combined nucleation, growth, and agglomeration mechanisms. However, the inclusion of crystallization mechanisms such as nucleation and growth occurring simultaneously with agglomeration requires innovative model development and further understanding of the interplaying kinetics. David et al. (1991) began tackling this issue by formulating an agglomeration rate kernel that incorporated particle concentration, supersaturation, energy dissipation, crystallizer size and size of agglomerating crystals.[165]

A SA process, particles are constantly changing in size until an equilibrium is reached. This change in particle size changes the hydrodynamic experience, or collision mechanism, for each particle. David et al. (1995, 2003) followed their initial work by developing a multi-layer agglomeration model that considers the efficiency of agglomeration based on the collision mechanism (i.e., Brownian, laminar, or turbulent).[166,167]

$$\beta_{i,j,b} = k_{Ab} G \frac{(S_i+S_j)^2}{S_i S_j} \tag{3.12}$$

$$\beta_{i,j,l} = k_{Al} G \left(S_i + S_j\right)^3 \left(\frac{P}{\nu}\right)^{1/2} \tag{3.13}$$

$$\beta_{i,j,t} = k_{At} G \frac{\left(S_j+S_i\right)^2}{S_j} f\left(\frac{S_i}{S_j}\right) ND \left(1 - \frac{\left(S_j+S_i\right)^2}{\lambda_c^2}\right) \tag{3.14}$$

In equations 3.12-3.14, $\beta_{i,j,b}$, $\beta_{i,j,l}$, and $\beta_{i,j,t}$ are the agglomeration rates at the Brownian, laminar, and turbulent scales, respectively. k_{Ab}, k_{Al}, k_{At}, are the agglomeration rate constants at the Brownian, laminar and turbulent scales, respectively. G is the growth rate and S_i (S_j) is the size of agglomerating particles. In equation 3.13, P is the dissipated power per unit mass and ν is the kinematic viscosity. In equation 3.14, f is the Marchal's relative size function, N is the stirring speed, D is the particle diffusivity, and λ_c is the Taylor microscale. Per David et al. (1991, 1995, 2003), Brownian collisions occur at or below the Batchelor microscale, laminar collisions occur above the Batchelor microscale and below the Kolmorgorov microscale, and turbulent collisions occur between the Kolmorgorov and Taylor microscale.[165,166,167] As particles increase in size, their collision mechanism (microscale/flow field) changes from Brownian (equation 3.12) to laminar (equation 3.13) to turbulent (equation 3.14). Above the Taylor microscale, equation 3.14 reduces to zero as the size of agglomerates becomes too large and the system is too turbulent to produce a successful agglomeration event.[167] The agglomeration rate kernels accounted for changes in the collision mechanism and was a function of the supersaturation and temperature through the growth rate which served as the efficiency term. Agglomeration is enhanced by inter-particle growth or agglomerative bond formation; when supersaturation increases, the strength of the liquid bridge between two particles increases leading to subsequent inter-particle growth and higher agglomeration efficiency.[37] It is important to note that the work of David et al. (2003) was not specific to agglomeration in suspension systems, but rather crystallization processes that exhibit agglomeration. This distinction is important because crystallization processes that exhibit agglomeration do not necessarily follow the same mechanisms or kinetics as agglomeration in suspension processes; since there is no bridging liquid addition. However, as shown experimentally, the effects of hydrodynamics, particle size and particle concentration are relevant to both.

Another area of opportunity is in the development of models that have ability to track the changes of the primary (internal) particles and multiple populations. Ochsenbein et al. (2015) developed a coupled PBM that tracked two populations during agglomeration in suspension for the agglomeration of needle-like crystals.[168,169] The coupled PBM framework is composed of a 2-D PBE that describes the 2-D growth of the needle-like primary crystals. The primary crystal population is coupled to a PBE that describes the

agglomeration of the needle-like crystals. The unique coupling of the PBM allowed the derivation of a 2-D agglomeration kernel, considering both characteristic lengths of the agglomerating particles as well as their orientation.

In all the modeling studies presented here, experimental observations drove the model development by describing and identifying critical mechanisms occurring during the agglomeration process. Different agglomerate growth regimes observed during experimentation lead to the development of a combined coalescence and breakage model to better predict those growth regimes.[154] Experimentally observed differences in agglomeration mechanisms as particles in size and fluid flow led to the development of a multilayer agglomeration kernel to describe changes in the hydrodynamics.[167] Consideration of more physically relevant mechanisms led to the incorporation the composition of bridging liquid in individual agglomerates as the efficiency term in a multidimensional agglomeration kernel.[161] Accounting for both mechanistic phenomena (e.g., deformability, collision efficiency, and compaction) and process conditions (e.g., energy dissipation, BSR, particle size) led to the development of a comprehensive model with the ability to predict size and porosity.[111] However, no generalization on the best model can be made as all the studies were very system specific. A challenge with the development of these more sophisticated models is validation. As the number of mechanisms represented by a model increases, so do the number of equations and parameters.

3.7 Continuous spherical crystallization

As outlined earlier, SA creates advantages in micromeritic properties of suspended particles that lead to the improved recovery of high-value solid particles. These advantages provide the opportunity for improved process design and efficiency, making SA a PI technique. Combining the inherent advantages of SA with the advantages of continuous operations can significantly improve process efficiency, adaptability and productivity. The first example of continuous SA was the preparation spherical wax matrices of sulfamethoxazole by Kawashima et al. (1982).[30] Their study focused on understanding the fundamental agglomeration mechanisms in a single-stage mixed suspension, mixed product removal (MSMPR) crystallizer. The most important observed difference between

batch and continuous SA was in the different growth regimes. Unlike batch, which undergoes a zero-growth period and then a fast growth period before leveling off at an equilibrium size, a continuous process undergoes a fast growth period immediately before undergoing a size reduction period then finally leveling off at an equilibrium size.[30,154] The initial fast growth period in a continuous process is a result of the buildup of bridging liquid and agglomerating particles during startup. However, as operation continues, the size reduction period can be attributed to the removal of particles and bridging liquid at a more balanced rate, i.e., steady state. With respect to most other process parameters, the same trends exist in terms of their effect on final agglomerate properties. Tahara et al. (2015) also used a single-stage MSMPR crystallizer for a SC technique via emulsion solvent diffusion (ESD).[170] Although a ESD technique differs from SA, their system used a solvent recycling technique that can potentially be incorporated into SA systems to allow for higher yield from the crystallization process. A MSMPR operates at a single point in the phase diagram which reduces yield, including a solvent recycle stream allows for yield closer to that of a batch system.

3.8 Conclusions

Spherical crystallization provides a direct path towards upstream and downstream integration of pharmaceutical unit operations. The technique can tailor micromeritic properties of crystals to produce final products of superior attributes. The enhanced micromeritic and flow properties potentially allow for a reduction in the number of unit operations during industrial processing, reducing time and costs. These attributes make the technique inherently a PI technique.

For the subset of SC techniques reviewed here, i.e., SA, studies show that there are many process parameters that influence the final agglomerates properties. Many of them focus on the optimization of the operating conditions to achieve desired product functionality. However, this has largely been carried out on a trial and error basis due to a lack of mechanistic understanding and PAT tools. Figure 3.4 details the various process considerations for developing a SA experiment. From solvent selection to final product properties there are many key decision variables that ultimate lead to a successful SA procedure, yielding desired properties. A bridging liquid should exhibit good wettability

(measured by capillary rise or Washburn's test) and low contact angle with the solid of interest. It should also be immiscible with the suspension solvent system to allow for preferential wetting of the solid particles. The combination of bridging liquid and crystallization solvent can influence the crystal polymorph and morphology so the method of bridging liquid addition and crystallization should be examined carefully. The size, morphology, and concentration of solids in the system can affect the optimal process parameters as well. The desired final agglomerate properties should dictate the critical operating range for all process parameters as changes in processing parameters can lead to a wide range of final product properties. Identifying the critical BSR and sufficient agitation rate appeared to be of top priority throughout the literature.

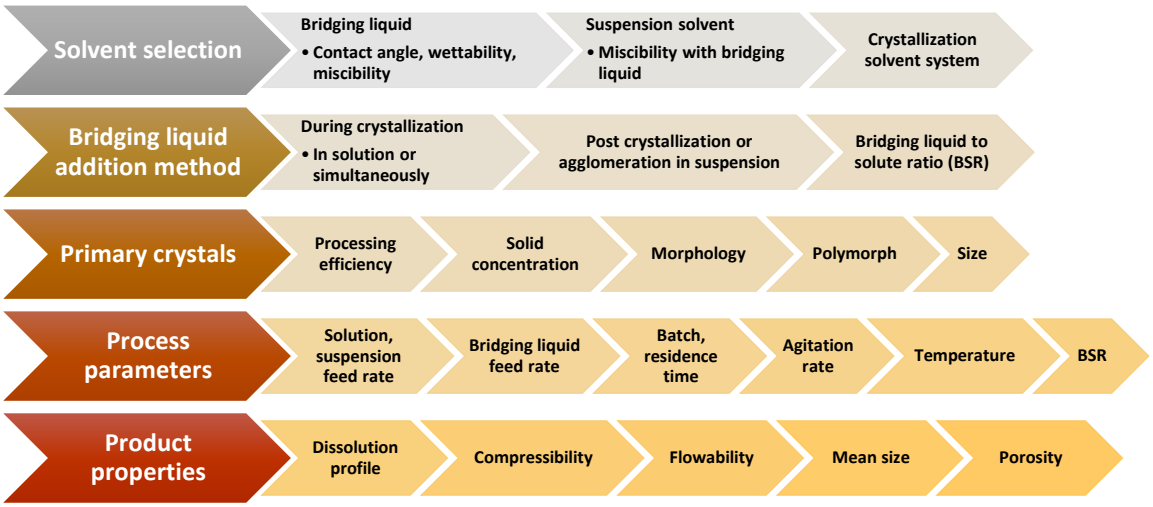

Figure 3.4 Workflow of process considerations when developing a spherical agglomeration process.

An understanding of the mechanisms occurring during the agglomeration process is imperative to control and predict final product properties. Studies have been reported which have given important insights into the mechanisms occurring during SA citing coalescence, consolidation, growth via layering, deformation, collision efficiency, microscale dependent collisions, composition of bridging liquid in agglomerate, fragmentation, and breakage. Models have been proposed that take into consideration these agglomeration phenomena. However, more mechanistic and modeling studies are required to enable experimental design and the tailoring of specific product properties. Moreover, models that can track the

different populations/phases (i.e., primary crystals, agglomerates, droplets) are needed so that physically relevant agglomeration kernels can be developed that take into consideration the effects of process conditions (i.e., agitation rate, BSR). Moving forward, a mechanistic understanding should be enhanced due to the emergence of sophisticated on-line analysis techniques and PAT tools (e.g., PVM, FBRM). Combined with the traditional off-line characterization methods, on-line PAT provides an opportunity to further enhance our understanding of the SA mechanisms and their effects on final product properties.

Most research thus far, has been carried out using batch systems. However, continuous SA processes have also been successfully reported. The pharmaceutical industry is experiencing a paradigm shift from batch to continuous processing. Continuous processing has the potential to significantly reduce plant size and footprint while generating a more consistent product at higher levels of productivity. Combining the PI benefits of SA with continuous processing can be the future of pharmaceutical manufacturing.

While this review focused only the SA subset of SC there are also many potential benefits from some of the other techniques. Co-agglomeration of APIs and excipients, can allow direct incorporation of final formulation blends into the spherical agglomerates. Co-agglomeration of API and excipients adds another PI attribute to SC that can lead to direct compression of agglomerates. This technique could further reduce the required number of unit operations and costs in pharmaceutical manufacturing. QESD is also a technique that has been employed in the co-agglomeration. QESD can allow the incorporation of API and excipients of different hydrophobicity into spherical agglomerates, providing a method of overcoming differences in wettability.

4. FURTHER UNDERSTANDING OF AGGLOMERATION MECHANISMS IN SPHERICAL CRYSTALLIZATION SYSTEMS THROUGH PAT TOOLS

4.1 Introduction

Spherical crystallization of active pharmaceutical ingredients is a technique used to alter and improve micromeritic properties of the crystals during or post the crystallization process. While there are different SC techniques, a commonly used technique in the bulk chemical industries is SA.[152,162] Spherical agglomeration requires the use of an appropriate bridging liquid that preferentially wets suspended particles causing agglomeration that under suitable hydrodynamics (agitation/mixing) produce spherical agglomerates. General guidelines for the selection of the appropriate bridging liquid and solvent system have been developed for common chemical compounds and pharmaceutical powders.[135] To further develop initial studies, investigations into the effects of the different operating parameters governing a SA process have been studied in detail. The effects of operating parameters such as the amount of bridging liquid, identification of the critical bridging liquid range, batch or residence time, agitation rates, solute concentration, polymorphic effects, and feed rate have been well studied in the literature.[22,26,29,30,131,133,137,141,143]

Blandin et al. (2003) and Subero-Couroyer et al. (2006) incorporated an *in-situ* visualization probe in their salicylic acid SA experiments to study bridging liquid injection time and wetting period.[142,143] Their imaging probe allowed for real time tracking of agglomeration mechanisms. Blandin et al. (2003) used the probe to monitor and measure particle size *in-situ*. Most of the study focused on the effects of process parameters on the agglomerate size and porosity. Subero-Couroyer et al. (2006) used the probe to identify mechanisms such as flocculation during the binder injection period and compaction. The study also investigated the effect of different initial particle sizes on the agglomeration process by comparing crystallized particles of salicylic acid with salicylic acid particles available commercially. While some insights as to how the agglomeration mechanism differs with different primary particles size was suggested, the operating conditions at which the differences in mechanisms occur were not clearly identified. Nonetheless, these two studies mark some of the few cases using process analytical technologies (PAT) tools

to study SA mechanisms. A recent few studies focused on understanding the differences in final agglomerate properties for different bridging liquid addition methods and different primary crystal properties.[26,29,116,140,141,144] However, these studies did not clearly elucidate differences in the agglomeration mechanism for different bridging liquid addition methods, likely due to having not employed PAT tools. Incorporating in-line PAT tools in SA processes has proven to be difficult due to fouling of the probes.[29,142]

As SC becomes more prevalent in pharmaceutical applications, process development will require knowledge of the effects primary crystal properties, interactions between crystals and bridging liquid, and mechanisms of various bridging liquid addition methods. A study on the differences in mechanisms for different bridging liquid addition methods is currently lacking. Moreover, a definitive mechanistic relationship between the primary crystal size and bridging liquid droplet size has yet to be established. Lastly, an analysis of flow characteristics as it pertains to the agglomeration mechanism has not been divulged.

In this work, PVM and FBRM probes are used to determine the properties of the primary crystals, examine the interactions between crystals and bridging liquid droplets, and assess the most suitable bridging liquid addition method for the SA of benzoic acid. For different bridging liquid additions methods, the PVM will elucidate the respective agglomeration mechanism. Particle size of bridging liquid droplets and primary crystals are characterized by the FBRM to establish the relationship between primary crystal size and bridging liquid droplet size that lead to different mechanisms. Characterization of final agglomerates for various flow properties will be related to mechanistic findings to provide guidelines for experimental design.

4.2 Materials and methods

4.2.1 Materials

Benzoic acid (≥99.5% purity, Sigma Aldrich) was used as the model compound for all experiments in this study. Benzoic acid typically exhibits thin plates or needle-like morphologies during crystallization; hence has been extensively used as a model compound for SA throughout the literature.[26,139] The solvent system consisted of ethanol-water-toluene. Ethanol (pure, 200 pf, USP grd, Decon Labs) served as the solvent in which

to prepare benzoic acid solutions, deionized water served as the anti-solvent, and toluene (≥99.5% assay, Fisher Scientific) as the bridging liquid.

4.2.2 Experimental setup

All experiments were carried out in a 500-mL lab scale jacketed crystallizer. Agitation was controlled by an overhead stirrer with a three-blade retreat curve impeller. At the agitation rates studied (300-500 rpm) particles were observed to be well suspended. Peristaltic pumps (Cole-Palmer) and platinum cured silicon tubing (MasterFlex L/S) fed solution, antisolvent and bridging liquid into the crystallizer. All liquids fed to the crystallizer were added at the surface, equidistant from the impeller and crystallizer wall. The chord length distribution and particle counts were monitored using a Mettler-Toledo Particle Track G400 (FBRM) and *in-situ* images of the process was taken using a Mettler-Toledo ParticleView V19 (PVM).

4.2.3 Methods

Benzoic acid solutions were prepared by dissolving benzoic acid in ethanol at 40 °C. The solution was then allowed to cool down to room temperature (20 °C) prior to the start of the experiment. The saturation temperature of the maximum concentration (0.375 g/mL) was 15 °C. Three different bridging liquid addition methods were studied to assess their respective agglomeration mechanism. The benzoic acid concentrations (BA conc.) of the solution feed studied were 0.15, 0.25, and 0.375 g/mL. The SASR studied were 0.175, 0.35, and 0.50. The BSR was equal to 1 for all experiments. The conc., SASR, and BSR were kept constant for each method to evaluate their mechanistic differences.

(i) Bridging liquid addition method 1 (BAM1): The bridging liquid is dissolved in the benzoic solution. To ensure homogeneity, the bridging liquid-solution mixture is stirred for a minute. Then the bridging liquid-solution mixture is fed (2 mL/min) to the crystallizer which contains water to induce simultaneously crystallization and agglomeration. The stirring speed is maintained at 500 RPM through the experiment.

(ii) Bridging liquid addition method 2 (BAM2): The benzoic acid solution is fed (2 mL/min) to the crystallizer containing water to initiate crystallization. The

crystallization process proceeds until the particles counts (FBRM) plateau. The bridging liquid is then fed (2 mL/min) to the crystallizer to induce agglomeration. In this case, the crystallization and agglomeration processes are decoupled. During the crystallization period the agitation rate is kept at 300 RPM to avoid agitation induced shear or secondary nucleation. The agitation rate is increased to 500 RPM upon bridging liquid addition.

(iii) Bridging liquid addition method 3 (BAM3): The benzoic acid solution and bridging liquid are simultaneously fed to the crystallizer. In this method, the solution is fed at 2 mL/min while the bridging liquid is fed per the BSR. For an experiment at a benzoic acid conc. of 0.15 g/mL and a SASR of 0.175 the benzoic acid weight percentage by volume would be 10%. Since the BSR = 1, the bridging liquid flowrate is set to 0.20 mL/min.

Total batch time for some experiments varied as the total amount of solution feed varied. For BAM1, the batch time for SASR = 0.175, 0.35, and 0.50 was 67, 95, and 113 min, respectively. For all BAM2, the crystallization process was carried for 120 min and the agglomeration process 30 min. The crystallization process was carried out for a long period to ensure the crystals had reached an equilibrium prior to agglomeration. For BAM3, the batch time for SASR = 0.175, 0.35, and 0.50 was 75, 130, and 167 min, respectively. The differences in batch time does not affect the mechanistic studies. Due to the decoupling of crystallization and agglomeration in BAM2, results from BAM2 are used to identify significant relationships between crystal size and agglomerate properties. The method is also used to study bridging liquid droplets. For bridging liquid droplet studies, the experiments were carried at the same experimental conditions but on a solute-free basis (no crystallization).

Offline images of the spherical agglomerates were taken using a Nikon SMZ1500 microscope. ImageJ was used to determine the ASD based on the Feret diameter. A Freeman FT4 Powder Rheometer was used to characterize the flow properties of the resulting agglomerates. The FT4 uses a blade that rotates and move down and up through a particle bed at a defined helix angle and speed. The instrument then measures the torque, force, and height as it traverses the particle bed. Given the blades ability to condition the particle bed through gentle clockwise slicing flow patterns, every test starts in a

homogeneous, low stress packing state. This conditioning process makes the FT4 ideal for comparative studies since all samples will have a similar start condition. Actual flow studies occur under a counter-clockwise aggressive flow pattern or for compressibility a vented piston is used to apply force on the particle bed.[171-173] Flow properties studied include: compression percentage (CPS), stability index (SI), flow rate index (FRI), and conditioned bulk density (CBD). The porosity of the final agglomerates was measured using the combination of an AccuPyc II 1340 Pycnometer and GeoPyc 1360 Envelope Density Analyzer.

4.3 Results and discussion

Table 4.1 details the experimental conditions. The BA conc. and SASR are the only variables varied for each experiment. The BSR and agitation rate (RPM) were set to values found suitable in the literature, BSR = 1 and RPM = 500.[26,137] The theoretical supersaturation (*S*) for each experiment was calculated from solubility data in the literature.[137,187] The SC procedure in this study is carried out using a reverse anti-solvent addition where the solution is fed to anti-solvent. This type of procedure results is a supersaturation profile which is not easily quantified. Therefore, *S* expressed as the ratio of g of benzoic acid in g of the solvent mixture (ethanol-water-toluene) to the solubility of benzoic acid in the solvent mixture (g/g). At a constant BA Conc., *S* doesn't have a linear response to changes in SASR. This observation is typical of benzoic acid in ethanol-water mixtures and has been detailed in the literature.[187] The bridging liquid to anti-solvent ratio (BASR) is also provided based on the BSR. The BASR is specified because it is the main parameter in the bridging liquid droplet studies. The table also details the success rate of the different bridging liquid addition methods. BAM2 was the most successfully at producing spherical agglomerates. BAM1 showed some success both also produced elongated agglomerates while BAM3 produced only elongated agglomerates. Experiments 3, 8 and 9 did not produce agglomerates for any of the methods. For experiment 3 and 9, it was observed that the high solubility at SASR = 0.5 was too high to produce the sufficient crystallization (experiment 3) or adequate immiscibility of the bridging liquid (experiment 9). For experiment 8, the supersaturation was too high, yield high nucleation and resulting in insufficient bridging liquid at a BSR = 1.

Table 4.1 Experimental conditions

Exp.	BA Conc.	SASR	BASR	*S*	BAM1	BAM2	BAM3
1	0.15	0.175	0.02	2.2	✓	✓	×
2	0.15	0.35	0.03	2.5	×	✓	×
3	0.15	0.5	0.05	1.5	-	-	-
4	0.25	0.175	0.03	3.5	✓	✓	×
5	0.25	0.35	0.06	4.0	✓	✓	×
6	0.25	0.5	0.08	2.4	×	✓	×
7	0.375	0.175	0.04	4.8	✓	✓	×
8	0.375	0.35	0.08	5.5	-	-	-
9	0.375	0.5	0.11	3.2	-	-	-

✓spherical agglomerates produced, × elongated agglomerates, - no agglomerates

4.3.1 Bridging liquid addition method 1 (BAM1)

Figure 4.1 shows the progression of Exp. 1 via BAM1 (i.e., bridging liquid is dissolved in solution). For BAM1, as the solution is fed to crystallizer bridging liquid droplets containing solution are formed due to the immiscibility of the solvent mixture. Droplet formation and stabilization is then proceeded by nucleation within the droplets; evidenced by changes in the turbidity of the droplet. As crystals grow through solvent diffusion they break the droplet barrier. This is apparent through a breakout period where bridging liquid droplets are no longer visible. It is important to notice the crystal morphology. Due to the slow nature of solvent diffusion through the droplet/water interface, long needle-like crystals for formed. As the crystals grow in length the bridging liquid droplet is distributed along the surface of the crystal which accounts for the disappearance of the droplets. The agglomerated needle-like particles formed within one droplet are now wet agglomerates

that go through further coalescence with other wet agglomerates. Figure 4.2 illustrates the mechanisms involved in this method.

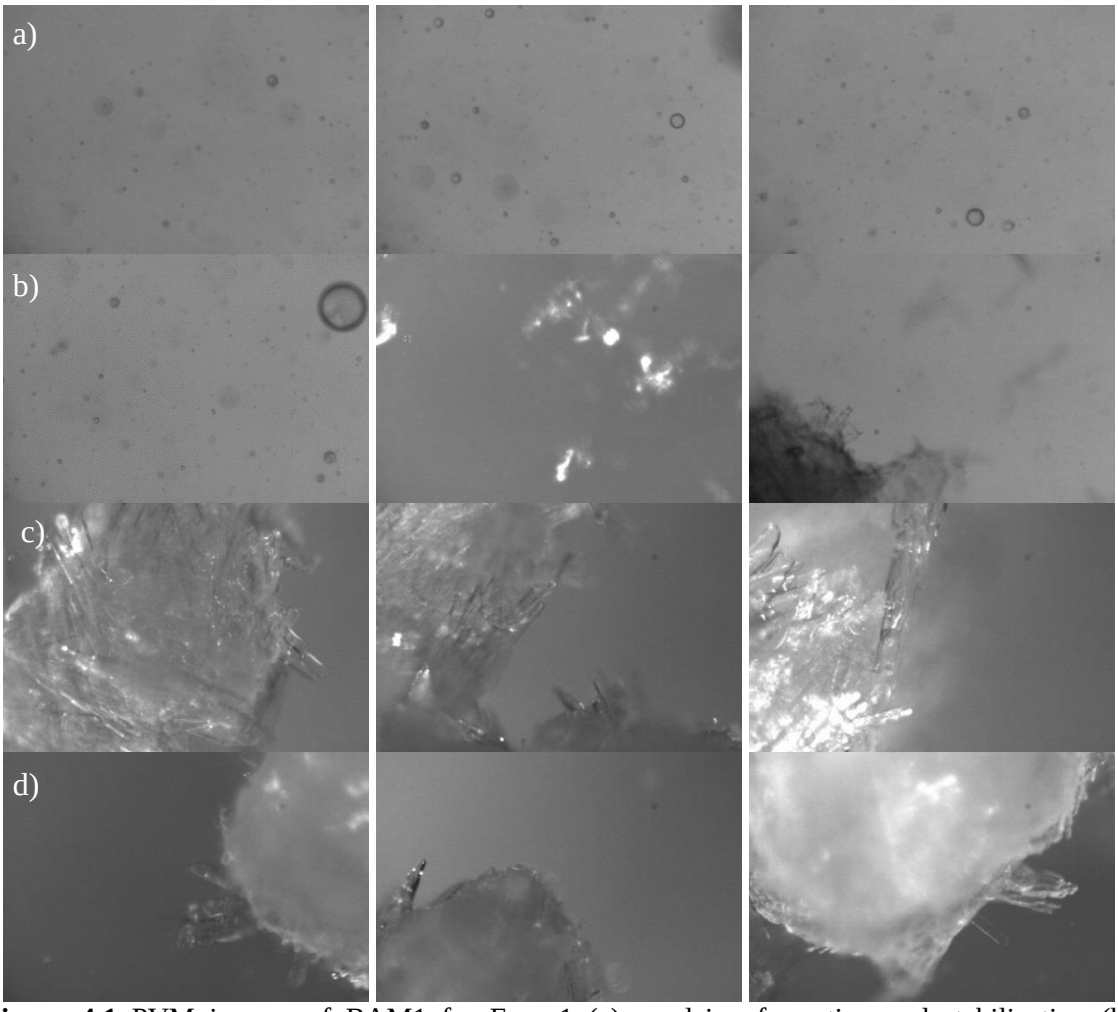

Figure 4.1 PVM images of BAM1 for Exp. 1 (a) emulsion formation and stabilization (b) crystallization and break out (c) coalescence (d) completion

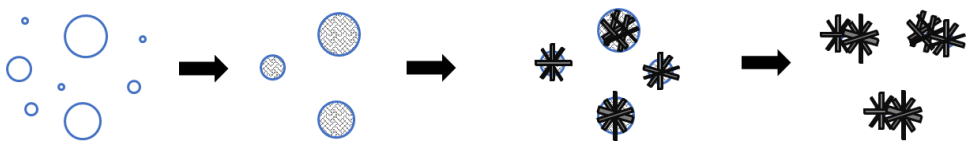

Figure 4.2 Schematic of agglomeration mechanism for BAM1

It is important to mentioned that this bridging liquid addition method did produce a significant amount of fouling on both the FBRM and PVM probes. While the PVM probe could provide images that detail the mechanisms, fouling of the FBRM made it impossible to record any significant particle counts or size data for this method; especially during the agglomeration period.

4.3.2 Bridging liquid addition method 2 (BAM2)

Figure 4.3 shows the progression of Exp. 1 via BAM2 (i.e., bridging liquid is introduced into the system after the crystallization). It is important to note the difference in crystal morphology from this method versus the previous method. Due to benzoic acid's low solubility in water, the high supersaturation generated by solution addition leads to the formation of fine plate-like crystals and some minor agglomeration. As the bridging liquid is introduced, flocculation of the fine crystals around the bridging liquid droplets occurs. Flocculation is also referred to as the wetting phase in SC. This observation is a key difference between the BAM1 and BAM2. Flocculation was not observed in BAM1 because the droplets are stabilized prior to crystallization and nucleation and growth occurs with the droplet. As the particles grow out of the droplet, their surfaces contain bridging liquid so there is no wetting phase for BAM1. After the flocculation period, the system goes through a consolidation period where the agglomerates become much more compact and begin to take their spherical shape. The crystal morphology of this method (i.e., small plate-like crystals) most likely leads to the better compaction and sphericity observed in the PVM images. The consolidation phase also leads to the movement of bridging liquid from the agglomerate core to the surface, and ultimately, liberation into the continuous phase. Thus, further coalescence of agglomerates is observed. The consolidation and bridging liquid liberation phase leading to further coalescence can be observed in Figure 4.4. These results agree well with the empirical findings in early literature.[154,155,160] Figure

4.5 illustrates all the mechanisms involved in this method. The consolidation phase was also not observed for BAM1.

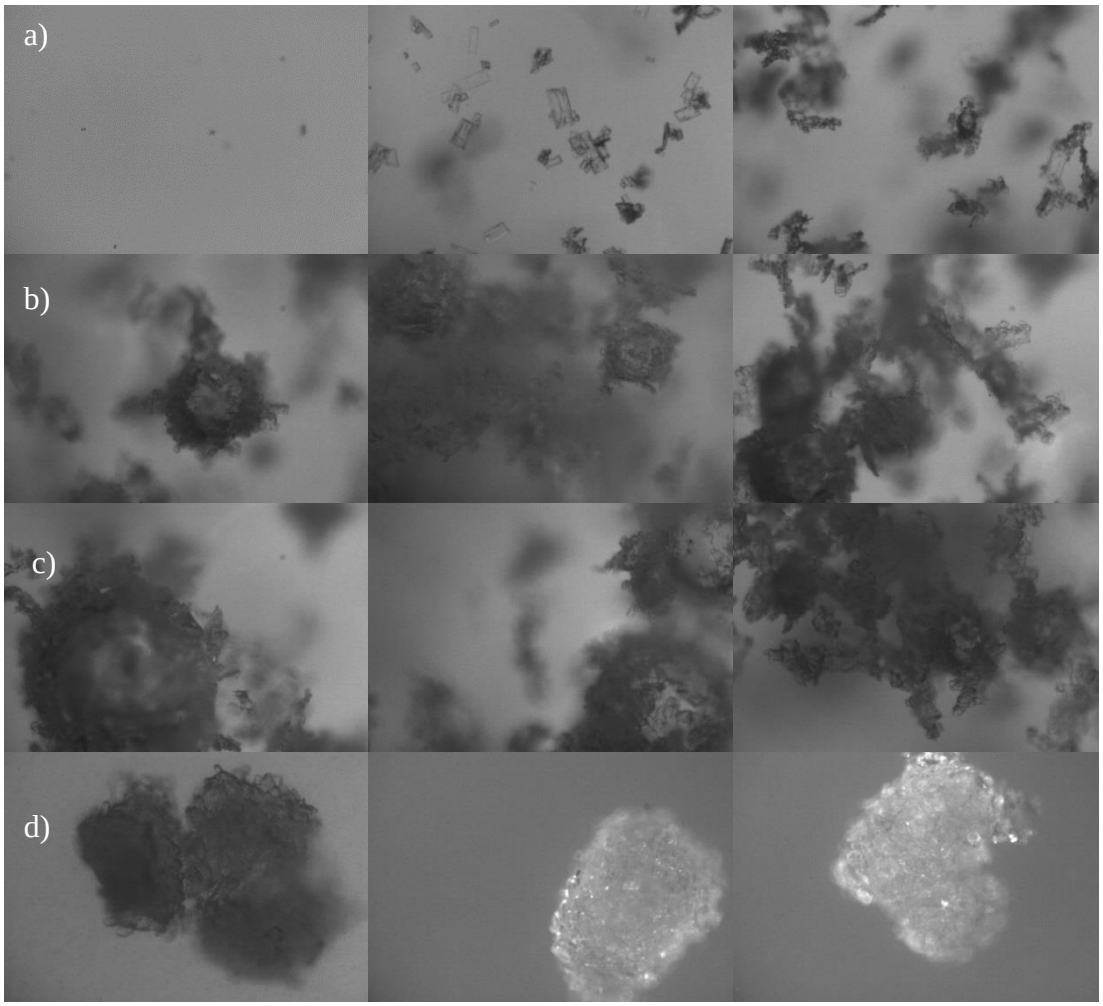

Figure 4.3 PVM images of BAM2 for Exp. 1 (a) crystallization (b) flocculation (c) consolidation (d) coalescence and completion

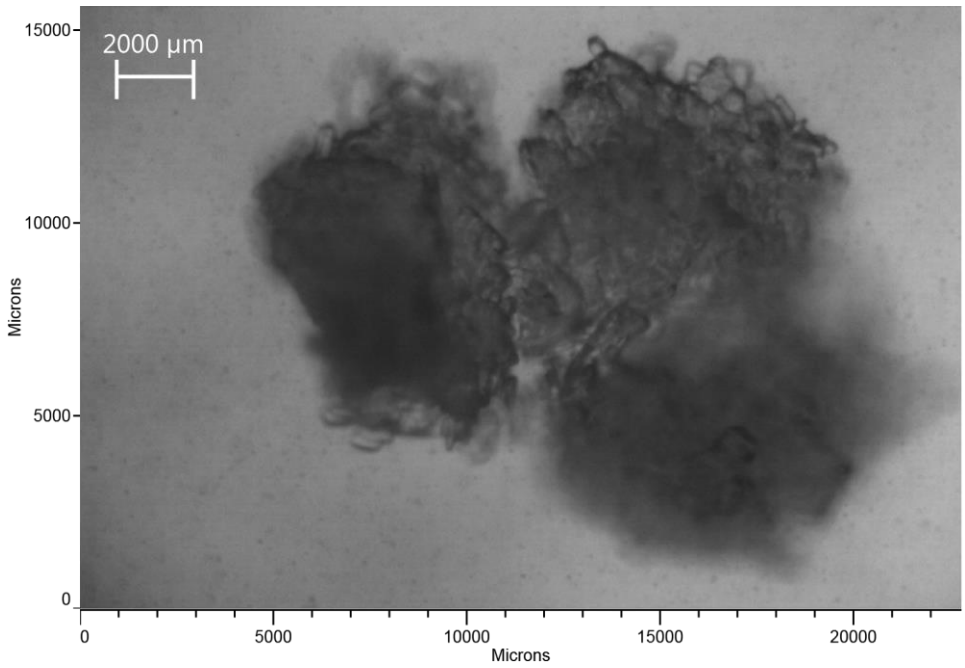

Figure 4.4 PVM of consolidation and agglomeration of multiple agglomerates and the liberation of bridging liquid droplets (Exp. 1)

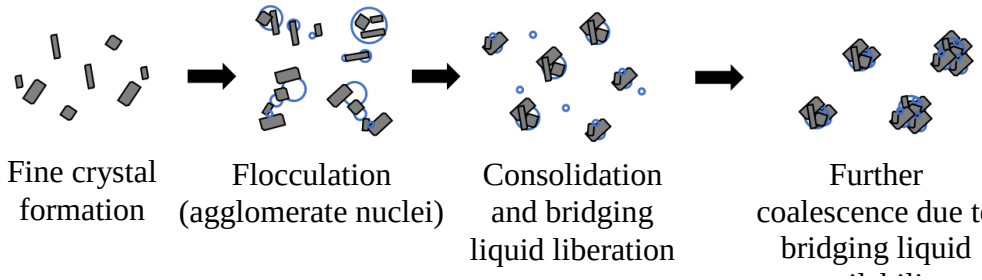

Figure 4.5 Schematic of agglomeration mechanism for BAM2

4.3.3 Bridging liquid addition method 3 (BAM3)

Figure 4.6 shows the progression of Exp. 1 via BAM3 (i.e., bridging liquid and solution are simultaneously introduced to anti-solvent). Here both very small crystals and droplets form at the onset. Although not entirely depicted in the images presented here, generally, the onset of the process includes a combination of crystals, crystals in droplet from ethanol-water emulsions, bridging liquid droplets, and bridging liquid droplets with crystals via immersion. However, the life span of droplets and emulsions are short and the process is governed by slow crystal growth that leads to long needle-like crystals, like BAM1. While the constituent particles are like those of BAM1, the final agglomerates have a much

different morphology. BAM3 results in elongated agglomerates that are not spherical in shape. This observation could be attributed to the significantly slower addition of bridging liquid for this method which results in agglomeration via layering of needle-like crystals as opposed to coalescence. Thus, the elongated agglomerates.

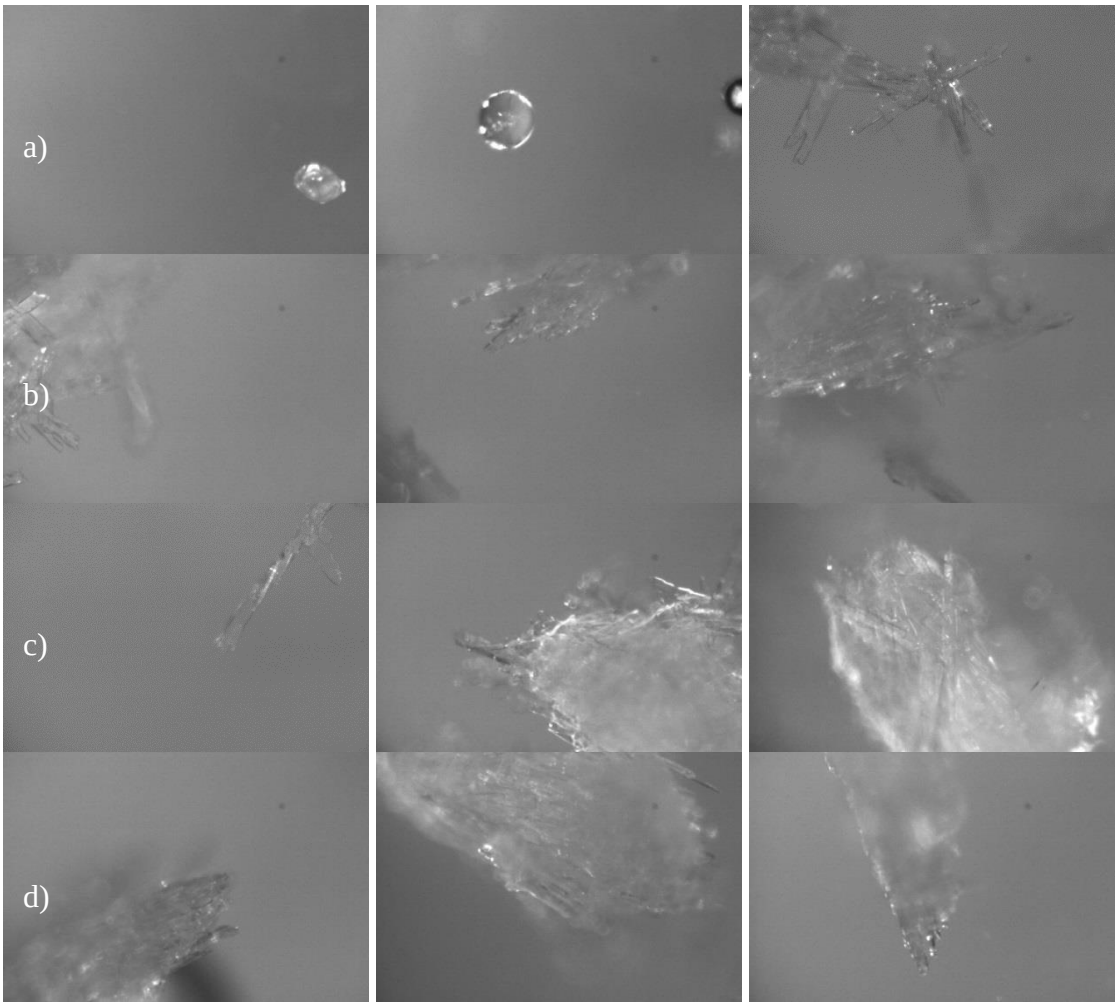

Figure 4.6 PVM images of BAM3 for Exp. 1 (a) droplet formation and crystallization (b) crystal growth and wetting (c) agglomeration via layering (d) completion

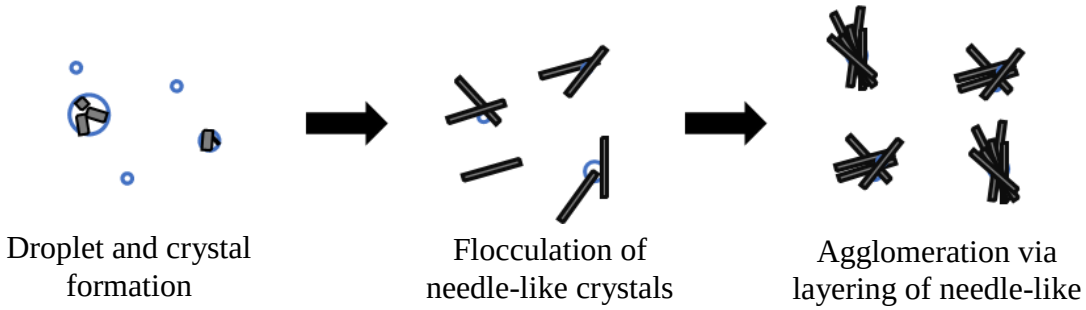

Figure 4.7 Schematic of agglomeration mechanism for BAM3

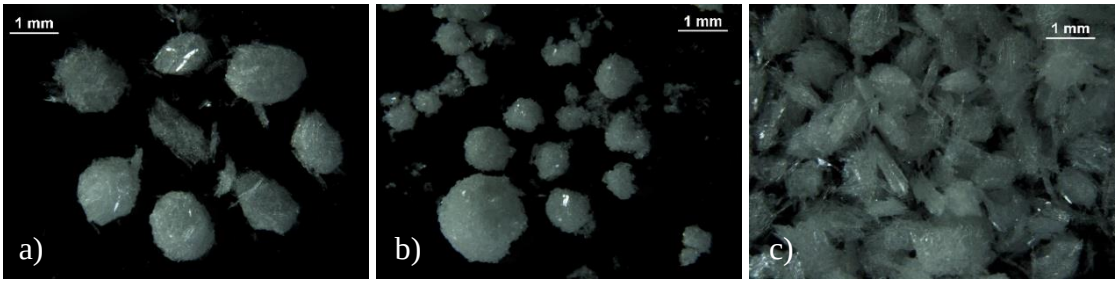

Figure 4.8 Offline images of agglomerates from Exp. 1 a) BAM1 b) BAM2 c) BAM3

Both BAM1 and BAM3 produce the same crystal morphology although the agglomeration mechanism ultimately differs. This observation is an indication that presence of the bridging liquid influences the crystallization process. The bridging liquid reduces the rate of supersaturation generation given that the bridging liquid increases the solubility of the system as appose to crystallizing with pure anti-solvent as with BAM2. Figure 4.7 illustrates the mechanisms involved in this method. Agglomerates from each method for experiment one are show in Figure 4.8. Given the elongated nature of the agglomerates produced via BAM3 (Figure 4.8c), this method was not considered for characterization.

4.3.4 Comparison of agglomerate properties from BAM1 vs BAM2

4.3.4.1 ASDs of BAM1 vs BAM2

Properties of spherical agglomerates from BAM1 and BAM2 were compared to assess how final product properties are effected by the bridging liquid addition method. Figure 4.9 shows the ASD for experiments 1, 4, 5 and 7. Aside from experiment 4, agglomerates made via BAM1 are shown to have broader and multi-nodal distributions. While agglomerates made via BAM2 have a uniform distribution with a long tail. These observations are a direct result of the difference in mechanisms between the two methods.

Agglomerates made via BAM1 are shown to have a fine agglomerate population and a large agglomerate population evidenced by the multi-nodes. The fine agglomerate population is likely a result of the size distribution of droplets formed at the beginning of the process. Smaller bridging liquid droplets that crystallize and coalesce with other smaller droplets lead to finer agglomerate formation. While large droplets can coalesce with larger

droplets to create very large agglomerates. Experiment 4 and 7 do not show significant fine agglomerate nodes nor very large agglomerate nodes, which suggests a more even distribution during droplet formation when compared to experiment 1 and 5. This could also suggest that the solvent composition (miscibility) and BSR of these experiments are optimal compared to the others. Except for experiment 4, agglomerates made via BAM1 also tend to be significantly larger than those of BAM2. Larger agglomerates can also be a result of the apparent larger constituent particles of BAM1 as evidence by the PVM images. Due to fouling of the FBRM for BAM1, this observation was difficult to quantify in terms of particle size. Lastly, since BAM1 did not show a consolidation mechanism, the mechanism could also be responsible for the very large agglomerate size.

Agglomerates made via BAM2 are shown to have a much smaller size distribution. This observation is due to the smaller constituent particles and the consolidation mechanism that follows the flocculation phase. The tailing displayed in the ASD of agglomerates made via BAM2 is a result of continued coalescence of agglomerates after the consolidation phase which liberates bridging liquid from the core to the surface of agglomerates (Figure 4.4). The small dark spots in the background of Figure 4.4 are liberated droplets.

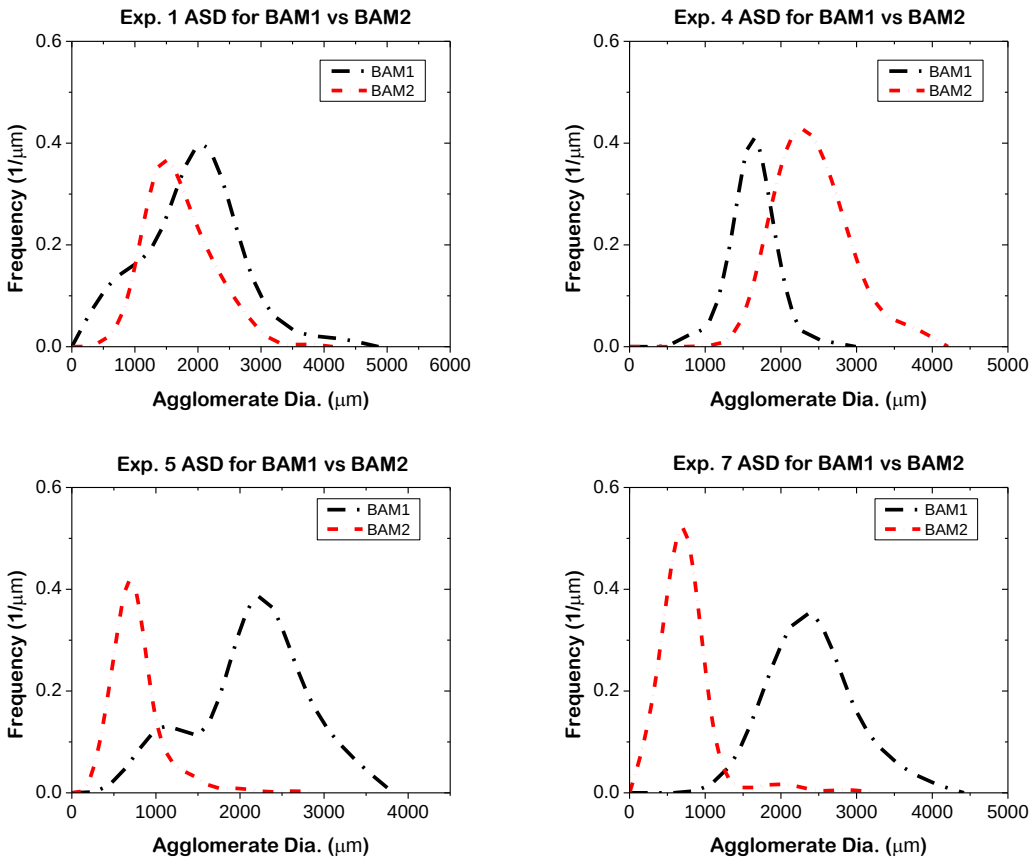

Figure 4.9 ASD of experiments 1,4, 5, and 7 for BAM1 and BAM2

4.3.4.2 Flow properties of BAM1 vs BAM2

Flow properties for agglomerates from both bridging liquid addition methods were also measured. The first set of flow studies were stability and variable flow. For stability studies using the FT4, the blade traverses downward through the particle bed at a set rotation speed for seven different tests (100 mm/s). The ratio of the energy required to traverse the particle bed during the seventh test to the energy required during first test is a measure of the stability of the particles. This ratio is called the Stability Index (SI). An SI = 1, or within the range 0.90 to 1.10, shows good agglomerate stability. As Figure 4.10a depicts, experiments 5 and 7 of BAM1 and experiments 2, 4, and 7 of BAM2 have acceptable stability. The rest display an SI below 0.90. The cause of instability is due to the de-agglomeration of the particles. Experiment 1 via BAM2 has a particularly low SI which can be attributed the de-agglomeration of large agglomerates into their primary agglomerates. As shown in Figure 4.4, BAM2 tends to over-agglomerate after the

consolidation phase due the liberation of bridging liquid. However, the liberated bridging liquid may be insufficient to create strong bonds between two agglomerates leading to de-agglomeration during flow studies.

For variable flow studies using the FT4, the blade traverses downward through the particle bed at decreasing rotational speeds for four different tests (100, 70, 40, 10 mm/s). The ratio of the energy required to traverse the particle bed during the fourth test to the energy required during the first test is called the Flow Rate Index (FRI), and is a measure of how sensitive the agglomerates are to being made to flow. An FRI between 1.5 and 3.0 displays average sensitivity to flow while an FRI = 1 is indicative of insensitivity to flow. As Figure 4.10b depicts, all experiments that display good stability also display average to low sensitivity to flow. This observation is typical of large particles and confirms the benefit of SC. For particles of low SI, particularly experiments 1 and 6 via BAM2, the FRI cannot be interpreted given the likelihood of de-agglomeration occurring.

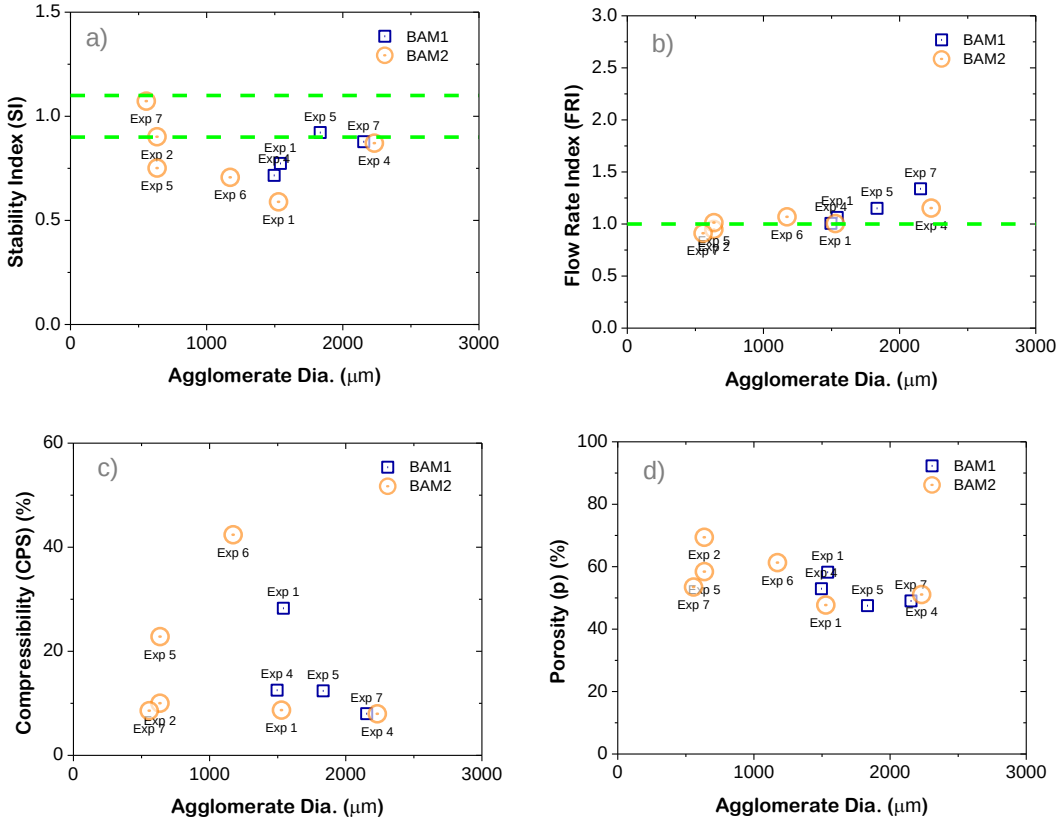

Figure 4.10 a) SI vs agglomerate dia., b) FRI vs agglomerate dia., c) CPS vs agglomerate dia., d) CPS vs p for agglomerates from BAM1 & BAM2

For compression studies using the FT4, a vented piston applies pressure the particle bed. The percentage in the height of the particle bed is Compression % (CPS). Figure 4.10c-d show the CPS vs agglomerate diameter and porosity (p) vs agglomerate diameter. For BAM1, CPS decreases with increase in agglomerate size. The decrease in CPS is related to the apparent increase in constituent particle size evidenced in PVM images. For BAM2, CPS increases as agglomerate size increases up to 1500 um. Larger agglomerates (>1500 um) display low compressibility. The low compressibility of smaller agglomerates (<1000 um) and larger agglomerates (>1500 um) is related to consolidation and continued coalescence mechanisms exhibited by this method. However, no significant or generalizable trends are observed between the CPS and agglomerate size for BAM2. For BAM1, the batch time could have impacted the compressibility as the compressibility decreases with increasing batch time for experiments 1, 4, 5 and 7. The porosity (p) was observed to decrease with increasing agglomerate size. Experiments of high porosity but low compressibility signal that the constituent particles are difficult to rearrange and are tightly packed even at high porosity. These results suggest the relationship in CPS and p are more likely correlated to the properties of the constituent particles. The following suggestions will focus on BAM2 and the relationship between primary crystal size and agglomerate properties.

4.3.5 Relationship between crystal CLD and ASD for BAM2

Understanding the relationship between the crystal size and agglomerate size is critical in optimizing a SA process for both crystal and agglomerate properties. Since BAM2 decouples crystallization and agglomeration, each mechanism can be studied separately and their effect on one another becomes more apparent. Figure 4.11a-b shows the chord length distributions (CLD) and square weighted mean chord length (SWMCL) of experiments 4,5, and 6 from the FBRM. For these experiments, the BA conc. of the solution feed is 0.25g/ml and SASR = 0.175, 0.35 and 0.50, respectively. Experiment 4 had the largest SWMCL and least number of particles in the CLD. At low SASR, as solution is added to the crystallizer the change in solubility as a function of SASR is not significant. Experiment 4, therefore, has much longer growth period than experiments 5 and 6. At higher SASR, like in experiments 5 and 6, as solution is feed into the crystallizer the

solubility increases rapidly and diminishes the supersaturation along with nucleation and growth. For this reason, as SASR increases the particle size decreases. Experiment 5 also exhibits the highest supersaturation likely driving the process towards nucleation and leading to a smaller SWMCL and higher counts. Figure 4.11c-d shows CLD and SWMCL of experiments 1,4, and 7. For these experiments, the SASR = 0.175 and BA conc. of the solution feed is 0.15, 0.25 and 0.375 g/ml, respectively. As the CLD depicts, the particle count increases significantly with increases BA conc. as expected. Experiment 7 with the highest BA conc. produced crystals of the smallest SWMCL. Experiment 4 produced larger crystals and higher counts than experiment 1 due to the faster depletion of supersaturation at the lower concentration of experiment 1 (0.15 g/mL).

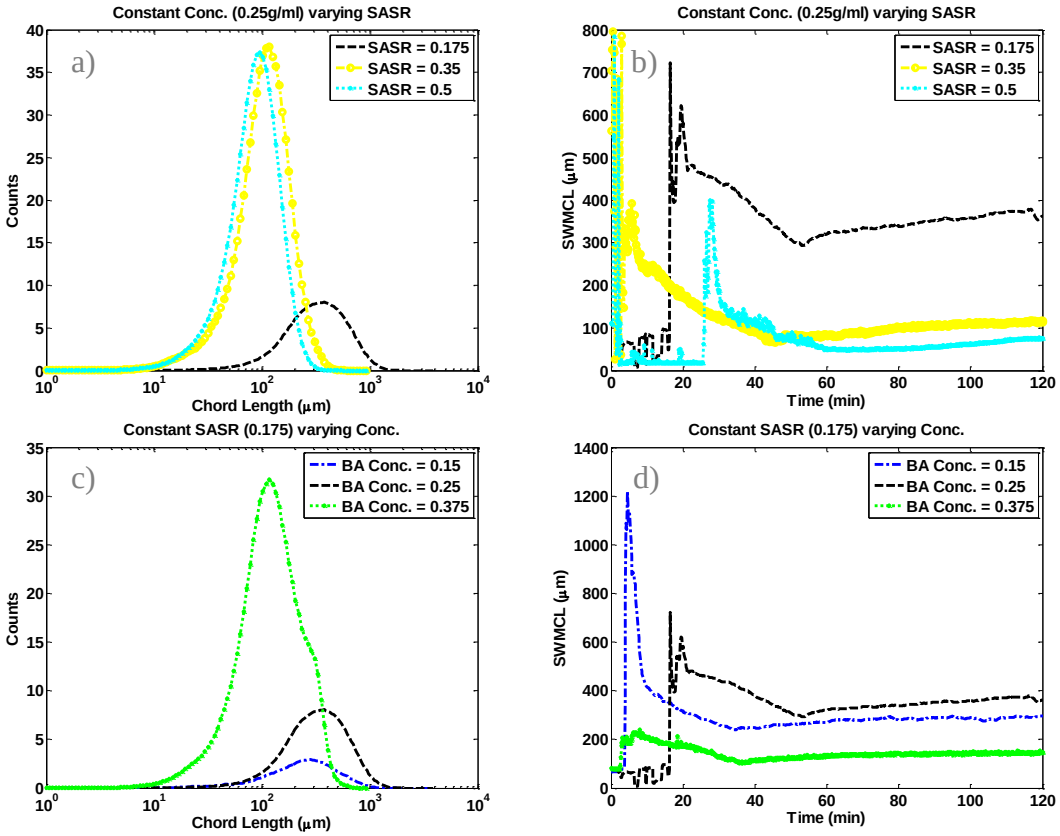

Figure 4.11 (a) CLD of Exp. 4, 5 and 6 and (b) SWMCL of Exp. 4, 5, and 6 for constant concentration (0.25 g/ml) with varying SASR. (c) CLD of Exp. 1, 4, and 7 and (d) SWMCL for constant SASR (0.175) with varying concentration.

With knowledge about the primary crystal properties from the crystallization process, an understanding of the relationship between primary crystal CLD and ASD can be

developed. Figure 4.12 shows the size distributions of the agglomerates for the experiments 4, 5, and 6 (constant concentration with varying SASR). As the figure shows, the experiments with the smallest primary crystal size produce agglomerate distributions with the smallest mean size. The experiment with the largest primary crystal size produced the agglomerates with the largest mean size. The images of agglomerates produced (Figure 4.13a-c) show a vast qualitative difference. The smaller agglomerates have less sphericity and appear to be less compact with evident void spaces. The larger agglomerates are of high sphericity and appear more dense/compact.

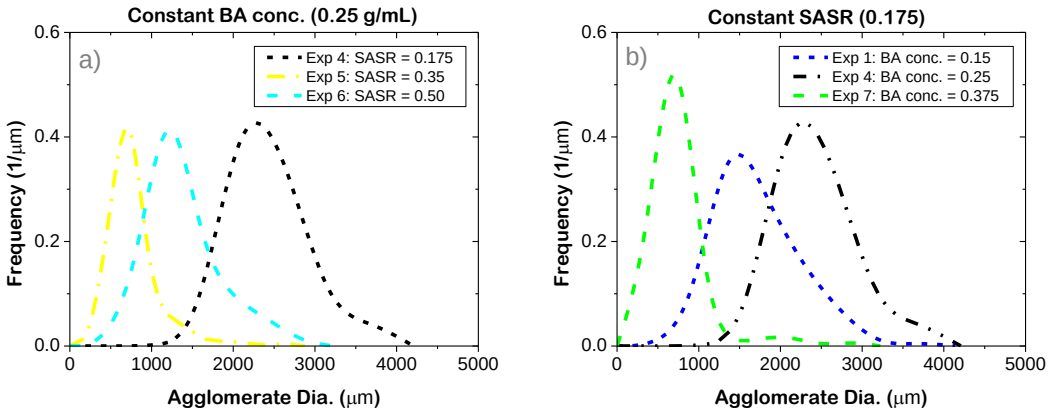

Figure 4.12 (a) ASD for constant BA conc. (0.25g/ml) and varying SASR (b) ASD for constant SASR (0.175) and varying BA conc.

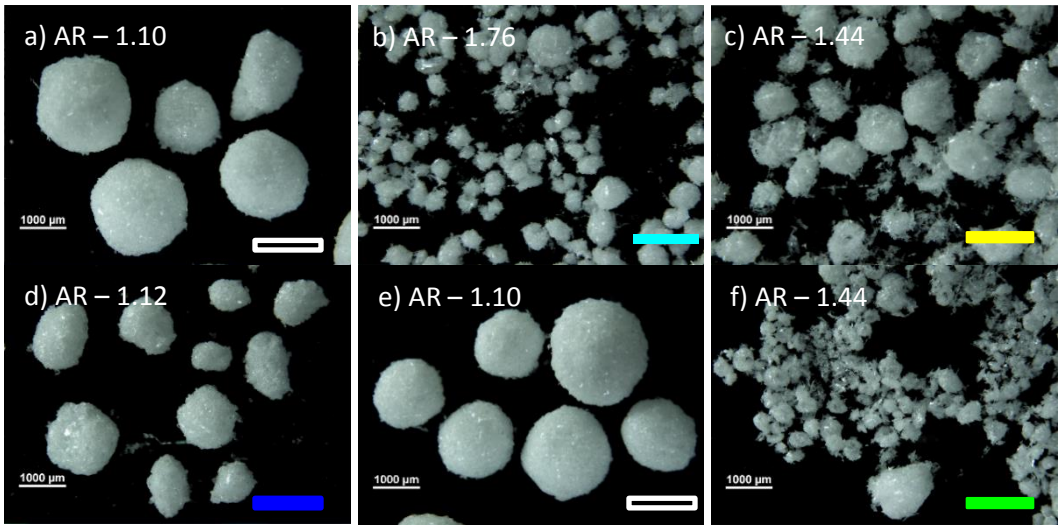

Figure 4.13 (top) Agglomerates corresponding to Exp. 4, 5, and 6 left to right (bottom) agglomerates corresponding to Exp. 1, 4, and 7 left to right.

Figure 4.13d-f shows the size distributions of the agglomerates for the experiments 1, 4, and 7 (constant SASR with varying concentration). The trend here is the same as previous scenario. The experiments that produced the smallest primary particles, produced the smallest agglomerates. The agglomerates show the same qualitative difference observed in the previous scenario. The smaller agglomerates have less sphericity and appear to be less compact with evident void spaces. The larger agglomerates also show higher sphericity and appear to more compact.

In comparing the spheres from Figure 4.12 and Figure 4.13, it is evident that the agglomeration efficiency is much better for experiments 1,4 and 7. This observation suggests that variations in the SASR affect the sphericity and agglomeration efficiency of the process. As the SASR increases, the miscibility of the bridging liquid increases and leads to a reduced amount of bridging liquid in the continuous phase. Therefore, the SASR effects the miscibility and operating point in the ternary (ethanol-water-toluene) phase diagram.

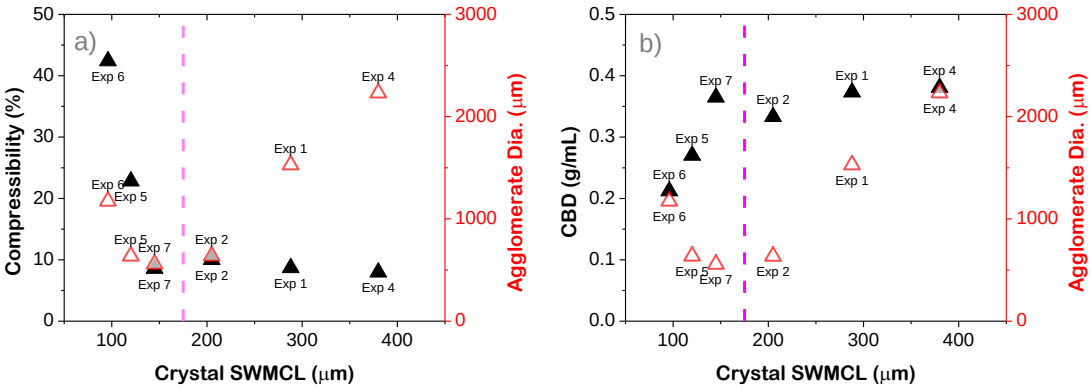

Figure 4.14 (a) Compressibility (CPS) % and (b) Condition Bulk Density (CBD) vs Crystal SWMCL and Agglomerate Dia.

Evaluating the performance properties of the agglomerates from BAM2 experiments shows a higher correlation with the size of the primary crystals as opposed to the agglomerate size. For example, Figure 4.14 shows the CPS and CBD vs Crystal SWMCL. Both figures can be divided up into two regions: primary crystals above and below 175μm. In the region below 175μm, as the primary crystal size increases the CPS and agglomerate size decrease while the CBD increases. From a mechanistic perspective, agglomerates in

this region undergo continued consolidation as primary crystal size increases, consolidating to a minimum CPS and agglomerate size and maximum CBD. In the region above 175μm, as the primary crystal size increases the CPS and CBD remain relatively constant while the agglomerate size continues to increase. From a mechanistic perspective, agglomerates in this region have reached a maximum consolidation leading to constant values in CPS and CBD as primary crystal size increases. However, as evidence in Section 3.2, the consolidation phase liberates bridging liquid which leads to continued coalescence and a larger agglomerate size. The results also suggest that as primary crystal size increases it becomes more difficult to compress and compact the resulting agglomerates. Smaller primary crystals have a greater ability to rearrange and compact during the consolidation phase as opposed to larger ones. These results provide a much clear picture than when only comparing performance with agglomerate size as in Figure 4.10. Moreover, it was observed in Figure 4.12 and Figure 4.13 that the sphericity increases with increase in primary crystal and agglomerate size. To further investigate to these differences in the agglomerate quality as a function of primary crystal size, the interaction between primary crystal size and bridging liquid droplet size is examined in the following section.

4.3.6 Interaction between crystals and bridging liquid droplets

To understand the influence of bridging liquid droplet size and primary crystal size on the final agglomerate size some experiments from Table 4.1 use BAM2 were run for bridging liquid droplet only scenarios. The experimental conditions were the same except without the crystallization process. Bridging liquid was fed to an ethanol-water mixture at the appropriate BASR and the resulting droplets were measured by an FBRM. Figure 4.15a-b shows the CLD for both crystals and droplets from experiments 1 and 4. The crystal SWMCL for these experiments were 288μm and 380μm, respectively, while the droplet SWMCL was 49μm. In both scenarios, the bridging liquid droplet SWMCL was at least 5X smaller than the primary crystal SWMCL. The resulting agglomerates from both experiments are very large and qualitatively show excellent agglomeration efficient, sphericity, and compaction (Figure 4.13a, d-e). Figure 4.15c-d shows the CLD for both crystals and droplets from experiments 5 and 6. The crystal SWMCL for these experiments were 121μm and 96μm, respectively, while the droplet SWMCL for each was 58μm and

50µm. In both scenarios, the bridging liquid droplet SWMCL was close to 2X smaller than the primary crystal SWMCL. The resulting agglomerates from both experiments are much smaller, less spherical and appear to be less compact (Figure 4.13b-c, f).

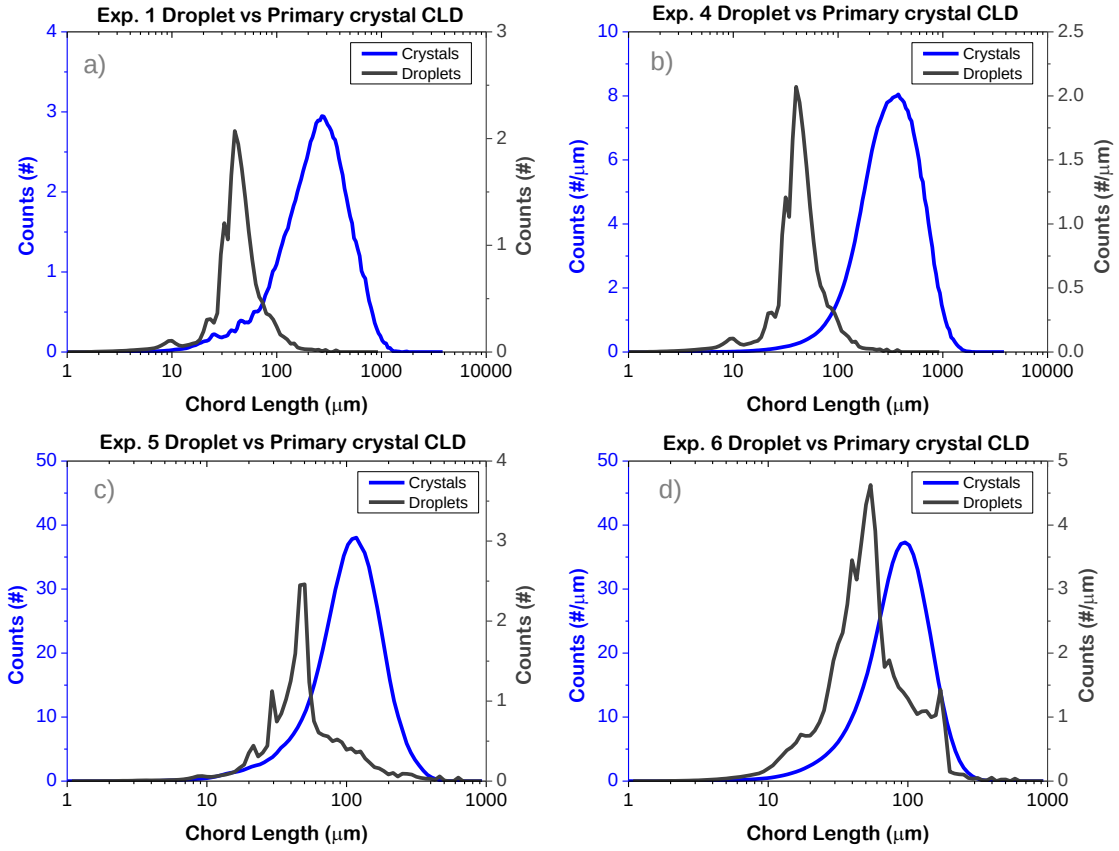

Figure 4.15 Crystal vs Droplet CLD from a) Exp. 1, b) Exp. 4, c) Exp. 5, and d) Exp. 6

The results here reveal the critical relationship between the primary crystal and bridging liquid droplet. As the ratio between crystal SWMCL and droplet SWMCL decreases the crystal-droplet interaction goes from distributive to immersive. The difference in crystal-droplet interaction is responsible for the CPS, P and CBD differences observed in Figure 4.10 and Figure 4.14. Experiments 5 and 6 showed much higher CPS and P compared to experiments 1 and 4. In Figure 4.14, Experiments 1 and 4 show a higher CBD compared to experiments 5 and 6. The images shown in Figure 4.13 qualitatively back these findings. Ratios of crystal to droplet SWMCL for four experiments (Exp. 1, 4, 5 and 6) are given in Table 4.2. For benzoic acid, the critical crystal to droplet size ratio (CPSR) is suggested to CPSR = 4. For a distributive crystal-droplet interaction, the crystal size should be at least 4X greater than the droplet size. For an immersive interaction, the

crystal size should be less than 4X the droplet size. Due to the polydispersity of both crystals and droplets of the droplets, it is likely that both immersive and distributive mechanisms occur at the same time. However, at the suggested CPSR one mechanism will be significantly more dominant than the other. The droplet experiments in this study did not differ significantly in SWMCL given the constant feed and agitation rates. These parameters can be adjusted to further reduce/increase the droplet size.

Table 4.2: Crystal vs bridging liquid droplet mean size

Exp.	Crystal SWMCL	Droplet SWMCL	Ratio	Resulting Agglomerate
1	288	49	5.9	Large, spherical, compact
4	380	49	7.8	Large, spherical, compact
5	120	58	2.1	Small, irregular, loose
6	96	50	1.9	Small, irregular, loose

4.4 Conclusions

This study uses PAT tools to provide insight and knowledge of the different phases of SC. Different bridging liquid addition methods were studied to assess how the agglomeration period differs for each bridging liquid incorporation method. BAM1 undergoes an emulsion dispersion and stabilization phase followed by crystallization of needle-like particles within the droplets. Once the particles grow in length, they breakout of the droplet and begin to coalescence other particles. BAM2 undergoes a wetting phase post crystallization. The wetting phase is characterized by the flocculation of particles. The flocs then go through a consolidation phase forms agglomerates and liberates bridging liquid to the surface of the agglomerate. The newly available bridging liquid then promotes continued coalescence. BAM3 undergoes simultaneous emulsion formation and crystallization. Due to the slow bridging liquid feed, this method undergoes a layering type of agglomeration mechanism that results in elongated agglomerates. Spherical crystallization via crystallization followed by agglomeration (BAM2) proved to be the most robust in terms of successfully producing spherical agglomerates as well as flow properties. This study also clearly outlines the role of droplet size and primary crystal size in the final agglomerate size. A critical crystal to droplet size ratio was established to

determine whether a crystal-droplet interaction would be dominated by an immersive or distributive mechanism.

5. MODELING AND OPTIMIZATION OF SPHERICAL AGGLOMERATION IN SUSPENSION THROUGH A COUPLED POPULATION BALANCE MODEL

This chapter is reprinted with minor modification with permission from Peña, R., Burcham, C. L., Jarmer, D. J., Ramkrishna, D., & Nagy, Z. K. (2017). *Chemical Engineering Science, 167*, 66–77.

5.1 Introduction

Since its introduction, the PBM has been widely used and accepted as the model formulation method for simulation and prediction of the size distribution and other properties of particulate systems.[83,174] PBMs allow for systems that include any or all of the following mechanisms: nucleation, growth, breakage and agglomeration. Following the initial work by Smoluchowski[175] (1917) on the rate of aggregation for spherical particles, there have been many contributions for systems that exhibit agglomeration including dispersion (bubble) coalescence[176,177], granulation[178,179] and particle aggregation during crystallization.[165,180,181] The shared limitation in the models between many of the previous studies is the loss of information of constituent particles. This limitation presents obstacles in the estimation of the kinetic parameters (nucleation and growth rate vs agglomeration rate) and in developing an understanding of the influence of process conditions on each in population (constituent particles vs agglomerates). Having information regarding the constituent particles would allow for improved particle design through more accurate parameter estimation, simulation, optimization, and control; particularly for the increasingly popular technique of agglomeration in suspension.

Agglomerating fine particles in suspension, using a bridging liquid, to improve particle properties and downstream process efficiency has been known since the late 1960s. Initially the technique was used mostly in bulk chemical industries (e.g., coal beneficiation[162]). Since then agglomeration in suspension techniques have been geared

towards application in the pharmaceutical industry to improve filtration and downstream processing of APIs during crystallization by eliminating granulation and milling unit operations.[27,28,29] In this respect the technique is often referred to as SC. Interest in the application of SC in pharmaceutical processes has increased through the continued development and understanding of the operating conditions[22,30,123], choice of binding agent[26], kinetics[152] and mechanisms[28,137,139,143] that govern experimental outcomes. Peña and Nagy[130] studied and showed the benefits of SC as a PI technique, whereby both internal (primary crystals) and external (agglomerates) properties can be controlled experimentally through a decoupled CSC approach; providing the means by which both biopharmaceutical (bioavailability, dissolution) and manufacturing (flowability, filtration, drying) properties can be simultaneously adapted to meet desired quality specifications. This technique opens the door for combined experimental and modeling approaches for the optimization and control of both the primary crystal and agglomerate properties in SC processes. However, many of the PBMs currently in literature would fail to accomplish this because of the limitations and loss of constituent particle information.

The limitations in previously developed PBMs are related to the complex crystallization phenomena occurring during SC processes. For previous models, agglomeration was either an incidental process occurring along with nucleation and growth during crystallization or the main process occurring in seeded or seed-fed systems with negligible nucleation and growth. This allowed for empirical agglomeration models often independent of system properties and solely dependent on fitting to experimental data.[182] The models are limited in accuracy, very system dependent and have difficulty capturing all the influencing process parameters on the system. Moreover, they only take into consideration the evolution of the agglomerates and not that of the constituent primary crystals. As previously mentioned, from the mechanistic point of view there are numerous studies in the literature that propose agglomeration mechanisms. However, there has yet to be a comprehensive correlation between the proposed mechanisms of SC, which include nucleation, growth and agglomeration, and the appropriate agglomeration kernel. This has largely been influenced by the inherit loss of information in the PBMs and the lack of PAT tools to help determine and validate proposed mechanisms.[17]

Bemer (1979) was one of the first to study agglomeration in suspension from both an experimental and modeling approach.[154] His work led to further implementations of combined experimental and modeling studies. David et al. (2003) developed a multi-layer agglomeration model that considers the efficiency of agglomeration based on the collision mechanism (i.e., Brownian, laminar, or turbulent).[167] As particles change in size their collision mechanism or flow field can change from Brownian to laminar to turbulent, as particle size increases. In their model, the kernel accounted for changes in the collision mechanism and was also a function of the supersaturation and temperature through the growth rate which was used as the efficiency term. It is known that agglomeration is enhanced by inter-particle growth or agglomerative bond formation; when supersaturation increases the subsequent inter-particle growth between two particles that come in contact increases allowing for higher agglomeration efficiency.[37] Madec et al. (2003) simplified the agglomeration model by incorporating a more relevant process parameter into the kernel, specifically their work accounted for the composition of bridging liquid in an agglomerate.[161] It has been shown that there is a critically optimal range for the ratio of bridging liquid to solute volume (BSR); below or above this critically optimal range would produce loosely compacted agglomerates or paste-like amorphous agglomerates, respectively.[27,137,139] This unique incorporation of the bridging liquid composition served as the efficiency term by which the process would reach equilibrium.

The most comprehensive study in this area is that of Blandin et al. (2005) In this combined experimental and modeling study, key aspects of agglomeration in suspension are noted:

(i) The agglomeration mechanism is a three-step process; a) bridging liquid droplets capture solid particles and form agglomerate nuclei, b) compaction of the agglomerate nuclei due to collisions with other particles causes a rapid decrease in the mean diameter, c) growth and consolidation then occur due to the hydrodynamics and process conditions of the system (i.e., collisions, BSR),

(ii) Agglomeration is only efficient in the critical BSR range; the agglomerate size increases with a strong dependence on BSR, weak dependence on solids concentration and inverse dependence on agitation rate,

(iii) Porosity decreases as mean diameter reaches equilibrium.

(iv) Agglomeration stops once the agglomerates become too compact to deform.[111]

Based on these fundamental experimental observations an agglomeration model considering the size and concentration of the agglomerating particles, with the agglomeration kernel expressed as a function of the *meeting probability* and agglomeration efficiency of the process, was developed. The meeting probability was described by a function of the target efficiency, agglomerate sizes, and collision velocity.[164] The simulations from this work agreed with experimental data when the necessary parameters were fit to the data. By identifying the critical experimental mechanisms, Blandin et al. (2005) could develop a comprehensive model that accounted for both the mechanistic phenomena (e.g., deformability, collision efficiency, and compaction) and process conditions (e.g., energy dissipation, BSR, primary particle size). Although this model showed significant superiority over many others observed in the literature, it still has the limitation of losing the information of the constituent particles. Moreover, the model relies on the assumption that the initial particles participating in the agglomeration are monodispersed. Table 5.1 summarizes various kernels found in the literature used for agglomeration in suspension modeling with r defined as the radius of the particle and is interchangeable with the characteristic length.

Table 5.1 Common agglomeration kernels

Size-independent	K_a
Product	$K_a(L_i L_j)^3$
Sum	$K_a(L_i^3 + L_j^3)$
Brownian[175]	$K_a \frac{(L_i + L_j)}{(L_i * L_j)}$
Shear	$K_a(L_i + L_j)^3$
Modified Shear	$K_a \alpha_{i,j}(L_i + L_j)^3$
Turbulent	$K_a(L_i + L_j)^2 \sqrt{\overline{U_i^2} + \overline{U_j^2}}$
Zauner and Jones[183]	$5.431 * 10^{-17}\left(1 + 2.29\varepsilon^{\frac{1}{2}} - 2.429\varepsilon\right)S^{2.15}$
Madec et al. (2003)[161]	$K_a(L_i^3 + L_j^3)\left((c_i + c_j)^{\alpha}\left(100 - \frac{c_i + c_j}{2}\right)^{\delta}\right)^{\alpha}$
Blandin et al. (2005)[111,164]	$K_a = f(L_i, L_j, t)eff(L_i, L_j, t)$

To overcome the issues of loss of information a coupled PBM formulation is required. A coupled PBM formulation could simultaneously tracks the evolution of the primary crystals and the evolution of the agglomerates. The relationship between primary crystal properties and their effect on final agglomerate properties would thereby be more evident and more efficient than in traditional approaches. To the best of our knowledge, the only previous work that presented this approach is that of Ochsenbein et al. (2015).[169] In their study, Ochsenbein et al. (2015) focused on the agglomeration of needle-like crystals in suspension. Through a coupled PBM framework Ochsenbein et al. (2015) could develop a PBE to describe the evolution of the primary crystals by a two-dimensional growth rate to represent the needle like structure of the crystal. Then another PBE was used to describe the evolution of the agglomerates as a function of the primary crystals. For the agglomeration kernel, they derived their own modified kernel that included both characteristic lengths of the primary crystals participating in the agglomeration. The new PBM formulation also allowed for the development of new parameters that add value to the simulations due to their experimental relevance. However, the work of Ochsenbein et al. (2015) neglected nucleation, something common to previously developed PBMs with agglomeration. The coupled PBM framework will be extended herein.

The contribution of this work is the extension of the coupled PBM framework for application in the simulation and optimization of an agglomeration in suspension system. A coupled PBM framework has been developed for a semi-batch, reverse addition, anti-solvent crystallization system with agglomeration. Reverse addition anti-solvent crystallization techniques entail the addition of solution to the anti-solvent. The technique is carried out for low SASR to produce very fine crystals due to very high supersaturation generation. The system includes nucleation and growth of primary crystals and subsequent agglomeration. The purpose of the work is to exploit the advantages presented by a coupled PBM framework; for example, the ability to optimize for specific primary and agglomerate sizes. This presents an opportunity to find optimal operating conditions that meet both bioavailability and manufacturability demands. It also allows for the ability to develop a first principles based parameter for agglomeration efficiency and a first principles based

estimate for porosity. Additionally, through the retention of the information of the primary particles, the interplay between the effects of operating conditions on the properties of the primary crystals versus the agglomerates will be clear.

5.2 Model development for agglomeration in suspension

Modeling the agglomeration in suspension system is decomposed into three populations: all primary crystals, un-agglomerated crystals and agglomerates. The system of coupled PBEs will be coupled with a mass balance equation to enable the modeling of the CSD properties and ASD properties simultaneously. The model will allow us to relate the CSD and ASD properties to micromeritic properties (e.g., porosity and agglomeration efficiency). The PBM will incorporate nucleation, growth and agglomeration mechanisms. This coupling allows for a PBE that describes the entire primary crystal population whether part of an agglomerate or not. However, the PBE does not track the location of the primary crystals. The inability to track the location of the primary crystals creates a difficulty in assessing the exposure of each individual crystal to supersaturated fluid; especially, once it is incorporated into an agglomerate. Hence, for simplicity, it is assumed that primary crystal growth rate is independent of its in environment (i.e., particles partaking in agglomeration have the same growth kinetics as particles remaining in suspension). This assumption is a limitation of the model but studies the literature have shown that agglomerate strength is dependent on supersaturation of the system due to growth of crystals within an agglomerate (agglomerative bond).[37]

The set of PBEs are as follows:

$$\frac{\partial}{\partial t}[V(t)n_{tc}(x,t)] = -\frac{\partial}{\partial x}\big(G(x)V(t)n_{tc}(x,t)\big) + \delta(x)V(t)B \qquad 5.1$$

In equation 5.1, $n_{tc}(x,t)$ is the volumetric number density (no. m^{-4}) representing the primary crystals in the system; regardless of whether the crystal is part of an agglomerate or not (total crystals). G (m s^{-1}) is the growth rate, B (no. $m^{-3}s^{-1}$) is the nucleation rate, $\delta(x)$ (m^{-1}) is the Dirac delta function, and $V(t)$ (m^3) is the suspension volume. x (m) represents the characteristic length and t is the batch time.

$$\frac{\partial}{\partial t}[V(t)n_{cs}(x,t)] = -\frac{\partial}{\partial x}\big(G(x)V(t)n_{cs}(x,t)\big) + \delta(x)V(t)B - D_{cs,agg}(x) \qquad 5.2$$

$$D_{cs,agg}(x) = V(t)n_{cs}(x,t)\int_0^{\infty}\beta(x,\lambda)n_{ca}(\lambda,t)d\lambda \quad 5.3$$

In equation 5.2, $n_{cs}(x,t)$ is the volumetric number density (no. m^{-4}) representing the un-agglomerated crystals (crystals in suspension). This equation differs from the first equation by the third term ($D_{cs,agg}(x)$ (no. m^{-1}s^{-1})) which represents the death (disappearance) of crystals due to agglomeration (equation 5.3). The death of crystals can occur through crystal agglomeration with other crystals or agglomerates. This is denoted by the volumetric number density $n_{ca}(\lambda,t)$ (no. m^{-4}) which represents both crystals and agglomerates of a characteristic size λ. In equation 3, $\beta(x,\lambda)$ represents the agglomeration rate (m^3 no.$^{-1}$s^{-1}) of a particle of characteristic size x with a particle of characteristic size λ.

$$\frac{\partial}{\partial t}[V(t)n_a(x,t)] = -\frac{\partial}{\partial x}\big(G(x)V(t)n_a(x,t)\big) + B_{a,agg}(x) - D_{a,agg}(x) \quad 5.4$$

$$B_{a,agg}(x) = \frac{x^2}{2}\int_0^{x}\frac{\beta\left(\left(x^3-\lambda^3\right)^{1/3},\lambda\right)n_{ca}\left(\left(x^3-\lambda^3\right),t\right)V(t)n_{ca}(\lambda,t)}{\left(x^3-\lambda^3\right)^{2/3}}d\lambda \quad 5.5$$

$$D_{a,agg}(x) = V(t)n_a(x,t)\int_0^{\infty}\beta(x,\lambda)n_{ca}(\lambda,t)d\lambda \quad 5.6$$

In equation 5.4, $n_a(x,t)$ is the volumetric number density (no. m^{-4}) representing the agglomerates produced from the birth ($B_{a,agg}(x)$ (no. m^{-1}s^{-1})) and death ($D_{a,agg}(x)$ (no. m^{-1}s^{-1})) of agglomerates from crystal-agglomerate and agglomerate-agglomerate agglomeration. $\beta(x,\lambda)$ is the same as the term in equation 5.3 and represents the agglomeration rate. It is important to note that traditionally the agglomeration birth and death terms are expressed with volume as the internal coordinate. However, since all the other mechanisms are expressed with respect to characteristic length a modification is made to express this in terms with respect to characteristic length following modification steps from the literature.[12,85,88] Equations 5.2 and 5.4 are coupled through equation 5.7.

$$n_{ca}(x,t) = n_{cs}(x,t) + n_a(x,t) \quad 5.7$$

Equation 5.7 is simply the addition of the un-agglomerated crystals and the agglomerates denoted by the number density function $n_{ca}(x,t)$ (no. m^{-4}). This combined population is used to account for crystal-crystal and crystal-agglomerate interactions and reduce the number of terms in the birth and death terms in equations 5.1-5.6. Equation 5.1 is intentionally made to stand alone based on the assumption of uniform kinetics for all

populations tracked in the system. The set of equations will all be coupled by the mass balance which will ultimately determine nucleation and growth kinetics.

5.3 Solution method

Most of the SC systems in literature are semi-batch with limited modeling work. For this reason, a semi-batch system with combined cooling and reverse addition anti-solvent is modeled. To account for the volume change in a semi-batch system the number density functions are expressed as a redefined number density ($\tilde{n}(x,t) = V(t)n(x,t)$).[15,184] The modified PBM will be as follow:

$$\frac{\partial}{\partial t}\tilde{n}_{tc}(x,t) = -\frac{\partial}{\partial x}\big(G(x)\tilde{n}_{tc}(x,t)\big) + \delta(x)V(t)B \quad 5.8$$

$$\frac{\partial}{\partial t}\tilde{n}_{cs}(x,t) = -\frac{\partial}{\partial x}\big(G(x)\tilde{n}_{cs}(x,t)\big) + \delta(x)V(t)B - \widetilde{D}_{cs,agg}(x) \quad 5.9$$

$$\frac{\partial}{\partial t}\tilde{n}_{a}(x,t) = -\frac{\partial}{\partial x}\big(G(x)\tilde{n}_{a}(x,t)\big) + \tilde{B}_{a,agg}(x) - \widetilde{D}_{a,agg}(x) \quad 5.10$$

$$\tilde{n}_{ca}(x,t) = \tilde{n}_{cs}(x,t) + \tilde{n}_{a}(x,t) \quad 5.11$$

$$\widetilde{D}_{cs,agg}(x) = \tilde{n}_{cs}(x,t)\int_0^{\infty}\beta(x,\lambda)\tilde{n}_{ca}(\lambda,t)d\lambda \quad 5.12$$

$$\tilde{B}_{a,agg}(x) = \frac{x^2}{2}\int_0^{x}\frac{\beta\Big(\big(x^3-\lambda^3\big)^{1/3},\lambda\Big)\tilde{n}_{ca}\Big(\big(x^3-\lambda^3\big),t\Big)\tilde{n}_{ca}(\lambda,t)}{\big(x^3-\lambda^3\big)^{2/3}}d\lambda \quad 5.13$$

$$\widetilde{D}_{a,agg}(x) = \tilde{n}_{a}(x,t)\int_0^{\infty}\beta(x,\lambda)\tilde{n}_{ca}(\lambda,t)d\lambda \quad 5.14$$

The above set of PBEs can be solved using the QMOM approximation for the redefined moments. [12,85,88,185]

$$\tilde{\mu}_k = \int_0^{\infty}x^k\tilde{n}(x,t)dx \approx \sum_{i=1}^{N}w_i{L_i}^k \quad 5.15$$

The quadrature approximation transformed set of PBEs can be written as:

$$\frac{d\tilde{\mu}_{tc,k}}{dt} = k\sum_{i=1}^{N}w_{tc,i}L_{tc,i}^{k-1}G(L_{tc,i}) + \delta(k)V(t)B \quad 5.16$$

$$\frac{d\tilde{\mu}_{cs,k}}{dt} = k\sum_{i=1}^{N}w_{cs,i}L_{cs,i}^{k-1}G\big(L_{cs,i}\big) + \delta(k)V(t)B - \widetilde{D}_{cs,agg}\big(w_{ca,i},L_{ca,i},w_{cs,i},L_{cs,i},k\big) \quad 5.17$$

$$\frac{d\tilde{\mu}_{a,k}}{dt} = k\sum_{i=1}^{N}w_{a,i}L_{a,i}^{k-1}G(L_{a,i}) + \tilde{B}_{a,agg}\big(w_{ca,i},L_{ca,i},k\big) - \widetilde{D}_{a,agg}\big(w_{ca,i},L_{ca,i},w_{a,i},L_{a,i},k\big) \quad 5.18$$

$$\widetilde{D}_{cs,agg}\left(w_{ca,i}, L_{ca,i}, w_{cs,i}, L_{cs,i}, k\right) = \sum_{i=1}^{N} w_{cs,i} L_{cs,i}^{k} \sum_{j=1}^{N} w_{ca,j} \beta(L_{cs,i}, L_{ca,j}) \quad 5.19$$

$$\tilde{B}_{a,agg}\left(w_{ca,i}, L_{ca,i}, k\right) = \frac{1}{2} \sum_{i=1}^{N} w_{ca,i} \sum_{j=1}^{N} w_{ca,j} \left(L_{ca,i}^{3} + L_{ca,j}^{3}\right)^{\frac{k}{3}} \beta(L_{ca,i}, L_{ca,j}) \quad 5.20$$

$$\widetilde{D}_{a,agg}\left(w_{ca,i}, L_{ca,i}, w_{a,i}, L_{a,i}, k\right) = \sum_{i=1}^{N} w_{a,i} L_{a,i} \sum_{j=1}^{N} w_{ca,j} \ \beta(L_{a,i}, L_{ca,j}) \quad 5.21$$

$$\tilde{\mu}_{ca,k} = \tilde{\mu}_{cs,k} + \tilde{\mu}_{a,k} \quad 5.22$$

The set of PBEs is solved with the product difference (PD) algorithm and the number of quadrature points used is $N = 3$ which solves for the weights (w_i) and abscissas (L_i). Details regarding the PD algorithm can be found in the literature.[84,86,185] Matlab ® *ode15s* is used to solve the set of ODEs.

5.4 Mass balance and kinetics

The mass balance equations used in the model for the semi-batch reverse addition anti-solvent crystallization of benzoic acid is derived as:

$$\frac{dV}{dt} = F_s \quad 5.23$$

$$\frac{dC_S}{dt} = \frac{(C_{BA_0} - C_S)}{V} F_s - \frac{3\rho_c k_v G \tilde{\mu}_{tc,2}}{V} \quad 5.24$$

$$\frac{dx_{SASR}}{dt} = \frac{F_s}{V_0} \quad 5.25$$

$$M = \frac{\rho_c k_v \tilde{\mu}_{tc,3}}{V} \quad 5.26$$

where V(mL) is the volume of mother liquor mixture, F_s (mL min^{-1}) is the flow rate of solution being added to the system, C_S (g mL^{-1}) is the solute (benzoic acid) concentration, C_{BA_0} (g mL^{-1}) is the solute concentration in the solution being fed, and x_{SASR} is the solution to anti-solvent ratio. In equation 5.24, ρ_c is the density of the crystal and k_v is the shape factor and are fixed at 1.316 (g mL^{-1}) and 0.524, respectively. For simplicity, it is assumed that the solvent mixture density change is negligible. M(g/mL) represents the magma density of the slurry.

The nucleation and growth rate kinetics for traditional anti-solvent crystallization of benzoic acid were used for this study and taken from the literature.[186]

$$B = k_b(\mathcal{N})(1 + i * M)(S - 1)^{b(\mathcal{N})} \quad 5.27$$

$$G = k_g(\mathcal{N})(S-1)^{g(\mathcal{N})} \quad 5.28$$

$$S = \frac{C_S}{C_{sat}} \quad 5.29$$

Here the nucleation and growth kinetics depend on supersaturation, S, (which is generated by changes in the $\mathcal{SASR}$ and temperature) and agitation rate, $\mathcal{N}$. The variable i is an empirical parameter that influences the extent to which a system is driven by primary or secondary nucleation. The i parameter is not given in the reference and hence will be used to do a parameter study on the effect of secondary nucleation on the results of the model formulation. The dependence of the rate constants on the agitation rate is shown in Table 5.2.

Table 5.2 Empirical kinetic constants retrieved from [186]

$\mathcal{N}$ - agitation rate (rpm)	k_g (10^{-6})	g	k_b (10^7)	b
400	1.5	3.1	1.2	1.6
600	2.6	3.5	3.2	1.9
800	3.2	3.8	3.6	2.3

There are limited complete studies of the solubility of benzoic acid in ethanol-water mixtures for various concentrations and temperatures except for O'Grady (2007).[187] In the study, various solubility experiments for benzoic acid at different temperatures and ethanol-water mixtures were carried out. The data from his work is taken and fit to a third order polynomial with respect to both temperature and $\mathcal{SASR}$ using the Matlab function *fit*. Figure 5.1, the y-axis (left) and z-axis (right) are read as the concentration of benzoic acid in ethanol expressed in g per mL.

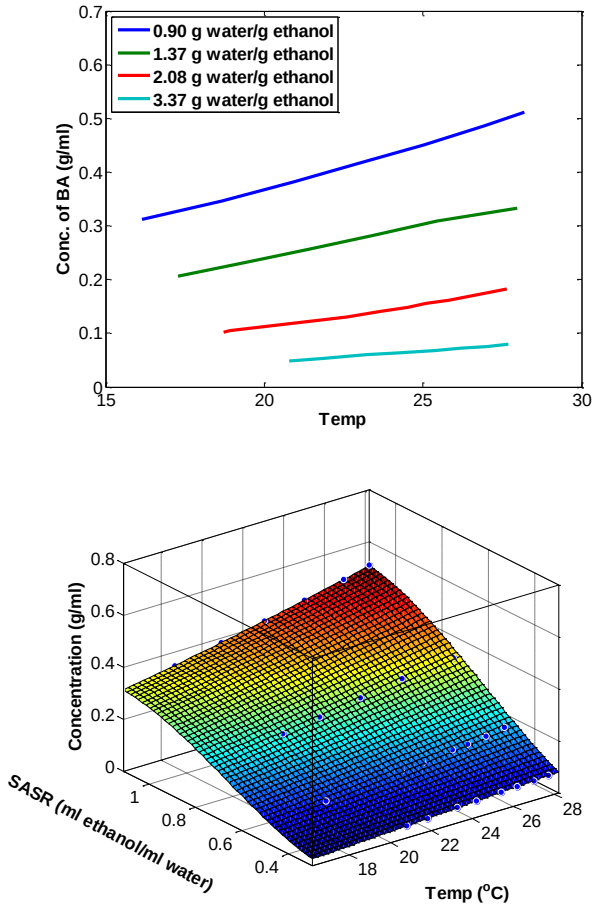

Figure 5.1 (top) Solubility data retrieved from [187] of benzoic acid in ethanol-water mixture with respect to temperature. (bottom) Resulting solubility surface as a function of SASR and temperature. The SASR from O'Grady were expressed as volume ratios for the solubility surface.

The agglomeration kernel used for this study is a homogeneous kernel derived from the combination of the Brownian diffusion kernel and the Zauner and Jones[183] and will be referred to as the Brownian+ kernel. It is expressed as:

$$\beta(L_i, L_j) = a\left(b + c\varepsilon^{\frac{1}{2}} - d\varepsilon\right) S^e \frac{k_a(L_i+L_j)^2}{L_i L_j} \qquad 5.30$$

The first portion of the agglomeration kernel is composed of the parameters and process conditions defined by Zauner and Jones[183] where a, b, c, d and e are constants, ε is the energy dissipation and S is the supersaturation. The energy dissipation is defined as follows:

$$\varepsilon = \frac{N_p d_s^5 \mathcal{N}^3}{V} \qquad 5.31$$

where N_p is the stirrer power number, d_s(m) is the diameter of the stirrer and $\mathcal{N}$ is the agitation rate over V, the volume of the slurry.[142] The second part of the kernel is the Brownian portion that takes into account the surface area effect of the two particles partaking in the agglomeration and is divided by the product of the two particles which allows for a determination effect; as the particles get larger the effect of the Brownian portion of the kernel is reduced. This is appropriate as this model allows the agglomeration rate to decreases as the particles get larger, a common behavior seen in agglomeration in suspension techniques like SC.

5.5 Agglomeration efficiency and porosity

As pointed out by Ochsenbein et al. (2015), one of the advantages of the coupled PBM is that it allows for the development of physically relevant parameters.[169] One parameter is the agglomeration efficiency. The coupled PBM framework allows for the population of all primary crystals, un-agglomerated crystals and agglomerates to be tracked, allowing for the determination of the efficiency of the agglomeration process with regards to the total number of crystals contained in the agglomerates.

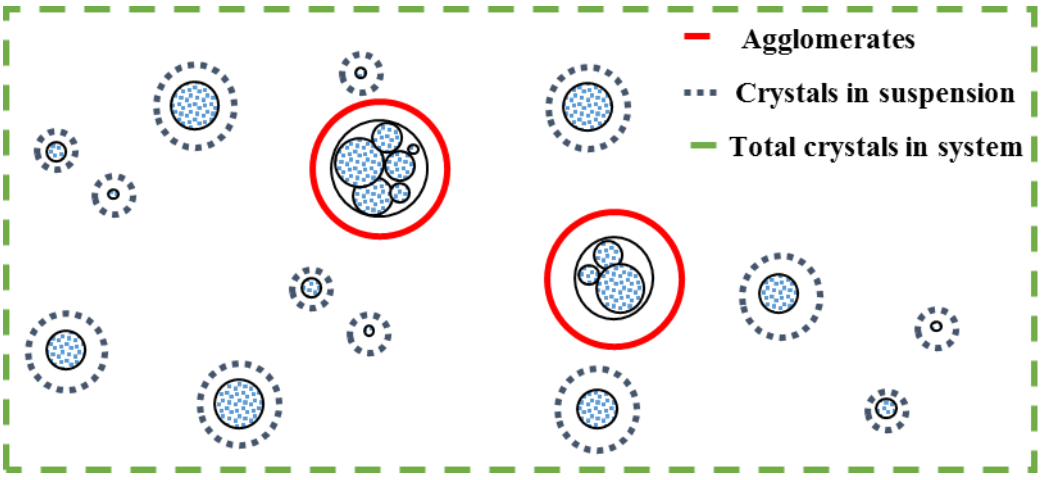

Figure 5.2 Schematic of the different populations being tracked by the coupled PBM framework.

Figure 5.2 is a schematic representation of the three populations being tracked by the coupled PBM framework. As the figure depicts, the primary crystals population consist of each individual crystal outlined in green within the green dashed box, the individual

crystals left in suspension consist of those crystals circled in blue dotted lines and lastly the agglomerates consist of those particles circled in red solid lines. Expressed in terms of volume, Figure 5.2 illustrates that the ratio of the volume of agglomerates to the volume of total primary crystals is a measure of the extent of agglomeration:

$$\%\ of\ agglomerated\ crystals = 100\left(\frac{V_a}{V_{tc}}\right) \tag{5.32}$$

This definition can be very easily defined using the moments of the PBM ($\tilde{\mu}_{tc,k}, \tilde{\mu}_{cs,k}, \tilde{\mu}_{a,k}$). Specifically, the third moment of each PBE which is a volume based moment can be used to express the agglomeration efficiency as:

$$\mathcal{AE} = 100\left(\frac{\tilde{\mu}_{a,3}}{\tilde{\mu}_{tc,3}}\right) \tag{5.33}$$

Porosity is a property of interest in agglomeration and granulation because it can have on other properties like dissolution and compressibility. Many times, a final desired porosity can determine the experimental conditions.

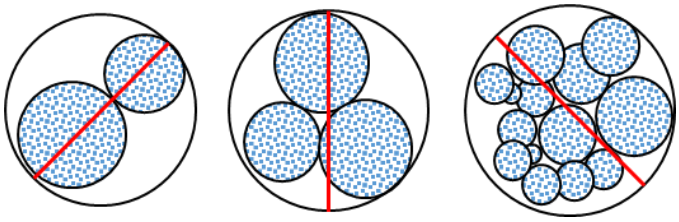

Figure 5.3 Schematic of agglomerates with similar characteristic lengths but different internal properties (i.e., porosity).

Figure 5.3 illustrates how the porosity of an agglomerate decreases as subsequent agglomeration continues over time. Due to the one-dimensional PBE, reconstructing the size of the agglomerate from the characteristic length assumes that the particle produced from an agglomeration event is a sphere. This assumption causes high porosity initially (see agglomerate on left in Figure 5.3) which is what occurs experimentally. As subsequent agglomeration continues the assumption of a sphere becomes more reasonable and the porosity decreases in the very same manner seen experimentally (left to right in Figure 5.3). Expressed in terms of volume Figure 5.3 states that volume of the pore (V_p) is equal to the volume of agglomerates minus the difference between the volume of primary crystals and

volume of un-agglomerated crystals. The porosity determined by dividing this difference by the volume of agglomerates.

$$V_p = V_a - (V_{tc} - V_{cs}) \quad 5.34$$

$$\varepsilon_p = 1 - \frac{(V_{tc} - V_{cs})}{V_a} \quad 5.35$$

Like the agglomeration efficiency, the porosity can be calculated with respect to the moments of the coupled PBM ($\tilde{\mu}_{tc,k}, \tilde{\mu}_{cs,k}, \tilde{\mu}_{a,k}$).

$$\mathcal{P} = 1 - \frac{\frac{\tilde{\mu}_{tc,3}}{\tilde{\mu}_{tc,0}} - \frac{\tilde{\mu}_{cs,3}}{\tilde{\mu}_{cs,0}}}{\tilde{\mu}_{a,3}/\tilde{\mu}_{a,0}} = 1 - \frac{\mathcal{V}_{tc,30} - \mathcal{V}_{cs,30}}{\mathcal{V}_{a,30}} \quad 5.36$$

The set of coupled PBEs and defined parameters are to be used in an optimization framework where internal properties like crystal mean size and external properties like agglomerate mean size can be optimized for subject to constraints on agglomeration efficient and yield, and other quality attributes or process constraints.

5.6 Optimization framework

Three optimization scenarios were analyzed: (i) minimizing primary crystal size, (ii) maximizing primary crystal size, and (iii) attaining bioavailability and manufacturability targets. For simplicity, the total particle mean size using the first and zeroth moment of the respective populations were used, $\mathcal{L}_{tc,10}$ and $\mathcal{L}_{a,10}$. The batch time is fixed at 300 min (~5 hr) which is typical for agglomeration in suspension systems like benzoic acid SC. The optimization variables are the dynamic operating profiles for temperature ($\mathcal{T}(t)$), agitation rate ($\mathcal{N}(t)$) and solution flow rate ($\mathcal{F}_s(t)$). The level of discretization for the optimization variables is 10. All the scenarios were subject to the same variable bounds and constraints. The bounds were chosen based on the range of the available solubility and kinetic data. The framework includes constraints on cooling/heating rate, ($\frac{\partial \mathcal{T}}{\partial t}$), solution addition ($\mathcal{SASR}$), agglomeration efficiency, ($\mathcal{AE}$), yield, ($\mathcal{C}_{final}$) and initial flow rate, ($\mathcal{F}_s(0)$). Since a reverse addition anti-solvent crystallization system was chosen for this study the constraint on the initial flow rate assures that a certain crystal mass will be generated otherwise the optimizer may try to crystalize one large particle towards the end of the batch. The optimization problem for the first two scenarios can be written as:

$$\min_{\mathcal{T}(t),\mathcal{N}(t),\mathcal{F}_s(t)} -\mathcal{L}_{tc,10} \text{ or } \mathcal{L}_{tc,10} \quad 5.37$$

$s.t.$

$$16 \leq \mathcal{T}(t) \leq 28\,°C \quad 5.38$$

$$400 \leq \mathcal{N}(t) \leq 800\,RPM \quad 5.39$$

$$0 \leq \mathcal{F}_s(t) \leq 2.5\,ml/min \quad 5.40$$

$$-0.4 \leq \frac{\partial \mathcal{T}}{\partial t} \leq 0.4°C/min \quad 5.41$$

$$0.25 \leq \mathcal{SASR} \leq 0.40 \quad 5.42$$

$$\mathcal{AE} \geq 50\% \quad 5.43$$

$$\mathcal{C}_{final} \leq 0.75\mathcal{C}_{max} \quad 5.44$$

$$\mathcal{F}_s(0) \geq 1.0\,ml/min \quad 5.45$$

The new variable $\mathcal{C}_{final}$ is the final concentration of solute in solution while C_{max} is the maximum concentration if all the solution is added to the system and no crystallization occurred. As written the constraint requires a 25% yield. The optimization problem is solved using the "interior point" method of *fmincon* in Matlab. The objective function of the optimization problem for the last scenario can be written as:

$$\min_{\mathcal{T}(t),\mathcal{N}(t),\mathcal{F}_s(t)} W_1\left(\mathcal{B}_T - \mathcal{L}_{tc,10}\right)^2 + W_2\left(\mathcal{M}_T - \mathcal{L}_{a,10}\right)^2 \quad 5.46$$

$\mathcal{B}_T$ and $\mathcal{M}_T$ represent bioavailability and manufacturability targets. For this scenario, the optimization problem is a multi-objective framework with W_1 and W_2 being the weights for each objective. The weights in equation 5.46 are shown as a generalization for situations in which bioavailability or manufacturability is more heavily weighted than the other. In this work, W_1 and W_2 each have values of one. This scenario is restricted to the same constraints previously described.

5.7 Results and discussion

5.7.1 Minimizing primary crystal mean size

The first scenario of interest is the minimization of the particle size. Minimization of primary crystal mean size is relevant in many industrial scenarios and helps with

micromeritic properties in pharmaceutical applications like bioavailability and dissolution. This scenario will also serve to illustrate the capabilities of the coupled PBM approach. The moments of this scenario illustrate the ability to keep track of all the populations in the PBE set. Figure 5.4 shows the zeroth moment for the three populations. The zeroth moment is representative of the total particle count. In Figure 5.4, the total particle count for the primary crystals in the system increases as solution is fed and the system becomes supersaturated. For this scenario, an inflection point occurs (at 105) indicating a significant increase in nucleation and a plateau is reached (at 220 min) indicative of zero supersaturation (zero nucleation).

Focusing on the zeroth moment of the un-agglomerated crystals and the agglomerates, an initial increase in un-agglomerated crystals that correlates with that of the primary crystals when the system first nucleates is evident. There is a delayed increase in the agglomerate counts since agglomeration cannot begin until there are crystals present. At 38 min, the un-agglomerated crystals count begins to spike but is then quickly reduced due to agglomeration. Since agglomerate formation can occur from crystal-crystal, crystal-agglomerate and agglomerate-agglomerate interactions, the zeroth moment of the agglomerates continues to decrease further; even though there is no longer nucleation (zeroth moment of primary crystals plateaus). The difference in magnitude of the primary crystals and un-agglomerated crystals in the beginning is also an indication of agglomeration.

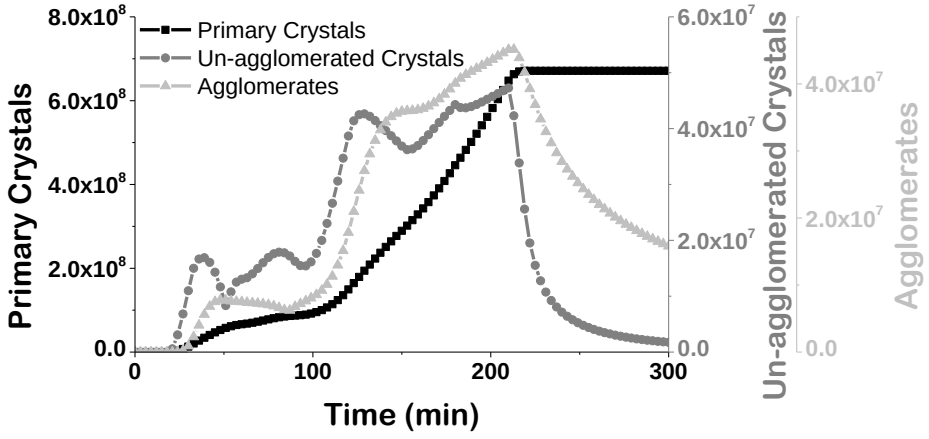

Figure 5.4 The zeroth moment for each population in the PBE set for the minimization of $L_{tc,10}$.

Figure 5.5 shows the third moment for the three populations. As the system begins to nucleate and grow the volume of the primary crystals increases steadily until the supersaturation is depleted. Comparing both Figure 5.4 and Figure 5.5 suggests that most of the particle volume is created at the onset with low total counts followed by secondary nucleation shown by the jump in the total counts but only a slight increase in total volume. The volume of un-agglomerated crystals is significantly smaller than the volume of primary crystals and agglomerates suggesting that most of the agglomeration happens at after the infliction (increase in nucleation) in primary crystals counts. The third moment of the three populations shows the same trend for all optimization scenarios investigated and hence will not be shown for other scenarios. Comparing Figure 5.4 and Figure 5.5 can be misleading given that in Figure 5.4 the total count of un-agglomerated crystals is increasing along with that of primary crystals, while in Figure 5.5 the total volume of un-agglomerated crystals rapidly decreases and is significantly smaller than that of the primary crystals. This can be clarified by looking at the mean sizes of the three populations.

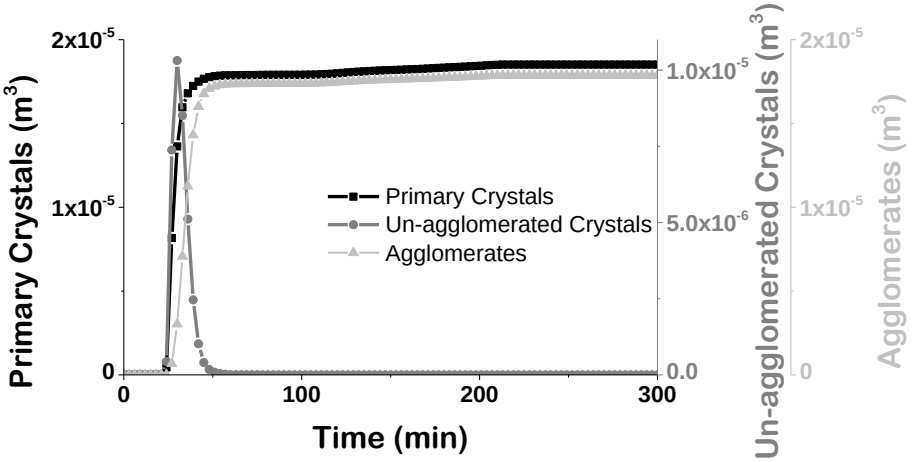

Figure 5.5 The third moment for each population in the PBE set for the minimization of $L_{tc,10}$.

The mean size optimization profiles of the three populations for this scenario are shown in Figure 5.6. The mean size is expressed as the first moment divided by the zeroth, $L_{tc,10}$. The minimum primary particle size achievable in this scenario is 2.5 μm. While the crystals left in suspension have a mean size of 0.1 μm and the agglomerates are of a mean size of 28.8 μm. The small size of the un-agglomerated crystals again suggests that the increase

seen in the total counts relates to secondary nucleation, which in turn corresponds to a small particle size and very small/negligible volume. The agglomerate mean size and the primary crystal mean size follow the trend observed from the zeroth moment. When the primary crystal mean size plateaus the agglomerate mean size increases otherwise they follow the same pattern as the primary crystal mean size increases the agglomerate mean size increases and vice versa.

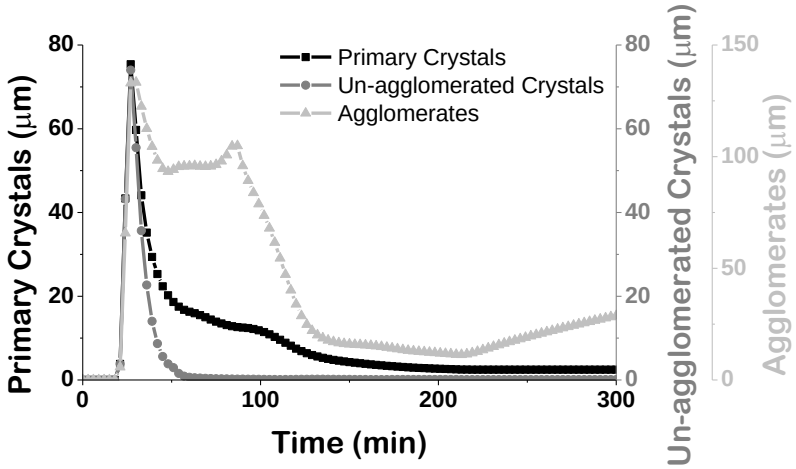

Figure 5.6 Primary crystal mean size ($L_{tc,10}$), un-agglomerated crystals mean size ($L_{cs,10}$) and agglomerate mean size ($L_{a,10}$) for Scenario 1.

Figure 5.7 shows the optimal flowrate, temperature and agitation rate profiles for the minimization of the primary crystals mean size. Flowrate is initialized at its upper bound, the temperature profile starts near its lower bound and the agitation rate is initialized at its upper bound. High nucleation or crashing out is characteristic of reverse addition anti-solvent crystallization. Thus, the optimizer begins the process by nucleating from the addition of solution to the anti-solvent, at lower temperatures and high agitation rate to promote nucleation and generate small crystals. This period lasts the first 15 min and allows for the system to reach a supersaturated state quickly.

Immediately following the initial period, the flow rate of solution is decreased to its lower bound, the temperature begins to decrease further and the agitation rate is decreased to 600 RPM. These changes allow the system to decouple the effects of solution addition, temperature and agitation on nucleation. Whenever solution addition is increased,

temperature is slightly increased and whenever solution addition is decreased, temperature is slightly decreased allowing for nucleation to be controlled by flowrate or temperature. This keeps the system supersaturated and in a nucleation phase, evident by the continued decrease in the primary crystals mean size, until the plateau in primary crystals is reached at 220 min. Nucleation is reduced in this period by an increase in temperature and solution addition. This period is continued until the end of the batch. This final addition of solution satisfies the SASR constraint and decreases supersaturation. Figure 5.8 shows the operating curve along the solubility surface for this scenario.

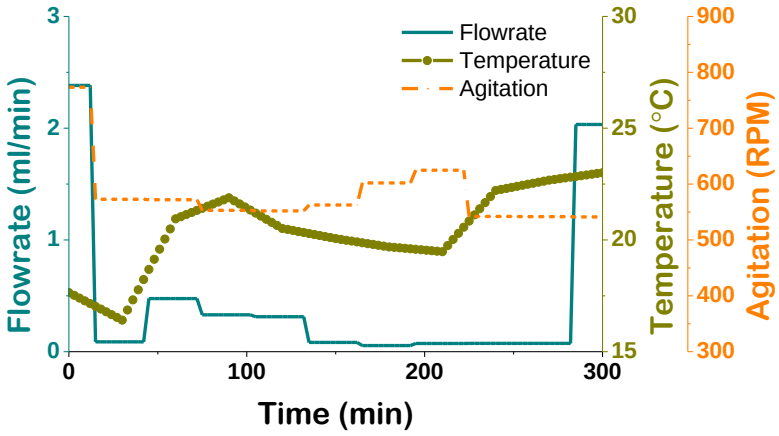

Figure 5.7 Optimal flowrate, temperature and agitation rate profiles for the minimization of $L_{tc,10}$.

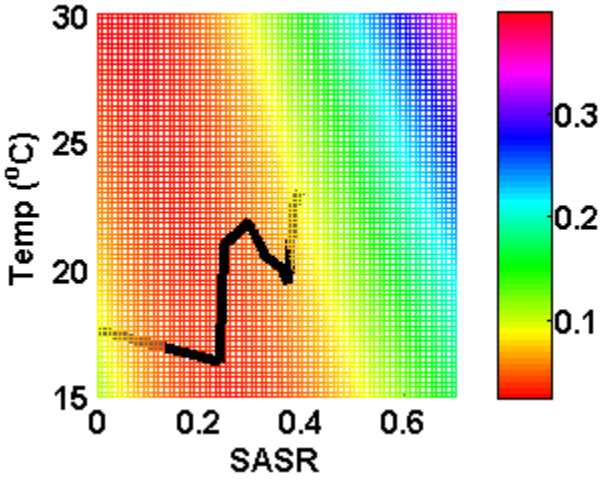

Figure 5.8 Operating curve along the solubility surface for the minimization of primary crystal size.

5.7.2 Maximizing primary crystal mean size

Maximizing particle size also has industrial relevance in that some systems exhibit low downstream processing efficiency when the particle size is too small. For this scenario, Figure 5.9 shows the primary crystal count very quickly reaching a plateau (100^{th} min) indicative of the system avoiding secondary nucleation. A similar behavior in the zeroth moment of un-agglomerated crystals and agglomerate population is observed. The initial spike in the number of un-agglomerated crystals increases similarly to the primary crystals, however once the primary crystal counts plateau the counts of un-agglomerated crystals decreases sharply. This is followed by an increase and then a decrease in the agglomerate counts as the system transitions from crystal-crystal agglomeration to agglomerate-crystal and agglomerate-agglomerate agglomeration.

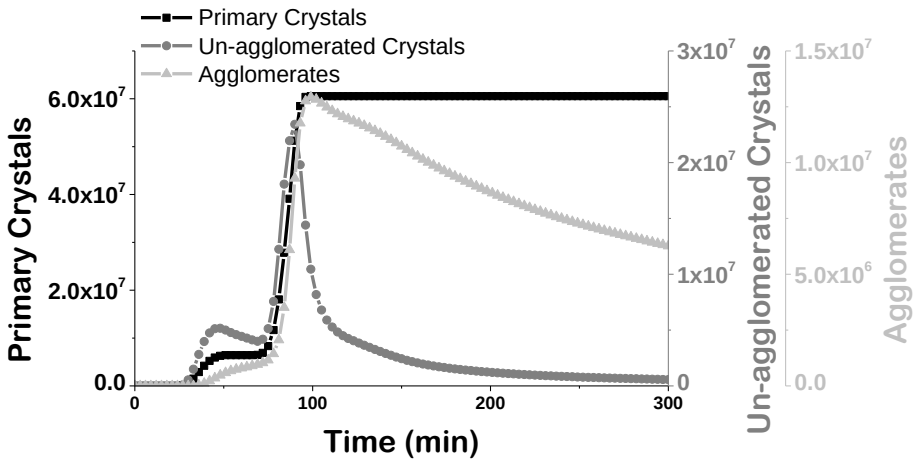

Figure 5.9 The zeroth moment for each population in the PBE set for the maximization of $L_{tc,10}$.

Figure 5.10 shows the optimization results for the maximization of the primary particle size. The maximum achievable primary particle size is 41.8 μm. While the un-agglomerated crystals left in suspension have a mean size of 61.6 μm and the agglomerates are of a mean size of 117.8 μm. With regards to the growth of the primary crystals and agglomerates the trends are like that of the first scenario. The mean size of the primary crystals remains constant after the 100^{th} min which aligns with the plateau in primary crystals counts indicative of little supersaturation or growth beyond this point. As in the previous scenario, the agglomerate mean size increases when the primary crystal mean size

is constant or when increasing. Interestingly, the un-agglomerated crystal mean size continues to increase even after the 100th min point. This is due to the agglomeration kernel used to describe the system. The Brownian+ kernel favors the agglomeration of smaller particles. Hence, once the system plateaus with regards to counts and has depleted supersaturation; agglomeration will favor smaller particles, which is the reason for the increase in mean size of un-agglomerated crystals, due to the removal of fine crystals from this distribution. This is also the reason why the increase in the mean size of un-agglomerated crystals increases with a higher order trend versus the agglomerate mean size which increases with a linear trend. Every small crystal that leaves the un-agglomerated crystals population increases the percentage of large crystals left behind while only marginally increasing the size of the agglomerate they attach to.

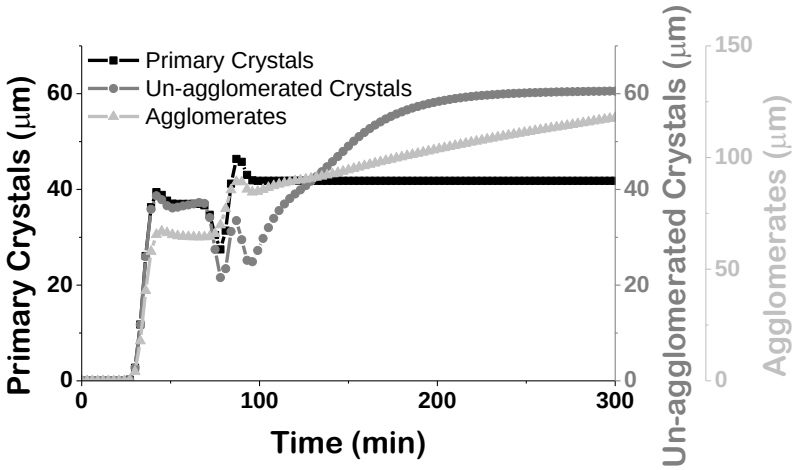

Figure 5.10 Primary crystal mean size ($L_{tc,10}$), un-agglomerated crystals mean size ($L_{cs,10}$) and agglomerate mean size ($L_{a,10}$) for Scenario 2.

Figure 5.11 shows the optimal process profiles for this scenario. The solution flow rate is initiated at 1.0 mL/min and quickly increased to the upper bound while the temperature is increased linearly to the upper bound (30 °C). As seen in Figure 5.12 (solubility surface), the system is not supersaturated at the onset, and thus the delayed start in counts and mean size. As the solution flow rate is increased to 2.5 mL/min and the temperature is held constant, the system becomes supersaturated and crystals begin to nucleate and grow. The addition of solution is continued through the 75th minute until the system again becomes undersaturated. A steady decrease in temperature follows, bringing the system back to a

supersaturated state. An increase in nucleation results as evident by the sharp increase in counts and subtle decrease in mean size. The process completes with another cycle of increasing temperature and decrease in agitation rate. This effectively serves to reduce the amount of supersaturation that is consumed due to nucleation and drives growth. This is evident by the increase in primary crystal mean size before the system plateaus and the temperature is brought to saturation.

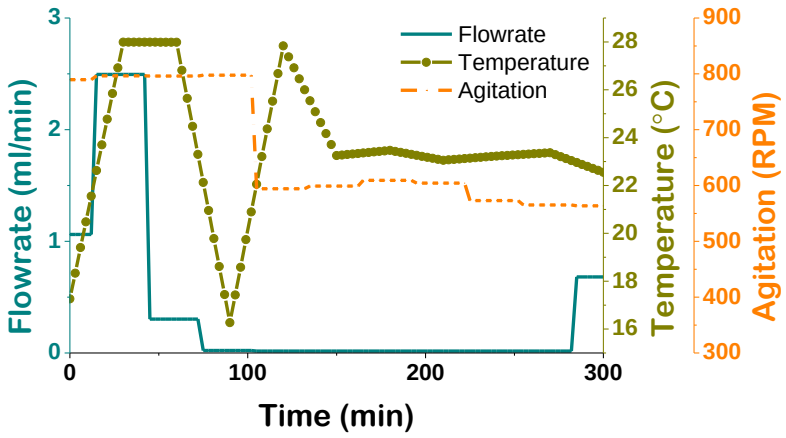

Figure 5.11 Optimal flowrate, temperature and agitation rate profiles for the maximization of $L_{tc,10}$.

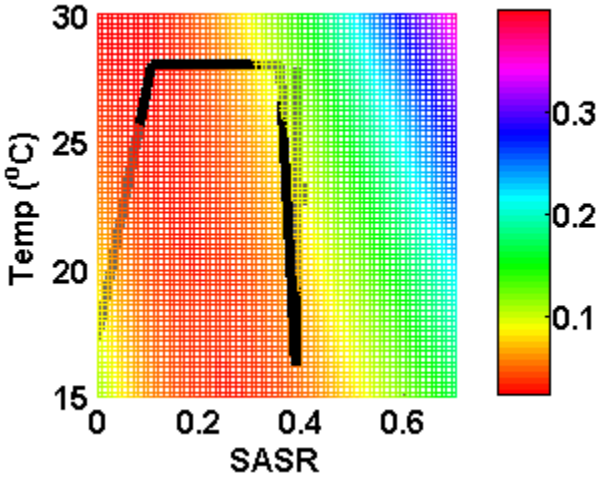

Figure 5.12 Operating curve along the solubility surface for the maximization of primary crystal size.

5.7.3 Multi-objective optimization for bioavailability and manufacturability

Optimizing for both bioavailability and manufacturability targets is the unique scenario that is made feasible by the proposed coupled PBM framework. Prior to evaluating the attainability of bioavailability and manufacturability targets, the maximization of agglomerate particles is evaluated to understand the range and limitation to the maximum agglomerate size; although the optimal profiles are not shown here. The maximum attainable agglomerate size for the fixed batch time and operating conditions used here is 154.4 μm. The minimum and maximum size for the primary crystal were 2.5 and 41.8 μm, respectively. Given these results, the bioavailability target, B_T, for the mean size is set to 10 μm and the manufacturability target, M_T, is set to 50 μm.

Figure 5.13 shows the results of the mean sizes for the bioavailability and manufacturability targets. Both the bioavailability and manufacturability target sizes were attained within 1 μm. B_T = 10.1 and M_T = 49.9 μm. The trends of mean size profiles described for the previous scenario is similar in this scenario. When the primary crystals mean size is increasing or constant the agglomerate mean size increases. While the primary crystal mean size is constant the un-agglomerated crystal mean size increases because agglomeration favors smaller particles due to the agglomeration kernel used in this case. All the mean sizes decrease when nucleation occurs due to the increase in smaller counts for all populations.

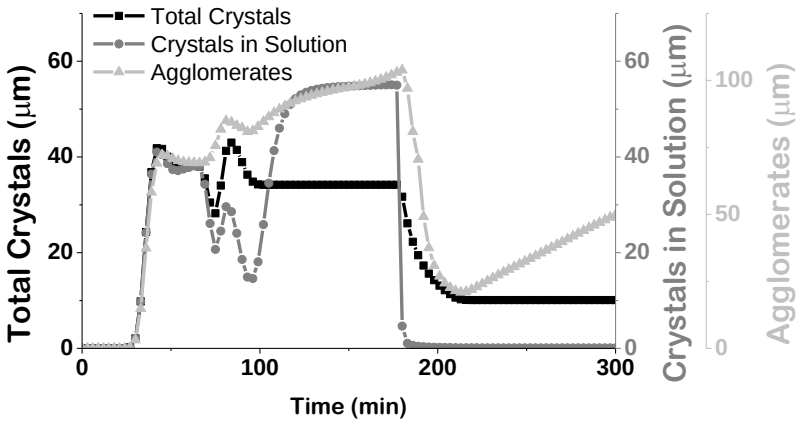

Figure 5.13 Primary crystal mean size ($L_{tc,10}$), un-agglomerated crystals mean size ($L_{cs,10}$) and agglomerate mean size ($L_{a,10}$) for Scenario 3.

Figure 5.14 shows the optimal process profiles for the solution flow rate, temperature and agitation and Figure 5.15 shows the operating line along the solubility surface. Analyzing these figures together, it is obvious that the optimal profile is a combination or interpolation of the previous two scenarios. One apparent difference is the number of temperature cycles observed in this scenario driven by the need to balance both nucleation and growth of the primary crystals so to attain both targets. From a solution flow rate perspective, the system is initiated and carried in the same manner as the previous scenario of maximizing primary particle size. The solution flow rate is initiated at 1.0 mL/min and then increased to the upper bound while the temperature is increased linearly to the upper bound (30 °C). As in the previous scenario, the system is undersaturated until the solution flow rate is increased (Figure 5.15). A temperature cycling phase then commences at a very low solution addition. This temperature cycles and low solution addition balance nucleation and growth allowing for both the bioavailability and manufacturability targets to be reached. The agitation rate follows the same trend as both previous scenarios.

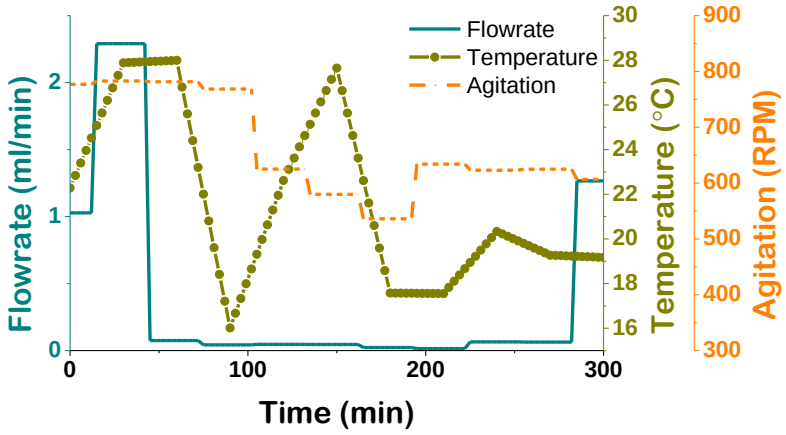

Figure 5.14 Optimal flowrate, temperature and agitation rate profiles for the bioavailability and manufacturability target.

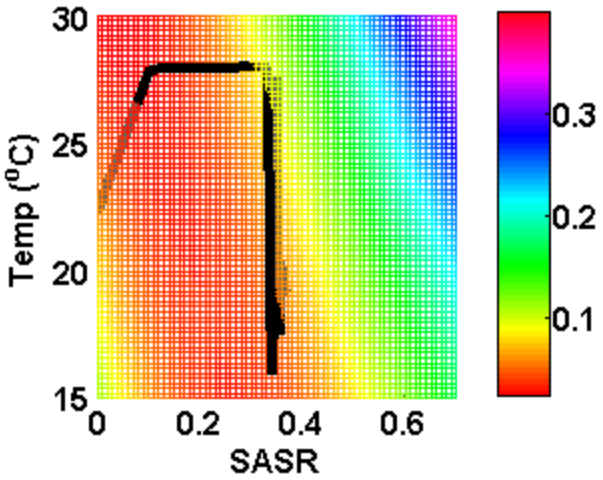

Figure 5.15 Operating curve along the solubility surface for the bioavailability and manufacturability targets.

The agitation profile is similar for all three scenarios indicating that agitation rate is impacting the nucleation and growth kinetics more than the agglomeration kinetics. Overall the trend in agglomerate size with respect to changes in agitation rate did not match those reported in the literature.[26, 27,123] This is most likely due to the set of nucleation and growth kinetic models used as both have an agitation rate dependence. The influence temperature profiles also had an impact on this results since most SA experiments had previously been conducted at constant temperature.

Table 5.3 Summary of optimization results with constraint values.

Parameters	***Min* $L_{tc,10}$**	***Max* $L_{tc,10}$**	B_T/M_T
$L_{tc,10}$ *(μm)*	2.5	41.8	10.1
$L_{a,10}$ *(μm)*	28.8	117.8	49.9
AE	96.5%	77.5%	75.6%
Yield	0.25	0.31	0.41
SASR	0.39	0.40	0.37

Table 5.3 summarizes the optimization results. All scenarios met the agglomeration efficiency (larger than 50%), yield (25% or greater) and SASR constraints (between 0.25 and 0.40). The bioavailability and manufacturing target scenario required the lowest amount of solution to the system but produced the highest yield. This is most likely due to the greater number of temperature cycles. The scenario to minimize primary crystal mean size had lowest yield most likely due to prevention of growth in the system. This scenario

also had the highest agglomeration efficiency which is also related to the high amount of nucleation in this scenario and the fact that agglomeration favors smaller particles.

5.8 Porosity profiles

Figure 5.16 shows the porosity profiles from the optimization scenarios. As detailed in the model development section, this approach to estimating porosity is unique and derived from the moments of the distributions. The benefits of calculating porosity in simulations is the ability to design process around the ideal porosity for specific dissolution and compression properties. The porosity is not included in the optimization studies as it would require an appropriate scaling parameter to make physical sense. The porosity for the different scenarios show similar final values with different profiles. The porosity profile for the maximization of primary crystal size increases initially and then decreases as the system continues to agglomerate without supersaturation or nucleation (Figure 5.9 and Figure 5.10). The profiles for the minimization of primary crystal size and target bioavailability and manufacturability both follow similar cycles of increasing and decreasing porosity, which correlates well with the temperature and nucleation cycles seen in optimal profiles and total counts.

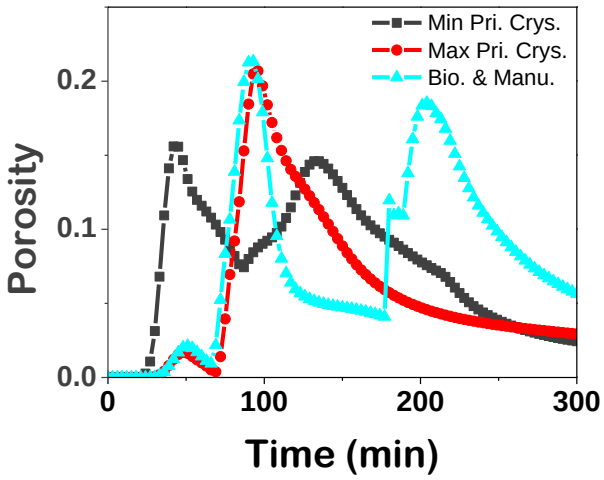

Figure 5.16 Porosity profiles for all three optimization scenarios.

5.9 Effects of secondary nucleation

The parameters used for the presented results were taken from literature values. However, the empirical parameter ***i*** found in the nucleation rate expression is not found in the literature and was not fit to experimental data prior to this study. A study to understand the effects of this parameter on the simulation and optimization results was conducted. Table 5.4 shows the differences in the results for minimization and maximization of primary crystal for ***i*** equal to 1 and 0.01.

Table 5.4 Comparison of optimization results with different ***i*** values

Empirical Parameter	***Min*** $L_{tc,10}$	***Max*** $L_{tc,10}$
	$L_{tc,10} / L_{a,10}$ (μm)	$L_{tc,10} / L_{a,10}$ (μm)
i *= 1*	2.5/ 28.8	41.8 / 117.8
i *= 0.01*	19.8 / 145.8	89.6 / 156.1

The results from shown in Table 5.4 show that a lower ***i*** value results in a significantly larger achievable minimum and maximum primary crystal mean size. Modulating ***i*** varies the extent of secondary nucleation in the system. A lower ***i*** value decreases the extent of secondary nucleation which in return allows more supersaturation to be consumed by growth.

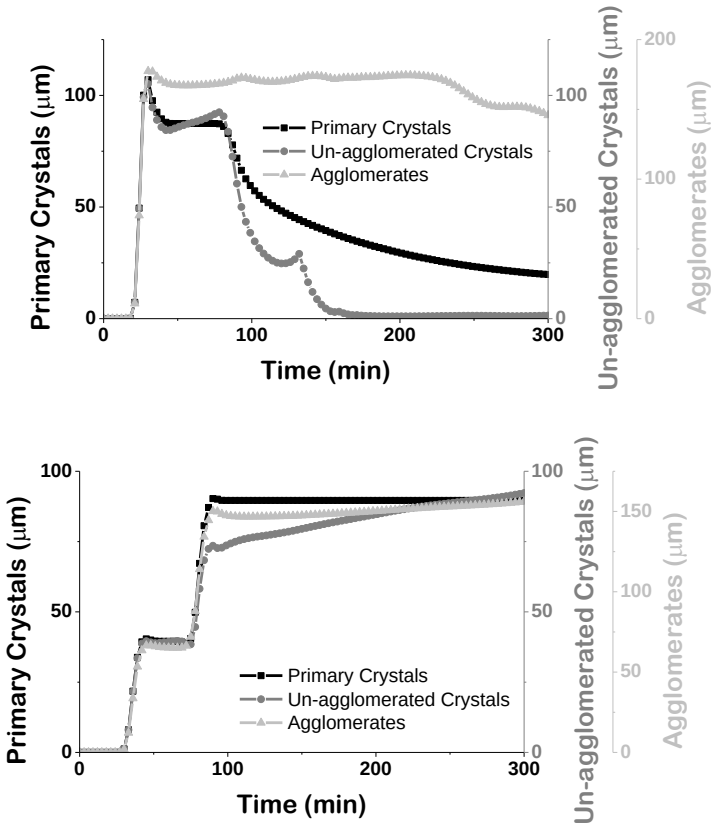

Figure 5.17 Primary crystal mean size ($L_{tc,10}$), un-agglomerated crystal mean size ($L_{cs,10}$) and agglomerate mean size ($L_{a,10}$) when $i = 0.01$ for both minimization (top) and maximization (bottom) of primary crystal size.

Figure 5.17 shows the mean size profiles for both the minimization and maximization of primary crystal size. The mean size profiles show a significant difference from that of the system with a higher value for $\boldsymbol{i}$. Most notably, changes in the mean size for the agglomerate follow more closely the changes in mean size of the primary crystals. The agglomerate mean size stays relatively constant, increases and decreases with the same trend as primary crystal mean size. This shows the impact that secondary nucleation can have on the final agglomerated size. The trends observed with lower values for $\boldsymbol{i}$ are more reasonable when compared to the experiments in the literature[137,139], but will need to be fit to experimental data to attain a system specific value.

5.10 Conclusions

In this work, a coupled PBM with nucleation, growth and agglomeration was developed. Three populations of interest are tracked: primary crystals, un-agglomerated crystals and agglomerate populations. Tracking these populations separately gives access to otherwise unattainable information in traditional PBMs. This allows for optimization frameworks and process design efforts tailored to the property specifications for each population.

An optimization framework has been developed to achieve optimal flowrate, temperature and agitation rate profiles for a reverse addition, anti-solvent crystallization system of benzoic acid with agglomeration. The results of this work show that operating parameters can be optimized to achieve the desired primary and/or agglomerate properties. The framework allows for bioavailability (primary crystal size) and manufacturability (agglomerate particle size) optimization. Moving forward this model formulation will allow for the development of better, more relevant kinetic and agglomeration parameters. Given that each population is tracked separately, kinetic parameters can be fit separately without having to lump all the kinetics into one population; thereby increasing accuracy of the parameter fit. Agglomeration kernel identification would greatly improve with this model formulation, and can begin the shift from purely empirical kernels to combination kernels that relate the physical mechanisms and operating conditions more accurately. Moving forward the proposed model formulation will be fit to data from various agglomeration in suspension systems to assess its capability to predict product properties.

6. PROCESS INTENSIFICATION THROUGH CONTINUOUS SPHERICAL CRYSTALLIZATION USING A TWO-STAGE MIXED SUSPENSION MIXED PRODUCT REMOVAL (MSMPR) SYSTEM

This chapter is reprinted with minor modification with permission from Peña, R., & Nagy, Z. K. (2015). *Crystal Growth and Design*, *15*(9), 4225–4236.

6.1 Introduction

Crystallization, originally conceived as a purification and separation process, has become a predominant technique in particle design technology. It is a unit operation in process systems in a broad range of industries including pharmaceuticals, bulk and fine chemicals, food, and electronics.[32] In most solid-liquid separation processes, crystallization is the characteristic and property-determining step. Given that it is also one of the initial steps, it has a major impact on downstream processes (e.g., filtering, drying, milling, handling, storage).[1]

Crystallization greatly influences API purification, final product properties, dosage form and the efficiency of intermediate unit operations leading to the final dosage form. Milling and granulation are unit operations that often follow crystallization with the purpose of improving crystal properties either for better bioavailability or for improved processing characteristics (e.g., flowability, compressibility). However, milling and granulation have some inherited inefficiencies and although the overall crystal size can improve, it is often at the expense of a wider crystal size distribution (granulation) and poor process properties (milling).

In the past, the pharmaceutical industry's manufacturing processes have been limited in efficiency due to their batch nature, costing the industry as much capital investment and development time as drug discovery. However, due to expiring patents and the fluctuating cost of energy most companies have begun to face the economic burden of inefficient manufacturing.[23] Of current interest in the industry is to move manufacturing processes from batch to continuous operation. Batch crystallization is a versatile, recipe based, mode

of operation that can be adapted for specific product properties and used for different products. Batch crystallizers are also relatively inexpensive compared to systems using other methods of operation and are simple to use. However, continuous operation allows for lower overall capital investment, production that is more efficient and reproducible, easier scalability, and better waste or off-specification product management.[25,83] Scale up of batch operations is not as straightforward as that of continuous operations because they occur at unsteady state and require greater understanding of the effects of the differences in scales. Continuous operation, although easier to scale, makes the process design more difficult because of all the interplaying parameters. Also according to standard economy of scale considerations it is only viable when production rates are very large (> 50 tons/day).[32] More recently, throughput requirements for continuous operations have been outweighed by considerations that are related to achieving operating conditions and levels of product consistency that are unattainable in the batch operations currently available; providing accepted benefits to continuous processes independently of the scale and production rate.

Common to most pharmaceutical products is the use of many unit operations, which is characteristic of batch operation and solid dosage formulations. This can decrease the overall yield and efficiency of the manufacturing process and often makes it difficult to maintain product safety and quality. Instead, intensifying the processes involved in pharmaceutical formulations can greatly improve efficiency. One method of improving product properties post-crystallization, reducing unit operations and easily implementing continuous manufacturing strategies is through PI. PI presents several advantages for the pharmaceutical industry including lower capital and operating costs, less handling, transfer and storage of intermediate products, and more robust and energy efficient operation. Implementing CSC allows for the elimination of downstream particle property enhancing unit operations like milling, grinding and granulation, and promotes the move from batch to continuous operation.

CSC of a model drug compound was first carried out by Kawashima et al. (1982) after Kawashima & Capes (1974) realized that resulting products from SA had very good flow properties.[30,152] In their work, a model continuous mixed suspension, mixed product removal (MSMPR) crystallizer consisting of one stage was fed an aqueous suspension. The

critical parameters were identified as agitation rate, suspension feed rate, and bridging liquid feed rate.[22] Since Kawashima et al. (1982) very little work has been done on CSC. An abundance of work exists on SC in batch operation. The first batch spherical crystallization (BSC) was carried out by Kawashima et al. (1982) who crystallized salicylic acid in ethanol by pouring the solution into a water-chloroform mixture and found the critical parameters to be similar to that in a continuous system: agitation rate, temperature, bridging liquid content, and residence time.[22] There are also very few references that make use of PAT tools for monitoring SC. This could be due to the increased difficulty of process monitoring when complex mechanisms like nucleation, growth, and agglomeration are happening simultaneously. However, the use of PAT tools for crystallization processes has been widely discussed in the literature[17,46,188] and has proven to be beneficial in the monitoring of both liquid-phase and solid-phase dynamics during crystallization. Blandin et al. (2003) provides the best example of the benefits of in-situ monitoring of a SC process.[143]

Rasmuson & co-workers[26,137,139] have done research on how changes in the key operating parameters of BSC affect the final product properties. In most of their work the solute was benzoic acid, the good solvent was ethanol, and the poor solvent was water. Longer residence times[30], or duration under agitation[137], produced stronger and highly spherical agglomerates. Katta & Rasmuson[26] also found that the agglomerate size increased with increasing solute concentration. Lower concentrations produced more fines and porous spherical agglomerates. Other properties found to be important in BSC include the feed rate of the solution into the poor solvent; an increase in feed rate led to decrease in agglomerate size. This is due to the difference in the rate of supersaturation generation at low versus high feed rates. Thati & Rasmuson[139] studied the effect of temperature on the SA process, and found that agglomerate size increased with a decrease in temperature. The decrease in solubility at lower temperatures increased supersaturation, which increased nucleation and subsequent inter-particle growth between colliding particles. There has also been a wide range of studies on the physiochemical, mechanical, and micromeritic properties of the spherical agglomerates to assess the possibility of direct tableting of the agglomerates.[28,118,123,134,137,139,189,190] However, none of the aforementioned studies looked into the interplay between the operating conditions and the trade-off between the size

distribution and properties of spherical agglomerates and the size distribution of constituting internal crystals. In almost all previous SC systems, crystallization and agglomeration occurred simultaneously; offering little or no control in tailoring the internal crystal size versus external agglomerate size. In this work, a novel two-stage CSC system is proposed in which the nucleation and growth processes are separated (in the first stage) from the agglomeration mechanism (in second stage), enabling precise and independent control of the internal CSD and ASD. This can enable the simultaneous control of product properties (e.g., dissolution profile) and processing requirements (e.g., flowability, compressibility). A FBRM was used to help identify the initiation and extent of the agglomeration process, although in-situ imaging microscope might be more suitable.

6.2 Spherical crystallization mechanisms

Kawashima et al. (1995) found that SC is also possible in two solvent systems and proposed the SC mechanism for both two and three solvent systems. In both systems, the proposed mechanism is the formation of an emulsion droplet of good solvent in which the drug is precipitated via diffusion of the good solvent to the poor solvent.[124] The difference in the techniques is the presence or absence of agglomeration. Figure 6.1 illustrates the SC mechanism for two and three solvent systems. Two solvent systems are usually emulsion based SC techniques where emulsions are formed by the immiscibility between the poor and good solvent (e.g., oil in water or water in oil) or by the good solvent's inherently greater affinity for the solute. Chadwick & Davey made spherical particulates from water in oil emulsions using a water-soluble compound and cooling as the method of supersaturation generation.[126] Spherical particulates can also be produced using anti-

solvent crystallization whereby counter diffusion of the poor solvent and good solvent into and out of the emulsion droplet promotes crystallization or ESD.

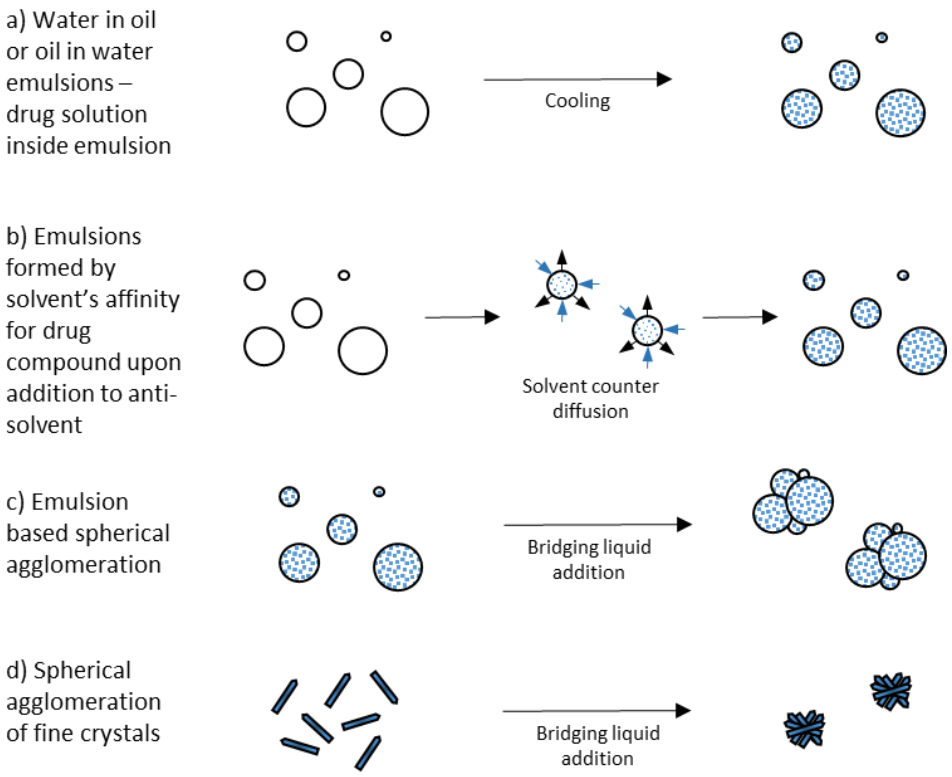

Figure 6.1 Agglomeration mechanism for different spherical crystallization techniques (c and d adapted from [28], d adapted from [23]).

The mechanism for three solvent systems is like two solvent systems except agglomeration is present. The third solvent is the bridging liquid. The bridging liquid preferentially wets the precipitated solute particles.[26,123,139,152] Collisions between wet particles causes the particles to adhere and create agglomerates. This method is commonly referred to as SA. Spherical particulates produced by ESD are usually smaller and more porous than the particulates produced by SA while agglomerates produced by SA are usually bigger and stronger. SA has more applicability as it does not require the creation and subsequent stability of emulsion droplets like ESD. Kawashima et al. (2003) states the SC mechanism taking place changes from SA to ESD as the SASR, essentially the concentration, is decreased.[28] Krishna et al. (2012) and Kovačič et al. (2012) propose methods to decide the best SC mechanism for different types of systems.[123,191]

Blandin et al. (2003) and Rasmuson & Thati (2011) found that the size of the spherical agglomerates significantly increases with increased bridging liquid content.[111,137] The BSR determines the bridging liquid content. Amaro-González & Biscans (2002), Subero-Couroyer et al. (2006), and Rasmuson & Thati (2011) established that there is a critical range for the BSR for which below the minimum spherical agglomerates will not form and above the maximum a paste like product will form. [29,142,137] Figure 6.2 illustrates the progression of an agglomerate, for both fine crystals and emulsions, as the BSR is increased. Initially, when an amount of bridging liquid is added at a ratio of BSR_1 below the critical ratio (BSR_{cric}) the agglomeration process begins and crystals (or emulsions) adhere and form agglomerates although there may be loose crystals still in the suspension. As the bridging liquid ratio is increased to the BSR_{cric} the agglomerate is more firmly held together, more particles adhere to one agglomerate and there are no longer loose particles in suspension. At a ratio BSR_3 above the BSR_{cric} a bridging liquid layer begins to form around the agglomerate. When the bridging liquid ratio is increased to BSR_4, the bridging liquid layer reaches its maximum. At ratios above BSR_4, there will be excess bridging liquid in the suspension, which causes the formation of bridging liquid droplets (Figure 6.2e). Further increase in the bridging liquid ratio can cause phase separation where the particles (or agglomerates) become surrounded by bridging liquid, which is suspended in the continuous phase (Figure 6.2f). In the case of excess bridging liquid, a more amorphous agglomerate is produced that behaves in a paste-like manner.

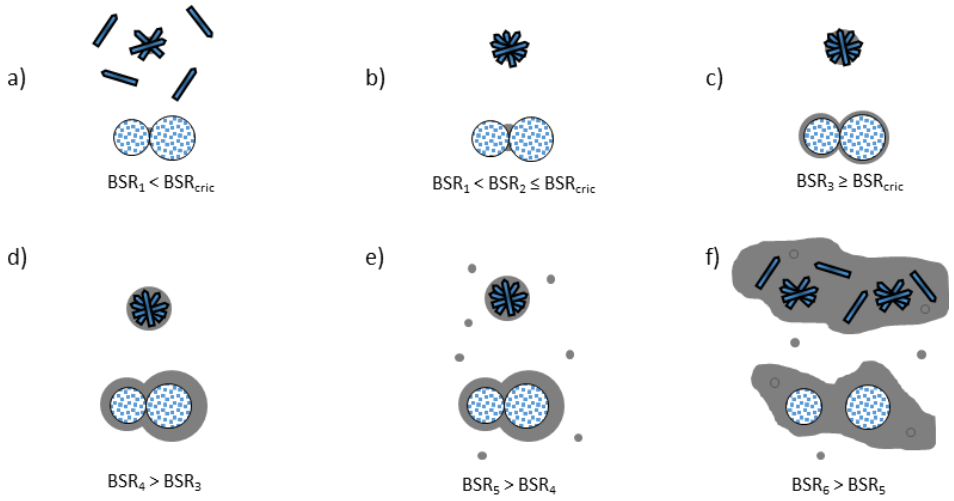

Figure 6.2 Agglomerate formation as bridging liquid content is increased. Adapted from [162].

The contribution of the work presented herein is CSC in a two-stage MSMPR crystallizer. The purpose of the proposed setup is to achieve two of the current major focuses of the pharmaceutical industry, which are PI and continuous manufacturing. PI occurs through the SC technique that will produce spherical particulates with the potential to be directly compressed. Continuous manufacturing in the proposed MSMPR setup will improve the process efficiency while reducing the handling of intermediate products and reducing the number of unit operations in a drug product line. The continuous production of spherical agglomerates allows for changes in operating parameters to produce agglomerates of different qualities, which is an improved method of product quality control over batch operation. The proposed two-stage MSMPR crystallizer setup also serves as a product design approach because of the ability to decouple nucleation/growth and agglomeration mechanisms. This ability to decouple mechanisms allows for direct product design whereby in one stage biopharmaceutical properties are enhanced, and in the other stage processing properties are improved. The benefits of the setup and production will also include the ease with which these spherical particulates can then be filtered, dried, and compressed when compared to traditional crystallization. The use of PAT tools in CSC-MSMPR setup will also add degrees of freedom to the operation allowing for the possibility of other model-free approaches from the literature[6,10,18,192] to be implement in the different stages as part of the continuous MSMPR system.

6.3 Experimental work

The two-stage continuous MSMPR crystallizer setup proposed for CSC allows the tailoring of internal and external properties of spherical agglomerates. As depicted in Figure 6.3, in the system the first stage serves as the nucleation and growth dominant stage where altering of the operating conditions produces crystals of a specific size distribution, morphology and dissolution properties. The second stage serves as the agglomeration dominant stage where the operating conditions produce agglomerates of specific size distribution, flow and disintegration properties. The decoupling of the crystallization and agglomeration mechanisms will provide flexibility in final product properties. For example, one combination could produce large spherical agglomerates of loosely packed fine crystals but alternatively one could potentially produce the same size agglomerates with densely

packed coarse crystals. This opens the door for better product specific design that can potentially achieve specification levels that granulation cannot. To the best of our knowledge, no previous work in the literature has taken this approach to SC and very little work exists on CSC.

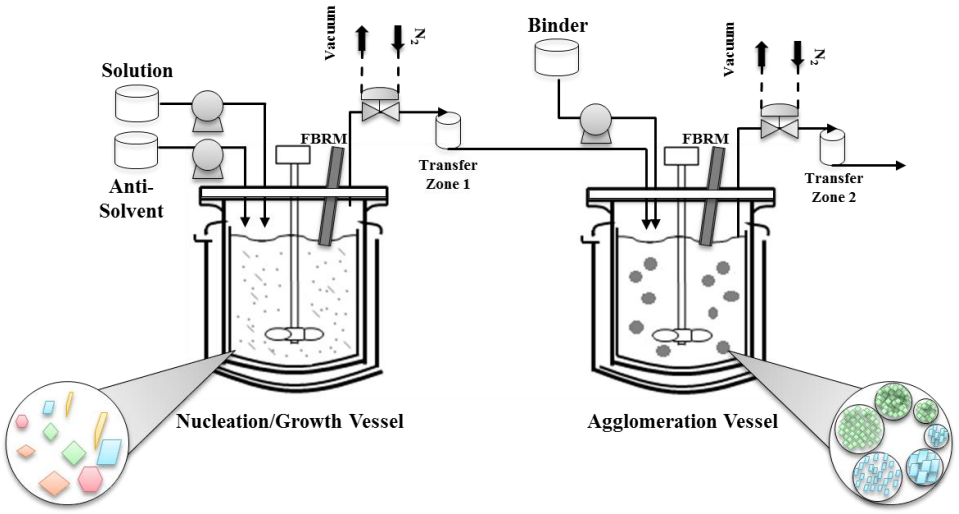

Figure 6.3 Schematic representation of proposed two-stage MSMPR setup for CSC.

To control the particulate properties in each stage, understanding of the critical operating parameters and their effect on each stage is important. Table 6.1 lists the critical parameters for each stage. The mean residence time will be a critical parameter for both stages as it will determine approximately the average time for crystal growth in the first stage and the average time for agglomerates to consolidate in the second stage. The agitation rate is critical in both stages. In the first vessel, it is important to limit secondary nucleation, reduce breakage and agglomeration so that crystal counts in the vessel are close to constant throughout the experiment. Keeping agitation at a moderate level will accomplish this. However, in the second vessel the opposite is true. It is important to operate the second stage at high agitation rates to produce more spherical and stronger agglomerates. The SASR in the first stage, and subsequently throughout both stages, will change the supersaturation and plays the most significant role in the CSD in the first vessel. These primary crystals then become the internal crystals that makeup the agglomerates. The last parameter of importance is the BSR. Proven in the literature, through batch experiments, there exists a critical range for the BSR.[139] In continuous experiments, the critical operating range to guarantee SA production needs to be developed. The BSR,

residence time in the second stage and agitation have a combined effect of the size distribution of agglomerates (ASD) and their micromeritic properties.

Table 6.1 Critical Operating Parameters in two-stage MSMPR

1st Stage	2nd Stage
Residence time (RT)	Residence time (RT)
Agitation rate (N)	Agitation rate (N)
Operating volume (V)	Operating volume (V)
Solution to anti-solvent ratio (SASR)	Bridging liquid to solute ratio (BSR)

6.3.1 Materials and methods

Lab grade benzoic acid (C_6H_5COOH) (>99% purity Fisher Science Education) was used as the model drug compound. Benzoic acid is a good model drug for SC given that its crystal habit from traditional crystallization techniques is poorly flowing thin plates or needles.[26] It was dissolved in ethanol (pure, 200 pf, KOPTEC, USP Grd) which served as the good solvent. Deionized water induced anti-solvent crystallization, and served as the poor solvent given its poor solubility of the model drug. Toluene (>99.5% Macron Fine Chemicals) served as the bridging liquid as it has proven to be a suitable bridging liquid in the literature.[137,139] Nitrogen (dry, 99.9% purity) and vacuum moved slurry into and out of the transfer zones. A Nikon microscope was used to take pictures of the resulting spherical agglomerates.

The proposed two-stage MSMPR system (shown in Figure 6.3) was used for the CSC studies. The stages consist of 500 ml lab scale jacketed crystallizers. An overhead stirrer with a three-blade retreat curve impeller was used to agitate the system. At agitation rates ranging from 250 to 500 RPM good mixing was observed. Peristaltic pumps (Cole-Palmer) and platinum cured silicon tubing (MasterFlex L/S) fed solution and anti-solvent into the first stage. A KDS 100 syringe pump or a Cole-Palmer peristaltic pump using MasterFlex L/S tubing fed bridging liquid into the second stage. All inlet liquids (solution, anti-solvent, and bridging liquid) were added to the vessel at the surface, equidistance from the impeller and crystallizer wall. The slurry transfer of each stage was carried out in a manner similar to the process described in Hou et al. (2014).[193] Using a dip tube intermittent slurry transfer occurred by a combined vacuum and pressure, which removed and then purged the slurry into and out of the transfer zone (Figure 6.3). For the first and second stage, withdrawal

was no more than 4.2% and 6.8% of the suspension, respectively. The ratio of the transfer zone volume to the volumetric feed rate determined the cycle times (CT), or the constant intervals at which transfer occurred. A programmable control unit allowed for the automation of the solenoid valves that controlled both vacuum and nitrogen (control unit and transfer line provided by Eli Lilly & Co). In all the experiments, bridging liquid is fed to the second stage at the same CT as the volume of slurry transferred from the first stage. Lasentec FBRM S400 and FBRM G400 by Mettler-Toledo were used to monitor the process in the first and second stage, respectively. The probes allowed the identification of nucleation/growth and agglomeration mechanisms as well as identification when the CSO was achieved.

Product samples used in this study were collected every residence time from the agglomeration stage using a wide-mouth pipette and were filtered. Samples were air dried at room temperature for 24hrs then off-line imaging and dissolution studies were conducted. During operation, the rest of products were continuously collected in a collection vessel. For the dissolution studies, an attenuated total reflection ATR-UV/Vis probe was used to measure absorbance of benzoic acid. The UV peak absorbance for benzoic acid is at a wavelength of about 220-240 nm. A 230-nm wavelength was used for this studies. A 27% ethanol and 73% water mixture served as the dissolution medium. The ethanol-water mixture improved the wettability of the spherical agglomerates and assured the spheres remained suspended. For each study, a 500-mL jacketed vessel was used with 100 mg of agglomerates dissolved in 300 ml of the dissolution medium. The temperature was constant at 37 °C and the agitation rate was set at 250 rpm for all dissolution studies. The dissolution differences were assessed based on the t_{80} of each respective experiment. The t_{80} represents the amount of time it takes to reach 80% of the maximum dissolved concentration. The studies were repeated three times and the standard deviation has been included as error bars in the dissolution profiles. SEM images were taken of the spheres from the experiments used for dissolution studies.

6.3.2 Procedure

Solution preparation consisted of dissolving benzoic acid in ethanol at 40 °C then allowing the solution cool to room temperature. The saturation temperature of the maximum

concentration used was 15 °C. The critical operating parameters for the present experiments were those presented in Table 6.1 combined with the bridging liquid, solution and anti-solvent flow rates and benzoic acid concentrations. Compared to the second stage, in the first stage agitation rate and operating volume were lower to promote the minimal amount of nucleation and growth by reducing secondary nucleation and residence time. Initially, the first stage is operated in semi-batch mode feeding the benzoic acid in ethanol solution into a specified amount of anti-solvent until the specific SASR is reached after which both solution and anti-solvent are fed and are then transferred from the first stage to the second is initiated. The second stage operated at a higher agitation rate and residence time to promote better agglomeration and allow the granules to mature. In a few experiments, bridging liquid feed to the second stage initiated after the first stage approached a CSO in terms of counts and mean size. For the dissolution studies, when the UV absorbance reached an equilibrium, the study was terminated and the equilibrium value was taken to be the maximum UV absorbance. The percent dissolution becomes the UV absorbance over the maximum multiplied by 100.

6.4 Results and discussion

In total 10 experiments were performed to assess the viability of the proposed CSC-MSMPR setup. Table 6.2 lists the specific operating conditions and outcomes of each experiment. The experiments consisted of conditions that proved to be successful for batch operation in the literature.[26] Two concentration levels were attempted 0.25 and 0.375 g/ml of benzoic acid in ethanol. The SASR and BSR range were 0.20-0.33 and 0.59-1.25, respectively. Two levels of agitation rate were attempted for each stage; 250 and 300 rpm for the first stage, and 400 and 500 rpm for the second stage. The volume of each stage was adjusted multiple times to assess the influence of residence time.

Table 6.2: Operating Conditions for CSC experiments in two-stage MSMPR

Exp.	Conc. of BA in Feed (g/ml)	Op. Stage	SASR	BSR	N (rpm)	V (ml)	RT (min)	CT (min)	Flow Rates (ml/min)				Result
									BL	S	AS	Overall	
1	0.250	*1st*	0.33	--	300	300	60.00	2.48	--	1.25	3.75	5.00	small, loosely compact and flakey spheres
		2nd	0.33	1.00	400	500	100.00	6.72	0.20	--	--	5.20	
2	0.250	*1st*	0.33	--	300	300	37.50	1.55	--	2	6	8.00	small, loosely compact and flakey spheres
		2nd	0.33	1.00	400	500	62.50	4.20	0.32	--	--	8.32	
3	0.250	*1st*	0.33	--	250	300	37.50	1.55	--	2	6	8.00	crystals, paste-like slurry
		2nd	0.33	1.25	400	500	62.50	4.20	0.40	--	--	8.40	
4	0.250	*1st*	0.20	--	250	300	33.33	1.37	--	1.5	7.5	9.00	large spheres
		2nd	0.20	1.00	500	500	55.56	3.73	0.24	--	--	9.24	
5	0.375	*1st*	0.33	--	250	250	31.25	1.55	--	2.00	6.00	8.00	irregular shaped agglomerates, spheres, and crystals
		2nd	0.33	0.59	400	400	50.00	4.20	0.26	--	--	8.26	
6	0.375	*1st*	0.33	--	250	200	25.00	1.55	--	2.00	6.00	8.00	spheres and crystals
		2nd	0.33	0.82	400	450	56.25	4.20	0.36	--	--	8.36	
7	0.375	*1st*	0.33	--	300	250	25.00	1.23	--	2.5	7.5	10.00	spheres and crystals
		2nd	0.33	1.00	400	450	45.00	3.37	0.55	--	-	10.55	
8	0.375	*1st*	0.33	--	250	250	25.00	1.23	--	2.5	7.5	10.00	spheres and crystals
		2nd	0.33	0.82	400	500	50.00	3.37	0.45	--	--	10.45	
9	0.375	*1st*	0.33	--	250	300	37.50	1.55	--	2	6	8.00	irregular shaped agglomerates and paste-like slurry
		2nd	0.33	1.25	400	500	62.50	4.20	0.56	--	--	8.56	
10	0.375	*1st*	0.23	--	300	300	37.50	1.55	--	1.5	6.5	8.00	uniform spheres
		2nd	0.23	1	500	500	62.50	4.20	0.33	--	--	8.33	

As shown, only two experiments produced solely spherical agglomerates (experiments 4 and 10). The other experimental conditions produced small, loosely compact spheres, irregularly shaped agglomerates, or combination of spheres and crystals. The most influential operating parameters that differentiated the product quality in these experiments were the agitation rate (N) in the second stage and the BSR. The agitation rate in the second stage for the two successful experiments was 500 rpm. The experiments that produced spheres and crystals and were in the mid-range of the BSR ratios attempted would have produced spheres had the agitation rate been sufficient. In previous batch experiments, 400 rpm was successful due to the smaller scale at which the experiments were conducted. At the scale of these continuous experiments, 400 rpm is not sufficiently high to produce the

necessary agglomeration needed for uniform spherical agglomerate products. Experiments at the lowest and highest BSR coincided with the experimental results found in the literature and the mechanisms described in Figure 6.2. At low BSR there is insufficient bridging liquid to promote complete agglomeration and at high BSR large, very porous and irregularly shaped agglomerates are formed. The SASR plays an important role in determining the supersaturation of the system. Higher SASR results in a lower supersaturation and therefore less yield. The combination of high SASR and high BSR will produce a paste-like slurry due to the lower crystal yield and excess bridging liquid as shown in Table 6.2. The remaining parts of this work will focus on examining the two successful experiments.

Table 6.2 has the operating conditions for experiment 4 and Figure 6.4 presents the in-situ FBRM data. As previously mentioned, initially the first stage operates in semi-batch mode to produce the crystals for the continuous experiment. This accounts for the ~50-min shift at the start of data collection in the second stage. In experiment 4, bridging liquid addition to the second stage was initiated after one RT (~55.6 min) and was fed continuously using a syringe pump. As can be seen in Figure 6.4b, the counts in the second stage immediately begin to decrease at the start of bridging liquid addition. There is also an immediate increase in mean chord length (Figure 6.4d). These are clear indications that agglomeration occurs in the system. In Figure 6.4d the mean chord length is seen to be oscillating this is potentially due to the to the competing phenomena of nucleation, growth, and agglomeration as slurry is being transferred from the first stage to the second. There has been work in the literature that shows how different operating conditions can cause continuous MSMPR to have multiplicity and oscillatory behavior due to changes in the complex interactions between the different crystallization mechanims.[39,194] Figure 6.4b shows the effect of nucleation as the counts <10 microns are the highest. Figure 6.2f shows the chord length distribution of the agglomerates and it shows a wide, almost bimodal distribution.

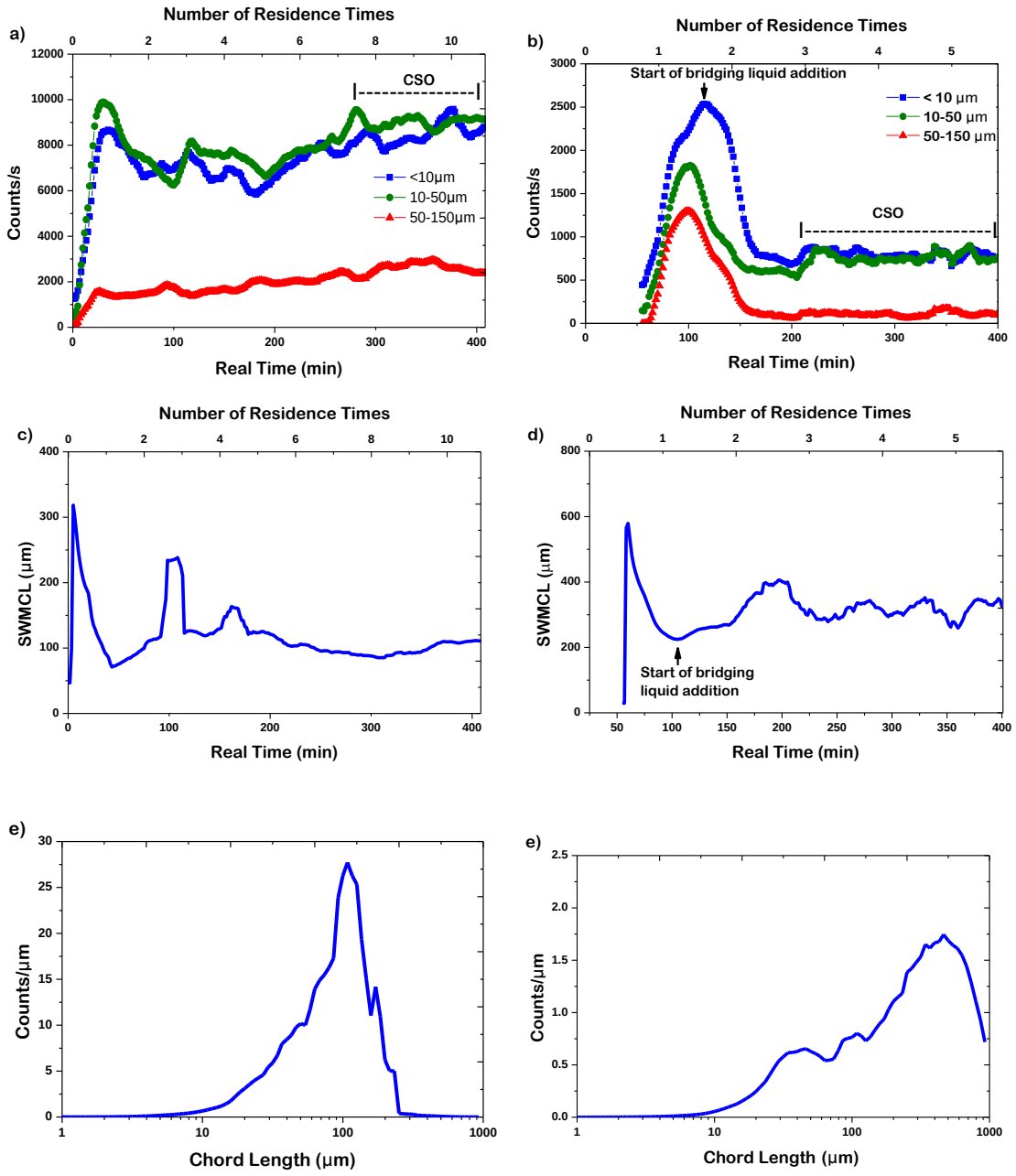

Figure 6.4 In-situ FBRM counts/s, mean chord length, and chord length distribution, (left) Stage1 (Nucleation/Growth): a) Counts/s; c) Square Weighted Mean Chord Length (SWMCL); e) Square Weighted Chord Length Distribution; (right) Stage 2 (Agglomeration): b) Counts/s; d) SWMCL; f) Square Weighted Chord Length Distribution. Note that bridging liquid addition to the second stage initiated after one RT (~55.6 min).

In approximately 1.5 RT from the start of bridging liquid addition, the counts in the second stage begin to reach a CSO (Figure 6.4b). However, Figure 6.4a shows the first stage lags, taking slightly longer to reach a CSO. The first stage begins to reach a CSO at

7 RT (7×33.3 min) and the second stage reaches a CSO at 2.5 RT (2.5×55.6 min). This is common from a two-stage operation as the second stage tends to attenuate future variations from the periodic addition of slurry from the first, and therefore reaches a CSO faster. These observations point out the key benefits of in-line PAT tools, such as FBRM, that it allows for the identification of different process mechanisms like agglomeration and process monitoring to determine that a suitable CSO is achieved.

Figure 6.5 shows pictures of agglomerates at different times after initiation of bridging liquid addition. As can be noted from the pictures, the agglomerates from experiment 4 are very irregular in shape and not very uniform in size. The two top pictures in Figure 6.5a show some agglomerates that are very spherical and somewhat uniform in size while Figure 6.5b shows an agglomerate that was so large that it was out of the view of the microscope used. The scale in each picture is 1000 μm. The irregularities in shape in this experiment can be attributed to several operating issues. For one, it appears that the bridging liquid was added prematurely and there were not enough particles in the second stage for bridging liquid being added. Also, because the bridging liquid was added to the second stage continuously but the slurry from the first stage was added in intervals there were periods of imbalance between the amount of bridging liquid and amount of crystals in suspension. This excessive amount of bridging liquid potentially caused excessive agglomeration and production of very large, irregularly shaped agglomerates. Another potential reason for the very large, irregularly shaped agglomerates and wide chord length distribution is the fact that as the agglomerates got bigger there may not have been representative withdrawal from the second stage. Combining that with the incoming crystals from the first stage would undoubtedly cause a wider agglomerate size distribution.

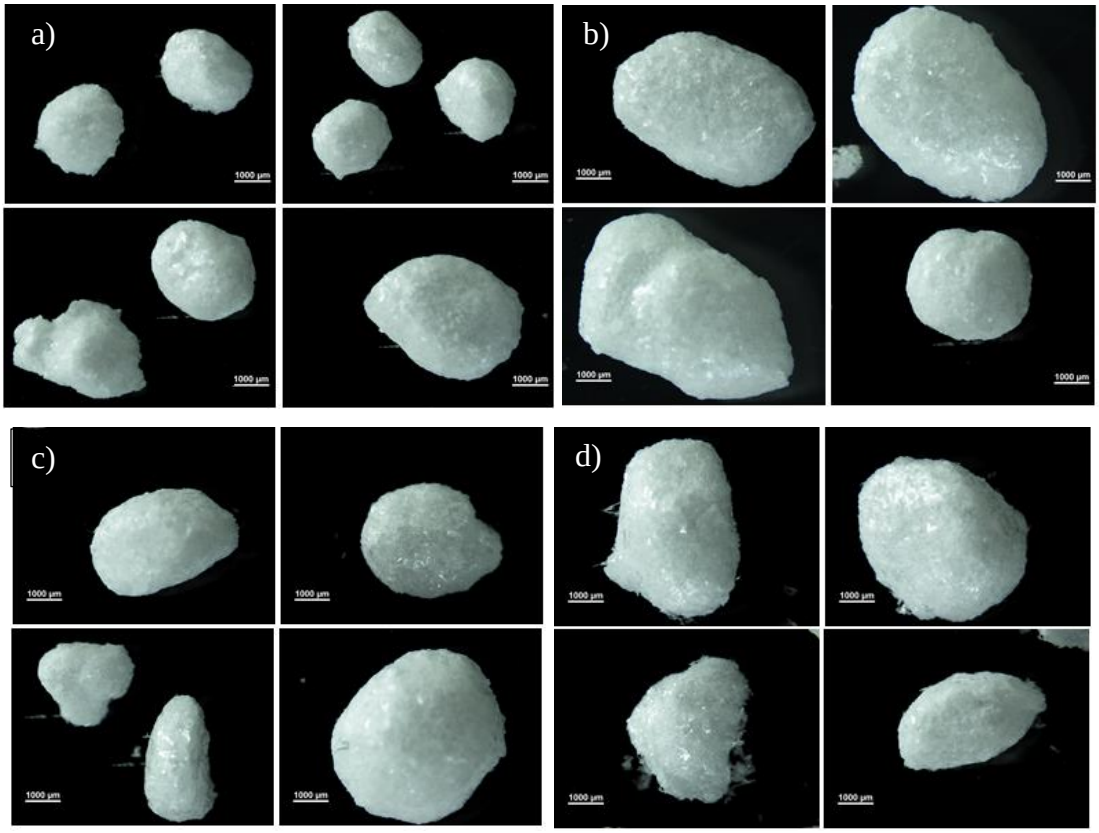

Figure 6.5 Spherical agglomerates at different times after bridging liquid addition: a) 1 RT after bridging liquid addition; b) 3 RT after bridging liquid addition; c) 4 RT after bridging liquid addition; d) 5 RT after bridging liquid addition.

Table 6.2 has the operating conditions for experiment 10 and Figure 6.6 below presents the in-situ FBRM data. The results from the experiments produced very spherical agglomerates and a more uniform ASD in comparison to experiment 4. Figure 6.6a shows that CSO was achieved in the first stage within approximately six residence times and maintained for approximately four residence times. The second stage approached a CSO at approximately 5 to 6 residence times (Figure 6.6b). In experiment 10, bridging liquid addition began after the first stage had reached a CSO (six residence times) and the second stage had nearly reached a CSO (three residence times) in terms of counts/s. In this experiment, the bridging liquid addition to the second stage occurred intermittently at the same cycle time as the slurry coming from the first stage. This allowed for bridging liquid addition at the exact BSR needed for the slurry coming in. The data from the second stage (Figure 6.6b and Figure **6.6**d) clearly depicts the decrease in counts/s and the increase in mean chord length after bridging liquid addition started, allowing for the clear

identification of agglomeration. One difference between experiment 4 and 10 is that once bridging liquid addition began the mean chord length increased and reached a new CSO rather than oscillating as it did in experiment 4. This is a sign of a more uniform size distribution (Figure 6.6f) as there are fewer fluctuations in the mean chord length. Figure 6.6f shows the chord length distribution to be uniform compared to in experiment 4. The chord length distributions before and after bridging liquid addition indicates a significant decrease in the counts/s. Overall, this experiment show less instability and oscillations when compared to the previous experiment. From the FBRM counts it appears that the effects of nucleation in the second-stage are also less pronounced in this experiment which could account for the improved stability in the mean chord length.

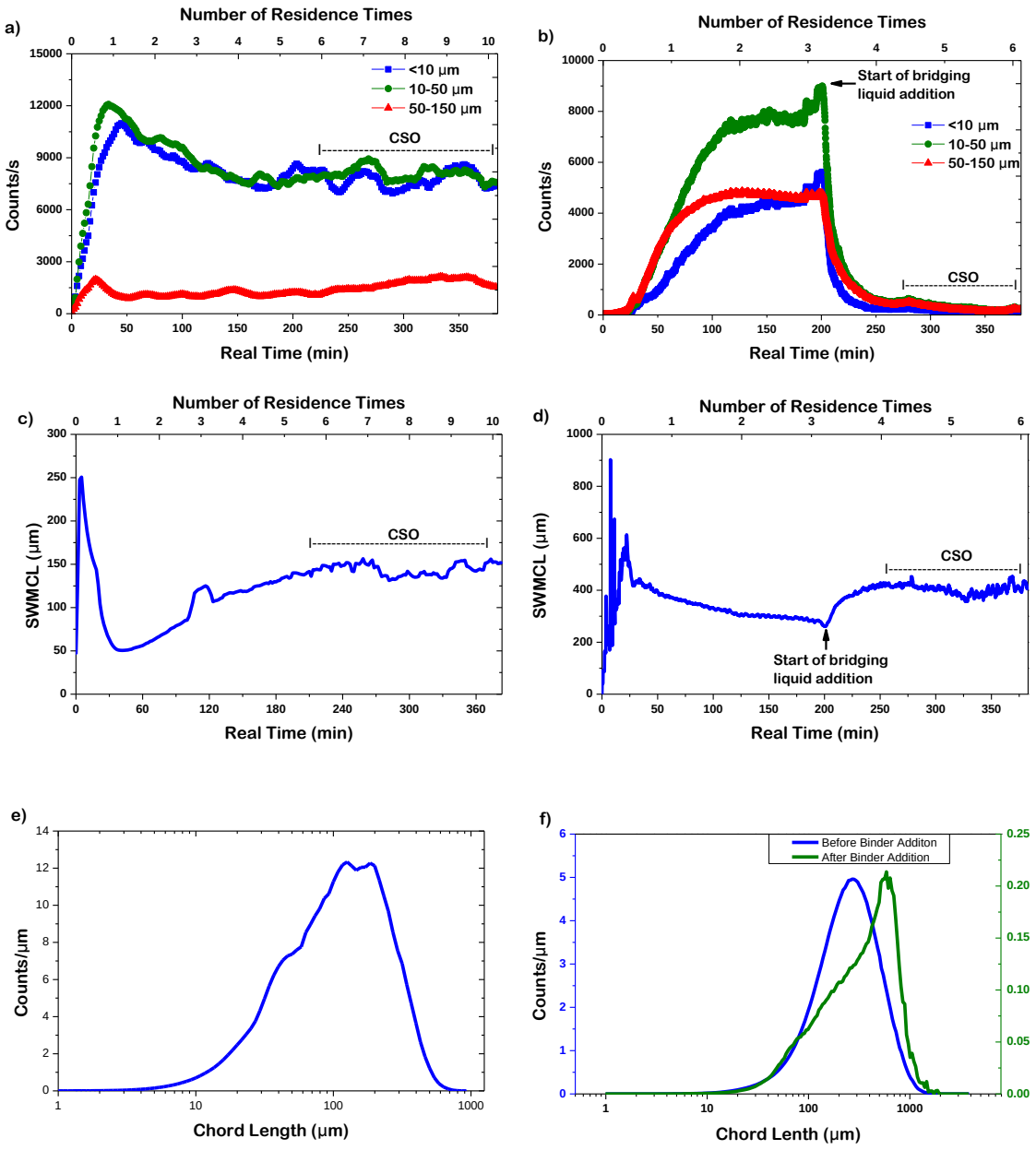

Figure 6.6 In-situ FBRM counts, mean chord length, and chord length distribution, (left) Stage1 (Nucleation/Growth): a) counts/s; c) SWMCL; e) Chord Length Distribution; (right) Stage 2 (Agglomeration): b) counts/s; d) SWMCL; f) Chord Length Distribution.

Visual and qualitative assessment of the improvement in agglomerate size and shape can been done through Figure 6.7, which shows pictures of the agglomerates at different times after the bridging liquid addition was initiated. Figure 6.7a-c shows the clear improvement in sphericity and size uniformity with time. The scale in each the picture is 1000 µm.

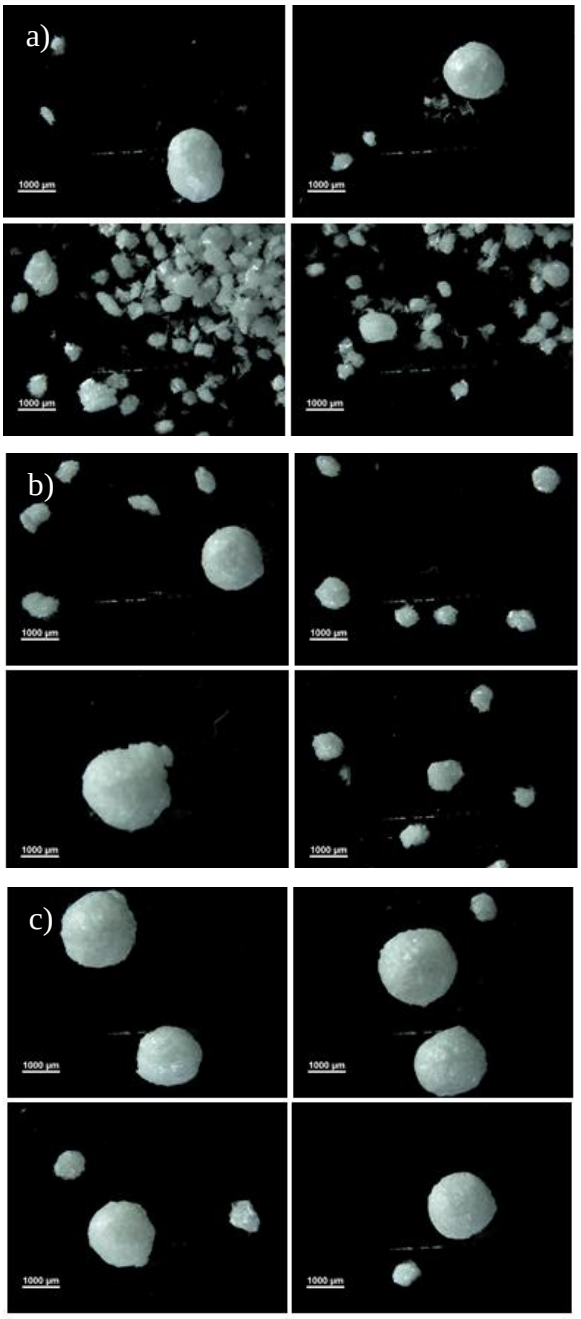

Figure 6.7 Spherical agglomerates at different times after bridging liquid addition: a) 1 RT after bridging liquid addition; b) 2 RT after bridging liquid addition; c) 3 RT after bridging liquid addition.

6.4.1 Dissolution studies

Comparison of dissolution properties from experiments at different conditions illustrates the potential ability of the proposed system for product design by producing agglomerates

with different release profiles based on tailoring the combination of internal CSD, external ASD and micromeritic properties through manipulating the operating conditions in each stage. The spherical agglomerates produced from experiments 9 and 10 were compared for these studies. The t_{80} for experiment 9 (higher BSR and SASR than experiment 10) is approximately 2.5 min whereas for experiment 10 is approximately 7.5 min (Figure 6.8). The dissolution results present a clear difference in biopharmaceutical properties, illustrating the potential control of dissolution rate, hence drug release profile, through varied operating conditions of the CSC system. The agglomerates obtained from the experiment with a higher BSR and higher SASR dissolved three times faster than at lower BSR and lower SASR.

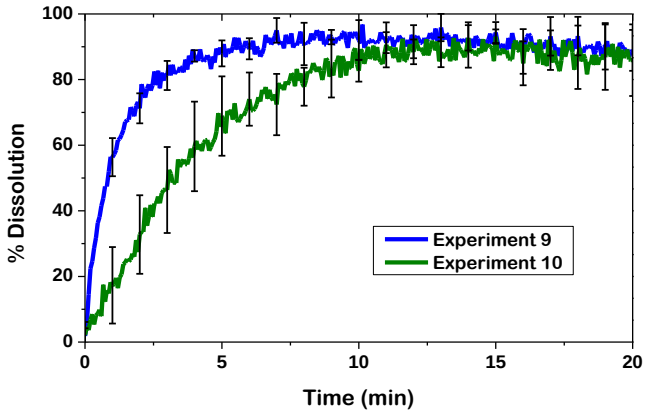

Figure 6.8 Dissolution profiles of spherical agglomerates obtained under different operating conditions.

There are two contributing reasons for this based on the two operating parameters that were changed. Figure 6.2 explains the contribution of an increased BSR to the dissolution properties. As the BSR is increased, it goes from suboptimal to critically optimal to excessive bridging liquid. When excess bridging liquid exists, it produces agglomerates with loose, very porous structures and more solvent inclusion (Figure 6.2f). Due to the fair solubility of the compound in the bridging liquid, when the agglomerate is filtered and dried, crystallization of fine crystals will occur. However, due to the porous nature of the agglomerate the new fine crystals do not pack into the structure of the agglomerates tightly.

These fine crystals and the loose structure of the agglomerate cause rapid disintegration and dissolution compared to the tightly packed spheres from experiment 10.

Figure 6.9 shows SEM images of the spheres produced from the experiments 9 and 10. The top pictures (a) are spheres from experiment 9 which show a more porous structure as well as irregularly shaped primary crystals. The bottom pictures (b) are of a spherical agglomerate from experiment 10, which show less porosity and void space and the primary crystals have a consistent structure (plate-like crystals). The spherical agglomerates from experiment 10 resemble the agglomerates corresponding to the SA mechanism stages given in Figure 6.2b-c. This is further validated by the fact that Thati & Rasmuson found the critical operating BSR range for a benzoic acid and ethanol-water-toluene system to be 0.47-1.16 (at 20 °C).[137] The higher SASR increases the rate of supersaturation generation. This level of supersaturation generation can also cause the system to precipitate fast, which can lead to unstructured crystals seen in the Figure 6.9a.

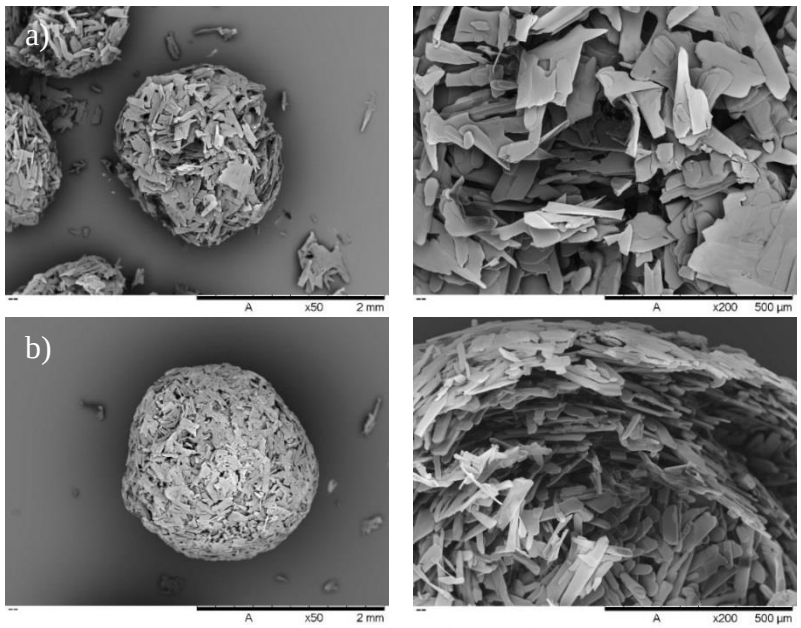

Figure 6.9 SEM Images of agglomerates form different operation (a) experiment 9 (b) experiment 10.

Figure 6.10 displays agglomerated particles from experiment 9. The figure indicates clearly the irregularly shaped agglomerates that are obtained from these operating conditions. From the figure, it is also clear that the agglomerates are far more ‘flaky’ than the spherical

agglomerates from Figure 6.7c. This is evident by the small fine crystals that appeared to have fallen off the agglomerates when placed on the slide. The agglomerates in Figure 6.7c correspond to the BSR level shown in Figure 6.2b-c, whereas the agglomerates from Figure 6.10 correspond to the BSR level shown in Figure 6.2e-f. The results of the dissolution study combined with the entire experimental design provide validation for the proposed CSC-MSMPR setup. The results presented demonstrate the ability to tailor the properties of the product for both biopharmaceutical and processing benefits.

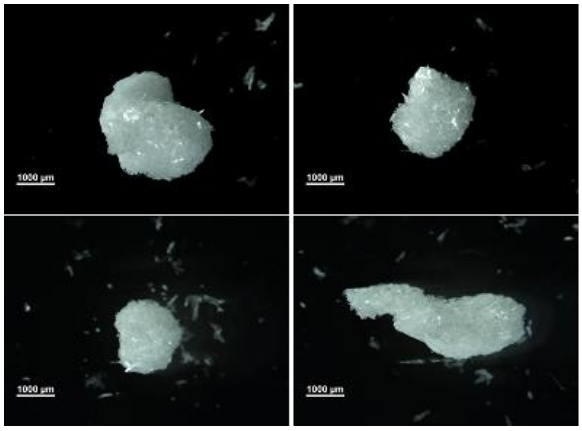

Figure 6.10 Agglomerate particulates from experiment 9 (BSR = 1.25, SASR = .33).

6.5 Conclusions

In this work a two-stage MSMPR setup for CSC is proposed that serves as a combined process and product design platform. To go along with the ability to decouple different mechanisms by allotting different stages for each mechanism, the setup allows for continuous spherical agglomerate production. This new process and product design approach represents a novel continuous manufacturing platform for pharmaceutical solid products; hence supporting current trends in the pharmaceutical industries to move toward continuous processes. By implementing CSC, the setup also serves as a PI technique thereby reducing the total number of unit operations that would be need in a pharmaceutical production line. The spherical agglomerates have the potential to be directly compressed and as proven by the dissolution results a specific drug compound can be produced in such a way as to have different final properties (size, dissolution, compactibility). The properties of the spherical agglomerates produced by the CSC platform can be altered by changes in operating parameters, which is an improved method of meeting product specifications over

batch crystallization and granulation. The benefits of the setup also include the ease with which these spherical particulates can be processed post-crystallization (filtering, drying, and compressing). In this study, the FBRM served as a useful PAT tool to indicate when the system reaches a CSO and in identifying the agglomeration process. However, due to the large size of the spherical agglomerates, true particle size analysis of the spherical agglomerates needs to be conducted offline as part of a characterization study. Transition from BSC to CSC-MSMPR should be straightforward and feasible. The results here have demonstrated that the critical operating parameters remain the same for both BSC and CSC. The extra parameters in CSC are mainly flow rate and crystallizer volume that control residence time. Given a sufficient residence time, increased or decreased residence time affects strength and sphericity more so than the ability to produce spherical agglomerates.

The proposed two-stage MSMPR-based approach for CSC allows for greater degrees of freedom to tailor product properties. The added benefit of the proposed approach is the ability to independently tailor the properties of the crystalline particulates that compose the spherical agglomerates and the characteristics of the agglomerates produced by CSC. Hence the proposed two-stage MSMPR system for CSC serves as both a product and process design approach.

7. PROCESS INTENSIFICATION THROUGH CONTINUOUS SPHERICAL CRYSTALLIZATION USING AN OSCILLATORY FLOW BAFFLED CRYSTALLIZER (OBCF)

This chapter is reprinted with minor modification with permission from Peña, R., Oliva, J. A., Burcham, C. L., Jarmer, D. J., & Nagy, Z. K. (2017). *Crystal Growth and Design*, acs.cgd.7b00731.

7.1 Introduction

As the pharmaceutical industry continues to adopt different aspects of continuous processing, PI will be a key driver towards more integrated unit operations. PI is defined as the integration of innovative techniques and technologies to create sustainable solutions to current industrial production difficulties. It is comprised of two parts: novelty in equipment[43,195] and novelty in processing techniques.[3,19,21,96,196-199] Continuous PI techniques lead to improved product quality, process safety and efficiency, and a reduction in waste/maintenance. These techniques allow for development and manufacturing at laboratory scale, ultimately reducing time to market and improving patent life utilization.[17,43,46,96,196]

Spherical crystallization is inherently a PI technique due to its ability to eliminate further downstream unit operations and improve particulate flow properties while promoting higher processing efficiency. CSC provides the ability to directly connect upstream reaction synthesis to separation and purification unit operations. Peña & Nagy (2015) and Tahara et al. (2015) implemented CSC using MSMPR systems.[130,170] Tahara et al. (2015) used a single-stage MSMPR to carry out a QESD SC technique with a solvent recycle stream.[125,200] The recycling of solvent from the mother liquor resolves two major issues common to SC: low yield and maintaining the low ratio of solvent (API carrier) to anti-solvent. Peña & Nagy (2015) used a SA technique in a two-stage MSMPR system where the first stage was the nucleation/growth dominated stage and the second stage was the agglomeration dominant stage through the use of a bridging liquid (binder).[26,123,139] Their work focused on the ability to alter both the properties of the internal (primary) crystals and the agglomerates by independently changing operating conditions in each

stage. Independent control of internal and external properties provides the ability to achieve a target primary crystal size for bioavailability and a target agglomerate size for drug product manufacturability. The ease of 'knowledge transfer' from batch to continuous operation using the design concept of a MSMPR was evident when comparing the feasibility of SC in Peña & Nagy (2015) and Tahara et al. (2015) to those of batch operations.[125,139]

The MSMPR framework provides a straightforward technology transfer from batch operations since the mixing dynamics for both systems can be similar (independent of the net flow). The MSMPR system can be expanded in capacity and degrees of freedom through the addition of a cascade of multiple stages.[200,202] These characteristics make the MSMPR one of the more flexible continuous systems. However, broad CSDs are typically obtained as a result of the broad residence time distributions (RTD) experienced by crystals.[38,203] Another concern when using multistage MSMPR systems is appropriately transferring crystal slurry through each stage while maintaining the crystallizer operating conditions.[40,130,193] Plug flow reactors (PFRs) are an alternative continuous system that are known to deliver narrower CSDs. However, PFRs usually require high flow rates to create the desired mixing quality via turbulence. This requirement can lead to physically unrealistic lengths to achieve appropriate residence times.[43,170] As a design alternative to PFRs, the oscillatory flow baffled reactor (OFBR) is a plug flow reactor where an oscillatory motion is superimposed on the net fluid flow through the use of a piston near the reactor inlet. Periodically spaced baffles along the reactor length create changes in the reactor internal diameter, leading to paired eddy propagation as the net flow oscillates back and forth.[43] The zone between each pair of baffles is assumed to be uniformly mixed and acts as a continuous stir tank reactor. Figure 7.1 is a schematic that illustrates the fluid flow pattern of the oscillatory system. In some cases, the mixing capabilities of an OFBR are enhanced relative to a PFR, leading to improved heat transfer, longer residence times, turbulent mixing with laminar net flow Reynolds (Re_n), smaller reactor volume, and narrower CSDs.[42,43,204,205]

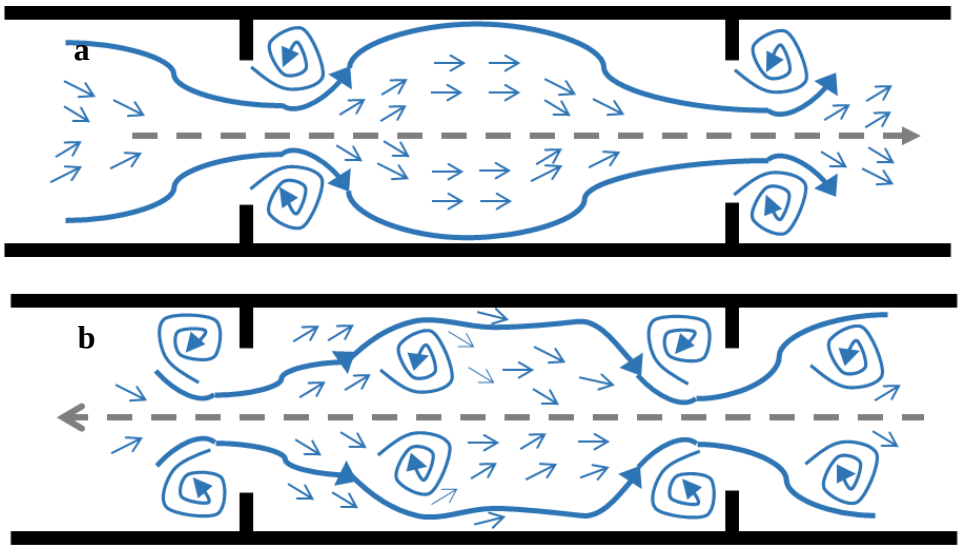

Figure 7.1 Schematic of the fluid flow pattern in an OFBR/C with net flow to the right: a) forward stroke b) backward stroke. Adapted with permission from [204] Copyright 2002 Elsevier and [42] Copyright 2003 Elsevier.

There are four key dimensionless parameters often used to define the fluid flow patterns in an OFBR, which include the oscillatory Reynolds number (Re_o), the net flow Reynolds number (Re_n), the Strouhal number (St), and Ψ, the ratio of oscillatory and net flows.

$$Re_o = \frac{2\pi x_0 f \rho D}{\mu} \quad 7.1$$

$$Re_n = \frac{\rho u D}{\mu} \quad 7.2$$

$$St = \frac{D}{4\pi x_0} \quad 7.3$$

$$\Psi = \frac{Re_o}{Re_n} \quad 7.4$$

The variables in equations 7.1-7.4 are as follows: x_0 is the piston amplitude, f is the oscillation frequency, ρ is the fluid density, D is the internal diameter of the tube segment, u is the mean superficial fluid velocity, and μ is the fluid viscosity. The Strouhal number (St) represents the effective eddy propagation through the ratio of the tube diameter to piston stroke length.[42,205] The Re_o measures the intensity of the oscillations generated by the piston and therefore, the turbulence level imposed on the fluid. The Reynolds number (Re_n) is the ratio of inertial to viscous forces. The volumetric flow rate limits the Re_n in the system, despite the impeding oscillatory flow imposed by the piston. The ratio of the Reynolds numbers (Re_o/Re_n) results in a dimensionless mixing parameter, Ψ, a measure

of oscillatory versus net flows. Large Ψ values result in "well-mixed" sections between the baffles.[42,206]

The objective of this study was to conduct CSC in an OFBC system. Conceptually, the system enables the application of various types of SC techniques; allowing for both simultaneous and independent nucleation, growth, and agglomeration mechanisms. The ability to have spatially independent zones within a crystallizer where only one crystallization mechanism is dominant offers additional degrees of freedom for the control of final product properties. This technique allows for products to be tailored for biopharmaceutical benefit and efficacy (e.g., bioavailability, dissolution rate, particle morphology) and processing efficiency (e.g., filtration and drying times). The feasibility of SC within a OFBC was studied via a series of experiments in which the control crystallization mechanisms and final product properties were investigated.

7.2 Materials and methods

7.2.1 Materials

Benzoic acid (C_6H_5COOH) (≥99.5% purity, Sigma Aldrich) was used as the model compound in this study. Benzoic acid SA has been studied in the literature making it an ideal candidate for this study.[26,130,139] The solvent system consisted of ethanol (pure, 200 pf, USP grd, Decon Labs), deionized water, and toluene (≥99.5% assay, Fisher Scientific). Ethanol served as the solvent in which to prepare benzoic acid solutions, water as the anti-solvent, and toluene as the bridging liquid. Acetic acid (≥99.5% assay, Fisher Chemical), water (Optima LC/MS grade, Fisher Chemical) and methanol (Optima LC/MS grade, Fisher Chemical) were used for ultra-performance liquid chromatography (UPLC) quantification of benzoic acid. The spherical agglomerates created were filtered and dried at 60 °C for 24 hours. A Nikon microscope was used to take images of the spherical agglomerates. Image analysis software (ImageJ) was used to determine the agglomerate size distribution (Feret diameter) and assess final agglomerate morphology.

7.2.2 Experimental setup

The OFBC was evaluated for a CSC process using a spatially distributed solvent/anti-solvent/binder addition strategy. In this system, nucleation and growth occur in the first

four segments due to supersaturation created by mixing solution and anti-solvent, while bridging liquid is added at the end of the fourth segment, leaving a four-segment agglomeration zone. Figure 7.2 is a picture of the experimental setup and illustrates the nucleation, growth, and agglomeration zones. Changing the binder addition location makes the agglomeration zone flexible in that adjusting this residence time allows one to tailor agglomerate size to a desired size target.

The OFBC used in this work (Figure 7.2) was a Nitech DN15 (Alconbury Weston Ltd) consisting of eight segments and a total volume of 1250 mL. All segments and elbows of the DN15 were jacketed for temperature control. The temperature was controlled by using four thermo-regulators (Huber Ministat 125/Julabo F25-ME) effectively dividing the OFBC into four temperature zones. The first zone (consisting of one segment) was kept at 40 °C to dissolve particles and prevent particles from reaching the piston which can lead to damage/leaking. The rest of the zones (consisting of seven segments) were kept at 22 °C. There is a temperature gradient from 40 °C to 22 °C at the interface between the first and second segments, however the temperature converges to 22 °C by the exit of the second segment and is uniform through the remaining segments of the OFBC. The solution was added at the end of the first zone to ensure an antisolvent process. Peristaltic pumps (MasterFlex L/S by Cole-Palmer) and platinum cured silicon tubing (MasterFlex L/S by Cole-Palmer) were used for both solution and anti-solvent feed into the OFBC (100-150 mL/min). A Waters 515 HPLC pump was used to feed toluene at the bridging liquid injection point through an injector (1.32-1.65 mL/min). A control unit allows for setting the oscillation amplitude (mm) and frequency (Hz). A Lasentec FBRM S400 was used for on-line monitoring of the particle chord length distribution within the system.

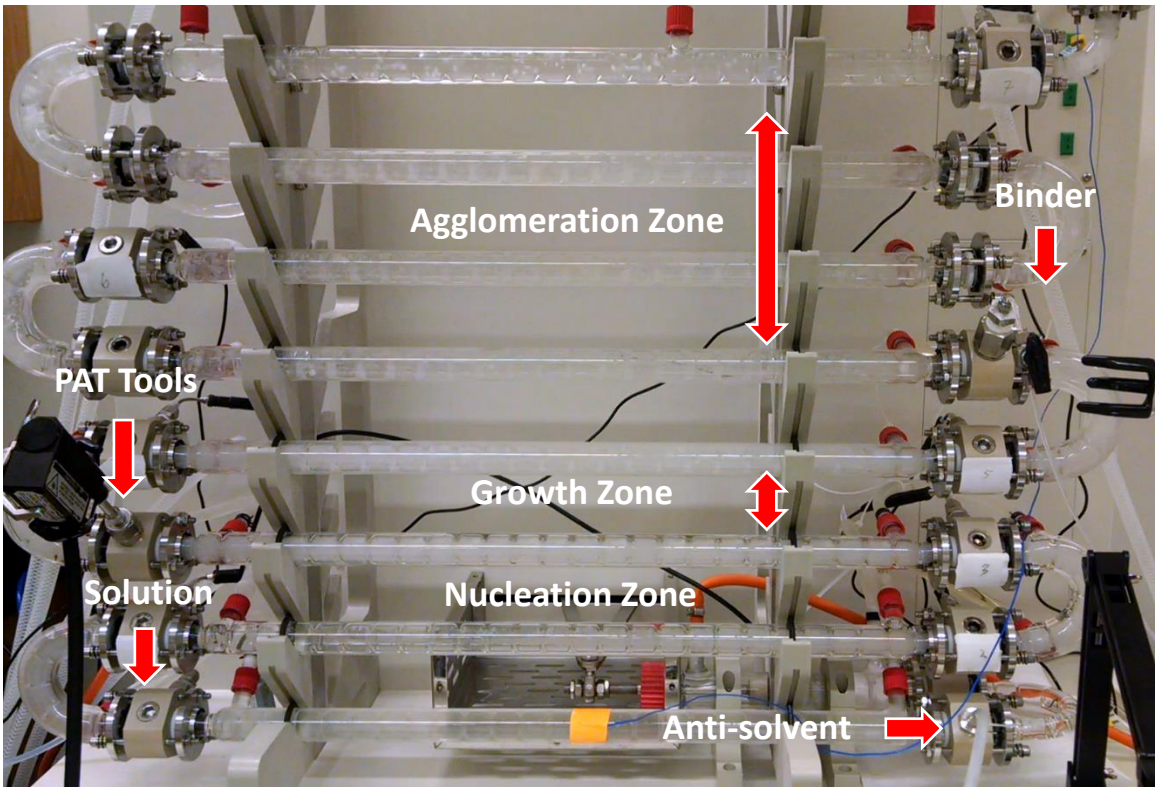

Figure 7.2 OFBC configuration indicating location of anti-solvent, solution and binder addition as well as PAT port (FBRM).

7.2.3 UPLC method of benzoic acid quantification

UPLC techniques differ from high performance liquid chromatography (HPLC) techniques in that they utilize columns with smaller diameters and particles (larger surface area to volume ratio), and therefore higher pressures to increase peak capacity (number of peaks resolved per unit time) and decrease retention time.[207] Benzoic acid quantification for both the determination of steady state and solubility data used an Acquity UPLC system (Waters Corporation). The system utilizes column, sample, and binary solvent managers coupled with Tunable Ultraviolet (TUV) detection in an offline setup to create an output signal that is later processed using the Empower 3.1 software (Waters Corporation). The stationary phase was an Acquity UPLC BEH C18 column 2.1 mm x 100 mm, 1.7µm, while the mobile phase was a combination of 1.5 % (v/v) acetic acid (in water) solution and HPLC grade methanol in an 85:15 ratio by volume. The diluent contains the same two solutions as the mobile phase, but in a 55:45 ratio by volume. Each sample injection was 10 µL and the

flow rate of the mobile phase was 0.5 mL/min. The temperature of the column was 40°C and the UV detection wavelength was 243 nm.

7.2.4 Benzoic acid solubility determination

Benzoic acid was dissolved in ethanol/water solutions of varying proportions (0.1-0.4 ethanol/water (v/v)) and were held at ambient conditions for 24 hours with intermittent mixing to reach equilibrium. The supernatant fluid was assumed to be at saturation. The samples were centrifuged for five minutes and the supernatant fluid was nano-filtered (200 nm pore size). Using this filtered saturated solution in a 10x dilution with ethanol and a manually prepared benzoic acid standard, the UPLC method generated a solubility curve as a function of SASR. To validate the equilibrium measurement, a second approach was also implemented. Benzoic acid was dissolved in pure ethanol (the solvent) before water (the anti-solvent) was added in a dropwise manner. This anti-solvent addition induced crystallization and the slurry was held at ambient conditions for 24 hours with constant mixing to reach equilibrium. With this additional step, both nucleation and dissolution rates are removed from the uncertainty as the measured concentration of benzoic acid in solution should be the same using either method. Figure 7.3 shows experimentally determined solubility data that was used for choosing operating conditions in the OFBC.

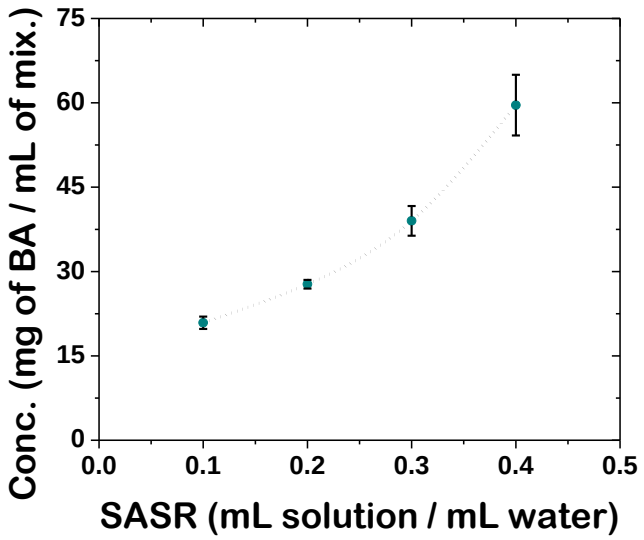

Figure 7.3 UPLC generated solubility of benzoic acid in ethanol solution-water mixtures of different ratios.

7.3 Experimental procedure

7.3.1 Degassing feed solution

An in-house degassing system was built to remove the risk of generating air bubbles during the operation of the OFBC. To remove the dissolved gas prior to injection, the solution was heated to 40°C with constant stirring (150 rpm) in a 5L jacketed vessel with a retreat curve stirrer (dia. 140 mm). In addition to the temperature shift, the vessel pressure was decreased using a vacuum pump (ultimate vacuum pressure of 110 torr, Welch by Gardner Denver). The decrease in pressure also decreases the solubility of air in solution. The entire system was held under these conditions for one hour before injection into the OFBC. The degassing process was limited to an hour because there is a tradeoff in removing trapped air and evaporating ethanol from the vessel. However, the concentration of benzoic acid was determined offline prior to injection, ensuring comparable starting conditions between experiments. The degassing process was a batch operation which impacted the length of each experimental run time.

7.3.2 OFBC concentration sampling

After reaching steady state based on stabilized particle counts measured by the FBRM, a sample was taken from the bridging liquid injection port before connecting the toluene feed line (refer to Figure 7.2). Once bridging liquid addition was initiated, samples (3 mL) were taken at the outlet to determine if steady state was also maintained in the liquid phase throughout the process. This approach serves to cross-validate the solid phase (particle counts) and liquid phase (concentration) based steady state assumption since crystallization processes depend on both phases. The samples taken at the outlet were filtered through (200 nm) pores before being diluted 10x with ethanol and inserted into the UPLC (Figure 7.4) shows an example of the concentration data used to monitor the process for 12 residence times (refer to experiment 3 from Table 7.1). The figure shows the benzoic acid concentration as a function of time for the duration of the experiment with the slight oscillation in the measurement due to the RTD in the liquid phase.[208] The measured concentration data corresponds to a steady state supersaturation of ΔC = 23 mg/mL (absolute supersaturation) or expressed as a ratio S = 1.6 ($S = C/C_{sat}$). S is the supersaturation ratio, C is the concentration, and C_{sat} is the saturation concentration.

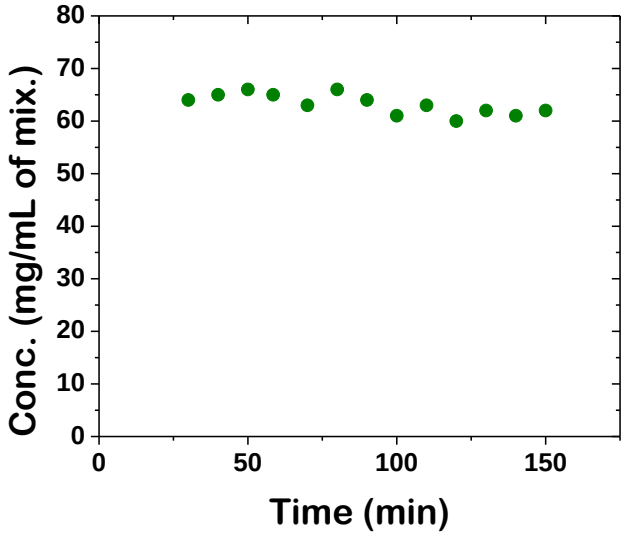

Figure 7.4 Concentration of benzoic acid as a function of time measured at the outlet of the OFBC.

7.4 Results and discussion

Several process parameters were varied between each experiment (Table 7.1). As previously mentioned, the lumped parameter Ψ determines the intensity of mixing within the OFBC. Five distinct values of Ψ (12, 33, 56, 58, and 82) were chosen to determine the sensitivity of agglomerate formation to the mixing conditions. The lower and upper values were chosen based on the manufacturer's recommendations for mixing and safe operation of the equipment; with two intermediate values to assess the operating range. Supersaturation, and hence slurry density, in the initial OFBC tube segments are varied by changing the SASR (0.18-0.30) and the benzoic acid (BA) concentration of the feed (0.08-0.125 g/mL). The BSR impacts both the extent of agglomeration and the agglomeration mechanism. The BSR was varied (0.6-1.2) to alter agglomeration size and decrease the number of un-agglomerated particles. The SASR, concentration, and BSR ranges were chosen based on previously successful SA experiments.[137] The remaining variables in Table 7.1 include the amplitude, frequency, residence time, oscillatory Reynolds (Re_o) and mean particle size (D_m).

Table 7.1 Summary of experimental conditions

Exp.	Conc. of BA (g/mL)	SASR	BSR	RT (min)	f (Hz)	x_0 (mm)	Re_o	Ψ	D_m (mm)
1	0.08	0.30	0.80	10.0	1.5	15	1974	12	3.0
2	0.08	0.30	0.80	8.33	3.0	25	6581	33	1.8
3	0.08	0.30	1.00	10.0	3.5	30	9213	56	2.3
4	0.08	0.30	0.80	12.5	3.5	35	10748	82	1.4
5	0.08	0.18	0.80	12.5	3.5	35	11015	82	1.6
6	0.08	0.25	0.80	12.5	3.5	35	10853	82	1.6
7	0.125	0.30	0.80	12.5	3.5	35	10748	82	1.5
8*	0.08	0.30	0.85	12.5	3.5	35	10748	82	1.7
9**	0.08	0.25	0.85	12.5	2.5	35	7752	58	1.3

**Agglomeration zone consisted of three segments, **Agglomeration zone consisted of two segments*

7.4.1 Evaluation of mixing conditions

Experiment 1 had the least turbulent mixing conditions (Ψ = 12) and resulted in a broad ASD as shown in Figure 7.5. In SA systems, the bridging liquid preferentially wets the crystals in suspension. Agglomerate formation then depends on particle collisions. Poor oscillatory mixing prevented uniform bridging liquid distribution, caused particle settling, and reduced collision events, resulting in a tri-modal ASD. This tri-modality is a result of particles left un-agglomerated due to reduced collisions, larger particles created due to particle settling, and very large particles created from over-agglomeration due to poor bridging liquid distribution. As mixing intensity increased (Ψ = 33 to 82), the ASD improved significantly, average agglomerate size decreased, and the system could run at a controlled state. The ASDs and images of agglomerates at the different mixing intensities are shown in Figure 7.5 and Figure 7.6. Note that images were not presented for experiment 1 due to the large particles that were out of the viewing field of the microscope and the broad size distribution that could not be represented in a single image. At a constant total flowrate, there was significant improvement in the ASD by increasing the amplitude and frequency of oscillations (experiment 1 vs. 3). Increasing residence time combined with increasing oscillatory mixing, allowed for improved agglomeration due to more sustained collisions and consolidation of agglomerates (experiment 1, 2 and 4). Overall, increased oscillatory mixing led to a narrower ASD, smaller average agglomerate sizes, and reduced particle settling/fouling. For these reasons, the mixing intensity remained high in each of the latter studies. Note that experiment 3 (Ψ = 56) does not follow the trend of decreasing

mean size and narrower ASD as mixing intensity increases due to the difference BSR value when compared to experiments 2 and 4.

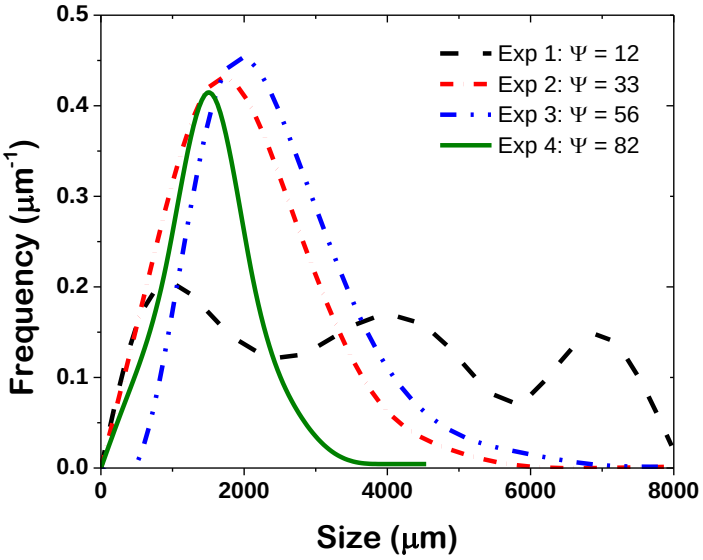

Figure 7.5 Agglomerate size distributions for different oscillatory mixing intensities.

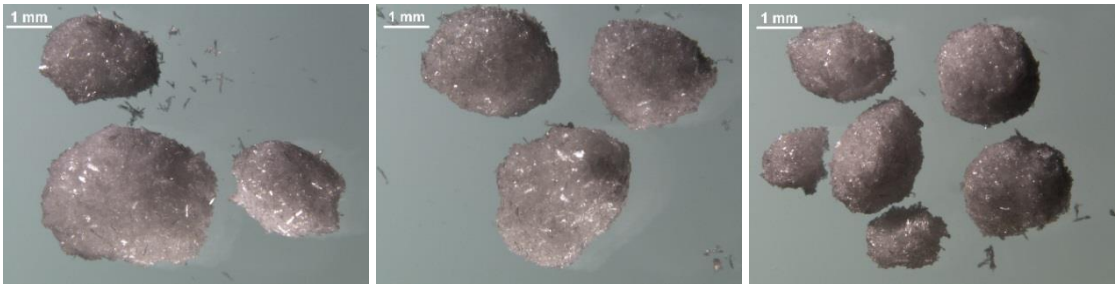

Figure 7.6 Agglomerates from experiments with increasing mixing intensity from left to right (exp. 2-4).

7.4.2 Initial supersaturation variations via SASR

Benzoic acid solution and anti-solvent are mixed in the first segment of the OFBC. Assuming the system is perfectly mixed, the SASR dictates the initial operating point in the phase diagram (initial supersaturation). In experiment 5, the SASR is low at 0.18, resulting in a higher initial supersaturation compared to experiments 4 and 6. Operating at such a low SASR (high supersaturation) increases slurry density due to higher nucleation. This supersaturation, and subsequent nucleation, is maintained throughout the agglomeration zone (refer to Figure 7.4), resulting in many un-agglomerated crystals (far

right of Figure 7.7) and a bimodal ASD (Figure 7.8). As the SASR increases from 0.18 to 0.25 to 0.30, the ASD narrows, the average agglomerate size decreases, and the maximum agglomerate size decreases as shown in Figure 7.8. It is important to note the maximum agglomerate size, or the breadth of the ASD, as it is related to the RTD of the system.[208] For each set of operating conditions, the maximum agglomerate size of each experiment captures a portion of the system dynamics. From Figure 7.8 it is apparent that increasing the slurry density (at constant net flow) broadens the ASD due to increased dispersion, suggesting that the RTD of the system is related to slurry density.[208] From a phase diagram perspective, a decrease in SASR can have the same effect on the RTD of the system as increases in concentration. At constant concentration, increasing the SASR past 0.30 results in an increase in the solubility of the system impeding sufficient supersaturation to crystallize. It is important to note that changes in the SASR (at a constant BSR) will also affect the operating point within the ternary phase diagram (ethanol-water-toluene).[137] Changes in the operating point in the ternary phase diagram affect the immiscibility of the bridging liquid which can cause changes in the agglomeration mechanism. Very low SASR increases the immiscibility of the bridging liquid moving it above the critical maximum BSR limit. Very high SASR will have the opposite affect; moving the bridging liquid below the critical minimum. At the SASR conditions studied, no significant differences in the agglomeration mechanisms were observed.

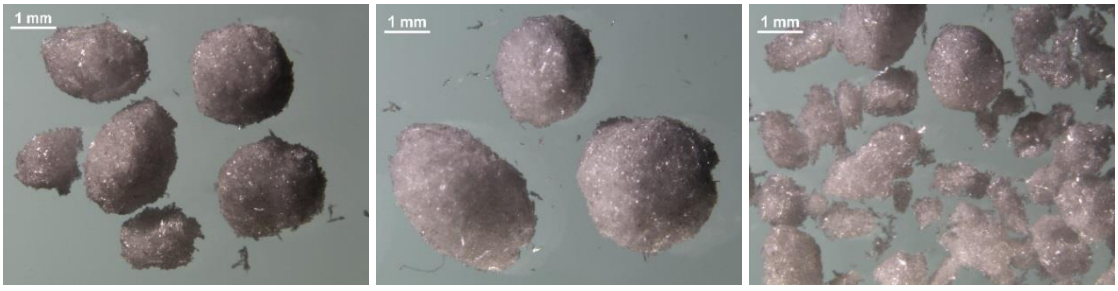

Figure 7.7 Agglomerates from experiments with decreasing SASR from left to right.

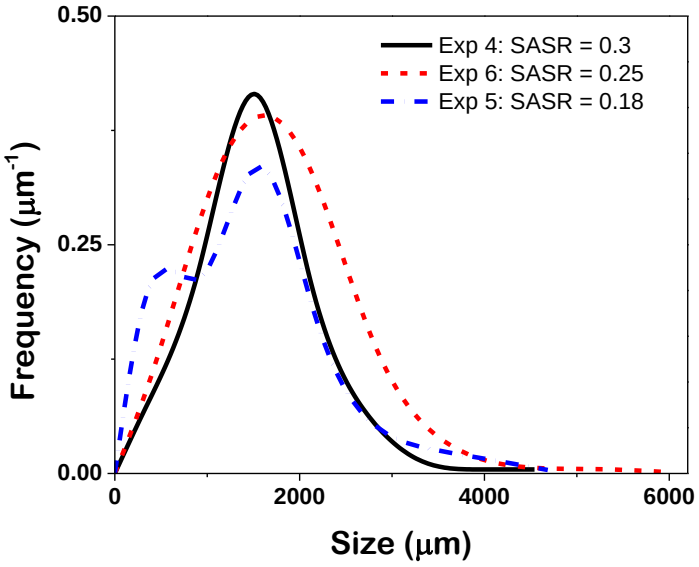

Figure 7.8 Agglomerate size distributions for different SASR ratios.

7.4.3 Initial supersaturation variations via benzoic acid concentration

At a constant SASR, the initial concentration of benzoic acid in solution dictates the crystallization starting point in the phase diagram (initial supersaturation). Increasing the concentration from 0.08 g/mL to 0.125 g/mL, induced more clogging/fouling in the system, broadened the ASD and the maximum agglomerate size dramatically increased (Figure 7.9). Increasing the initial supersaturation increases both primary and secondary nucleation. As with changes in the SASR, an increase in slurry density via increases in concentration can result in inconsistent agglomerate sizes and clogging/fouling. As concentration increases, the effects of RTD contribute significantly to the broadening of the ASD and the increase of the maximum agglomerate size. Concentrations above the values reported here were attempted but were unsuccessful due to clogging/fouling. Based on the observed trends, there is an optimal slurry density that minimizes the effects of RTD and avoids clogging/fouling.

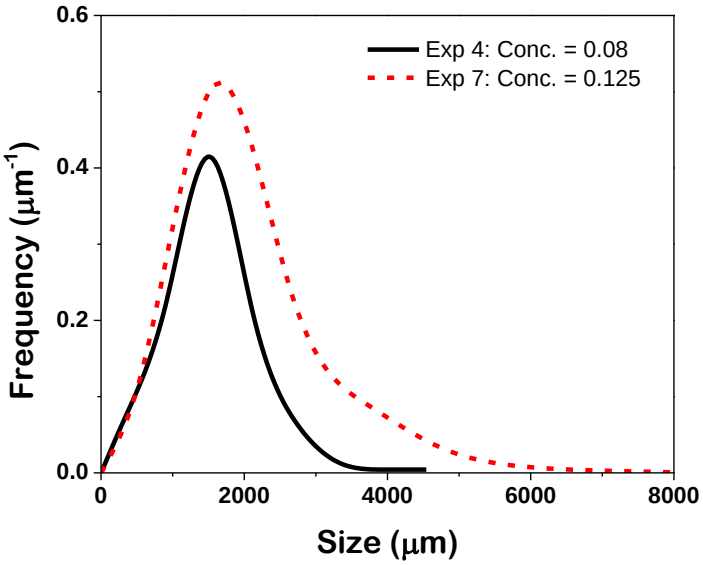

Figure 7.9 Agglomerate size distributions for different solution concentrations of benzoic acid.

7.4.4 Variations in BSR

Spherical agglomeration techniques generally have narrow BSR operating ranges which induce spherical agglomerate formation.[26,130,139] Changing this ratio drastically changes the final ASD and can change the agglomeration mechanism.[137] After increasing the BSR from 0.8 to 1.0, the average agglomerate size increased from 1.4 to 2.3 mm. The ASD broadened and the maximum agglomerate size dramatically increased as shown in Figure 7.10. As the bridging liquid is increased to the critical range, the agglomeration mechanism becomes increasingly adhesive as the particles have a greater bridging liquid film. The increased adhesiveness of the particles results in a greater propensity for successful collisions (collisions that result in agglomerate formation), particularly in agglomerate-agglomerate collisions. When two agglomerates adhere, the system generates large particles and results in the broad distributions shown in Figure 7.10.

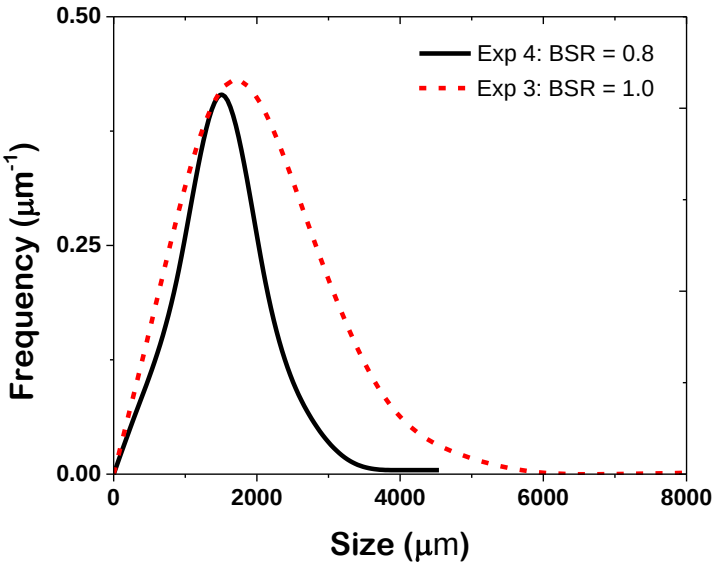

Figure 7.10 Agglomerate size distributions for different BSR.

7.4.5 Set point variations in BSR

One of the proposed advantages of continuous processes is the ability to make set point changes to operating conditions to adjust final product properties. For this study, set point changes in BSR were investigated to assess the feasibility of adjusting the final agglomerate properties while maintaining constant primary crystal properties. Set point changes in BSR were carried out at intermediate time steps during experiment 6 (Table 7.1) before setting the system to its original operating conditions afterwards. Figure 7.11 shows the FBRM total counts and SWMCL data over time as well as images of primary crystals from the experiment. The data shows that a CSO was attained after four residence times (50 min). The primary crystals in the images were collected at the end of the third residence time at the outlet of OFBC after which binder addition was initiated. The images of the primary crystals show the needle/rod-like morphology of the benzoic acid crystals and their relatively large size.

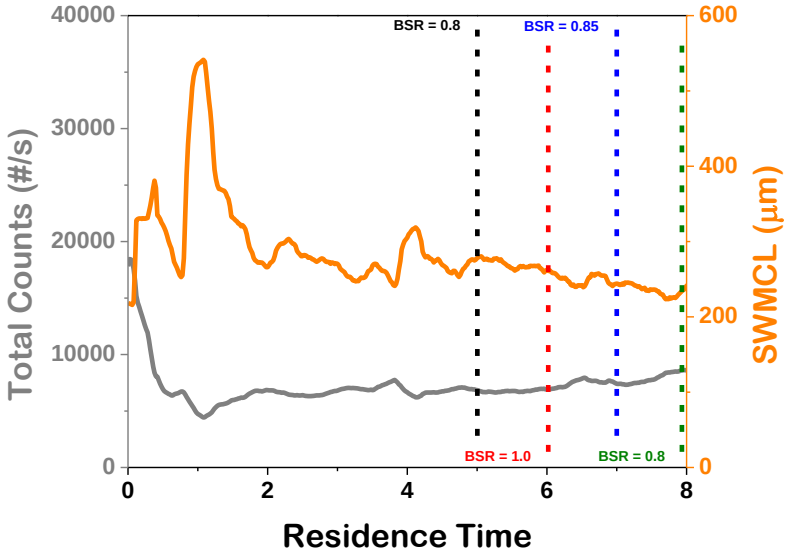

Figure 7.11 Total counts and SWMCL from FBRM probe.

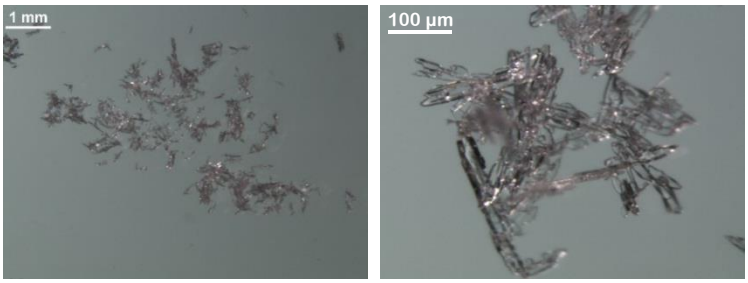

Figure 7.12 Images of the primary crystals prior to agglomeration.

Once under a CSO, the BSR was changed at the end of each residence time. The following set point changes in BSR took place: the system began operation with a BSR of 0.80, increased to a BSR of 1.0, decreased to 0.85 and then brought back to its original value of 0.80. Figure 7.13 shows the ASDs and images of agglomerates after the various set point changes. The fifth residence time corresponds to the first residence time after a CSO is reached per the FBRM data. However, given the breadth and maximum frequency of the ASD at the fifth residence, it is apparent that the agglomeration portion of the OFBC was not yet in a CSO. This observation suggests that there is a delay in the CSO of the primary crystals versus that of the agglomerates. However, the observation is not unexpected given that the binder addition was not initiated until the third residence time.

When the BSR is increased to 1.0 (RT 6) the ASD has a significant shift to the right as expected. Due the fact that only one RT was allowed for the step change response there is still a portion of the distribution corresponding to the original ASD prior to the change (RT 5). This observation suggests that one RT is not enough to achieve a CSO after a set point change. After the BSR is decreased to 0.85 and then to 0.80, the ASD shifts to the left returning to the uniform, normal distributions observed in previous sections. From the ASDs and images, it is evident that agglomerate properties can be adjusted throughout operation by set point changes in the operating conditions.

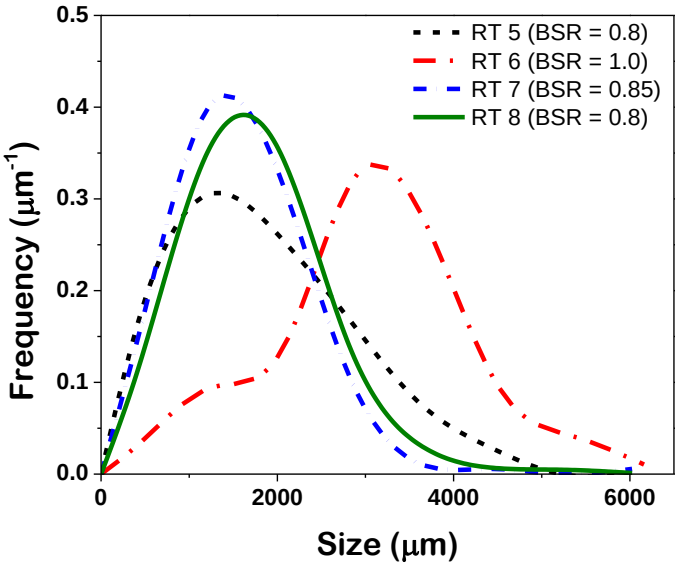

Figure 7.13 Agglomeration size distributions for step changes in BSR.

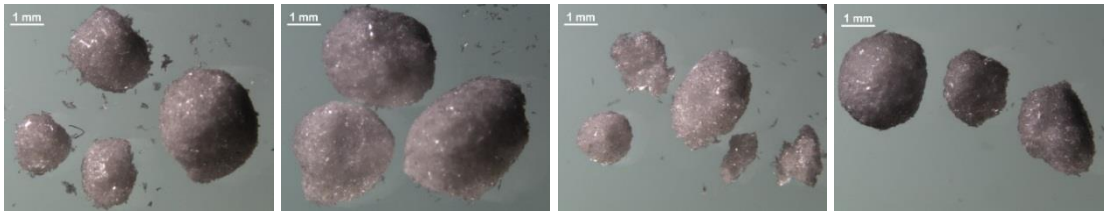

Figure 7.14 Images of agglomerates at different residence times and BSR (top left) BSR = 0.8, (top right) BSR = 1.0, (bottom left) BSR = 0.85 and (bottom right) BSR = 0.8.

7.4.6 Evaluation of different agglomeration zone lengths

The ability to easily change the configuration of the OFBC is a major advantage of the Nitech DN15. Changes in the jacket temperature of individual segments and location of

injection points can allow for optimized experimental conditions. The previous results used the configuration shown in Figure 7.2. Injecting the binder at the beginning of the fifth segment created an agglomeration zone consisting of the final four segments. For the studies that evaluated the impact of the agglomeration zone, the system is reconfigured by changing the location of the binder injection to change the length of the agglomeration zone while keeping the total length of the OFBC constant. Experiments were run for agglomeration zones consisting of three, two and one segment(s) with the operating conditions of experiment 4 used as reference.

When the operating conditions were held at the reference point, none of the configurations produced spherical agglomerates. Decreasing the agglomeration zone by one segment decreases the volume of the zone by approximately 1/7 or 14%. This decrease in volume, along with an already short residence time (12.5 min), does not provide sufficient time for agglomeration to occur. To create spherical agglomerates, changes in the operating conditions must compensate for the lost time for agglomeration. Experiment 8 (Table 7.1) used a three-segment agglomeration zone and required an increase in BSR to produce spherical agglomerates. Experiment 9 (Table 7.1) used a two-segment agglomeration zone and required an increase in BSR and a decrease in Ψ. Figure 7.15 shows the ASDs for experiment 4, 8 and 9 along with images of the spherical agglomerates.

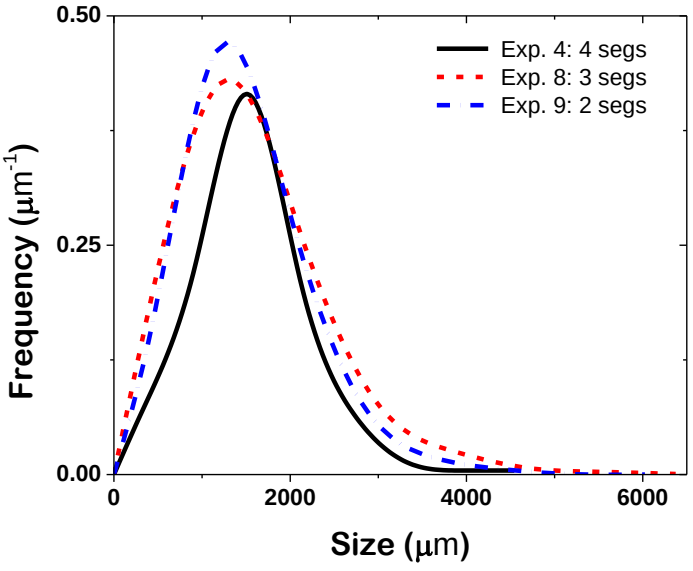

Figure 7.15 Agglomerate size distributions for different agglomeration zone configurations.

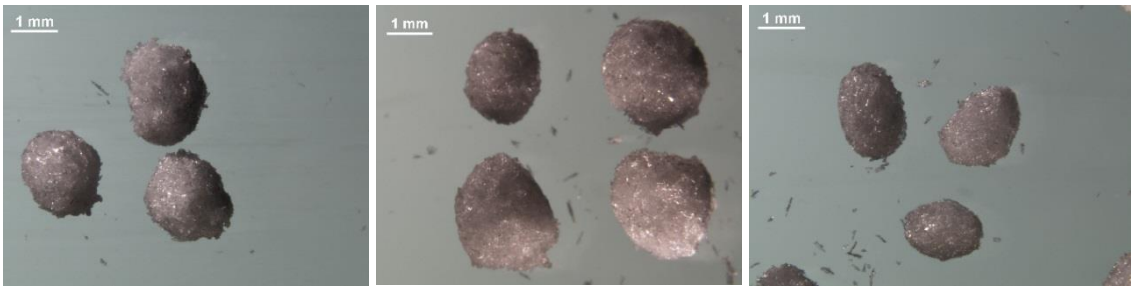

Figure 7.16 Images of agglomerates from experiments 4, 8 and 9 (left to right).

As evident by the ASDs and images of the agglomerates the experiments produced agglomerates of similar size distributions and mean sizes; with experiments 8 and 9 having broader ASDs and slightly larger mean sizes. The broader ASD can be attributed to the larger growth zone compared to experiment 4 which would contribute to a broader and larger crystal size distribution prior to agglomeration. As the agglomeration zone length decreases, the effects of dispersion/back mixing have a greater effect on the nucleation and growth than on the agglomeration mechanism with proper adjustments of the BSR. Experiment 8 required an increase in BSR to increase agglomeration and counteract the reduced agglomeration zone residence time. Experiment 9 required an increase in BSR to increase agglomeration and a decrease in the mixing intensity to reduce the dispersion of crystals from the growth zone. Reducing the crossing particles from the growth zone into the agglomeration zone allows the agglomeration to proceed without the effects of introducing new particles. Two segment agglomeration zone experiments at higher mixing intensities consistently produced a combination of spherical agglomerates and fine crystals. The effects at the interface between the growth and agglomeration can be overcome when the agglomeration zone is larger.

7.5 Summary of results

Spatially distributing API solution, anti-solvent, and bridging liquid along the length of the crystallizer led to independent control of mechanisms within the OFBC system. Various crystallization operating conditions were evaluated in the OFBC. Knowledge of the initial point in the phase diagram and the mixing ability of the OFBC allowed for an assessment of the effects of various operating parameters on the implementation of a SA technique. Increased mixing intensity significantly improved the final agglomeration size distribution

(narrower, smaller mean size). A Ψ = 82 was found to be optimal in this study. Ψ = 82 was the limit attempted in this study due to the stability of system as excessive vibrations can affect the crystallization process. However, further increasing the Ψ parameter should follow the same trends observed in this study at the expense of increased back mixing/dispersion. To achieve successful SA experiments, residence time (8.33-12.5 min) and benzoic acid solution concentration (0.08 and 0.125 g/mL) were kept relatively low. The slurry density should be limited to avoid fouling, clogging and particle settling, and decrease the effects of residence time distributions. Broadening of the residence time distribution can be limited with decreased slurry density which leads to more narrow/uniform distributions. The supersaturation and slurry density was controlled by maintaining the solution concentration and the SASR at appropriate levels (BA conc. at 0.08 g/mL, SASR at 0.30). Higher flow rates and mixing intensities also slow the buildup of fouling on crystallizer walls by reducing the possibility of particle settling. A solution concentration of 0.08 g/mL benzoic acid in ethanol and a SASR of 0.3 were found to be the optimal values in this study. The experimental conditions present in this study were largely determined by the avoidance of fouling. Thus, the experiments created very large primary crystals and spherical agglomerates. Higher nucleation rates could lead to smaller primary particle sizes and ultimately much smaller agglomerate sizes. However, fouling will be a bottleneck in such a process unless a continuously seeded system is studied. Lastly, as has been shown in the literature, the critical BSR range narrows for continuous systems.[130] A BSR of 0.80 was found to be the optimal in this study, with minimum room for adjustment. Table 7.2 summarizes the overall trends in mean size and ASD for the various process parameters.

Table 7.2 Summary of experimental results

Properties		**Effect of Process Parameters**				
Mean Size	decreases with	Ψ ↑	SASR ↓	Conc. ↓	BSR ↓	Agg. Segs ↓
	increases with	Ψ ↓	SASR ↑	Conc. ↑	BSR ↑	Agg. Segs ↑
ASD	narrows with	Ψ ↑	SASR ↑	Conc. ↓	BSR ↓	Agg. Segs ↑
	broadens with	Ψ ↓	SASR ↓	Conc. ↑	BSR ↑	Agg. Segs ↓

7.6 Conclusion

The OFBC is a viable option for applications in continuous crystallization. Given the OFBC's ability to be configured to optimize specific properties of interest, it also has application in PI. The benefit of a plug flow type of crystallizer is the ability to achieve product of narrower final properties. The broad agglomerate size distributions observed throughout this study contradict this fact. The results presented here suggest the OFBC deviates from an ideal PFC; with the effects of dispersion of the residence time distribution appearing to be most significant factor in that deviation. The findings in this study agree with RTD studies in literature that suggest the operating ranges studied here could cause significant dispersion.[208] The results show RTD to be related to slurry density. Increases the slurry density appeared to have led to increases in dispersion and back mixing. The effects of slurry density should be investigated further, especially for SA processes. Overall the agglomerate size distributions show improvement (narrower, more uniformity) over the distributions observed in an MSMPR.[130] A series of staged MSMPRs proves to be more efficient in decoupling the crystallization mechanisms because the stages are physically separated and are completely independent from one another. In the OFBC, the mixing (expressed through the Ψ) was the same through and between the different crystallization zones which can lead to multiple mechanisms occurring at the interface of different zones due to dispersion or back-mixing. Within the experimental framework studied here and in Peña & Nagy (2015), the MSMPR does not exhibit fouling issues allowing it to operate at much higher supersaturation ratios; leading to finer smaller primary crystals.[130] However, for optimal operating conditions, the OFBC proves effective in producing agglomerates of consistent quality. The superimposed oscillatory mixing of OFBC allows for process development at a wide range of productivity levels (from benchtop to pilot to manufacturing scale) without changes in equipment volume.

8. EVALUATION OF MIXED SUSPENSION MIXED PRODUCT REMOVAL CRYSTALLIZATION PROCESSES COUPLED WITH A CONTINUOUS FILTRATION SYSTEM

This chapter is reprinted with minor modification with permission from Acevedo, D., Peña, R., Yang, Y., Barton, A., Firth, P., & Nagy, Z. K. (2016). *Chemical Engineering and Processing: Process Intensification*, *108*, 212–219.

8.1 Introduction

Various works have been performed in the design, optimization and control of crystallization processes in order to improve and maintain crystal product qualities such as crystal size, shape and purity, among others.[6,7,15,21,47,209,210] However, batch operations are well known to affect the overall efficiency of pharmaceutical manufacturing processes and often affect the quality of products due to the significant batch-to-batch variability. Therefore, the study on the design and control of continuous operations has increased significantly. Continuous processing offers the advantage of consistency in product quality and achievement of operating conditions unattainable in batch processes. Other advantages of implementing continuous processing involve the reduction of cost by asset utilization, shorter down time and ease of scale up. Continuous processing has been identified as a key paradigm shift in the pharmaceutical industries with high potential of improving pharmaceutical production.[102,104,211]

The two-main type of continuous crystallizer designs for pharmaceutical applications are the plug flow and mixed suspension mixed product removal (MSMPR) crystallization systems. Advanced optimization and control strategies have been implemented in these types of crystallizers such as recycle and fines reduction.[194,212-214] The choice of which type of continuous processing to use depends mainly on the kinetics of the process. However, the MSMPR system offers the advantage of simple transfer of existing batch capacity to continuous.[211] The MSMPR crystallizer is an idealized vessel in which supersaturation is generated continuously while crystals nucleate and grow from a feed of homogeneous solution. It is assumed that the product slurry removed continuously has the same

composition and crystal properties as the vessel content. This is an important assumed property of an MSMPR crystallizer and leads to specific designs of downstream processes.

Filtration has long been developed through practical and empirical understanding instead of exact theory because of the complex nature of the development of the filter cake.[215,216] Due to this, many issues have arisen in terms of scaling from laboratory to industrial scale and process transfer from batch to continuous operation. Traditionally, laboratory filtration has taken place in batch mode with vacuum as the main driving force. At the manufacturing scale, filtration has mostly been carried out in batch mode consisting of very different geometries and introducing greater uncertainties because of interactions between filter feed and mechanical movement of the filter. Filtration is often assessed in terms of two parameters: mass of solids recovered from the slurry and the moisture content of the recovered solids.[216] Since the majority of the liquid content in a solid-liquid suspension is removed during the filtration process, the effectiveness of unit operations that proceed filtration are directly correlated to these two factors. Drying, for example, is a unit operation that typically proceeds filtration, but is only accountable for a small fraction of the liquid removed from the solids. Therefore, incremental improvements in the filtration process can significantly improve the efficiency and energy consumption of a drying unit.[217]

8.2 Materials and methods

Crystallization precedes filtration, and poor filterability of the crystallization product is a common problem for industrial scale pharmaceutical crystallizations. However, it has been shown in the literature that improvements in CSD can greatly improve the efficiency and time of filtration.[216,218,219] The filtration efficiency impacts the crystallization design as different operating conditions produce markedly different crystal properties. Jones et al. (1987) conducted a study analyzing the filterability of potassium sulfate crystals from a batch crystallization carried out through cooling or anti-solvent addition for both seeded and unseeded cases.[218] They found that the unimodal nature of unseeded crystallization processes greatly improved the permeability of the filter cake allowing for greater liquid removal and lower moisture content. The bimodal nature of seeded crystallization processes introduced greater uncertainty in the filter cake development causing reduced

permeability. The study showed no significant effect on filterability from changes in the cooling rate. However, for seeded processes Matthews et al. (1998) proposed an optimization framework to reduce the mass of nucleated crystals by controlling the temperature profile and found significantly reduced filtration times when fines were reduced.[219] Jones et al. (1987) also pointed out that there is a greater room for improvement in filterability for anti-solvent crystallization as opposed to cooling due to the smaller crystal size, faster rate of supersaturation generation, and potential for agglomeration of the crystals.[218] Fines reduction is not only important during crystallization but during and after filtration, too. Nucleation at the point of filtration is also commonly observed in industrial processes caused by rapid removal of saturated solution from the filter and residual solution dried up on filter parts.[220, 221]

There have been numerous studies on the integration of continuous filtration systems coupled to continuous crystallization systems within integrated continuous manufacturing (ICM) systems.[103, 222] However, this studies do not delve into much detail regarding the actual filtration process efficiency, productivity and operating parameters. This is partly due to simple filtration setups with minimal operating parameters built around other unit operations. A few continuous filtration setups are worth mentioning, in Ley et al. (2015) work two systems are discussed: (1) the rotating sintered glass filter system which is usually used for liquid collection, is a simple setup with a rotating filtration plate that collects solids while the filtrate can be sent to other unit operations; (2) vacuum assisted filter system that works similar to the sintered glass filter system but is used for solids collection equipped with a slurry dispenser, scraper, wash solvent.[223] The vacuum assisted system was used by Mascia et al. (2103).[102] Lastly, Gursch et al. (2015, 2016) have conducted studies of a dynamic cross-flow filtration (CFF) system which is a membrane based system for the filtration of model APIs.[105,224] Their results show the CFF to be a suitable continuous filtration technology with a material-specific linear relationship between feed and permeate rate. However, the effects of shear on the crystals was not studied although membrane based systems have a high dependence on shear rate.

In this work, the feasibility of coupling a CFC system with a continuous crystallization process is demonstrated. The aim is to demonstrate the impact of the type of crystallization: (a) cooling and (b) antisolvent on the operation, productivity and product obtained from

the continuous filtration system. Paracetamol (PCM) in ethanol is used as the model system for the case study for the cooling crystallization due to the high nucleation and slow growth kinetics, which make the product crystals difficult to filter. Furthermore, benzoic acid (BA) in ethanol drowned out by water was used as the model system for the antisolvent crystallization case study. This system produces crystal morphologies (i.e., needles and plates) common to many APIs. The variation in the crystal properties produced from the crystallization processes assessed the practicability of the continuous filtration system coupled with a MSMPR crystallizer for pharmaceutical crystallization processes.

8.2.1 Materials

4-Acetaminophenol (paracetamol, PCM, Alfa Aesar) with a purity of 98.0% in mass fraction was used in the cooling crystallization experiments. Benzoic acid (BA, Fisher Scientific Education) with a purity of 99.0% was used during the antisolvent crystallization case studies. Solubility data for paracetamol in ethanol and benzoic acid in water-ethanol were obtained from the literature.[187,225]

8.2.2 System setup

The continuous MSMPR crystallizer consists of a 500-mL round-bottom jacketed vessel and a transfer line, as shown in Figure 8.1a. The transfer line has a similar structure and working mechanism as the one described in literature.[19,130,193,198,199] The transfer line contains a transfer zone and four valves, which are used to control nitrogen gas, vacuum, inlet and outlet of the transfer zone, respectively. The slurry is transferred intermittently. Within one transfer, first the vacuum valve is opened for 5 seconds to evacuate the transfer zone, followed by 5 seconds opening of the inlet valve that allows slurry to be vacuumed into the transfer zone. Then the nitrogen valve as well as the outlet valve are opened simultaneously for 5 seconds to push the slurry out into the next vessel. The volume of the transfer zone is 32mL. The transfer interval is controlled by a controller box to maintain constant slurry levels in both vessels.

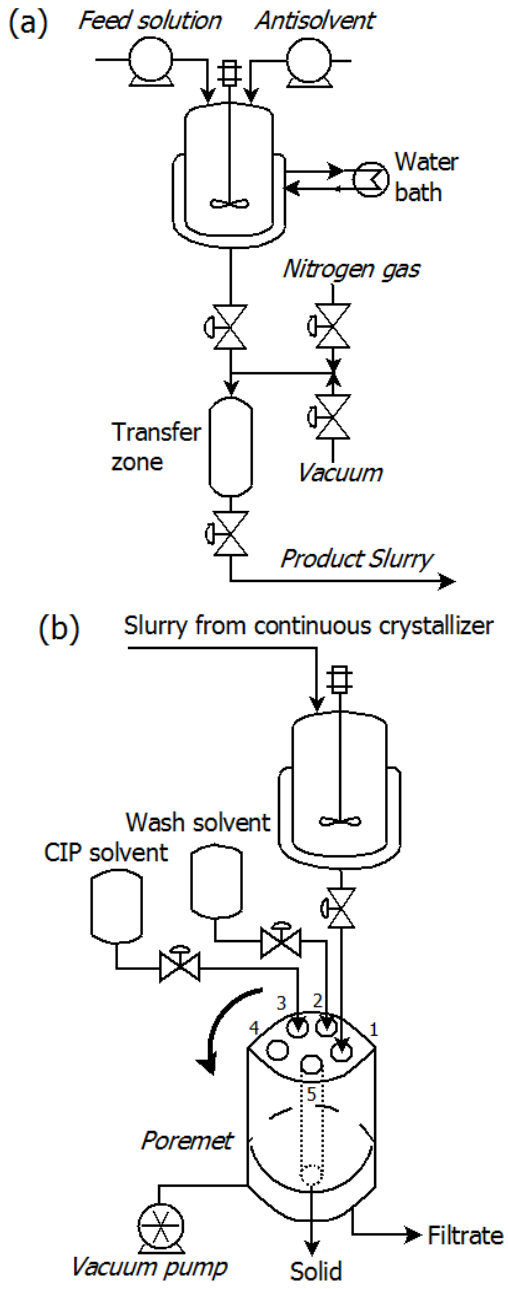

Figure 8.1 Schematics of (a) continuous MSMPR crystallizer using a transfer line and (b) CFC system.

A commercially available CFC system (Alconbury Weston Ltd, UK) is coupled with the continuous MSMPR crystallizer to filter the product slurry. As presented in Figure 8.1b, the CFC system contains a 2.5-liter slurry vessel, a wash solvent vessel, a clean-in-place (CIP) solvent vessel, a filtration unit, and three valves that are used to control slurry, wash

solvent and CIP solvent, respectively. The filtration unit consists of five cylindrical-shaped chambers (0.6'' diameter and 3.5'' height) and a poremet 10 (five-layer plate-type filter medium, 2.5'' diameter, 21μm geometrical pore size, 1.7 mm thickness) at the bottom. The filter medium spans the chambers located in positions 1, 2, 3 and 4. The chambers rotate counterclockwise every one filtration time. Slurry is fed into the chamber at position 1, as shown in Figure 8.1b. The slurry in that chamber is then washed in position 2 before being filtered through positions 3 and 4, and finally discharged at position 5. The bottom of position 5 is open, which allows the cake to be discharged through a chute by a piston. Therefore, the filtration unit works as a sequential-batch or semi-continuous operation, like a semi-batch Nutsche type filter. The bottom of the filtration unit is connected to a vacuum pump, which typically works at around 200 mmHg. The filtration time, as well as the slurry valve open time (or slurry time) and the wash solvent valve open time (or wash time) within every one filtration time are parameters that are controllable from the built-in user interface. Each chamber, therefore, operates under variable pressure and filtration rate as these parameters can be controlled and adjusted by the filtration, slurry, or wash timer. In addition, the inner pressure is monitored by the CFC system. Once the pressure drop increases past a user-defined normal operation pressure level, due to blockage of the poremet, an auto-clean function is actuated automatically by feeding CIP solvent into the chambers to dissolve the solids that cause blockage. The filtration unit returns to normal operation once the pressure drop normalizes after auto-clean. However, the small cross-sectional area of each chamber allows for slow ramp in pressure drop which allows for continued productivity without blockage. The appearance of the coupled continuous MSMPR crystallizer and CFC is shown in Figure 8.2.

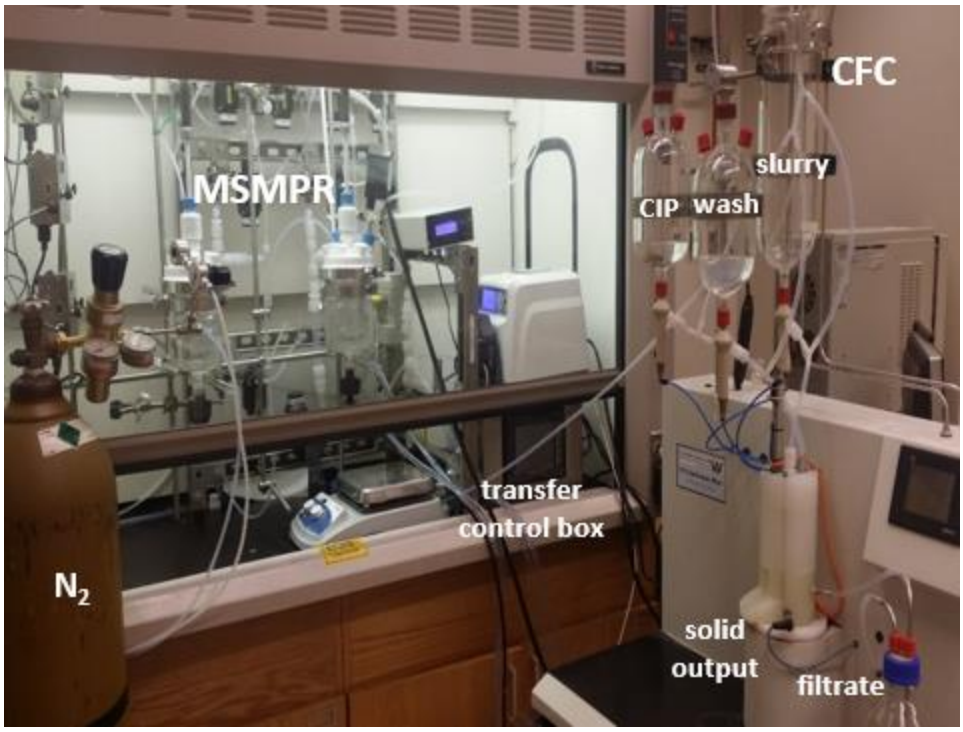

Figure 8.2 Coupled continuous MSMPR crystallizer and CFC.

8.2.3 Methods

The continuous crystallization was performed in the MSMPR-CFC system described in section 2.2. The temperature in a 500-mL lab scale glass jacketed vessel was controlled with a PT100 thermocouple using a Huber Ministat 125 refrigerated and heating circulator. An overhead stirrer with a three-blade retreat curve impeller was used to agitate the system. The saturated solution or antisolvent was fed to the MSMPR system using a Masterflex L/S pump. An S400 FBRM probe was used to monitor the dynamics and chord length distribution in-situ during the continuous experiments in order to infer the product CSD.[226,227] The data was collected every 15 s in the range of 0.1-1000μm. The crystals obtained from the CFC were weighed every half residence time to monitor the productivity and dynamics of the filtration system. Samples of filtrated crystals were collected every residence time to measure the moisture content by weight loss. Two types of continuous crystallization experiments were performed using PCM and BA.

The cooling crystallization of PCM in ethanol was performed in a one stage MSMPR crystallizer as described in section 2.2. A saturated feed solution was prepared by dissolving PCM in 2 L of ethanol in a beaker at a concentration of 0.24 g/g solvent. The initial saturated solution in the crystallizer was prepared at a similar concentration as the feed solution. The feed temperature was set to above the saturation temperature to avoid crystallization throughout the feed tubes. The crystallizer temperature was set to 20 °C to avoid significant impact of temperature variation between the MSMPR stage and CFC slurry stage shown in Figure 8.1. The agitation speed was set to be 300 rpm throughout the experiments, which is enough to guarantee the suspension of particles. The total residence time was set to 60 minutes to ensure significant growth of the crystals since PCM is a relatively slowly growing and mainly nucleation dominated system. The set of experimental conditions for the MSMPR-CFC system for the cooling crystallization experiments are shown in Table 8.1. The crystals were continuously washed with solvent to minimize the CIP steps which can affect the steady state operation.

Table 8.1 Experimental conditions for cooling crystallization of PCM in ethanol in a 1 stage MSMPR crystallizer coupled with continuous filtration (CFC) system.

Variable	Description	Value	Units
C_0	initial conc.	0.24	g/g
RPM	agitation	300	rpm
T_F	feed temp.	50	°C
T_C	cryst. temp.	20	°C
T_{sat}	sat. temp.	40	°C
F	flow rate	5.0	mL/min
τ	res. time	60	min
τ_F	filter time	90	s
τ_S	slurry time	0.4	s
τ_W	wash time	0.4	s

The antisolvent crystallization of BA in ethanol-water was performed in a one stage MSMPR crystallizer as described in section 2.2. The feed solution was prepared by dissolving BA in 700 mL of ethanol in a beaker at a concentration of 0.285 g/g solvent at 50 °C. The initial solution in the crystallizer was an ethanol-water mixture prepared at the same solution to antisolvent ratio (SASR) of the inlet streams. The SASR used for this experiment was 0.43 determined by the ratio of the solution flow rate (S_{FR}) to antisolvent flow rate (AS_{FR}). This allowed for a slow progression in the crystallization of BA crystals

as opposed to initializing with pure water which causes a crashing out effect. The inlet streams, crystallizer and CFC unit were all operated at ambient temperature (~20°C). The agitation speed was set to be 350 rpm throughout the experiments, which is enough to guarantee the suspension of particles. The total residence time was set to 40 minutes, which was enough to show significant growth of the crystals. The set of experimental conditions for the MSMPR-CFC system for the antisolvent crystallization experiments are shown in Table 8.2. During operation two CIP procedures were needed due to pressure drop increases from clogging of the filter plate.

Table 8.2 Experimental conditions for antisolvent crystallization of BA in ethanol-water in a 1 stage MSMPR crystallizer coupled with continuous filtration (CFC) system.

Variable	Description	Value	Units
C_0	initial conc.	0.285	g/g
RPM	agitation	350	rpm
Sol_{FR}	sol. flow rate	3	mL/min
AS_{FR}	antisol. flow rate	7	mL/min
$SASR$	Ratio	0.43	-
F	overall flow rate	10.0	mL/min
τ	res. time	40	min
τ_F	filter time	120	s
τ_S	slurry time	1	s
τ_W	wash time	0.15	s

8.3 Results and discussion

8.3.1 Cooling crystallization of paracetamol

The cooling crystallization of paracetamol was performed in a one stage MSMPR system and monitored using the FBRM. The SWMCL is shown in Figure 8.3a. First order dynamics are observed, which is expected since the continuous process was initiated with a saturated solution in the MSMPR vessel. The dynamic variation of the SWMCL demonstrates that the system achieved steady state behavior around 3 residence times (180 min). The oscillations in the dynamic profile, shown in Figure 3a, are commonly observed during the continuous crystallization in a MSMPR system.[15,39,194,228] The oscillations in the SWMCL are within ±8μm. Therefore, the system is considered to reach a CSO after three residence times. The SWMCL achieved at steady state shows that the system does not grow

significantly, which is expected for a nucleation dominated system, such as PCM.[6] The small size achieved will impact the filtration behavior as observed in Figure 8.3a.

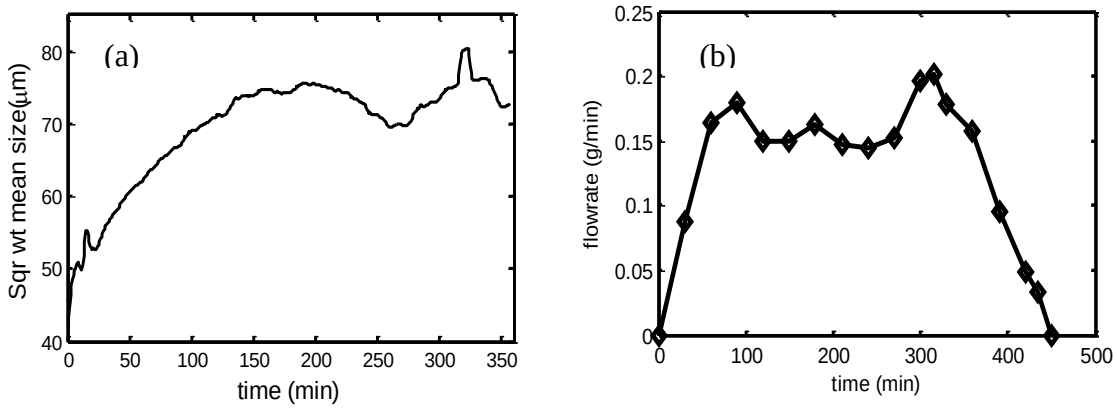

Figure 8.3 (a) SWMCL (μm) and (b) mass flowrate from CFC (g/min) during cooling crystallization of PCM in a MSMPR crystallizer coupled with CFC system.

The mass flowrate of PCM crystals obtained from the continuous filtration system (CFC) shows higher order dynamics. The continuous filtration processes were not started until half residence time to allow the filtration vessel to reach a minimum working volume in which the system could be operated with low fluctuations. Furthermore, the system was operated at low volume to avoid further growth or dissolution of crystals. Figure 8.4 shows microscope images of slurry samples taken after the system reached steady state, and filtered crystals after drying. No significant growth was observed between samples from the MSMPRS and filtered crystals. There is no clear evidence of breakage or attrition on the final crystals, which could affect the final crystal quality. Figure 8.4 demonstrates no significant variation in the crystal habit of PCM before and after the continuous filtration. Therefore, there is no observable impact due to growth, breakage or attrition on the PCM crystals that can occur while the slurry is in the filtration feed vessel or in the filtration chambers. These results indicate that the CFC system is a good isolation platform for the studied system as the crystallization product properties are preserved during the filtration.

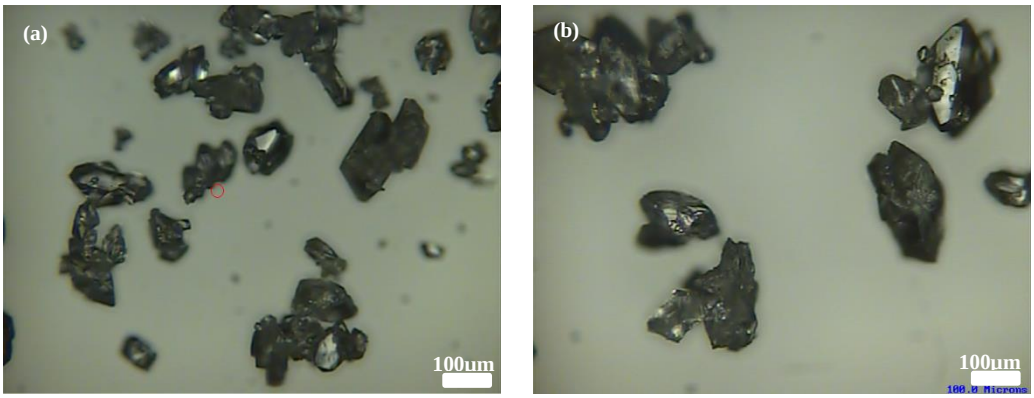

Figure 8.4 Microscope images obtained of (a) slurry at outlet of MSMPR and before the CFC and (b) filtered crystals after the CFC. Samples were obtained at steady-state.

The startup of the filtration system depends on the control of the volume at which the CFC is operated but also on the dynamics of the continuous crystallization process. As observed, steady state behavior was achieved between 2 to 2.5 hours of operation. A mean mass flow rate of 0.17±0.03 g/min during the steady state operation was achieved. The low productivity obtained can be attributed to the use of wash during the process to avoid disturbances in the continuous operation due to the CIP programmed step. However, higher productivity can be achieved by increasing the filtration timer which will maintain the same throughput and loose some running time to CIP. The continuous crystallization experiment was continued for 3.5 residence times after the system reached steady state as observed in Figure 8.3a. However, the continuous filtration system was operated until all the slurry in the vessel was filtered. This allowed the observation of the impact of decreasing working volume on the mass flowrate of crystals as demonstrated in Figure 8.3b. A monotonic decrease in the mass flowrate was observed after stopping the transfer from the MSMPR vessel to the filtration system. The startup and shutdown period observed in Figure 8.3b demonstrates that it is necessary to operate the CFC at constant volume since this has a direct impact in the output from the system; the amount of slurry pushed from the vessel when the filtration valve opens depend on the working volume dynamics (refer to section 2.2).

The moisture content was determined for the samples collected at each residence time from the filtered crystals at the outlet of the CFC. Figure 8.5 shows the moisture content (MC) dynamics calculated by weight loss after a 24 h drying period. The dynamics

demonstrated that the system reaches a steady state behavior after two residence times. An average MC of 22.2 ± 2.8 % was achieved at steady state. The MC before reaching steady state is significantly lower due to the lower amount of material in the filtration chambers. As demonstrated before, the mass flowrate before reaching steady state is lower, thus the vacuum system can remove solvent more efficiently. If the filtration operating conditions are constant throughout the processes, higher removal of solvent should be expected during startup due to the lower amount of material in the chambers.

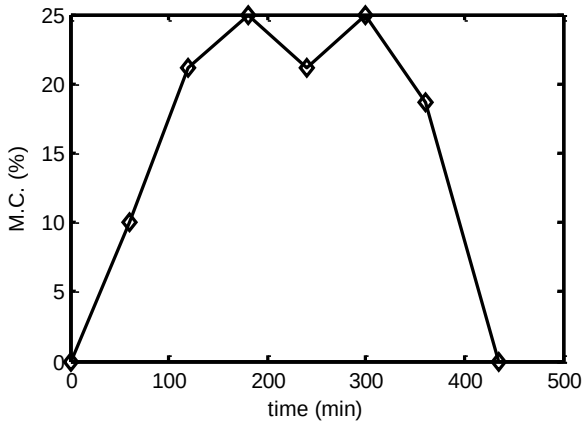

Figure 8.5 Moisture content (%) of filtered crystals obtained at each residence time throughout the cooling crystallization of PCM in a one stage MSMPR crystallizer coupled with the CFC system.

8.3.2 Anti-solvent crystallization of benzoic acid

The antisolvent crystallization of benzoic acid was performed in a one stage MSMPR system and monitored using the FBRM. The SWMCL is shown in Figure 8.6a. Higher order dynamics is observed, during the startup indicated by the initial overshoot and oscillations in the system behavior, which is generally expected for a continuous antisolvent crystallization process. The dynamic variation of the SWMCL demonstrates that the system achieved a steady state behavior at around four residence times (160 min). The oscillations in the dynamic profile after reaching steady state in this case study were negligible and can be attributed to intermittent operation. The steady state mean chord length was around 110 µm. This mean size showed good filtration properties aside from the two CIP procedures required at 120 and 200 min.

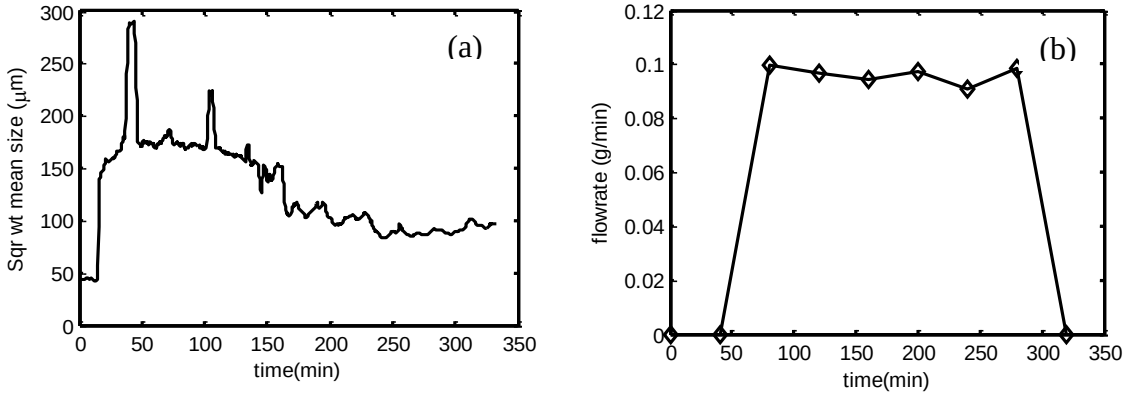

Figure 8.6 (a) SWMCL (μm) and (b) mass flowrate (g/min) during antisolvent crystallization of BA in a MSMPR crystallizer coupled with the CFC system.

The mass flowrate of BA crystals (Figure 8.6b) obtained from the CFC shows well maintained dynamics and was unaffected by the CIP procedures. Like the case of PCM, the continuous filtration process was not started until half residence time and there was no observable impact on BA crystal attributes due to the added holdup filtration period. The startup of the filtration system depends on the operating volume the CFC but also on the dynamics of the continuous crystallization process. Since antisolvent crystallization technique was used for BA there the induction time for crystallization was shorter and there was a significant amount of crystal mass in the slurry from the onset, although the solid concentration was relatively small. A mean mass flow rate of 0.10±0.003 g/min during the steady state operation was achieved. The low productivity obtained can be attributed to low solids concentration in the slurry. Given that filtration was not initiated until the appropriate working volume was achieved the mass flow rate for the antisolvent system was sufficiently constant. This is also attributed to the fact that the antisolvent system produces a constant solids concentration from the onset due to the short induction time

Figure 8.7 shows the morphology of the BA crystals obtained from the antisolvent crystallization. As the microscope images show, the morphologies present are both rigid plates and needles. This had a significant impact on the filtration process, specifically on the moisture content. The moisture content was determined for the samples collected at each residence time from filtered crystals at the outlet of the CFC.

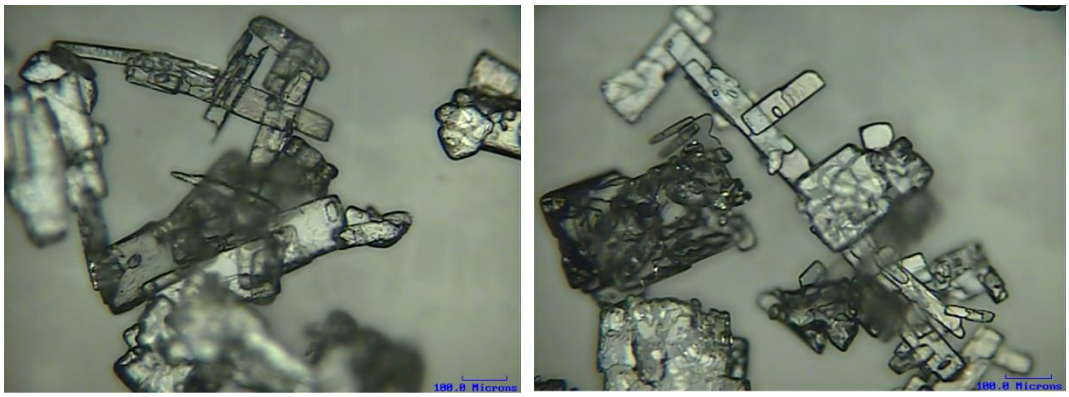

Figure 8.7 Microscope images of filtered crystal samples obtained at steady-state.

Figure 8.8 shows the MC dynamics obtained for BA after a 24-hour drying period; an average MC of 45±4% was achieved at steady state. The high moisture content can be attributed to the different morphologies of the benzoic acid crystals present. This directly impacts the development of the filter cake inside the filtration chambers and has a liquid entrapment affect. This is evident from the microscope images in which the crystals appear clustered together due the liquid entrapment. From Figure 8.8 two points of decreased moisture content are observed at 120 and 200 min. These points coincide with the two CIP procedures. The results show that after a CIP there is a significant improvement in the amount of solvent removed and shortly after the moisture content increases again. This proves that there is a combination of crystals that clog the pores of the filter medium as well as liquid entrapment in the filter cake that cause gradual increase in moisture content. The crystals clogging the pores of the medium are easily removed by the CIP solvent allowing for continued operation with small deviation in the process output.

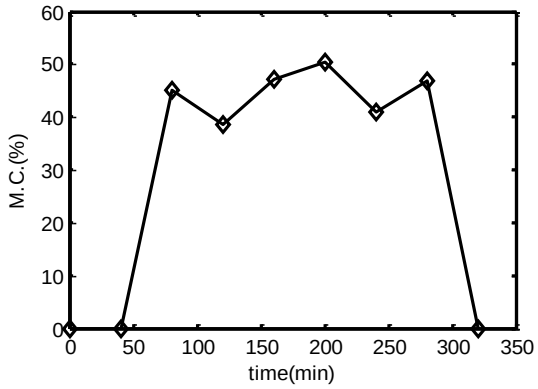

Figure 8.8 Moisture content (%) of filtered crystals obtained at each residence time throughout the antisolvent crystallization of BA in a one stage MSMPR crystallizer coupled with the CFC system.

8.3.3 Assessment of continuous filtration system

The CFC system presented in our work also allows washing the filter as a wash vessel and injection port onto the filter cake is available. Cleaning is also made easier by the presented system given the CIP vessel, which can contain a solvent that has a high solubility for the solids being recovered so that efficient cleaning can take place. However, whenever the CIP takes place the filtration step shows small deviation from steady state operation and the properties, including the moisture content, change. The impact of the CIP on the filtration step was observed for both scenarios studied but it was more frequent for the antisolvent crystallization of BA compared to the cooling crystallization of PCM. This could be attributed to the differences in crystal habit between the two systems as observed in Figure 8.7 and Figure 8.4b. Needle-like and plate shape crystals were obtained for BA during steady state operation. The PCM crystals obtained show a prismatic crystal habit. Hence, clogging occurred more frequently during the crystallization of BA due to the wide crystal shape distribution. The operating conditions of the CFC system would depend on the type of process and crystallization system. An important observation is that the performance of the filtration step depends significantly on the crystallization system and process. The achievable productivity and moisture content are correlated with the filtration parameters, which will also depend on the crystallization system. However, the small variability in the productivity and moisture content observed for both processes, demonstrate the robustness of the continuous crystallization process coupled with the CFC system. The highest variation in the moisture content occurs for both systems whenever a

CIP step initiates. Therefore, the variance observed throughout the operation of the CFC should be minimized if optimal operating conditions are implemented. Furthermore, the filtration buffer vessel should be operated at small residence times to avoid significant impact on the quality of the crystals produced from the continuous crystallization process. The temperature in the filtration buffer vessel should also be controlled, to avoid additional nucleation or growth. In our study the MSMPR stage was operated close or at ambient temperature to avoid any impact of the filtration buffer vessel temperature variation on the product.

The presented study demonstrated that the CFC system is a viable process for the continuous filtration of pharmaceuticals compounds and can be easily coupled with continuous crystallization to form a fully integrated platform. The ease of use and controllability of the CFC system make it feasible to operate continuously, while coupled with a continuous crystallization process

8.4 Conclusions

The operation of a continuous crystallization coupled with a novel continuous filtration system (CFC) was demonstrated through different case studies, (a) cooling crystallization of paracetamol and (b) antisolvent crystallization of benzoic acid. The continuous filtration showed significant dependence on the crystallization system due to the variations in crystal properties such as size and shape. This could lead to operation of the CFC system at sub-optimal conditions that could affect the efficiency of the process. However, the robustness of the system is demonstrated due to the low variability during steady-state operation. The continuous operation of the MSMPR coupled with the CFC system shows significant promise due to the robustness and fast start-up observed for the cooling and antisolvent crystallization of paracetamol and benzoic acid, respectively.

9. CONCLUSIONS AND FUTURE DIRECTIONS

9.1 Conclusions

Drug substance purification by crystallization is a key interface in going from drug substance synthesis to final formulation and can often be a bottleneck in process efficiency. Of utmost importance in the crystallization of APIs, in the pharmaceutical industry, is to produce crystals of desired physical, processing, and biopharmaceutical properties. The desired physical properties depends on what the end goal and the drug formulation that the crystals will be a part of, but often processing and biopharmaceutical properties are competing interests. In most cases, the crystallization process is tailored to improve downstream process efficiency rather than improve drug molecule efficacy in the human body. Thus, there has been increased importance in the development of continuous crystallization systems of APIs to produce crystals with targeted physical and biopharmaceutical properties.

Spherical crystallization can potentially completely alter a typical pharmaceutical product manufacturing line. By improving both bioavailability and manufacturability, the technique enables processes to be complimentary to biopharmaceutical and processing properties. The unique value proposition and ability to consolidate unit operations make SC an example of PI. Moreover, CSC as a PI technique can address many of the present flaws (e.g., size distribution, downstream processing efficiency) of traditional crystallization systems. Understanding the current state of SC will be essential to the development of new strategies and finding knowledge gaps that can be improved. In this thesis, a thorough literature review of SC was conducted followed by a study focused on gaining insight of SC mechanisms and applications of CSC. Moreover, a first principles model was developed that enabled to optimization of both bioavailability and manufacturability. Lastly, to further the concept of PI, a continuous filtration unit was evaluated to assess its application with an MSMPR system.

A review of SC literature aimed at identifying the controlling process parameters, understanding the mechanisms involved, and evaluating the current state of modeling was conducted. The controlling parameters were identified as: solvent system composition,

temperature, amount of bridging liquid, constituent particle properties, agitation rate and batch/residence time. An understanding of agglomeration mechanisms proposed in literature provided fundamental knowledge that guided experimental and modeling studies conducted herein. The current state-of-the-art in modeling of SC and agglomeration in suspension systems was reviewed, and combined with the mechanistic understanding, a PBM was developed to include the simulation of both primary crystal and agglomerate population. Evaluation of the current state of CSC lead to the development of the CSC processes outlined in this thesis.

To this point, mechanistic studies of SC systems had not used process analytical technologies to assist in developing an understanding of the complex mechanisms occurring in a SC technique. Here common process analytical technologies were used to conclusively determine the mechanisms of SC. Moreover, since there a many different implementations of SC, the study here focused on a subset referred to as SA or agglomeration in suspension; SA uses a bridging liquid to agglomerate fine crystals into spherical particles. The study evaluated how different methods of incorporating the bridging liquid affect the mechanisms that ultimately form agglomerates. The results showed that the most robust method of incorporating the bridging liquid is post crystallization. The study then further evaluated how the properties of the constituent particles and their interaction with the bridging liquid droplet affects agglomerate size and flow properties. The results prove that there is a critical relationship between bridging liquid droplet size and crystal size that determines whether the agglomeration mechanism is immersive or distributive. The difference in mechanism leads to different size, flow and compression properties.

In regards to modeling, the PBM is the common approach to simulation and prediction of the size distribution and other properties of particulate systems. Population balance models can include nucleation, growth, breakage and agglomeration mechanisms that are relevant to a particulate process. However, there are some limitations to many of the previous PBM formulations for systems with agglomeration. These limitations have prevented the use of PBMs to accurately predict and simulate agglomeration in suspension techniques such as SC. To overcome these limitations, an extension of the concept of a coupled PBM was presented for application in the simulation and optimization of a SA in

suspension system. A coupled PBM formulation was developed for a semi-batch, reverse addition, anti-solvent crystallization system with agglomeration. The system included nucleation and growth of the primary crystals and subsequent agglomeration. The advantages presented by a coupled PBM formulation include the ability to optimize for specific primary and agglomerate sizes. Allowing for identification of optimal operating conditions that meet both bioavailability and manufacturability demands.

Relating to CSC, a method to help satisfy both processing and biopharmaceutical interests was proposed, based on performing crystallization and SA in a two-stage continuous MSMPR system and in an OFBC. For the MSMPR, under suitable operating conditions, the system enabled the decoupling of nucleation and growth from the agglomeration mechanisms, while performing efficient continuous manufacturing of particles with desired properties. Decoupling offers more degrees of freedom for the control of each mechanism, and in turn, provides how properties can be tailored to those of most biopharmaceutical benefit and efficacy (e.g., bioavailability, dissolution, morphology). While allowing agglomeration to be tailored to produce spherical agglomerates of the most processing efficiency (e.g., filtering, drying, friability). OFBCs are comparable to PFCs in that they are both tubular crystallizers, however, the OFBC has periodically spaced orifice baffles with oscillatory motion overlapped on the net flow. Independent crystallization mechanisms can theoretically be achieved through spatially distributed solution, solvent, anti-solvent, and bridging liquid addition; offering more control of each mechanism. However, the studies here showed that the OFBC allowed for spatially distributed addition of solvents but achieving control of each mechanism individually was not attainable due to the back mixing of the system.

Lastly, as the pharmaceutical industry evolves and goes through the paradigm shift from batch to continuous crystallization, innovative processes will need to be developed to replace unit operations that have historically been batch operations. This requires innovation in downstream processes (e.g., filtration, drying, milling, and granulation). Herein a commercially available CFC was assessed for its feasibility of continuous filtration while coupled with a continuous MSMPR crystallizer. The filtration system was assessed using two different crystallization systems (i.e., cooling and antisolvent) with significantly different kinetics and morphologies to assess the robustness of the integrated

platform. With proper optimization of the various filtration parameters, each crystallization system could achieve a CSO. The crystal product from the CFC system shows good consistency with the crystals in the slurry in the MSMPR. Moisture content and productivity of the filtration system were reported and show dependency on crystal properties. The CFC system was equipped with solvent vessels that aided the continuous filtration by acting as a wash or a clean-in-place solvent, preventing or removing filter clogging, respectively.

9.2 Future Directions

Recommendations for future work are provided here:

- Supersaturation control (SSC) and direct nucleation control (DNC) have been widely used to control and attained crystals of optimal quality as well as crystals of different properties. Given the effects constituent particle properties can have on final agglomerate properties, SSC and DNC can be implement during the crystallization phase of a SC process to create optimal crystals for the agglomeration phase. Since supersaturation determines the growth of different crystal faces, SSC can be used to evaluate of the wetting ability of a bridging liquid on different faces of a crystal can also been evaluated by either control approach. DNC can be used to evaluate the efficient of an agglomeration process at different solids concentrations by studying various particle count set points. Final properties of traditional SC can be compared with SSC/DNC-SC to evaluate differences and identify any significant improvement final properties.
- Both the MSMPR and the OFBC proved to be suitable CSC platforms in this thesis. However, both platforms had significant operational pitfalls. In the MSMPR, the broad particle residence times can make particle design of the constituent particle difficult. In the case of the OFBC, fouling due to nucleation is a constant operational issue caused by its high surface area to volume ratio. Moreover, the operating conditions required to make spherical agglomerates are not recommended because of a significant level of dispersion is created which negates plug-flow. Since the MSMPR has a much longer induction time for fouling, it can be used as a nucleator to feed crystals into the OFBC. The OFBC can then be used

as a cooling crystallization system operating at close to plug-flow conditions, allowing for uniform growth of crystals. The outlet of the OFBC can be then fed back to an MSMPR where an over stirrer can induce agglomeration. The MSMPR-OFBC-MSMPR setup would be a novel coupling of equipment that lead to superior spherical agglomerates than the units individually.

- The two-stage MSMPR studies presented here successfully show the used of one stage as nucleation and growth stage and another as a agglomeration stage. The two-stage approach can be reconfigured and extended to include other unit operations. For example, the first stage can be replaced with a wet mill unit. The wet mill would serve as a nucleator that can provide micronized particles to the second stage for agglomeration. The wet mill (WM) can also be coupled in the same manner to the OFBC which would grow the crystals uniformly and then feed those particles to the an MSMPR. The WM-OFBC-MSMPR setup would be a novel coupling of unit operations that can lead to superior spherical agglomerates.
- The CFC was successfully coupled with the continuous crystallization processes in an MSMPR. However, due to clogging and other configuration limitations, the first version of the CFC was not coupled with CSC in an MSMPR. The newer versions of the CFC appear to be avoid of such technical issues and coupling of CSC in an MSMPR/OFBC with a CFC could prove to be another milestone in PI of pharmaceutical manufacturing.
- PCA can be employed as a method of bridging liquid selection from simple physical properties data for solvents and compounds. Analysis of the principal components could lead to rapid solvent system selection. Combined with regime maps, process development of tailored spherical agglomerates for specific compounds and solvent systems can be achieve with greater success.
- Multiple hypothesis-based iterative robust model identification approach can be used to develop an iterative model-based experimental design approach (IMED). This approach uses a constrained model-based optimization framework to determine the optimal experimental conditions within the feasible operating region that maximize the information content of the experiments to obtain the model parameters with minimum uncertainty. The model with improved parameters is

then used to design the next experiments and the procedure is repeated until no further improvement are observed in the parametric uncertainties. Typical optimality-criteria (e.g., A-opt, D-opt, E-opt, etc.) can be used in the IMED depending on how the information content in the experiment is quantified. When the actual mechanism for which the model parameters are identified is unknown, the same procedure is repeated for the candidate set of mechanisms and the model with the mechanism or combination of mechanisms that provide prediction with lowest uncertainty will be selected based on quantitative model discrimination procedures. Therefore, this approach provides an automated structural and parametric model identification procedure that enables not only the determination of a robust predictive model for model-based optimization using the minimum number of experiments, but also enables the elucidation of the correct mechanisms that govern a manufacturing process.

APPENDIX A. PRODUCT DIFFERENCE ALGORITHM

The PD algorithm enables the estimation of the weights and abscissas used in the QMOM approach detailed in Chapter 5. The first step in the estimation is to construct a triangular $\boldsymbol{P}$ matrix. The $\boldsymbol{P}$ matrix has components P_{ij} constructed from the moments. The components of the first column of $\boldsymbol{P}$ are:

$$P_{i,1} = \delta_{i1}, \quad i \in 1, \dots, 2N+1 \tag{A.1}$$

where δ_{i1} is the Kronecker delta. The components in the second column of $\boldsymbol{P}$ are:

$$P_{i,2} = (-1)^{(i-1)}\mu_{i-1}, \quad i \in 1, \dots, 2N+1 \tag{A.2}$$

The calculations can be done assuming $\mu_0 = 1$ (i.e., a normalized distribution). The final weights can be multiplied by the true μ_0 afterwards. The remaining components of the $\boldsymbol{P}$ are found using the PD algorithm (equation A.3).

$$\begin{aligned} &P_{i,j} = P_{1,j-1}P_{i+1,j-2} - P_{i,j-2}P_{i+1,j-1} \\ &j \in 3, \dots, 2N+1 \quad and \quad i \in 1, \dots, 2N+2-j \end{aligned} \tag{A.3}$$

A simple example is the case of $N = 2$ quadrature points. For this case $\boldsymbol{P}$ becomes:

$$\boldsymbol{P} = \begin{bmatrix} 1 & 1 & \mu_1 & \mu_2 - \mu_1^2 & \mu_3\mu_1 - \mu_2^2 \\ 0 & -\mu_1 & -\mu_2 & -\mu_3 + \mu_2\mu_1 & 0 \\ 0 & \mu_2 & \mu_3 & 0 & 0 \\ 0 & -\mu_3 & 0 & 0 & 0 \\ 0 & 0 & 0 & 0 & 0 \end{bmatrix} \tag{A.4}$$

Moment inversion of the first row is then used to find the coefficients of the continued fraction (α_i). The coefficients are generated by setting the first element equal to zero ($\alpha_1 = 0$) and computing the remaining coefficients via the following recursive relationship:

$$\alpha_i = \frac{P_{1,i+1}}{P_{1,i}P_{1,i-1}}, \quad i \in 2, \dots, 2N \tag{A.5}$$

The Jacobi matrix is then constructed as a symmetric tridiagonal matrix obtained from sums and products of α_i,

$$\begin{aligned} a_i &= \alpha_{2i} + \alpha_{2i-1}, \quad i \in 1, \dots, 2N-1 \\ b_i^2 &= \alpha_{2i+1}\alpha_{2i-1}, \quad i \in 1, \dots, 2N-2 \end{aligned} \tag{A.6}$$

where a_i and b_i are the diagonal and off-diagonal of the Jacobi matrix. Once the tridiagonal Jacobi matrix is constructed the weights and abscissas are obtained from the eigenvalue problem around the matrix $\boldsymbol{J}$. The abscissas (L_j) are simply the eigenvalues of $\boldsymbol{J}$ and the weights (w_j) can be obtained from the first component of the jth eigenvector (v_{j1}).

$$w_j = \mu_0 v_{j1}^2 \qquad \text{A.7}$$

APPENDIX B. DIMENSIONAL ANALYSIS OF SPHERICAL CRYSTALLIZATION SYSTEMS

This section details the use of regime maps and dimensional analysis to aid in the development of SC processes. Here it is demonstrated how the critical process parameters are reduced to dimensionless quantities that can be used to determine the mechanism or the final product properties. The first step is to identify parameters that are critical to a SC process and develop relationships that allow of dimensional analysis.

As the previous sections detail, the most important process parameters include: the BSR, supersaturation, agitation rate, and batch or residence time. For the BSR, there is a critical range for which a SC process will be successful. This range is identified by the BSR_{min} and BSR_{max}. Both quantities are system specific and are found empirically through trial and error. The supersaturation is the main control variable in determine the size and concentration of the particles in suspension which influence the agglomeration mechanism and final agglomerate properties. For agitation rate, there is a lower bound where below the bound agglomeration would not be successful and agitation rates slightly above bound increases agglomerate size. However, the generally observed trend is agglomerate size decreases with increasing agitation rate above the sufficient agitation rate. Batch or residence time is also an important parameter as it determines the consolidation phase which directly affects final properties of agglomerates.

With knowledge of these parameters, two dimensionless numbers can be development. The first is the bridging liquid saturation ratio (S_B). S_B expressed as the ratio of the difference between the BSR and the BSR_{min} to the difference between the BSR_{min} and BSR_{max} (equation B.1).

$$S_B = \frac{BSR - BSR_{min}}{BSR_{max} - BSR_{min}} \qquad \text{B.1}$$

S_B serves as to balance BSR between the sufficient low bound and maximum upper bound. A negative ratio or a ratio above 1 would indicate that the process is outside the ideal range for SA. S_B directly relates to and can determine the agglomeration process. To further

incorporate the crystallization process, S_B is multiplied by the supersaturation (S). The combined term is referred to as SS.

$$SS = S_B * S \quad \text{B.2}$$

The second dimensionless number is time under agitation. Time under agitation (ν) is the multiplication of agitation rate (N) and the batch or residence time (t or τ) (equation B.3). By considering the agitation speed and residence, the time under agitation directly relates to the agglomeration and consolidation phases of SC.

$$\nu = N * t \text{ or } \nu = N * \tau \quad \text{B.3}$$

Here the time under agitation is calculated for the formation and agglomeration phases. The formation phase (ν_F) refers to the solution or bridging liquid addition phase. This represents the initial forming and flocking of agglomerate particles. The agglomeration phase (ν_{agg}) refers to the post solution or bridging liquid addition phases. Table B.1 shows the experimental conditions for the dimensional analysis of batch studies carried using a BAM1 technique. It is important to note that the effect of flow rate is not accounted for the set of dimensionless parameters evaluated here. Table. B.2. shows the dimensionless parameters from those experiments.

Table B.1 Experimental conditions for batch regime maps

Exp.	F (min)	Agg (min)	BA conc. (g/mL)	SASR	S	BSR	RPM	FR
1	1,5	20,30	0.25	0.09	1.9	0.9	600	5
2	2,5	10,20,30	0.25	0.18	3.5	0.9	600	5
3	-	30	0.25	0.35	4.6	0.9	400	5
4	-	30	0.38	0.35	6.7	1.0	600	2.4
5	-	0,30,60	0.38	0.35	6.7	0.9	400	5
6	3,6,9,12	15	0.38	0.35	6.7	0.9	600	5

Table B.2 Dimensionless parameters

Exp.	S_b	SS	ν_F ($x10^3$)	ν_{agg} ($x10^3$)
1	0.623	1.2	0.6,3	12,18
2	0.623	2.2	1.2,3	6,12,18
3	0.623	2.9	-	12
4	0.768	5.1	-	12
5	0.623	4.2	-	0,12,24
6	0.623	4.2	1.8, 3.6, 5.4, 7.2	9

The dimensionless parameters for plot against each other to assess the different regimes of the various experiment. Figure B.1 shows the regime map for the formation phase of the SC process. The corresponding agglomerates from these times are shown in Figure B.2. From the regime map and the images, it is evident that the formation phase occurs within the first three minutes of the process. For experiments at lower concentration, the initially formed agglomerate nuclei are much larger in size. By five minutes into the process agglomeration of multiple nuclei is apparent. Significant agglomerate growth is observed after nine minutes.

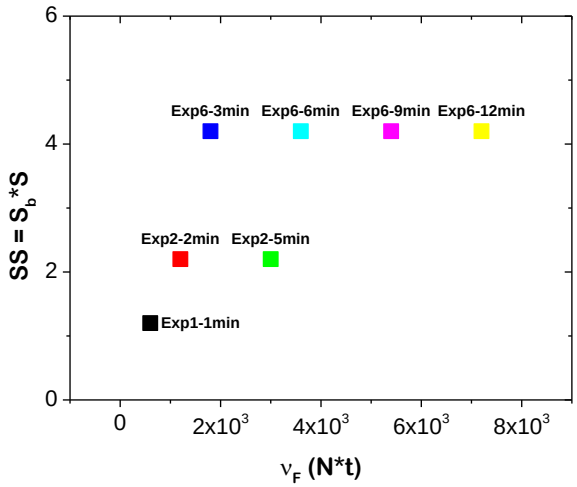

Figure B.1

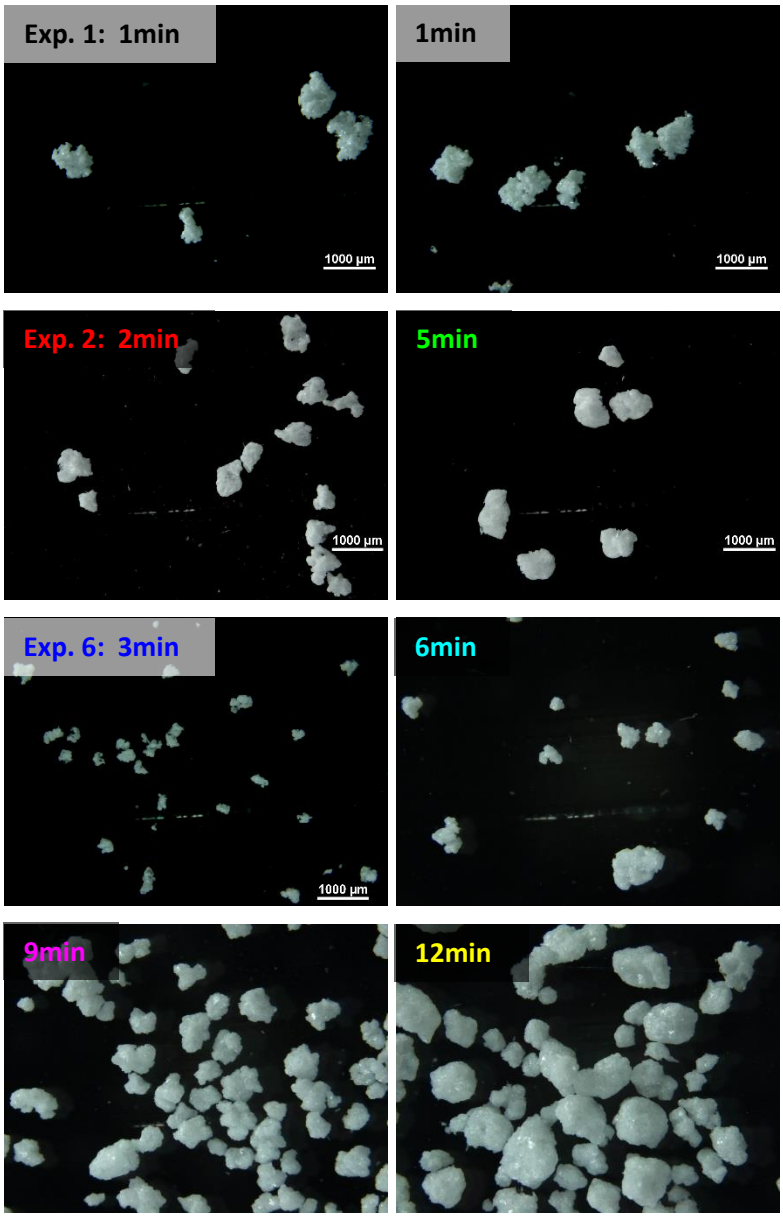

Figure B.2

Figure B.3 shows the regime map for the agglomeration phase of a SC process. The agglomeration phase can be divided into low *SS*, medium *SS*, and high *SS* regimes. At low *SS* (< 2), final agglomerates are small and there is minimal agglomerate growth with increase in time under agitation. As evidenced by the minimal increase in agglomerate size over time for experiment 1 (Figure B.4). The medium *SS* (> 2, < 4) regime corresponds to experiments 2 and 3. The agglomerates produced in this regime are spherical and appear uniform in size. It is also observed that this regime seems insensitive to increases in the

time under agitation (Figure B.4). The high *SS* (> 4) regime corresponds to experiments 4, 5, and 6. This regime shows rapid agglomerate growth with increase in time under agitation. Agglomerates in this regime show over agglomeration with evident smaller agglomerates on their surface (Figure B.4). At low to moderate ν_{agg} (<15x10^3), agglomerate sphericity is maintained. Higher ν_{agg} (>15x10^3) displays excess agglomeration. However, the *SS* parameter shows the most sensitivity to agglomerate properties. At constant ν_{agg} (12x10^3), experiments 1, 2, 3, 4 and 5 in Figure B.3 and B.4, increase in *SS* shows agglomerate growth from consolidation (experiments 1) to layering (experiments 2, 3) to coalescence (experiments 4, 5).

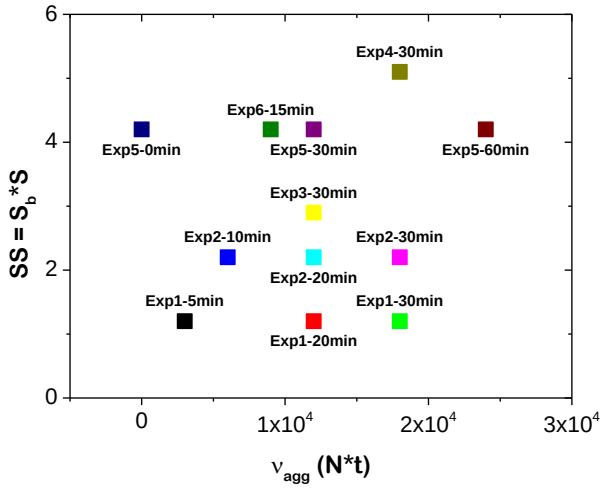

Figure B.3

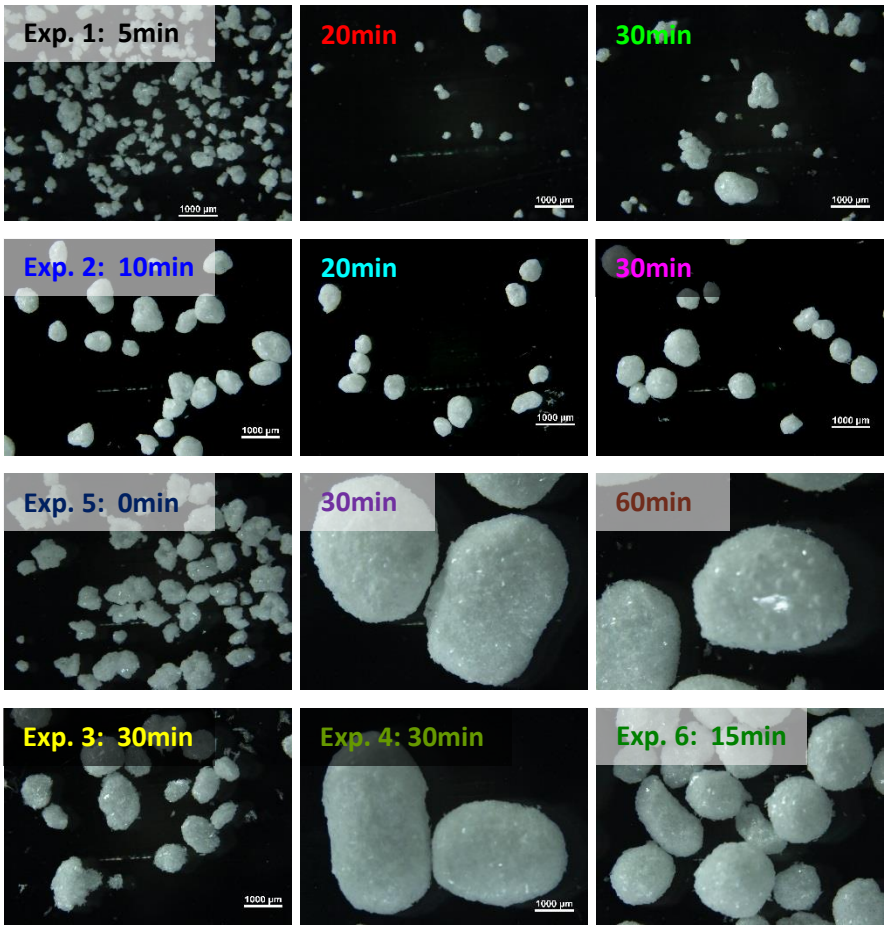

Figure B.4

Table B.3 shows the experimental conditions and dimensionless numbers for the MSMPR experiments. The SS and ν_{agg} are plotted against each other in Figure B.5. Similar trends are observed in the low, medium and high SS regimes for the MSMPR compared to the batch. However, for the MSMPR, the low SS exhibits low agglomeration efficiency with fine crystals evident. While the high SS exceeds that of the batch experiments and displays very porous and unstructured agglomerates. For $3.5<SS<5$ the agglomerates the same qualitative properties as the equivalent regime for the batch, i.e., excessive agglomeration leading to significant agglomerate growth (Figure 5.6).

Table B.3 Experimental conditions and dimensionless parameters for MSMPR

Exp.	Agg (min)	BA conc. (g/mL)	SASR	BSR	RPM	*S*	S_b	SS	ν_{agg} (x10^3)
1	50.00	0.38	0.33	0.59	400	6.9	0.174	1.2	20.0
2	56.25	0.38	0.33	0.82	400	6.9	0.507	3.5	22.5
3	62.50	0.38	0.23	1.00	500	6.2	0.768	4.8	31.3
4	62.50	0.38	0.33	1.25	500	6.9	1.130	7.8	31.3
5	55.56	0.25	0.20	1.00	500	4.7	0.768	3.6	27.8
6	29.50	0.38	0.10	0.76	400	3.0	0.420	1.3	11.8
7	60.00	0.38	0.10	1.08	400	3.0	0.884	2.7	24.0

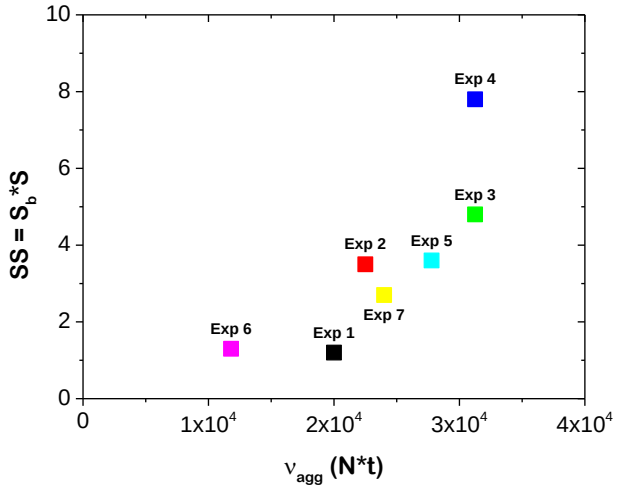

Figure B.5

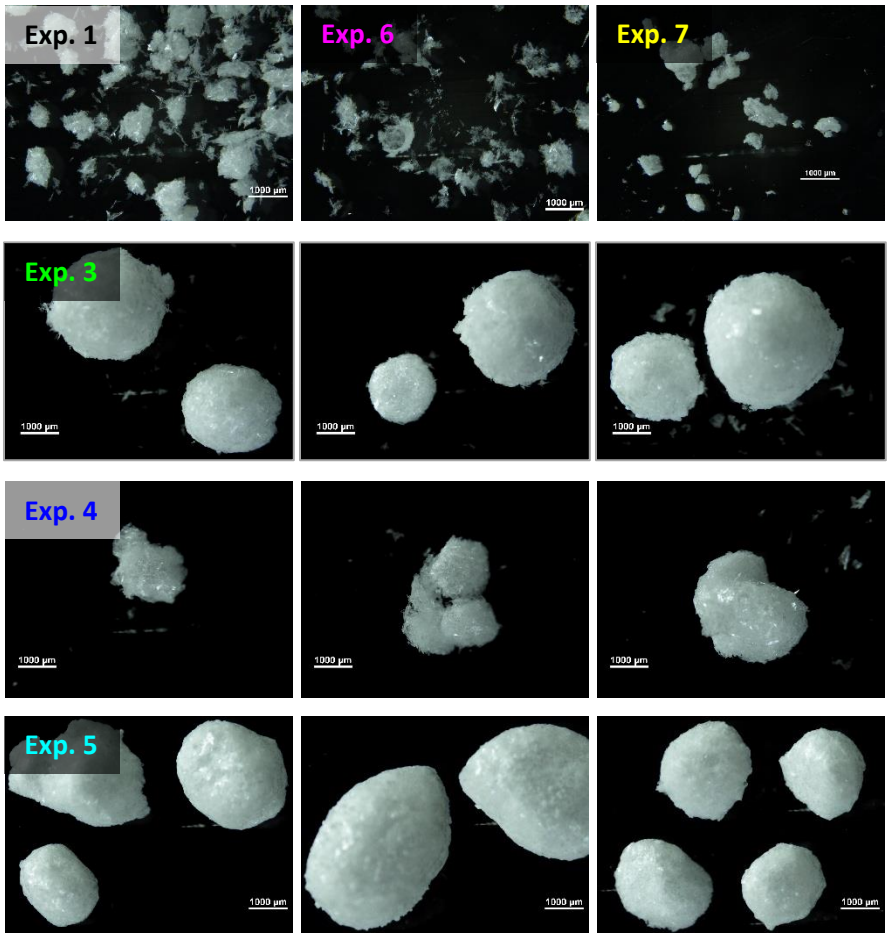

Figure B.6

REFERENCES

1. Lovette, M. A.; Browning, A. R.; Griffin, D. W., Sizemore, J. P.; Snyder, R. C.; Doherty, M. F. Crystal Shape Engineering. *Ind. Eng. Chem. Res.* 2008, 47(24), 9812–9833.
2. WHO. Pharmaceutical Industry. 2014.
3. Alvarez, A.J.; Myerson, A.S. Continuous Plug Flow Crystallization of Pharmaceutical Compounds. *Cryst. Growth Des.* 2010, 10(5), 2219–2228.
4. Holmbäck, X.; Rasmuson, Å. C. Size and morphology of benzoic acid crystals produced by drowning-out crystallization. *J. Cryst. Growth.* 1999, 198-199, 780–788.
5. Holmbäck, X. Drowning-out crystallization of benzoic acid: Influence of processing conditions and solvent composition on crystal size and shape. Ph.D. Thesis. Royal Institute of Technology. 2002.
6. Acevedo, D.; Nagy, Z. K. Systematic classification of unseeded batch crystallization systems for achievable shape and size analysis. *J. Cryst. Growth.* 2014, 394, 97–105.
7. Acevedo, D.; Tandy, Y.; Nagy, Z. K. Multiobjective Optimization of an Unseeded Batch Cooling Crystallizer for Shape and Size Manipulation. *Ind. Eng. Chem. Res.* 2015, 54(7), 2156–2166.
8. Leyssens, T.; Baudry, C.; Hernandez, M. L. E. Optimization of a crystallization by online FBRM analysis of needle-shaped crystals. *Org. Process Res. Dev.* 2011, 15(2), 413–426.
9. Simone, E.; Saleemi, A. N.; Tonnon, N.; Nagy, Z. K. Active polymorphic feedback control of crystallization processes using a combined Raman and ATR-UV/Vis spectroscopy approach. *Cryst. Growth Des.* 2014, 14, 1839–1850.
10. Simone, E.; Saleemi, A. N.; Nagy, Z. K. Application of quantitative Raman spectroscopy for the monitoring of polymorphic transformation in crystallization processes using a good calibration practice procedure. *Chem. Eng. Res.Des.* 2014, 92(4), 594–611.

11. Yang, Y.; Zhang, C.; Pal, K.; Koswara, A.; Quon, J.; McKeown, R.; Nagy, Z. K. Application of Ultra-Performance Liquid Chromatography as an Online Process Analytical Technology Tool in Pharmaceutical Crystallization. *Cryst. Growth Des.* 2016, 16(12),7074-7082.
12. Costa, C. B. B.; Maciel, M. R. W.; Filho, R. M. Considerations on the crystallization modeling: Population balance solution. *Comput. Chem. Eng.* 2007, 31(3), 206–218.
13. Mostafa Nowee, S.; Abbas, A.; Romagnoli, J. A. Antisolvent crystallization: Model identification, experimental validation and dynamic simulation. *Chem. Eng. Sci.* 2008, 63(22), 5457–5467.
14. Ridder, B. J.; Majumder, A.; Nagy, Z. K. Population Balance Model Based Multi-Objective Optimization of a Multi-Segment Multi-Addition (MSMA) Continuous Plug Flow Antisolvent Crystallizer. *Ind. Eng. Chem. Res.* 2014, 53(11), 4387–4397.
15. Yang, Y.; Nagy, Z. K. Model-Based Systematic Design and Analysis Approach for Unseeded Combined Cooling and Antisolvent Crystallization (CCAC) Systems. *Cryst. Growth Des.* 2014, 14(2), 687–698.
16. Barrett, M.; McNamara, M.; Hao, H.; Barrett, P.; Glennon, B. Supersaturation tracking for the development, optimization and control of crystallization processes. *Chem. Eng. Res. Des.*, 2010, 88(8), 1108–1119.
17. Nagy, Z. K.; Fevotte, G.; Kramer, H.; Simon, L. L. Recent advances in the monitoring, modelling and control of crystallization systems. *Chem. Eng. Res. Des.* 2013, 91(10), 1903–1922.
18. Su, Q.; Nagy, Z. K.; Rielly, C. D. Pharmaceutical crystallization processes from batch to continuous operation using MSMPR stages: Modelling, design, and control. *Chem. Eng. Process.* 2015, 89, 41–53.
19. Yang, Y.; Song, L.; Nagy, Z. K. Automated Direct Nucleation Control in Continuous Mixed Suspension Mixed Product Removal Cooling Crystallization. *Cryst. Growth Des.*, 2015, 15(12), 5839–5848.
20. U.S. Department of Health and Human Services, Food and Drug Administration Guidance for Industry: PAT – A Framework for Innovative Pharmaceutical Development, Manufacturing and Quality Assurance. 2004.

21. Nagy, Z. K.; Braatz, R. D. Advances and New Directions in Crystallization Control. *Annu. Rev. Chem. Biomol. Eng.* 2012, 3, 55–75.
22. Kawashima, Y.; Okumura, M.; Takenaka, H. Spherical crystallization: direct spherical agglomeration of salicylic acid crystals during crystallization. *Sci.* 1982, 216 (4550), 1127–1128.
23. Mahanty, S.; Sruti, J.; Patra, C. N.; Rao, M. E. B. Particle Design of Drugs by Spherical Crystallization Techniques. *Int. J. Pharm. Sci. Nanotech.* 2010, 3(2), 912–918.
24. Willburn, K. R. The Business Case for Continuous Manufacturing of Pharmaceuticals. M.S. Thesis. Massachusetts Institute of Technology. 2010.
25. Schaber, S. D.; Gerogiorgis, D. I.; Ramachandran, R.; Evans, J. M. B.; Barton, P. I.; Trout, B. L. Economic Analysis of Integrated Continuous and Batch Pharmaceutical Manufacturing: A Case Study. *Ind. Eng. Chem. Res.* 2011, 50(17), 10083-10092.
26. Katta, J.; Rasmuson, Å. C. Spherical crystallization of benzoic acid. *Int. J. Pharm.* 2008, 348(1-2), 61–69.
27. Kawashima, Y. Development of spherical crystallization technique and its application to pharmaceutical systems. *Arch. Pharmacal Res.* 1984, 7(2), 145-151.
28. Kawashima, Y.; Imai, M.; Takeuchi, H.; Yamamoto, H.; Kamiya, K.; Hino, T. Improved flowability and compactibility of spherically agglomerated crystals of ascorbic acid for direct tableting designed by spherical crystallization process. *Powder Technol.* 2003, 130(1-3), 283-289.
29. Amaro-González, D.; Biscans, B. Spherical agglomeration during crystallization of an active pharmaceutical ingredient. *Powder Technol.* 2002, 128, 188-194.
30. Kawashima, Y.; Kurachi, Y.; Takenaka, H. Preparation of spherical wax matrices of sulfamethoxazole by wet spherical agglomeration technique using a CMSMPR agglomerator. *Powder Technol.* 1982, 32(2), 155-161.
31. Sirianni, A. F.; Capes, C. E.; Puddington, J. E.; Recent experience with the spherical agglomeration process. *Can. J. Chem. Eng.* 1969, 47(2), pp.166–170.
32. Myerson, A. *Handbook of industrial crystallization*. Butterworth-Heinemann. 2002.

33. Mullin, J. W. *Crystallization*. Butterworth-Heinemann. 2001.
34. Davey, R. J.; Garside, J. *From molecules to crystallizers. An introduction to crystallization*. New York, Oxford University Press. 2001.
35. Turnbull, D.; Fisher, J. C. Rate of Nucleation in Condensed Systems. *J. Chem. Phys.* 1949, 17(1), 71.
36. Beckmann, W. *Crystallization: Basic Concepts and Industrial Applications*. John Wiley & Sons. 2013.
37. Brunsteiner, M.; Jones, A. G.; Pratola, F.; Price, S. L.; Simons, S. J. R. Toward a molecular understanding of crystal agglomeration. *Cryst. Growth Des.* 2005, 5(1), 3–16.
38. Garside, J.; Tavare, N. S. Mixing, reaction and precipitation: Limits of micromixing in an MSMPR crystallizer. *Chem. Eng. Sci.* 1985, 40(8), 1485–1493.
39. Lakatos, B. G.; Sapundzhiev, T. J.; Garside, J. Stability and dynamics of isothermal CMSMPR crystallizers. *Chem. Eng. Sci.* 2007, 62(16), 4348–4364.
40. Ferguson, S.; Morris, G.; Hao, H.; Barrett, M.; Glennon, B. Characterization of the anti-solvent batch, plug flow and MSMPR crystallization of benzoic acid. *Chem. Eng. Sci.* 2013, 104, 44–54.
41. Tavare, N.S. *Industrial Crystallization: Process Simulation Analysis and Design*. Plenum Press, New York. 1995
42. Ni, X.; Mackley, M. R.; Harvey, A. P.; Stonestreet, P.; Baird, M. H. I.; Rama Rao, N. V. Mixing Through Oscillations and Pulsations – A Guide to Achieving Process Enhancements in the Chemical and Process Industries. *Chem. Eng. Res. Des.* 2003, 81(3), 373–383.
43. Lawton, S.; Steele, G; Shering, P.; Zhao, L.; Laird, I.; Ni, X. Continuous Crystallization of Pharmaceuticals Using a Continuous Oscillatory Baffled Crystallizer. *Org. Process Res. Dev.* 2009, 13(6), 1357–1363.
44. Hinz, D. C. Process analytical technologies in the pharmaceutical industry: The FDA's PAT initiative. *Anal. Bioanal. Chem.* 2006, 384(5), 1036–1042.

45. Wu, H.; Dong, Z.; Li, H.; Khan, M. An integrated process analytical technology (PAT) approach for pharmaceutical crystallization process understanding to ensure product quality and safety: FDA scientist's perspective. *Org. Process Res. Dev.* 2015, 19(1), 89–101.

46. Simon, L. L.; Pataki, H.; Marosi, G.; Meemken, F.; Hungerbühler, K.; Baiker, A.; Tummala, S.; Glennon, B.; Kuentz, M.; Steele, G.; Kramer, H. J. M.; Rydzak, J. W.; Chen, Z.; Morris, J.; Kjell, F.; Singh, R.; Gani, R.; Gernaey, K. V.; Louhi-Kultanen, M.; O'Reilly, J.; Sandler, N.; Antikainen, O.; Yliruusi, J.; Frohberg, P.; Ulrich, J.; Braatz, R. D.; Leyssens, T.; von Stosch, M.; Oliveira, R.; Tan, R. B. H.; Wu, H.; Khan, M.; O'Grady, D.; Pandey, A.; Westra, R.; Delle-Case, E.; Pape, D.; Angelosante, D.; Maret, Y.; Steiger, O.; Lenner, M.; Abbou-Oucherif, K.; Nagy, Z. K.; Litster, J. D.; Kamaraju, V. K.; Chiu, M. Assessment of recent process analytical technology (PAT) trends: A multiauthor review. *Org. Process Res. Dev.* 2015, 19(1), 3–62.

47. Yu, L. X.; Lionberger, R. A.; Raw, A. S.; D'Costa, R.; Wu, H.; Hussain, A. S. Applications of process analytical technology to crystallization processes. *Adv. Drug Deliv. Rev.* 2004, 56(3), 349-369.

48. Barrett, P.; Smith, B.; Worlitschek, J.; Bracken, V.; O'Sullivan, B.; O'Grady, D. A review of the use of process analytical technology for the understanding and optimization of production batch crystallization processes. *Org. Process Res. Dev.* 2005, 9(3), 348–355.

49. Yu, Z. Q.; Chew, J. W.; Chow, P. S.; Tan, R. B. H. Recent Advances in Crystallization control. *Chem. Eng. Res. Des.* 2007, 85(7), 893–905.

50. Barrett, P.; Glennon, B. Characterizing the Metastable Zone Width and Solubility Curve Using Lasentec FBRM and PVM. *Chem. Eng. Res. Des.* 2002, 80(October), 799–805.

51. Aamir, E.; Nagy, Z. K.; Rielly, C. D. Optimal seed recipe design for crystal size distribution control for batch cooling crystallization processes. *Chem. Eng. Sci.* 2010, 65(11), 3602–3614.

52. Schöll, J.; Bonalumi, D.; Vicum, L.; Mazzotti, M.; Müller, M. In Situ Monitoring and Modeling of the Solvent-Mediated Polymorphic Transformation of L-Glutamic Acid. *Cryst. Growth Des.* 2006, 6(4), 881–891.

53. Scott, C.; Black, S. In-Line Analysis of Impurity Effects on Crystallisation. *Org. Process Res. Dev.* 2005, 9(6), 890–893.

54. Schöll, B. J.; Vicum, L.; Müller, M.; Mazzotti, M. Precipitation of L-Glutamic Acid: Determination of Nucleation Kinetics. *Chem. Eng. Technol.* 2006, 29(2), 257–264.

55. Kim, S.; Lotz, B.; Lindrud, M.; Girard, K.; Moore, T.; Nagarajan, K.; Alvarez, M.; Lee, T.; Nikfar, F.; Davidovich, M.; Srivastava, S. Kiang, S. Control of the Particle Properties of a Drug Substance by Crystallization Engineering and the Effect on Drug Product Formulation. *Org. Process Res. Dev.* 2005, 9(6), 894–901.

56. Abu Bakar, M. R.; Nagy, Z. K.; Saleemi, A. N.; Rielly, C. D. The Impact of Direct Nucleation Control on Crystal Size Distribution in Pharmaceutical Crystallization Processes. *Cryst. Growth Des.* 2009, 9(3), 1378–1384.

57. Woo, X. Y.; Nagy, Z. K.; Tan, R. B. H.; Braatz, R. D. Adaptive Concentration Control of Cooling and Antisolvent Crystallization with Laser Backscattering Measurement. *Cryst. Growth Des.* 2009, 9(1), 182–191.

58. Schöll, J.; Kempkes, M.; Mazzotti, M. Focused Beam Reflectance Measurement. *Industrial Crystallization Process Monitoring and Control*. Weinheim, Germany: Wiley-VCH Verlag GmbH & Co. KGaA. 2012, 21–28.

59. Heath, A. R.; Fawell, P. D.; Bahri, P. A.; Swift, J. D. Estimating average particle size by focused beam reflectance measurement (FBRM). *Part. Part. Sys. Char.* 2002, 19(2), 84–95.

60. FBRM Method of Measurement. www.mt.com/FBRM-mom

61. Wynn, E. J. W. Relationship between particle-size and chord-length distributions in focused beam reflectance measurement: stability of direct inversion and weighting. *Powder Technol.* 2003, 133(1–3), 125–133.

62. Li, M.; Wilkinson, D. Determination of non-spherical particle size distribution from chord length measurements. Part 1: Theoretical analysis. *Chem. Eng. Sci.* 2005, 60, 3251–3265.

63. Li, M.; Wilkinson, D.; Patchigolla, K. Determination of non-spherical particle size distribution from chord length measurements. Part 2: Experimental validation. *Chem. Eng. Sci.* 2005, 60, 4992–5003.

64. Worlitschek, J.; Hocker, T.; Mazzotti, M. Restoration of PSD from chord length distribution data using the method of projections onto convex sets. *Part. Part. Sys. Char.* 2005, 22(2), 81–98.

65. Kempkes, M.; Eggers, J.; Mazzotti, M. Measurement of particle size and shape by FBRM and in situ microscopy. *Chem. Eng. Sci.* 2008, 63, 4656–4675.

66. Kail, N.; Briesen, H.; Marquardt, W. Analysis of FBRM measurements by means of a 3D optical model. *Powder Technol.* 2007, 185(3), 2008, 211–222.

67. Yu, W.; Erickson, K. Chord length characterization using focused beam reflectance measurement probe - methodologies and pitfalls. *Powder Technol.* 2008, 185(1), 24–30.

68. Rudolph, G.; Lindner, P.; Bluma, A.; Joeris, K.; Martinez, G.; Hitzmann, B.; Scheper, T. Optical inline measurement procedures for counting and sizing cells in bioprocess technology. *Adv. Biochem. Engin. /Biotechnol.* 2010, 116, 125–142.

69. Höpfner, T.; Bluma, A.; Rudolph, G.; Lindner, P.; Scheper, T. A review of non-invasive optical-based image analysis systems for continuous bioprocess monitoring. *Bioprocess Biosys. Eng.* 2010, 33(2), 247–256.

70. Liu, W.; Wei, H.; Black, S. An Investigation of the Transformation of Carbamazepine from Anhydrate to Hydrate Using in Situ FBRM and PVM. *Org. Process Res. Dev.* 2009, 13(3), 494–500.

71. Jia, C.-Y.; Yin, Q.-X.; Zhang, M.-J.; Wang, J.-K.; Shen, Z.-H. Polymorphic Transformation of Pravastatin Sodium Monitored Using Combined Online FBRM and PVM. *Org. Process Res. Dev.* 2008, 12(6), 1223–1228.

72. Boxall, J. A.; Koh, C. A.; Sloan, E. D.; Sum, A. K.; Wu, D. T. Measurement and Calibration of Droplet Size Distributions in Water-in-Oil Emulsions by Particle Video Microscope and a Focused Beam Reflectance Method. *Ind. Eng. Chem. Res.* 2010, 49(3), 1412–1418.

73. ParticleView. www.mt.com/ParticleView

74. Förster, H. UV/VIS Spectroscopy, In: Karge H.G., Weitkamp J. (eds) *Characterization I. Molecular Sieves – Science and Technology*. Springer, Berlin, Heidelberg. 2004, 4, 337–426.

75. Thermo Spectronic. Basic UV-Vis Theory, Concepts and Applications Basic. *ThermoSpectronic*, 2013, 1–28.

76. Thompson, D. R.; Kougoulos, E.; Jones, A. G.; Wood-Kaczmar, M. W. Solute concentration measurement of an important organic compound using ATR-UV spectroscopy. *J. Cryst. Growth*, 2005, 276(1–2), 230–236.

77. Billot, P.; Couty, M.; Hosek, P. Application of ATR-UV spectroscopy for monitoring the crystallization of UV absorbing and nonabsorbing molecules. *Org. Process Res. Dev.*, 2010, 14(3), 511–523.

78. Saleemi, A. N.; Rielly, C. D.; Nagy, Z. K. Comparative investigation of supersaturation and automated direct nucleation control of crystal size distributions using ATR-UV/vis spectroscopy and FBRM. *Cryst. Growth Des.* 2012, 12, 1792–1807.

79. Wold, S.; Esbensen, K.; Geladi, P. Principal Component Analysis. *Chemometr. Intell. Lab.* 1987, 2, 37–52.

80. Tobiszewski, M.; Tsakovski, S.; Simeonov, V.; Namieśnik, J.; Pena-Pereira, F. A solvent selection guide based on chemometrics and multicriteria decision analysis. *Green Chem.* 2015, 17(10), 4773–4785.

81. Pöllänen, K.; Häkkinen, A.; Reinikainen, S. P.; Rantanen, J.; Minkkinen, P. Dynamic PCA-based MSPC charts for nucleation prediction in batch cooling crystallization processes. *Chemometr. Intell. Lab.* 2006, 84(1–2 Spec. Iss.), 126–133.

82. García-Muñoz, S.; Kourti, T.; MacGregor, J. F.; Mateos, A. G.; Murphy, G. Troubleshooting of an industrial batch process using multivariate methods. *Ind. Eng. Chem. Res.*, 2003, 42(15), 3592–3601.

83. Randolph, A. D.; Larson, M. A. *Particulate Processes: Analysis and Techniques of Continuous Crystallization*. Academic Press. 1988.

84. Mcgraw, R. Description of aerosol dynamics by the quadrature method of moments. *Aerosol Sci. Technol.* 1997, 27(2), 255–265.

85. Marchisio, D. L.; Pikturna, J. T.; Fox, R. O.; Vigil, R. D.; Barresi, A. A. Quadrature method of moments for population-balance equations. *AIChE J.* 2003, 49(5), 1266–1276.

86. Gordon, R. G. Error Bounds in Equilibrium Statistical Mechanics. *J. Math. Phys.* 1968, 9(5), 655.

87. Marchiso, D. L.; Barresi, A. A.; Garbero, M. Nucleation, growth, and agglomeration in barium sulfate turbulent precipitation. *AIChE J.* 2002, 48(9), 2039–2050.

88. Marchisio, D. L.; Vigil, R. D.; Fox, R. O. Quadrature method of moments for aggregation–breakage processes. *J. Colloid Interface Sci.* 2003, 258, 322–334.

89. Nowee, S. M.; Abbas, A.; Romagnoli, J. A. Optimization in seeded cooling crystallization: A parameter estimation and dynamic optimization study. *Chem. Eng. Process.* 2007, 46(11), 1096–1106.

90. Nagy, Z. K.; Chew, J. W.; Fujiwara, M.; Braatz, R. D. Comparative performance of concentration and temperature controlled batch crystallizations. *J. Process Contr.* 2008, 18(3–4), 399–407.

91. Sanzida, N.; Nagy, Z. K. Iterative learning control for the systematic design of supersaturation controlled batch cooling crystallization processes. *Comput. Chem. Eng.* 2013, 59, 111–121.

92. Trifkovic, M.; Sheikhzadeh, M.; Rohani, S. Kinetics estimation and single and multi-objective optimization of a seeded, anti-solvent, isothermal batch crystallizer. *Ind. Eng. Chem. Res.* 2008, 47(5), 1586–1595.

93. Sarkar, D.; Rohani, S.; Jutan, A. Multi-objective optimization of seeded batch crystallization processes. *Chem. Eng. Sci.* 2006, 61(16), 5282–5295.

94. Nocedal, J.; Wright, S. J. *Numerical Optimization*. *Springer Series in Operations Research*. Springer. 2006.

95. Byrd, R. H.; Hribar, M. E.; Nocedal, J. An interior point algorithm for large-scale nonlinear programming. *SIAM Journal Optimization*, 1999, 9(4), 877–884.

96. Stankiewicz, A.; Moulijn, J. A. Process intensification. *Ind. Eng. Chem. Res.* 2002, 41(8), 1920–1924.

97. Charpentier, J. C. In the frame of globalization and sustainability, process intensification, a path to the future of chemical and process engineering (molecules into money). *Chem. Eng. J.* 2007, 134(1–3), 84–92.

98. Calder, R. HEX reactors reduce process time by 98.6%. *BHR News*, 2000, 4.

99. Stankiewicz, A. Process intensification in in-line monolithic reactor. *Chem. Eng. Sci.* 2001, 56(2), 359–364.

100. Oxley, P.; Brechtelsbauer, C.; Ricard, F.; Lewis, N.; Ramshaw, C. Evaluation of Spinning Disk Reactor Technology for the Manufacture of Pharmaceuticals. *Ind. Eng. Chem. Res.* 2000, 39(7), 2175–2182.

101. Malone, M. F.; Doherty, M. F. Reactive Distillation. *Ind. Eng. Chem. Res.* 2000, 39(11), 3953–3957.

102. Mascia, S.; Heider, P. L.; Zhang, H.; Lakerveld, R.; Benyahia, B.; Barton, P. I., Braatz, R. D.; Cooney, C. L.; Evans, J. M. B.; Jamison, T. F.; Jensen, K. F., Myerson, A. S.; Trout, B. L. End-to-End Continuous Manufacturing of Pharmaceuticals: Integrated Synthesis, Purification, and Final Dosage Formation *Angew. Chem. Int. Ed.* 2013, 52(47), 12359–12363.

103. Zhang, H.; Lakerveld, R.; Heider, P. L.; Tao, M.; Su, M.; Testa, C. J.; D'Antonio, A. N.; Barton, P. I.; Braatz, R. D.; Trout, B. L.; Myerson, A. S.; Jensen, K. F.; Evans, J. M. B. Application of continuous crystallization in an integrated continuous pharmaceutical pilot plant. *Cryst. Growth Des.* 2014, 14(5), 2148–2157.

104. Lakerveld, R.; Benyahia, B.; Heider, P. L.; Zhang, H.; Wolfe, A.; Testa, C. J.; Ogden, S.; Hersey, D. R.; Mascia, S.; Evans, J. M. B.; Braatz, R. D.; Barton, P. I. The Application of an Automated Control Strategy for an Integrated Continuous Pharmaceutical Pilot Plant. *Org. Process Res. Dev.* 2015, 19(9), 1088–1100.

105. Gursch, J.; Hohl, R.; Toschkoff, G.; Dujmovic, D.; Brozio, J.; Krumme, M.; Rasenack, N.; Khinast, J. Continuous Processing of Active Pharmaceutical Ingredients Suspensions via Dynamic Cross-Flow Filtration. *J. Pharm. Sci.* 2015, 104(10), 3481–3489.

106. Smith, H.; Puddington, I. Spherical agglomeration of barium sulphate. *Can. J. Chem.*, 1960, 38, 1911–1916.

107. Farnand, J. R.; Smith, H. M.; Puddington, I. E. Spherical agglomeration of solids in liquid suspension. *Can. J. Chem. Eng.* 1961, 39(2), 94–97.

108. Sutherland, J. P. The agglomeration of aqueous suspensions of graphite. *Can. J. Chem. Eng.* 1962, 40(6), 268–272.

109. Kawashima, Y.; Capes, C. Further studies of the kinetics of spherical agglomeration in a stirred vessel. *Powder Technol.* 1976, 13, 279–288.

110. Zhang, H.; Chen, Y.; Wang, J.; Gong, J. Investigation on the spherical crystallization process of cefotaxime sodium. *Ind. Eng. Chem. Res.* 2010, 49, 1402–1411.

111. Blandin, A. F.; Mangin, D.; Subero-Couroyer, C.; Rivoire, A.; Klein, J. P.; Bossoutrot, J. M. Modelling of agglomeration in suspension: Application to salicylic acid microparticles. *Powder Technol.* 2005, 156(1), 19–33.

112. Maghsoodi, M., & Yari, Z. Effect of drying phase on the agglomerates prepared by spherical crystallization. *Iran. J.Pharm. Res.* 2015, 14(1), 51–57.

113. Kawashima, Y.; Okumura, M.; Takenaka, H. The effects of temperature on the spherical crystallization of salicylic acid. *Powder Technol.* 1984, 39(1), 41–47.

114. Sano, A.; Kuriki, T.; Kawashima, Y.; Takeuchi, H.; Hino, T.; Niwa, T. Particle design of tolbutamide by the spherical crystallization technique. III. Micromeritic properties and dissolution rate of tolbutamide spherical agglomerates prepared by the quasi-emulsion solvent diffusion method and the solvent change method. *Chem. Pharm. Bull. (Tokyo)* 1990, 38(3), 733–739.

115. Kenji, M.; Yoshiaki, K.; Hirofumi, T.; Toshiyuki, N.; Tomoaki, H.; Yoichi, K. Tabletting properties of bucillamine agglomerates prepared by the spherical crystallization technique. *Int. J. Pharm.* 1994, 105(1), 11–18.

116. Usha, A. N.; Mutalik, S.; Reddy, M. S.; Ranjith, A. K.; Kushtagi, P.; Udupa, N. Preparation and, in vitro, preclinical and clinical studies of aceclofenac spherical agglomerates. *Eur. J. Pharm. Biopharm.* 2008, 70(2), 674–683.

117. Zhang, H.; Chen, Y.; Wang, J.; Gong, J. Investigation on the spherical crystallization process of cefotaxime sodium. *Ind. Eng. Chem. Res.* 2010, 49, 1402–1411.

118. Maghsoodi, M. Effect of process variables on physicomechanical properties of the agglomerates obtained by spherical crystallization technique. *Pharm. Dev. Technol.* 2011, 16(5), 474–82.

119. Jbilou, M.; Ettabia, A.; Guyot-Hermann, A.-M.; Guyot, J.-C. Ibuprofen Agglomerates Preparation by Phase Separation. *Drug Dev. Ind. Pharm.* 1999, 25(3), 297–305.

120. Maghsoodi, M. How spherical crystallization improves direct tableting properties: A review. *Adv. Pharm. Bull.* 2012, 2(2), 253–257.

121. Sano, A.; Kuriki, T.; Kawashima, Y.; Takeuchi, H.; Hino, T.; Niwa, T. Particle design of tolbutamide by the spherical crystallization technique. V. Improvement of dissolution and bioavailability of direct compressed tablets prepared using tolbutamide agglomerated crystals. *Chem. Pharm. Bull.* 1992, 40(11), 3030–3035.

122. Varshosaz, J.; Tavakoli, N.; Salamat, F. A. Enhanced dissolution rate of simvastatin using spherical crystallization technique. *Pharm. Dev. Technol.* 2011, 16(5), 529–35.

123. Kovačič, B.; Vrečer, F.; Planinšek, O.Spherical crystallization of drugs. *Acta Pharm. (Zagreb, Croatia)* 2012, 62(1), 1–14.

124. Kawashima, Y.; Cui, F.; Takeuchi, H.; Toshiyuki, N.; Hino, T.; Kiuchi, K. Parameters determining the agglomeration behaviour and the micromeritic properties of spherically agglomerated crystals prepared by the spherical crystallization technique with miscible solvent systems. *Int. J. Pharm.* 1995, 119, 139–147.

125. Kawashima, Y.; Niwa, T.; Handa, T.; Takeuchi, H.; Iwamoto, T.; Itoh, K. Preparation of controlled-release microspheres of ibuprofen with acrylic polymers by a novel quasi-emulsion solvent diffusion method. *J. Pharm. Sci.* 1989, 78(1), 68–72.

126. Chadwick, K.; Davey, R. J.; Mughal, R.; Marziano, I. Crystallisation from water-in-oil emulsions as a route to spherical particulates: Glycine and the hydrochloride salts of glutamic acid and ephedrine. *Org. Process Res. Dev.* 2009, 13(6), 1284–1290.

127. Ueda, M.; Nakamura, Y.; Makita, H.; Imasato, Y.; Kawashima, Y. Particle design of enoxacin by spherical crystallization technique. I. Principle of ammonia diffusion system (ADS). *Chem. Pharm. Bull.* 1990, 38(9), 2537–2541.

128. Pawar, A. P.; Paradkar, A. R.; Kadam, S. S.; Mahadik, K. R. Crystallo-co-agglomeration: A novel technique to obtain ibuprofen-paracetamol agglomerates. *AAPS PharmSciTech*, 2004, 5(3), 57–64.

129. Sano, A.; Kuriki, T.; Handa, T.; Takeuchi, H.; Kawashima, Y. Particle design of tolbutamide in the presence of soluble polymer or surfactant by the spherical crystallization technique: Improvement of dissolution rate. *J. Pharm. Sci.* 198, 76(6), 471–474.

130. Peña, R.; Nagy, Z. K. Process Intensification through Continuous Spherical Crystallization Using a Two-Stage Mixed Suspension Mixed Product Removal (MSMPR) System. *Cryst. Growth Des.* 2015, 15(9), 4225–4236.

131. Shekunov, B. Y.; York, P. Crystallization processes in pharmaceutical technology and drug delivery design. *J. Cryst.Growth*. 2000, 211(1), 122–136.

132. Sano, A.; Kuriki, T.; Kawashima, Y.; Takeuchi, H.; Hino, T.; Niwa, T. Particle design of tolbutamide by the spherical crystallization technique. II. Factors causing polymorphism of Tolbutanide Spherical Agglomerates. *Chem. Pharm. Bull.* 1989, 37(8), 2183–2187.

133. Kawashima, Y.; Niwa, T. Characterization of polymorphs of tranilast anhydrate and tranilast monohydrate when crystallized by two solvent change spherical crystallization techniques. *J. Pharm Sci.* 1991, 80(5), 472–478.

134. Szabó-Révész, P.; Hasznos-Nezdei, M.; Farkas, B.; Göcző, H.; Pintye-Hódi, K.; Erős, I. Crystal growth of drug materials by spherical crystallization. *J. Cryst. Growth*. 2002, 237-239, 2240–2245.

135. Chow, A. H. L.; Leung, M. W. M. A study of the Mechanisms of Wet Spherical Agglomeration of Pharmaceutical Powders. *Drug Dev. Ind. Pharm.* 1996, 22(4), 357–371.

136. Di Martino, P.; Barthé lé my, C.; Piva, F.; Joiris, E.; Palmieri, G. F.; Martelli, S. Improved Dissolution Behavior of Fenbufen by Spherical Crystallization. *Drug Dev. Ind. Pharm.* 1999, 25(10), 1073–1081.

137. Thati, J.; Rasmuson, Å. C. On the mechanisms of formation of spherical agglomerates. *Eur. J. Pharm. Sci.* 2011, 42(4), 365–379.

138. Jitkar, S.; Thipparaboina, R.; Chavan, R. B.; Shastri, N. R. Spherical Agglomeration of Platy Crystals: Curious Case of Etodolac. *Cryst. Growth Des.* 2016, 16(7), 4034–4042.

139. Thati, J.; Rasmuson, Å. C. Particle engineering of benzoic acid by spherical agglomeration. *Eur. J. Pharm. Sci.* 2012, 45(5), 657–67.

140. Kawashima, Y.; Okumura, M.; Takenaka, H.; Kojima, A. Direct preparation of spherically agglomerated salicylic acid crystals during crystallization. *J. Pharm. Sci.* 1984, 73(11), 1535–1538.

141. Wu, S.; Li, K.; Zhang, T.; Gong, J.Size Control of Atorvastatin Calcium Particles Based on Spherical Agglomeration. *Chem. Eng. Technol.* 2015, 38(6), 1081–1087.

142. Subero-Couroyer, C.; Mangin, D.; Rivoire, A.; Blandin, A. F.; Klein, J. P. Agglomeration in suspension of salicylic acid fine particles: Analysis of the wetting period and effect of the binder injection mode on the final agglomerate size. *Powder Technol.* 2006, 161(2), 98–109.

143. Blandin, A. F.; Mangin, D.; Rivoire, A.; Klein, J. P.; Bossoutrot, J. M. Agglomeration in suspension of salicylic acid fine particles: Influence of some process parameters on kinetics and agglomerate final size. *Powder Technol.* 2003, 130(1–3), 316–323.

144. Kawashima, Y.; Furukawa, K.; Takenaka, H. The physicochemical parameters determining the size of agglomerate prepared by the wet spherical agglomeration technique. *Powder Technol.* 1981, 30(2), 211–216.

145. Kawashima, Y.; Lin, S.Y.; Naito, M.; Takenaka, H. Direct agglomeration of sodium theophylline crystals produced by salting out in liquid. *Chem. Pharm. Bull.*, 1982, 30(5), 1837–1843.

146. Kawashima, Y.; Naito, M.; Lin, S. Y.; Takenaka, H. An experimental study of the kinetics of the spherical crystallization of sodium theophylline monohydrate. *Powder Technol.* 1983, 34, 255–260.

147. Bos, A. S.; Zuiderweg, F. J. Kinetics of Continuous Agglomeration in Suspension. *Powder Technol.* 1985, 44(1), 43–51.

148. Paradkar, A. R.; Pawar, A. P.; Chordiya, J. K.; Patil, V. B.; Ketkar, A. R. Spherical crystallization of celecoxib. *Drug Dev. Ind. Pharm.* 2002, 28(10), 1213–20.

149. Ikegami, K.; Kawashima, Y.; Takeuchi, H.; Yamamoto, H.; Isshiki, N.; Momose, D. I.; Ouchi, K. Primary crystal growth during spherical agglomeration in liquid: Designing an ideal dry powder inhalation system. *Powder Technol.* 2002, 126(3), 266–274.

150. Kawashima, Y.; Aoki, S.; Takenaka, H. Spherical agglomeration of aminophylline crystals during reaction in liquid by the spherical crystallization technique. *Chem. Pharm. Bull.* 1982, 30(5), 1900–1902.

151. Morishima, K.; Kawashima, Y.; Kawashima, Y.; Takeuchi, H.; Niwa, T.; Hino, T. Micromeritic characteristics and agglomeration mechanisms in the spherical crystallization of bucillamine by the spherical agglomeration and the emulsion solvent diffusion methods. *Powder Technol.* 1993, 76(1), 57–64.

152. Kawashima, Y.; Capes, C. An experimental study of the kinetics of spherical agglomeration in a stirred vessel. *Powder Technol.* 1974, 10, 85–92.

153. Kawashima, Y.; Niwa, K.; Takeuchi, H.; Hino, T. Penetration of outer layered particles of agglomerate into inner intersticies of agglomerate during spherical agglomeration in liquid. *Chem. Pharm. Bull.* 1997, 45(2), 384–388.

154. Bemer, G. G. Agglomeration in suspension: A Study of Mechanisms and Kinetics. Technische Hogeschool Delft, The Netherlands. 1979.

155. Müller, M., & Löffler, F. Development of agglomerate size and structure during spherical agglomeration in suspension. *Part. Part. Sys. Char.* 1996, 13(5), 322–326.

156. Iveson, S. M.; Litster, J. D.; Hapgood, K.; Ennis, B. J. Nucleation, growth and breakage phenomena in agitated wet granulation processes: A review. *Powder Technol.* 2001, 117(1–2), 3–39.

157. Litster, J. Design and processing of particulate products. 1st ed. Cambridge University Press. 2016.

158. Rossetti, D.; Simons, S. J. R. A microscale investigation of liquid bridges in the spherical agglomeration process. *Powder Technol.* 2003, 130, 49–55.

159. Rossetti, D.; Pepin, X.; Simons, S. J. R. Rupture energy and wetting behavior of pendular liquid bridges in relation to the spherical agglomeration process. *J. Colloid Interface Sci.* 2003, 261, 161–169.

160. Blandin, A. F.; Rivoire, A.; Mangin, D.; Klein, J. P.; Bossoutrot, J. M. Using In Situ Image Analysis to Study the Kinetics of Agglomeration in Suspension. *Part. Part. Sys. Char.* 2000, 17(1), 16–20.

161. Madec, L.; Falk, L.; Plasari, E. Modelling of the agglomeration in suspension process with multidimensional kernels. *Powder Technol.,* 2003, 130, 147–153.

162. Petela, R. Prediction of the product size in the agglomeration of coal particles in a water-oil emulsion. *Fuel*, 1991, 70, 509–517.

163. Madec, L.; Falk, L.; Plasari, E. Simulatuion of agglomeration reactors via a coupled CFD/direct Monte-Claro method. *Chem. Eng. Sci.* 2001, 56(4), 1731–1736.

164. Kuboi, R.; Nienow, A.W.; Conti, R. Mechanical attrition of crystals in stirred vessels. *Ind. Crystall.* 1984, 84, 211–216.

165. David, R.; Marchal, P.; Klein, J. P.; Villermaux, J. Crystallization and precipitation engineering-III. A discrete formulation of the agglomeration rate of crystals in a crystallization process. *Chem. Eng. Sci.* 1991, 46(1), 205–213.

166. David, R.; Marchal, P.; Marcant, B. Modelling of Agglomeration in Industrial Crystallization from Solution. *Chem. Eng. Technol.* 1995, 18(1 995), 302–309.

167. David, R.; Paulaime, A. M.; Espitalier, F.; Rouleau, L. Modelling of multiple-mechanism agglomeration in a crystallization process. *Powder Technol.* 2003, 130, 338–344).

168. Ochsenbein, D. R.; Vetter, T.; Schorsch, S.; Morari, M.; Mazzotti, M. Agglomeration of Needle-like Crystals in Suspension: I. Measurements. *Cryst. Growth Des.* 2015, 15, 1923–1933.

169. Ochsenbein, D. R.; Vetter, T.; Morari, M.; Mazzotti, M. Agglomeration of Needle-like Crystals in Suspension. II. Modeling. *Cryst. Growth Des.* 2015, 15(9), 4296–4310.

170. Tahara, K.; O'Mahony, M.; Myerson, A. S. Continuous Spherical Crystallization of Albuterol Sulfate with Solvent Recycle System. *Cryst. Growth Des.* 2015, 15(10), 5149–5156.

171. Freeman, R. Measuring the flow properties of consolidated, conditioned and aerated powders - A comparative study using a powder rheometer and a rotational shear cell. *Powder Technol.* 2007, 174(1–2), 25–33.

172. Fu, X.; Huck, D.; Makein, L.; Armstrong, B.; Willen, U.; Freeman, T. Effect of particle shape and size on flow properties of lactose powders. *Particuology*, 2012, 10(2), 203–208.

173. Freeman, R. Measuring the flow properties of consolidated, conditioned and aerated powders - A comparative study using a powder rheometer and a rotational shear cell. *Powder Technol.* 2007, 174(1–2), 25–33.

174. Ramkrishna, D. *Population balances: Theory and applications to particulate systems in engineering*. Academic press, 2000.

175. Smoluchowski, M.V., 1917. Z. Phys. Chem. 19, 129–168.

176. Coulaloglou, C. A.; Tavlarides, L. L. Description of interaction processes in agitated liquid-liquid dispersions. *Chem. Eng. Sc.* 1977, 32(11), 1289–1297.

177. Prince, M. J.; Blanch, H. W. Bubble coalescence and break-up in air-sparged bubble columns. *AIChE J.* 1990, 36(10), 1485–1499.

178. Iveson, S. M. Limitations of one-dimensional population balance models of wet granulation processes. *Powder Technol.* 2002, 124(3), 219-229.

179. Liu, L. X.; Litster, J. D. Population balance modelling of granulation with a physically based coalescence kernel. *Chem. Eng. Sci.* 2002, 57(12), 2183-2191.

180. Marchal, P.; David, R.; Klein, J. P.; Villermaux, J. Crystallization and precipitation engineering—I. An efficient method for solving population balance in crystallization with agglomeration. *Chem. Eng. Sci.* 1988, 43, 59–67.

181. Kumar, S.; Ramkrishna, D. On the solution of population balance equations by discretization—III. Nucleation, growth and aggregation of particles. *Chem. Eng. Sci.* 1997, 52(24), 4659-4679.

182. Seyssiecq, I.; Veesler, S.; Mangin, D.; Klein, J. P.; Boistelle, R. Modelling gibbsite agglomeration in a constant supersaturation crystallizer. *Chem. Eng. Sci.* 2000, 55, 5565–5578.

183. Zauner, R.; Jones, A. G. Determination of nucleation, growth, agglomeration and disruption kinetics from experimental precipitation data: the calcium oxalate system. *Chem. Eng. Sci.* 2000, 55(19), 4219-4232.

184. Nagy, Z. K.; Fujiwara, M.; Braatz, R. D. Modelling and control of combined cooling and antisolvent crystallization processes. *J. Process Contr.* 2008, 18(9), 856–864.

185. Gimbun, J.; Nagy, Z. K.; Rielly, C. D. Simultaneous Quadrature Method of Moments for the Solution of Population Balance Equations, Using a Differential Algebraic Equation Framework. *Ind. & Eng. Chem. Res.* 2009, 48(16), 7798–7812.

186. Ramisetty, K. Ultrasound-Assisted Antisolvent Crystallization of Benzoic Acid: Effect of Process Variables Supported by Theoretical Simulations. *Ind. Eng Chem. Res.* 2013, 52(49), 17573–17582.

187. O'Grady, D. Multiscale characterization of anti-solvent crystallization. Ph.D. thesis, University College Dublin, Ireland. 2007.

188. Simon, L.L. ; Merz, T.; Dubuis, S.; Lieb, A.; Hungerbuhler, K. In-situ monitoring of pharmaceutical and specialty chemicals crystallization processes using endoscopy–stroboscopy and multivariate image analysis. *Chem. Eng. Res. Des.* 2012, 90, 1847-1855.

189. Kachrimanis, K.; Ktistis, G.; Malamataris, S. Crystallisation conditions and physicomechanical properties of ibuprofen-Eudragit® S100 spherical crystal agglomerates prepared by the solvent-change technique. *Int. J. Pharm.* 1998, 173, 61–74.

190. Maghsoodi, M.; Tajalli Bakhsh, A. S. Evaluation of physico-mechanical properties of drug-excipients agglomerates obtained by crystallization. *Pharm. Dev. Technol.* 2011, 16, 243–249.

191. Krishna, E.; Gupta, D.; Jyothi, S. Spherical crystallisation – A modern technique for direct compression of pharmaceutical substances. *Asian J. Pharm. Clin. Res.* 2012, 5, 3–6.

192. Powell, K. A.; Saleemi, A. N.; Rielly, C. D.; Nagy, Z. K. Periodic steady-state flow crystallization of a pharmaceutical drug using MSMPR operation. *Chem. Eng. Process.* 2015, 97(November), 195–212.

193. Hou, G.; Power, G.; Barrett, M.; Glennon, B.; Morris, G; Zhao, Y. Development and Characterization of a Single Stage Mixed-Suspension, Mixed-Product-Removal Crystallization Process with a Novel Transfer Unit. *Cryst. Growth Des.* 2014, 14, 1782–1793.

194. Griffin, D. W.; Mellichamp, D. A.; Doherty, M. F. Reducing the mean size of API crystals by continuous manufacturing with product classification and recycle. *Chem. Eng. Sci.* 2010, 65, 5770-5780.

195. Roberge, D. M.; Zimmermann, B.; Rainone, F.; Gottsponer, M.; Eyholzer, M.; Kockmann, N. Microreactor technology and continuous processes in the fine chemical and pharmaceutical industry: Is the revolution underway? *Org. Process Res. Dev.* 2008, 12(5), 905–910.

196. Acevedo, D. A.; Ling, J.; Chadwick, K.; Nagy, Z. K. Application of Process Analytical Technology-Based Feedback Control for the Crystallization of Pharmaceuticals in Porous Media. *Cryst. Growth Des.* 2016, 16(8), 4263–4271.

197. Acevedo, D. A.; Peña, R.; Yang, Y.; Nagy, Z. K. Evaluation of Mixed Suspension Mixed Product Removal Crystallization Processes Coupled with a Continuous Filtration System. *Chem. Eng. Process.* 2016, 108, 212-219.

198. Yang, Y.; Song, L.; Zhang, Y.; Nagy, Z. K. Application of wet milling-based automated direct nucleation control in continuous cooling crystallization processes. *Ind. Eng. Chem. Res.* 2016, 55, 4987-4996.

199. Yang, Y.; Song, L.; Gao, T.; Nagy, Z. K. Integrated Upstream and Downstream Application of Wet Milling with Continuous Mixed Suspension Mixed Product Removal Crystallization. *Cryst. Growth Des.* 2015, 15, 5879-5885.

200. Nocent, M.; Bertocchi, L.; Espitalier, F.; Baron, M.; Couarraze, G. Definition of a solvent system for spherical crystallization of salbutamol sulfate by quasi-emulsion solvent diffusion (QESD) method. *J. Pharm. Sci.* 2001, 90, (10), 1620–1627.

201. Cole, K. P.; Campbell, B. M.; Forst, M. B.; Mcclary Groh, J.; Hess, M.; Johnson, M. D.; Miller, R. D.; Mitchell, D.; Polster, C. S.; Reizman, B. J.; Rosemeyer, M. An Automated Intermittent Flow Approach to Continuous Suzuki Coupling. *Org. Process Res. Dev.* 2016, 20(4), 820-830.

202. Cui, Y.; O'Mahony, M.; Jaramillo, J. J.; Stelzer, T.; Myerson, A. S. Custom-Built Miniature Continuous Crystallization System with Pressure-Driven Suspension Transfer. *Org. Process Res. Dev.* 2016, 20(7), 1276–1282.

203. Randolph, A. D.; White, E. T. Modeling size dispersion in the prediction of crystal-size distribution. *Chem. Eng. Sci.* 1977, 32, (9), 1067–1076.

204. Ni, X.; Jian, H.; Fitch, A. Computational fluid dynamic modelling of flow patterns in an oscillatory baffled column. *Chem. Eng. Sci.* 2002, 57(14), 2849–2862.

205. Ni, X.; Liao, A. Effects of mixing, seeding, material of baffles and final temperature on solution crystallization of l-glutamic acid in an oscillatory baffled crystallizer. *Chem. Eng. J.* 2010, 156, (1), 226–233.

206. Stonestreet, P.; Harvey, A. P. A Mixing-Based Design Methodology for Continuous Oscillatory Flow Reactors. Chem. Eng. Res. Des. 2002, 80,31–44.

207. Swartz, M. E. UPLC™: An Introduction and Review. *J. Liq. Chromatogr. Relat. Technol.* 2005, 28, (7-8), 1253–1263.

208. Kacker, R.; Regensburg, S. I.; Kramer, H. J. M. Residence Time Distribution of Dispersed Liquid and Solid Phase in a Continuous Oscillatory Flow Baffled Crystallizer. *Chem. Eng. J.* 2017, 317, 413–423.

209. King, J.C.; Li, H.; Grover, M.A.; Kawajiri, Y.; Rousseau, R.W. Optimization of two-stage cooling profile in unseeded batch cooling crystallization. *IFAC-PapersOnLine.* 2015, 48(8), 297–302.

210. Costa, C. B.; Maciel, R. Evaluation of optimisation techniques and control variable formulations for a batch cooling crystallization process. *Chem. Eng. Sci.* 2005, 60, 5312–5322.

211. Chen, J.; Sarma, B.; Evans, J.M.B.; Myerson, A.S. Pharmaceutical crystallization. *Cryst. Growth Des.* 2011, 11, 887–895.

212. Majumder, A.; Nagy, Z. K. Fines removal in a continuous plug flow crystallizer by optimal spatial temperature profiles with controlled dissolution. *AIChE J*. 2013, 59, 4582–4594.

213. Eder, R. J. P.; Radl, S.; Schmitt, E.; Innerhofer, S.; Maier, M.; Gruber-Woelfler, H.; Khinast, J. G. Continuously seeded, continuously operated tubular crystallizer for the production of active pharmaceutical ingredients. *Cryst. Growth Des.* 2010, 10, 2247–2257.

214. Yang, Y.; Nagy, Z. K. Adanced control approached for combined cooling/antisolvent crystallization in continuous mixed supension mixed product removal cascade crystallizers. *Chem. Eng. Sci.* 2015, 127, 362–373.

215. Tien, C.; Bai, R.; Ramarao, B.V. Analysis of cake growth in cake filtration: Effect of fine particle retention. *AIChE J.* 1997, 43, 33–44.

216. Reynolds, T.; Boychyn, M.; Sanderson, T.; Bulmer, M.; More, J.; Hoare, M. Scale-down of continuous filtration for rapid bioprocess design: recovery and dewatering of protein precipitate suspensions. *Biotechnol. Bioeng.* 2003, 83, 454–464.

217. Chen, W. Optimization of sludge dewatering through pretreatment, equipment selection, and testing. *Drying Technol.* 2013, 31, 193–201.

218. Jones, A. G.; Budz, J.; Mullin, J. W. Batch crystallization and solid-liquid separation of potassium sulphate. *Chem. Eng. Sci.* 1987, 42, 619–629.

219. Matthews, H. B.; Rawlings, J. B. Batch crystallization of a photochemical: modeling, control, and filtration. *AIChE J.* 1998, 44, 1119–1127.

220. Zaitseva, N.; Atherton, J.; Rozsa, R.; Carman, L.; Smolsky, I.; Runkel, M.; Ryon, R.; James, L. Design and benefits of continuous filtration in rapid growth of large KDP and DKDP crystals. *J. Cryst. Growth*. 1999, 197, 911–920.

221. Chayen, N.E. Rigorous filtration for protein crystallization. *J. Appl. Cryst.* 2009, 42, 743–744.

222. Ingham, R. J.; Battilocchio, C.; Fitzpatrick, D. E.; Sliwinski, E.; Hawkins, J. M.; Ley, S. V. A Systems Approach towards an Intelligent and Self-Controlling Platform for Integrated Continuous Reaction Sequences. *Angew. Chem. Int. Edit.* 2015, 54 , 144–148.

223. Ley, S. V.; Fitzpatrick, D. E.; Ingham, R.; Myers, R. M. Organic synthesis: march of the machines. *Angew. Chem. Int. Edit.* 2015, 54, 3449–3464.

224. Gursch, J.; Hohl, R.; Dujmovic, D.; Brozio, J.; Krumme, M.; Rasenack, N.; Khinast, J. Dynamic cross-flow filtration: enhanced continuous small-scale solid-liquid separation. *Drug Dev. Ind. Pharm.* 2016, 42, 977–984.

225. Mitchell, N. A.; Frawley, P. J.; Ó'Ciardhá, C. T. Nucleation kinetics of paracetamol-ethanol solutions from induction time experiments using Lasentec FBRM. *J. Cryst. Growth.* 2011, 321, 91–99.

226. Li, H.; Kawajiri, Y.; Grover, M. A.; Rousseau, R. W. Application of an empirical FBRM model to estimate crystal size distributions in batch crystallization. *Cryst. Growth Des.* 2014, 14, 607–616.

227. Li, H.; Grover, M. A.; Kawajiri, Y.; Rousseau, R. W. Development of an empirical method relating crystal size distributions and FBRM measurements. *Chem. Eng. Sci.* 2013, 89, 142–151.

228. Yang, Y.; Nagy, Z. K. Application of nonlinear model predictive control in continuous crystallization systems. *Proceed. ACC.* 2015, 4282–4287.

VITA

Ramon Peña was born on April 4th in the lower east side (LES) of Manhattan, NYC, NY and grew up in a small, mostly Latino, town in central New Jersey. Having always had a passion for chemistry and mathematics, Ramon majored in chemical engineering at Rutgers University upon completing high school. While at Rutgers University, Ramon became a Ronald E. McNair and Louis Stokes Alliance for Minority Participation (LSAMP) Scholar. Through these organizations, Ramon received a National Action Council for Minorities in Engineering (NACME) research grant that funded his undergraduate research activities. Having research experience in the Engineering Research Center (ERC) and Center for Structure Organic Particulate Systems (C-SOPS) and industrial experience via internships at Bristol-Myers Squibb and BASF, Ramon decided to join the Davidson School of Chemical Engineering at Purdue University to pursue his doctoral degree in chemical engineering. Upon receiving his Ph.D., he will be joining Exxon Mobil as a Products Research Technologist.

PUBLICATIONS

Peña, R., & Nagy, Z. K. (2015). Process Intensification through Continuous Spherical Crystallization Using a Two-Stage Mixed Suspension Mixed Product Removal (MSMPR) System. *Crystal Growth and Design*, *15*(9), 4225–4236.

Acevedo, D., Peña, R., Yang, Y., Barton, A., Firth, P., & Nagy, Z. K. (2016). Evaluation of mixed suspension mixed product removal crystallization processes coupled with a continuous filtration system. *Chemical Engineering and Processing: Process Intensification*, *108*, 212–219.

Peña, R., Burcham, C. L., Jarmer, D. J., Ramkrishna, D., & Nagy, Z. K. (2017). Modeling and optimization of spherical agglomeration in suspension through a coupled population balance model. *Chemical Engineering Science*, *167*, 66–77.

Peña, R., Oliva, J. A., Burcham, C. L., Jarmer, D. J., & Nagy, Z. K. (2017). Process Intensification through Continuous Spherical Crystallization Using an Oscillatory Flow Baffled Crystallizer (OFBC). *Crystal Growth & Design*, acs.cgd.7b00731.